DOE/JPL/954331-82/1
(DE82009390)

SILICON MATERIALS TASK OF THE LOW COST SOLAR ARRAY PROJECT

Effect of Impurities and Processing on Silicon Solar Cells

Final Report

By
R. H. Hopkins
J. R. Davis
A. Rohatgi
M. H. Hanes
P. Rai-Choudhury
H. C. Mollenkopf

February 1982

Work Performed Under Contract No. NAS-7-100-954331

Westinghouse R & D Center
Pittsburgh, Pennsylvania

and

Hemlock Semiconductor Corporation
Hemlock, Michigan

U.S. Department of Energy

Solar Energy

DISCLAIMER

DISCLAIMER

DRD No. SE-7
DRL No. 58

DOE/JPL/954331-82/1
(DE82009390)
Distribution Category UC-63b

SILICON MATERIALS TASK OF THE LOW COST SOLAR ARRAY PROJECT

Effect of Impurities and Processing on Silicon Solar Cells

Final Report

February 1982

R. H. Hopkins, J. R. Davis, A. Rohatgi,
M. H. Hanes, and P. Rai-Choudhury
Westinghouse Research and Development Center
and
H. C. Mollenkopf
Hemlock Semiconductor Corp.

Contract No. 954331

The JPL Low Cost Silicon Solar Array Project is sponsored by the U. S. Dept. of Energy and forms part of the Solar Photovoltaic Conversion Program to inititate a major effort toward the development of low-cost solar arrays. This work was performed for the Jet Propulsion Laboratory, California Institute of Technology by agreement between NASA and DOE.

Westinghouse R&D Center
1310 Beulah Road
Pittsburgh, Pennsylvania 15235

THIS PAGE

WAS INTENTIONALLY

LEFT BLANK

PREFACE

This report presents an analysis of the data developed during a study entitled "An Investigation of the Effects of Impurities and Processing on Silicon Solar Cells" conducted under JPL Contract 954331.

A number of individuals contributed to the study; the most recent areas of responsibility for each are listed below.

R. H. Hopkins - Program Manager and Silicon Web Studies

J. R. Davis - Device Testing, Data Synthesis and Modeling

A. Rohatgi - Detailed Device Analysis and Deep Level Spectroscopy

M. H. Hanes and R. B. Campbell - Thermochemical Processing and Aging Studies

P. Rai-Choudhury - Device Processing

H. C. Mollenkopf - Principal Investigator, Crystal Growth and Analysis

We are indebted to the following individuals for their capable technical assistance: D. N. Schmidt (cell processing and testing), B. F. Westwood, J. McNally, R. R. Adams, J. M. Bronner and W. Cifone (process experiments and photolithography), A. M. Stewart (material characterization and web growth), H. F. Abt (metallization), S. Karako (DLTS measurements), T. Zigarovich (mask preparation).

Debbie Labor prepared the report manuscript; the text was edited by G. Law.

Dr. Alan Yamakawa served as technical monitor for the program at the Jet Propulsion Laboratory.

THIS PAGE

WAS INTENTIONALLY

LEFT BLANK

TABLE OF CONTENTS

TABLE OF CONTENTS (Cont.)

LIST OF FIGURES

LIST OF FIGURES (Cont.)

LIST OF FIGURES (Cont.)

LIST OF FIGURES (Cont.)

LIST OF TABLES

LIST OF TABLES (Cont.)

1. SUMMARY

This is the Final Report of a multiphase program conducted as part of the Silicon Materials Task of the LSA Project. The object of the program has been to investigate the effects of various processes, metal contaminants, and contaminant-process interactions on the properties of silicon and on the performance of terrestrial silicon solar cells. The study has encompassed topics such as thermochemical (gettering) treatments, base-doping concentration, base-doping type (n vs. p), grain boundary-impurity interaction in polycrystalline devices, and long-term effects of impurities and impurity impacts on high-efficiency cells, as well as a preliminary evaluation of some potential low-cost silicon materials. The work is now completed, and some of the highlights are given below.

We have studied the effects of various metallic impurities, introduced singly or in combination into Czochralski, float zone, and polycrystalline silicon ingots and into silicon ribbons grown by the dendritic web process. The metals were added in controlled and reproducible fashion with a primary boron or phosphorus dopant to produce n- or p-type conductivity. All crystals were analyzed chemically microstructurally, electrically, and via solar cell fabrication and testing.

Taken in toto, the solar cell data (collected from 238 experimental ingots) indicate that impurity-induced performance loss is caused primarily by a reduction in base diffusion length. An analytical model based on this observation has been developed and verified experimentally for both n- and p-base material. It predicts quite well the performance of silicon cells bearing multiple contaminants. Only Fe, Cu, Ni, and to a lesser extent, Co deviate from the model assumptions; cell degradation in these cases is caused by precipitate-induced junction effects. Several metal contaminants, noteably Ti and V, produce considerably less cell performance reduction in n-base devices than in the p-base cells.

Studies of polycrystalline ingots containing impurities indicate that solar cell behavior is species sensitive and that a fraction of the impurities are segregated to the grain boundaries during cooling of the ingots from the growth temperature. Cr, a rapidly diffusing species in silicon, exhibits a tenfold reduction in electrical activity at grain boundaries while Mo,a slow diffuser,shows no measureable activity reduction. Twin boundaries do not act as impurity sinks. Detailed analysis of contaminated poly cells via I-V, spectral response, and DLTS measurements showed that the impurity concentration and lifetime within grains is similar to that expected for a single crystal containing the same impurity.

HCl and POCl gettering improve the performance of single-crystal solar cells containing Fe, Cr, and Ti. In contrast Mo-doped material is barely affected by the treatment,apparently because Mo diffuses only slowly in silicon. Qualitatively similar behavior was observed for the gettering of polycrystalline devices, although cell efficiency improvements are smaller due to the presence of the grain boundaries. Argon ion implant damage does not significantly enhance gettering. Gettering of Ti, and probably other species as well, is a thermally activated, diffusion-controlled process.

The efficiencies of solar cells fabricated on impurity-doped wafers is lower when the front junction is formed by ion implantation than when conventional diffusion techniques are used.

When subjected to accelerated aging at high temperatures, most impurity-doped solar cells exhibit rates of cell performance reductions which, extrapolated to operating temperatures, would assure stability for projected times beyond 20 years. Ag and Cr-doped cells degrade at a more rapid rate consistent with the higher diffusion rate of these elements in silicon. No long-term effects due to impurity interactions with the internal electrical field of solar cells was measured at temperatures up to 280°C.

Feedstock impurity concentrations below one part per million for elements like V, or 100 parts per million for more benign impurities like Cu or Ni,will be required even with crystal growth methods like Czochralski or silicon web,which exhibit large melt segregation effects. The exact value of the acceptable impurity content for Solar Grade Silicon depends on tolerable cell efficiency, crystal growth method, melt replenishment strategy and cell process sequence. Our data base and the model equations permit each manufacturer to assess the utility of a solar grade of silicon to his specific process sequence.

2. INTRODUCTION

This is the Final Report of a multi-year study conducted under JPL Contract 954331. The program's objective was to define the effects of impurities and processing on the characteristics of silicon and terrestrial silicon solar cells so that poly-silicon manufacturers, wafer manufacturers, and the producers of solar cells can develop cost-benefit relationships for the use of cheaper, less pure solar grades of silicon.

The program evolved in four phases. In Phases I and II,[1,2] we established empirically what concentrations of commonly encountered impurities could be tolerated in typical p or n-base solar cells, then developed a preliminary analytical model from which the cell performance could be projected depending on the kinds and amounts of contaminants in the silicon base material. During Phase III,[3] the impurity data base was expanded to include construction materials, and the impurity-performance model was refined to account for additional effects such as base resistivity, grain boundary interactions, thermal processing, synergic behavior, and non-uniform impurity distributions. A preliminary assessment of long-term (aging) behavior of impurities was also undertaken. The objectives of the Phase IV activity were to complete the studies of thermochemical processing and aging effects, to examine in greater detail impurity behavior in polycrystalline and high-efficiency solar cells, and to evaluate the properties of some potentially low-cost silicon materials.

Our general approach was to: (1) grow silicon single crystals containing a baseline boron or phosphorus dopant and specific impurities which produce deep levels in the forbidden band gap; (2) assess crystal quality by chemical, microstructural, electrical, and solar cell tests; (3) correlate impurity type and concentration with crystal quality and

device performance; and (4) define how impurities and processing affect subsequent silicon solar cell performance.

The program is now completed. We have presented comprehensive summaries of previous work in references 1 to 3, so a major portion of this report concerns the Phase IV activities and an analysis of overall results. Key findings from earlier phases are reiterated where necessary for clarity and completeness. Previous analytical results and device data have been updated where possible to reflect the most current information. Tabulations of Phase IV data appear in Appendices I to V.

We have highlighted here the analysis of experimental results and their implications with respect to the use of "solar" grades of silicon. Readers interested in our experimental methodology - for example, deep-level spectroscopy, detailed dark I-V measurements, recombination lifetime determinations, scanned-laser photo-response, conventional solar cell I-V techniques, and silicon chemical analysis – are referred to Vol. 1 of reference 3, which also contains extensive tabulations of the chemical, electrical and solar cell characteristics of impurity-doped silicon gathered during Phases I to III. A list of related papers on impurity effects on silicon is collected in Appendix VI.

3. THE IMPACT OF IMPURITIES ON SILICON AND SILICON SOLAR CELLS

3.1 Impurity Selection

Our study was directed to the needs of potential makers and users of less pure but cheaper solar grades of silicon: polycrystalline silicon producers, crystal growers who transform the silicon to sheet or wafers, and solar cell and array manufacturers. Thus, to develop the impurity matrix (Table 1) for this study, the impurity species chosen were those which: (1) commonly occur in metallurgical grade silicon, a feedstock for many low-cost silicon processes,[2] (2) may be introduced during silicon production, (3) are used to construct crystal growth or silicon process equipment, or (4) may be employed as device contact metals.

The concentration ranges used for a given species depended on (1) the solid solubility in silicon,[4] (2) the maximum tolerable concentration for single-crystal growth,[5] (3) the threshold for solar cell performance reduction,[1,2] and (4) the analytical detection limits.[6,7] The targeted base resistivities, 4 to 6 Ω-cm for p-type ingots and 1 to 3 Ω-cm for n-type ingots (Ref. 3 and Appendix I), lie close to the range obtained typically in commercial practice. Resistivities as low as 0.2 Ω-cm and as high as 30 Ω-cm were examined in selected ingots to test for any interactions between the base dopant and the metal contaminant. A few boron-doped, phosphorus-compensated ingots were also produced.[3]

3.2 Ingot Growth and Evaluation

3.2.1 Crystal Growth

All ingots save five which were float-zoned[3] were prepared by Czochralski pulling. This method offers several advantages including: (1) a relatively flat doping profile, (2) the addition of impurities either before or after melt-down, (3) the ability to vary significantly growth conditions, and (4) the possibility to sample the melt at the completion of crystal growth to determine melt impurity concentration.

TABLE 1 IMPURITY MATRIX

Impurity	Approximate Concentration Range ($10^{15}cm^{-3}$)
Aluminum*	3-120
Boron*	
Calcium	0.1
Carbon**	20-500
Chromium (+)	0.1-1.1
Cobalt	0.054-3.0
Copper (+)	0.4-60
Gadolinium	<0.07
Gold	0.6
Iron (+)	0.02-1.5
Lead (+)	<0.1
Magnesium	0.003-0.03
Manganese (+)	0.01-4.0
Molybdenum	0.000046-0.0042
Nickel	0.4-10
Niobium	<0.044
Oxygen**	500-1700
Palladium	6.5
Phosphorus* (+)	1.0-150
Silver	2.2-4.5
Tantalum	0.000065-0.004
Tin	4846
Titanium (+)	0.0036-0.36
Tungsten	0.00014-0.0015
Vanadium (+)	0.0004-0.4
Zinc	<0.001
Zirconium	<0.0007

* Boron, phosphorus, and aluminium are electrically active impurities and therefore cause variations in resistivity when used as a secondary impurity.

** Oxygen and carbon concentrations measured in approximately 110 ingots doped with additional impurities. Two carbon-doped ingots prepared to determine effect of carbon.

\+ See text, Ref. 3.

TABLE 2 CHARACTERISTICS OF DOPANT MATERIALS

Element	Purity (%)	Form	Melting Point (°C)
Aluminum	99.99	wire	660
Calcium	99.9	block	851
Carbon	99.999	graphite rod	3550
Chromium	99.999	pellets	1900
Cobalt	99.99	polycrystal rod	1555
Copper	99.9997	zone-refined ingots	1083
Gadolinium	99.9	chips	1312
Gold	99.999	slugs	1063
Iron	99.999	sponge	1535
Lead	99.999	polycrystal rod	327
Magnesium	99.99	ingot	651
Manganese	99.99	flake	1244
Molybdenum	99.98	pellets	2610
Nickel	99.98	sponge wire	1455
Niobium	99.99	polycrystal rod	2468
Palladium	99.99	polycrystal rod	1555
Silver	99.999	polycrystal rod	960.8
Tantalum	99.99	polycrystal rod	2996
Tin	99.9995	polycrystal rod	232
Titanium	99.95	crystal	1668
Tungsten	99.999	polycrystal rod	3410
Vanadium	99.9	dendrite	2190
Zirconium	99.99	foil	2127

Two crystal-growth furnaces were used during the program. Phase I ingots were prepared in an NRC-2805 crystal-growth furnace. To provide more material, subsequent ingots were grown in the HAMCO CG-800 crystal-growth furnace. The characteristics of both pieces of equipment as well as the details of the growth procedure are given in Volume 1 of reference 3.

The majority of the ingots studied were single crystals seeded to grow in the <111> direction. In selected cases, polycrystalline ingots were grown from seeds containing 3 to 4 randomly oriented grains; typical polycrystalline ingot grain sizes averaged 1mm in diameter. A limited number of ribbon crystals produced by the dendritic web process were also studied.[8]

Number-one Dow Corning semiconductor-grade silicon nuggets or one-piece crucible charges were used throughout the entire program. Typical characteristics of this material can be found in reference 3. The impurities in the polycrystalline silicon are sufficiently low in concentration that their presence does not affect solar cell performance.[1-3]

High purity (99.99% or better) metal dopants were employed throughout the program. The form, purity, and melting points of these materials are listed in Table 2. Impurities with high melting points and low vapor pressures are added to the crucible charge prior to melt-down. Impurities melting at temperatures below silicon, or which exhibit high vapor pressure, are added to the molten silicon prior to initiation of crystal growth. The amount of impurity added to the melt was based on the target impurity concentration in the ingot and the best available value for the effective segregation coefficient.

3.2.2 Crystal Characterization

Subsequent to growth each ingot was sampled,[1-3] analyzed chemically (Section 3.4), then subjected to a variety of physical, electrical, and device-related tests including:

etch pit density	detailed I-V analysis
resistivity	spectral response
carbon analysis	laser-scanned photoresponse
oxygen analysis	recombination lifetime
deep-level transient spectroscopy	solar cell I-V analysis

Volume 1 of reference 3 describes these procedures in considerable detail.

3.3 Impurity-Induced Microstructural Breakdown

Two hundred-thirty-eight ingots have been produced and characterized as part of this study. Etch pit densities were typically less than 10^3 cm^{-2} on material from which all solar cells were made (Reference 3 and Appendix I). About 30 per cent of the ingots had zero dislocation densities although no special effort was made to achieve this result.

In heavily doped ingots, however, constitutional supercooling often initiated a microstructural degeneration manifested by inclusion entrapment within the ingots and the formation of a roughened, "feathery" surface pattern.[1-3] The onset of "breakdown" took place at liquid-impurity concentrations near 2×10^{20} cm^{-3} in the 3-cm diameter ingots pulled at 7cm/hr. In larger 7.6-cm ingots or those grown at higher speeds, proportionately less impurity was required to cause breakdown. Lower breakdown thresholds were also observed in purposely polycrystalline ingots than in comparably doped single crystals. Because breakdown ultimately limits the yield of useful solar cell material, a detailed review of this phenomena is presented here.

3.3.1 Constitutional Supercooling: Structural Aspects

3.3.1.1 Single-Crystal Ingots

Besides the direct electrical impact on silicon, impurities also limit the range of conditions for which single crystals can be grown. This is because a planar crystal-liquid interface can degenerate into a cellular morphology when the liquid impurity concentration exceeds

a critical value C_ℓ^*. The phenomenon, termed constitutional supercooling,[5,13] produces a microstructure in which a metal-rich second phase is distributed as a cell-like network, (e.g, Figure 1,) or as individual particles located preferentially near grain boundaries or twins in the silicon, (Figure 2). Particle morphologies are round, faceted, or sometimes blade-like as illustrated in Figure 3. These inclusions act as electrical shunts and render the silicon useless for solar cells.[3]

Using the energy dispersive x-ray analysis (EDAX) capability of the scanning electron microscope, we evaluated the chemical compositions of three to four inclusions from typical ingots which had undergone structural degeneration during growth: W166Fe, W171W, W226Mn, and W228Gd. In each case, the x-ray energy spectrum from a polished ingot section revealed that the inclusions contained only silicon and the purposely added metal contaminant, (e.g, Figure 4).

Standardless quantitative EDAX analyses were then performed using the computer program MAGIC5 to make appropriate absorption, fluorescence, and atomic number corrections.[9] Listed in Table 3 are the compositions of the inclusion phases obtained by averaging data from several particles in each specimen. The compositions are estimated reliable to about 2 w/o. Also listed in the table are the compositions of the most silicon-rich compounds and eutectics in the pertinent binary systems (Mn-Si, W-Si, Fe-Si, and Gd-Si).

In general, we found the phase diagrams[10-12] are good predictors of the inclusion phases formed during structural breakdown. One might expect the inclusions formed during constitutional supercooling to be the most silicon-rich phase in the given binary system. The close match between the measured impurity compositions and the equilibrium compositions of $Mn_{11}Si_{19}$[9], WSi_2[10], and ξ-$FeSi_2$[10], (Table 3) bear out this expectation. Agreement for the Gd-Si system is less clear, a fact which may be attributable to the general lack of data pertaining to this system.[12]

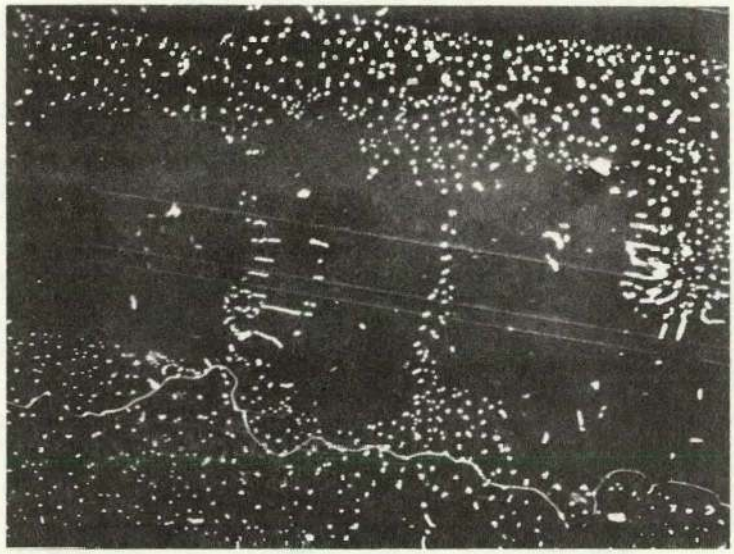

Figure 1 Aligned twin structure and second-phase network of WSi_2 formed in ingot W145W001 after structural breakdown. (130X) Scanning Electron Micrograph.

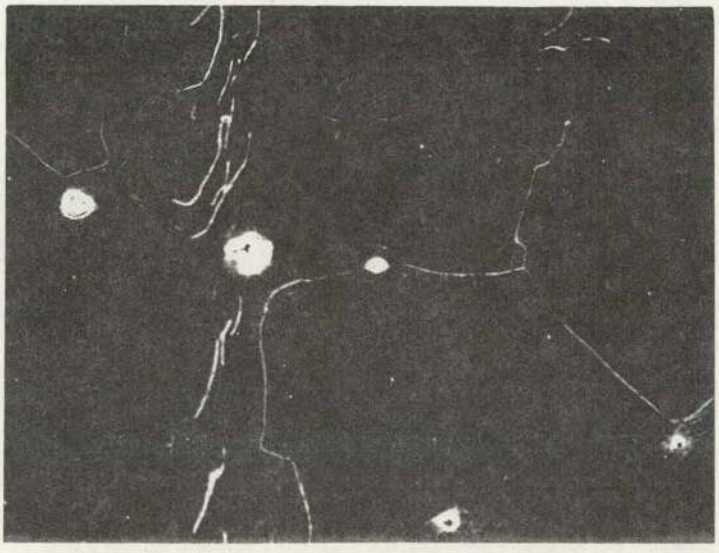

Figure 2 Inclusions of an Fe-rich ("Fe-Si_2") phase formed in ingot W166Fe007 due to constitutional supercooling. (130X) Scanning Electron Micrograph.

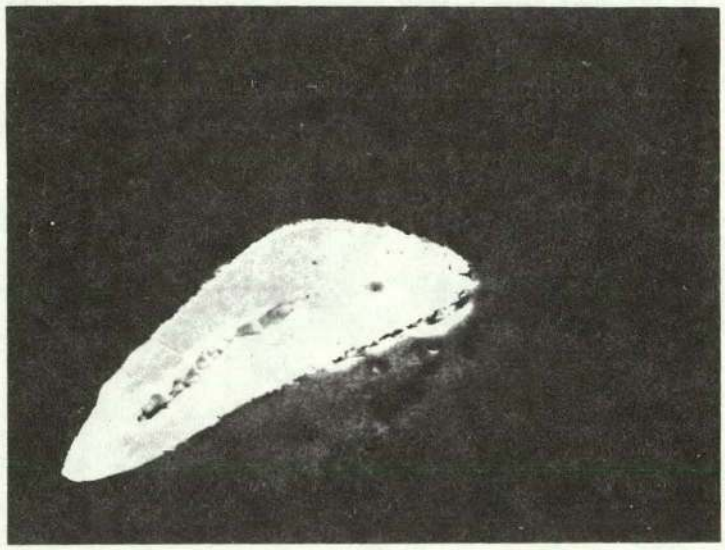

Figure 3 Blade-like $Mn_{11}Si_{19}$ second-phase particle identified by EDAX analysis of ingot W226Mn-010.

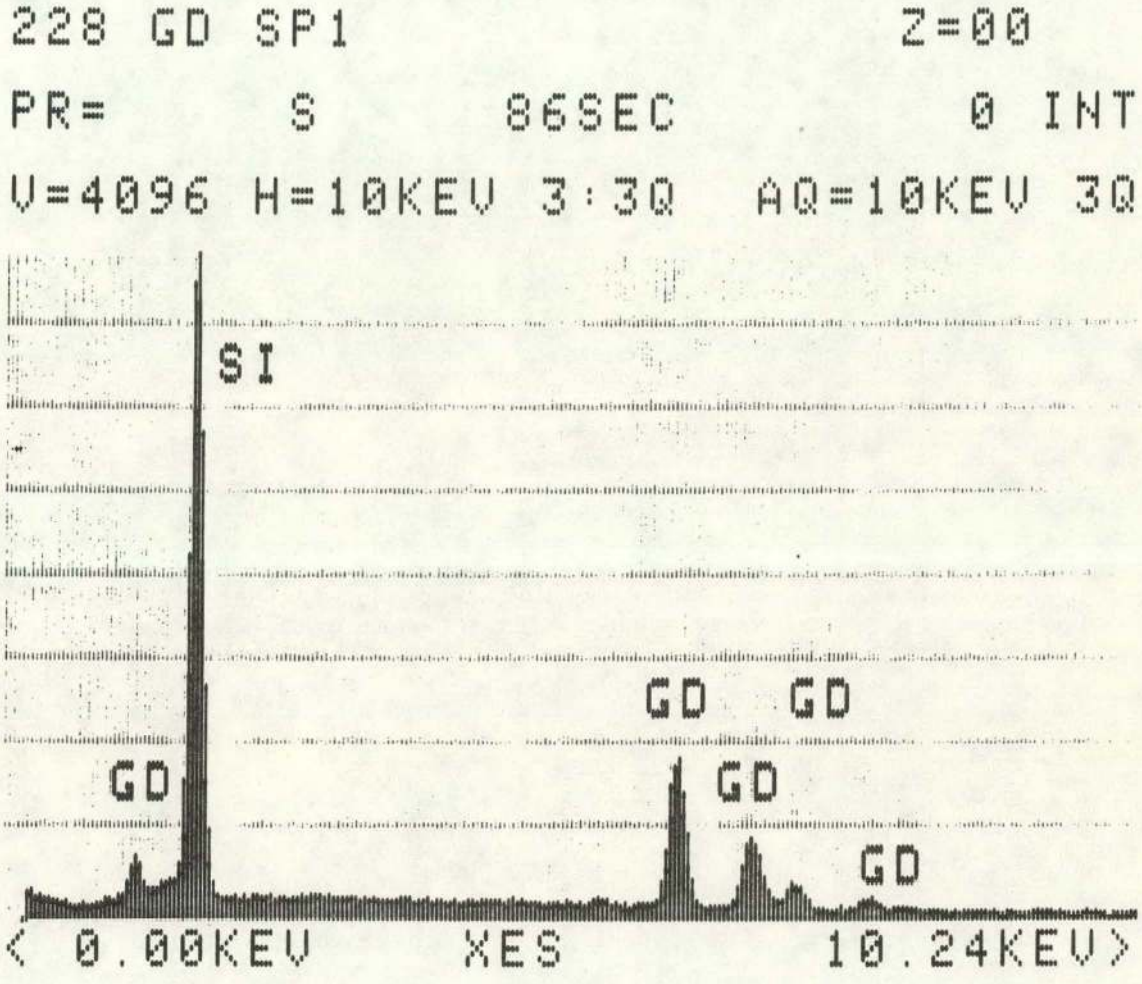

Figure 4 Electron beam-excited energy spectrum from an inclusion in ingot W228Gd001. Only Gd and Si were detected.

TABLE 3

ANALYSIS OF INCLUSIONS FORMED DURING STRUCTURAL BREAKDOWN OF SILICON INGOTS GROWN FROM CONTAMINATED MELTS

Ingot	Average Composition[+] of Inclusion Phase(w/o)		Composition from Phase Diagram (%)	Eutectic Composition (w/o)
W226Mn	45.12	% Si	47% Si[9]	51.5% Si[9]
	54.88	% Mn	53% Mn	48.5% Mn
			($Mn_{11}Si_{19}$)	($Mn_{11}Si_{19}$ + Si)
W171W	26.42	% Si	25% Si[10]	95% Si[10]
	73.58	% W	75% W	5% W
			(WSi_2)	(WSi_2 + Si)
W166Fe	49.44	% Si	53-57% Si[10]	58% Si[10]
	50.56	% Fe	47-43% Fe	42% Fe
			(ξ-"$FeSi_2$")	("$FeSi_2$"+Si)
W228Gd	37.92	% Si	26.33[11]	undetermined
	62.08	% Gd	73.67	
			("$GdSi_2$")	

[+]Standardless EDAX Method in Scanning Electron Microscope

Of the systems we chose for analysis, the W-Si system has a eutectic whose composition lies within a few percent of pure silicon, (Table 3). Apparently, impurity-rich liquid formed during structural breakdown of the W-doped crystal reached the eutectic composition, which would account for the eutectic-like intergrowth observed in this specimen, (Figure 1).

3.3.1.2 Polycrystalline Ingots

During this program, purposely polycrystalline ingots have been grown and contaminated with various impurities in order to evaluate impurity-grain boundary interactions (see Section 3.0). These ingots were nucleated from seeds having several 0.5 to 1mm-sized grains; the polycrystalline structure propagated the length of the ingot. For the most heavily doped melts, these ingots also underwent impurity-induced structural degradation: metal rich inclusions formed within the grains, (e.g. Figure 5) or eutectic material formed at the grain boundaries (Figure 6). After inclusion formation the grain size abruptly diminished to a fine network of twins and grain boundaries well below the 1mm diameters originally present.

For three impurities we examined in detail—V, Mo, and Cr—the threshold for structural degradation appears to be smaller in the polycrystalline ingots than in silicon single crystals grown under comparable conditions, (viz. Table 4). The greatest difference in behavior occurs at V, where C_ℓ^* for the polycrystalline ingot is nearly an order of magnitude smaller than for the single crystal grown under comparable conditions.

All our single crystals were grown in the [111] direction so the crystal-liquid interace is a (111) facet. Such singular faces stabilize a planar solid-liquid interface against constitutionally induced breakdown. Thus, one might expect structural breakdown to occur at lower values of C_ℓ^* in polycrystals which contain a multiplicity of growth orientations, as well as grain boundaries which perturb an otherwise smooth solid-liquid interface and are thus favored sites to initiate

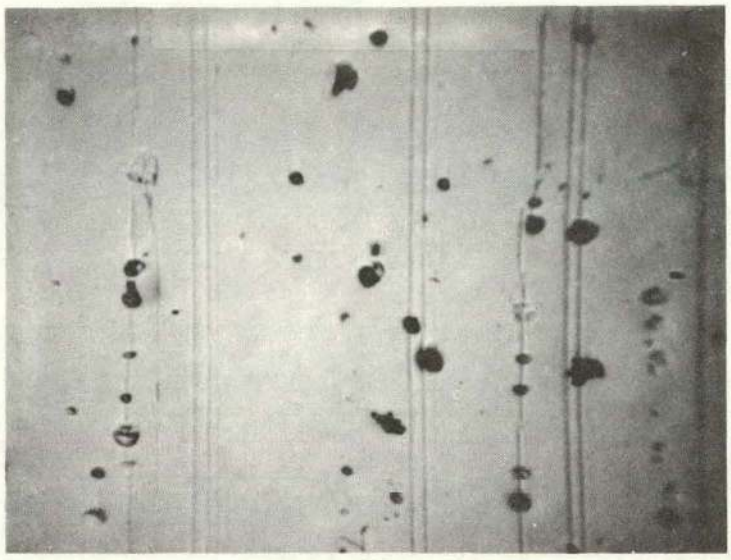

(a)

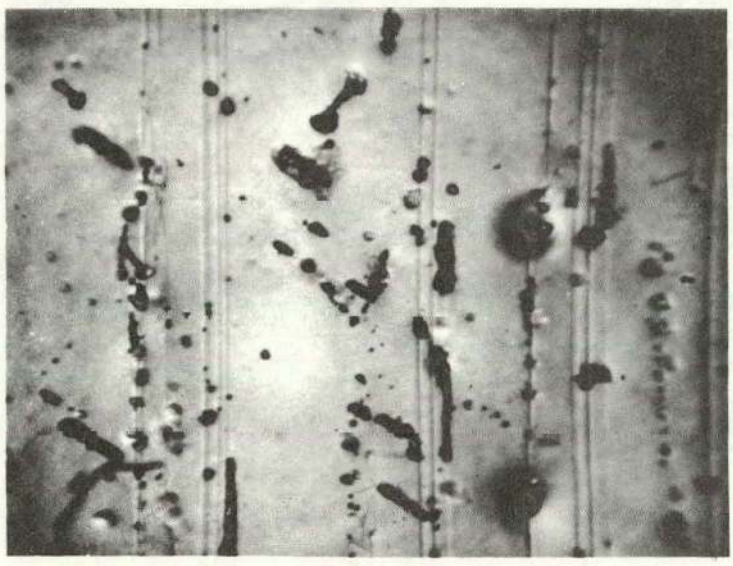

(b)

Figure 5 Cr silicide inclusions caused by constitutional supercooling during the growth of Ingot W204Cr: (a) Inclusions outcrop on the wafer surface, a reflected light photomicrograph; (b) Infrared transmission photomicrograph of the same area showing the inclusions threading through the same area of the bulk wafer. (60X).

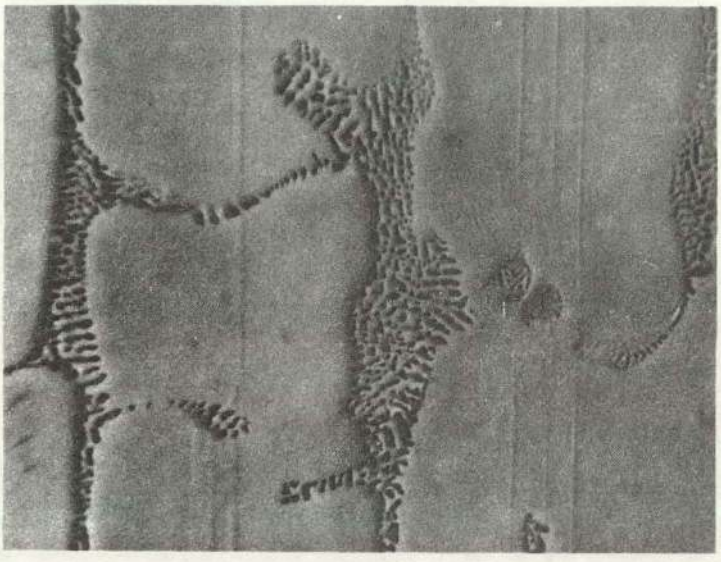

Figure 6 Optical photomicrograph from a section cut normal to the growth direction of Ingot W201Mo007. The eutectic-like network is composed of Mo silicide intertwined with the silicon host crystal. The second-phase network extends in the growth direction and also lies parallel to twin boundaries ({111} traces) on the plane of polish. 100X magnification.

TABLE 4

COMPARISON OF CRITICAL IMPURITY CONCENTRATIONS FOR STRUCTURAL BREAKDOWN IN SINGLE AND POLYCRYSTALLINE INGOTS

Ingot	Impurity	Measured Breakdown Concentration C_ℓ^*, 10^{20} cm^{-3}
W009	V	2.4
W203-Poly+	V	0.15
W139	Mo	1.3
W201-Poly+	Mo	0.9
W004	Cr	3.6
W216-Poly+	Cr	1.5

+ nucleated from a polycrystalline seed

breakdown. The rather sizeable difference in behavior between poly- and single-crystal V-doped ingots is not yet explained.

3.3.2 Constitutional Supercooling: Model for Onset of Breakdown

For a crystal freezing at a steady-state velocity R under an imposed liquid thermal gradient G_ℓ, the conditions for stable growth from a liquid whose impurity concentration is C_ℓ are that[5,13]:

$$G_\ell/R > \frac{(-m\, C_\ell)}{D_\ell}\left[\frac{1-k_o}{k_o}\right] \qquad (1)$$

The liquidus slope, m, and the equilibrium distribution coefficient, k_o, are obtained from the respective phase diagram ($m < 0$ for $k < 1$), and D_ℓ is the impurity diffusion coefficient in the liquid. Hurle[14] reformulated the expression to account for stirring in the liquid during Czochralski growth[14]:

$$\frac{G_\ell}{R} > \frac{(-m\, C_\ell)}{D_\ell}\,\frac{1-k_o}{\{k_o + (1-k_o)e^{-\Delta}\}} \qquad (2)$$

where $\Delta = \frac{R\delta}{D}$; δ is the thickness of the diffusion-dominated boundary layer.

Equation (2) may be recast in terms of the solid thermal gradient G_s, a quantity more readily calculated, or measured, than is the gradient in the liquid, G_ℓ:

$$\frac{K_s G_s - LR}{K_\ell R} > \frac{-mC_\ell}{D_\ell}\,\frac{1-k_o}{\{k_o + (1-k_o)e^{-\Delta}\}} \qquad (3)$$

where K_s and K_ℓ are the solid and liquid thermal conductivities and L is the latent heat of fusion per unit volume. When k_o is small, equation 3 can be simplified to give the critical impurity concentration for breakdown as

$$C_\ell^* = \frac{D_\ell}{-m}\left[\frac{K_s G_s}{K_\ell R} - \frac{L}{KL}\right]e^{-\Delta}. \qquad (4)$$

The critical impurity concentration depends strongly on the growth parameters but less so on the species of metal impurity.

G_s can be calculated from the heat flow through the growing crystal. For simplicity, we choose a solution derived for a crystal of radius r, and constant conductivity K_s, which loses heat by radiation to a 0 K environment[15],

$$G_s = (2\varepsilon\sigma/5K_s r)^{1/2} T_m^{5/2}. \qquad (5)$$

Substituting this in equation 4 and evaluating the resulting expression with[15] $\varepsilon_s = 0.46$, $K_s = 0.216$ W/cm^{-1}K^{-1}, $K_\ell = 0.6$W/cm^{-1}K^{-1}, L = 4128.5 J cm^{-3}, $\sigma = 5.67\text{x}10^{-12}$W/cm^{-2}K^{-4}, $T_m = 1685$ K, gives

$$C_\ell^* = \frac{D_\ell}{-m}\left[\frac{A}{r^{1/2}R} - B\right]e^{-\Delta} \qquad (6)$$

where A = 92.44 and $B = 6.88\text{x}10^3$ with r in cm and R in cm/sec.[13]

For dilute solution the liquidus slope depends on the number rather than kind of atom in the liquid and can be obtained from the data of Thurmond and Kowalchik[16]: $m \cong -464$ K (at. fract)$^{-1}$. Liquid diffusion coefficient data for silicon are sparse — but D generally ranges around the value 10^{-4} cm^2/sec which we have adopted for purposes of calculation. Finally, we chose $\delta/D \sim 130$ as characteristic of our experiments.

For the assumed conditions; the critical impurity concentration for breakdown varies with growth rate and crystal diameter as shown in Figure 7. At low velocities where latent heat evolution is negligible, C_ℓ^* changes inversely with R. At higher velocities, C_ℓ^* falls rapidly as the velocity (R_{max}) for which G_L goes to zero is approached. For any given R, C_ℓ^* decreases as ingot radius increases.

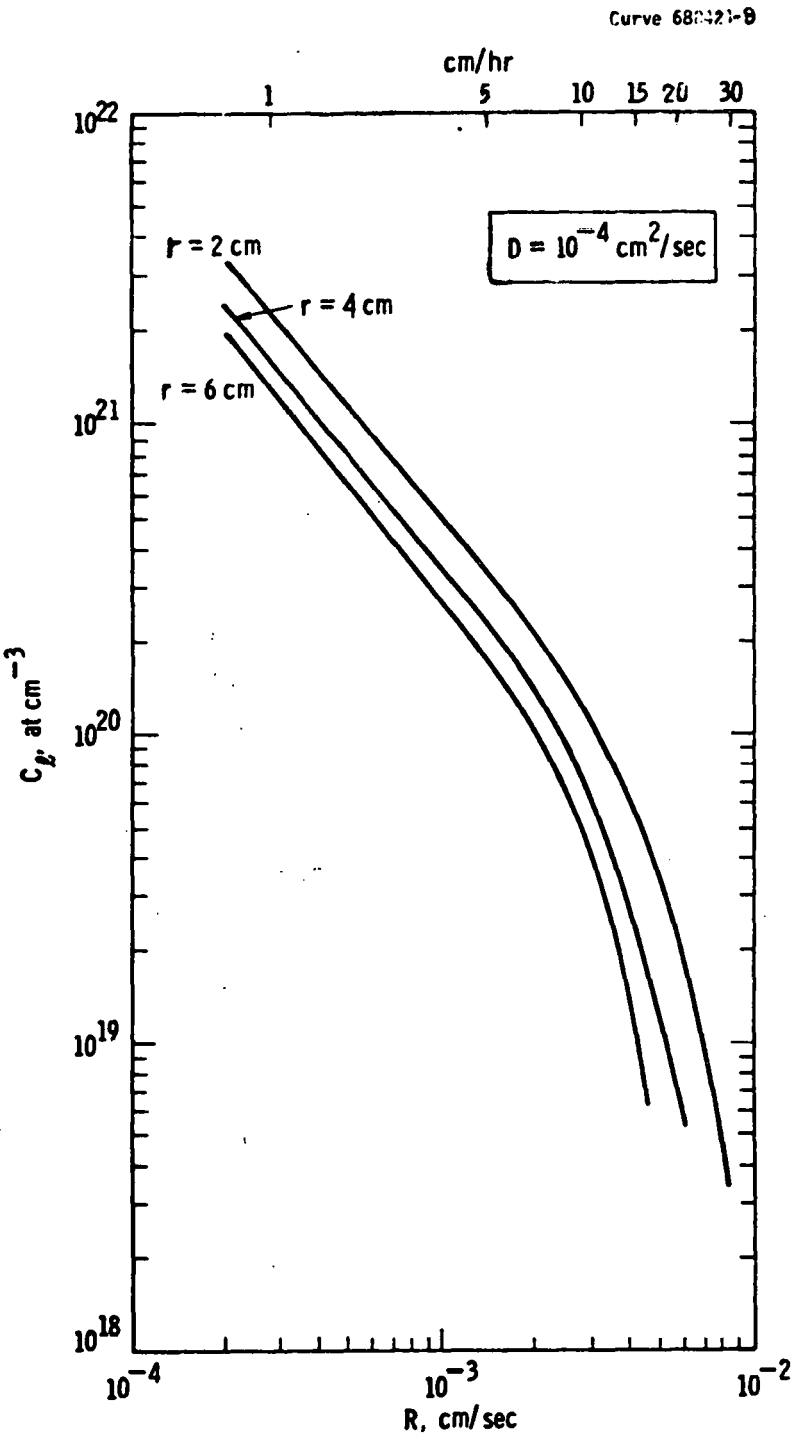

Figure 7 Predicted variation of critical liquid-impurity concentration for crystal breakdown with crystal-growth velocity during Czochralski pulling of silicon. Metal concentrations for which breakdown actually occurred are indicated by the data points.

Using equation (6) and the constants given above, we computed the values of C_ℓ^* for a variety of growth velocities and ingot diameters pertaining to our experiments. In Figure 8, we compare the computed values with the impurity concentrations corresponding to the onset of structural breakdown experimentally observed for ingots ranging in diameter from 2.5 to 8 cm and grown at rates between 1 and 15 cm/hr. The agreement between theory and experiment is quite good. The critical breakdown concentrations typically fall in the low to mid 10^{20} cm^{-3} (few thousand ppma) range for our studies.

As we have noted,[13] the model can be improved by modifications to account better for actual thermal conditions, exact values of liquid diffusion coefficients, and effects of grain boundaries. However, even without correcting these deficiencies, the model is a very useful tool for estimating the effects of impurities on ingot structure (see Sec. 4).

3.3.3 Liquid Diffusion Constants Calculated from Breakdown Data

In our calculations, we have assumed a value of $D_\ell = 10^{-4} cm^2/sec$. While this is clearly a good approximation, it is evident that the value of D_ℓ will vary somewhat from impurity to impurity. The data in Figure 8 in fact imply that this is so since the measured values of C_ℓ^* for some impurities lie above the unity correlation line, while those for others fall below the line.

We can use equation (6) and the measured values of C_ℓ^* to estimate D_ℓ in the following way. We use the relation[17]

$$\frac{\delta}{D} = 1.6 D^{-2/3} \nu^{1/6} \omega^{-1/2} \qquad (7)$$

to eliminate δ from $\Delta = \frac{R\delta}{D} - 1$. Using $\nu = 0.0106$ cm/sec for kinematic viscosity[17] and $\omega = 0.167 s^{-1}$ (typical of our experiments), we obtain

$$\delta/D = 1.8 D^{-2/3}. \qquad (8)$$

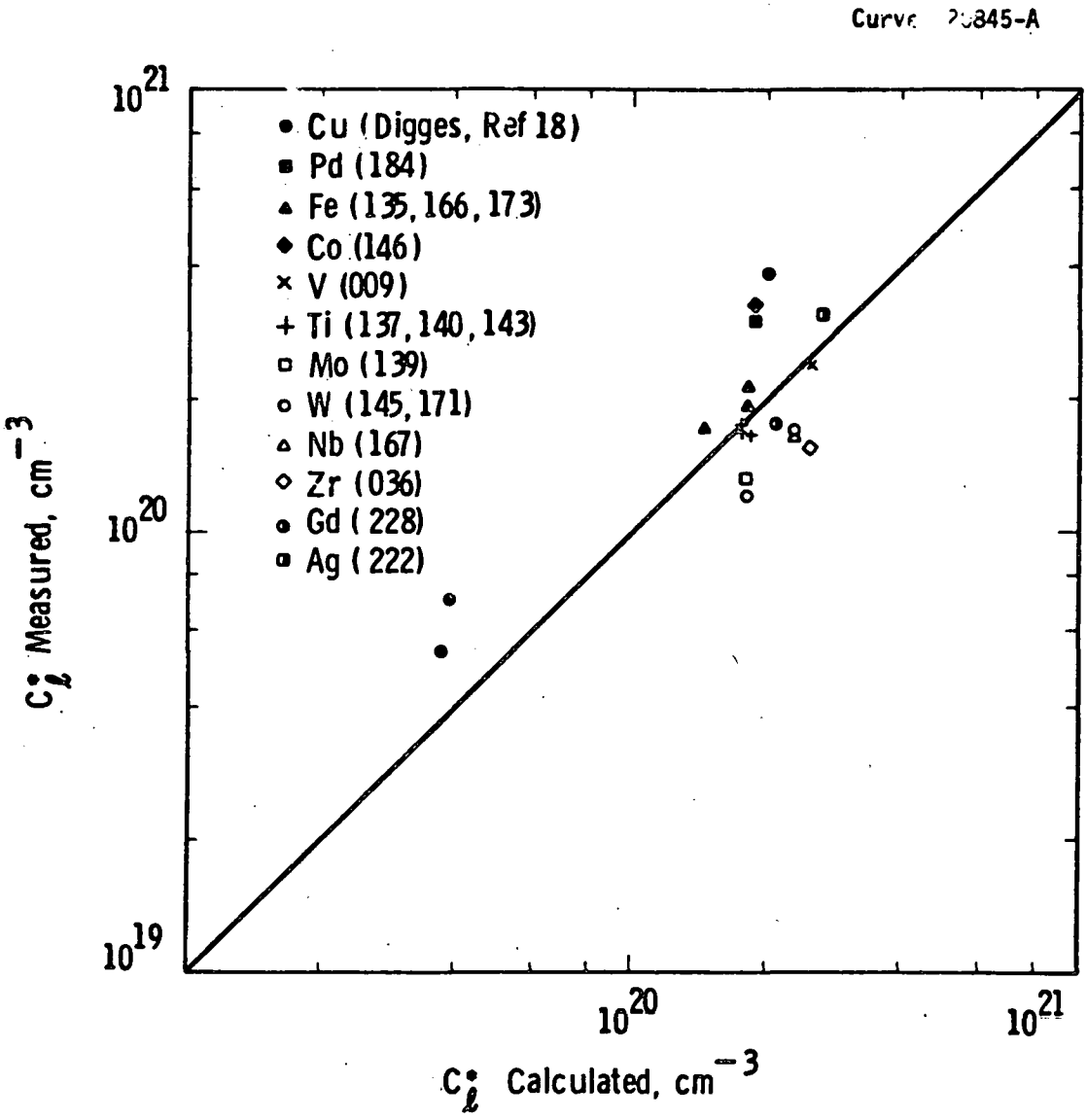

Figure 8 Measured and calculated values of the critical impurity concentration (C_ℓ^*) for which ingot structure transforms from single to polycrystal.

Substituting (8) in equation (6) and introducting numerical constants from Section 3.3.2 gives

$$C_{\ell}^{*} = 1.07(10^{20})D_{\ell}e^{-1.8RD_{\ell}}{}^{-2/3}\left[\frac{92.44}{r^{1/2}R} - 6.88(10^{3})\right] \qquad (9)$$

We introduced sets of data (C_{ℓ}^{*}, r, and R) for each impurity into equation (9) and solved for D_{ℓ} interactively with a programmable hand calculator. The results compiled in Table 5 indicate values of D_{ℓ} ranging from 1.51 to 4.2 x 10^{-4} cm^2/sec for the impurities. We caution that these values cannot be exact owing to imprecision in numerical constants, the simple thermal model we used, and the error in precisely identifying the initiation of breakdown. However, relative comparisons should be quite good.

3.4 Ingot Impurity Concentrations

In order to derive a quantitative relationship between the solar cell performance (or other electrical properties of silicon) and the ingot impurity content, an accurate determination of the metal concentration is required for each test ingot. In Table 6 are listed specific phenomena that limit the amount of a given impurity species which can be incorporated in a silicon ingot.

Carbon and oxygen concentrations – readily measured by infrared spectroscopy – fell in the ranges $2x10^{16}$ to $5x10^{17}$, and $5x10^{17}$ to $1.5x10^{18}$, respectively (See Ref. 3 and Appendix II). These values are common in Czochralski silicon.

It is important to recognize that the melt concentration at which structural breakdown occurs, coupled with the extremely small effective segregation coefficients for many of the impurities (see Table 7), results in ingot concentrations of the metal elements ranging from less than 10^{12} atoms cm^{-3} to values only as high as $1x10^{17}$ atoms cm^{-3}. This corresponds to required analytical detection limits of from 0.02 parts per billion to 2 parts per million.

TABLE 5

DIFFUSION CONSTANTS FOR METALS IN LIQUID SILICON CALCULATED FROM INGOT BREAKDOWN DATA

Ingot	Impurity	C_{ℓ}^{*} (10^{20} cm^{-3})	D_{calc} (10^{-4} cm^{2}/sec)
W228	Gd	1.8	1.51
W011	Zr	1.5	1.80
W145	W	1.2	1.88
W139	Mo	1.3	1.96
W009	V	2.4	2.04
W140	Ti	1.7	2.00
W143	Ti	1.7	2.27
W137	Ti	1.7	2.37
W166	Fe	1.9	2.41
W173	Fe	1.9	2.46
W135	Fe	2.1	2.55
W146	Co	2.1	2.55
W184	Pd	3.0	2.56
W222	Ag	3.0	2.60
Ref. 18	Cu	0.7	4.20

TABLE 6 LIMITS TO INGOT DOPING

INGOT IMPURITY CONCENTRATION LIMITED BY:

Impurity	Small k_{eff}	Volatility	Solid Solubility	Breakdown
Aluminum*				
Boron*				
Calcium		X		
Carbon			X	
Chromium			X	X
Cobalt			X	X
Copper			X	X
Gadolinium				X
Gold			X	
Iron			X	
Lead		X		
Magnesium		X		
Manganese			X	
Molybdenum	X			X
Nickel			X	
Niobium	X			
Oxygen			X	
Palladium			X	
Phosphorus*				
Silver			X	
Sodium		X		
Tin			X	
Titanium	X			X
Tantalum	X			X
Tungsten	X			X
Vanadium	X			X
Zinc		X		
Zirconium	X			X

*Concentration limited by electrical activity and resistivity desired.

TABLE 7 SEGREGATION COEFFICIENTS

Element	Segregation Coefficient
Ag	1.7×10^{-5}
Al	3×10^{-2} (2.8×10^{-3})
Au	2.5×10^{-5}
B	8×10^{-1}
C	5×10^{-2}
Ca	?
Co	2×10^{-5}
Cr	1.1×10^{-5}
Cu	8.0×10^{-4}
Fe	6.4×10^{-6}
Gd	$<4.0 \times 10^{-7}$
Mg	3.2×10^{-6}
Mn	1.3×10^{-5}
Mo	4.5×10^{-8}
Nb	$<4.4 \times 10^{-7}$
Ni	1.3×10^{-4}
P	3.5×10^{-1}
Pb	?
Pd	5×10^{-5}
Sn	3.2×10^{-2}
Ta	2.1×10^{-8}
Ti	2.0×10^{-6}
V	4×10^{-6}
W	1.7×10^{-8}
Zn	1.0×10^{-5}
Zr	$<1.6 \times 10^{-8}$

Spark source mass spectroscopy (SSMS) and neutron activation analysis (NAA) are the only methods generally applicable to these ranges. Thus, samples[3] from all ingots were analyzed by spark-source mass spectroscopy and selected samples were subjected to neutron activation analysis.* A vacuum-cast melt sample for each ingot analyzed by atomic absorption or emission spectroscopy completed the analytical data. (An evaluation of the accuracy of the analytical methods is given in Vol. 2 of Ref. 3.) By taking the ratio of the ingot impurity concentration C_S to the liquid-impurity concentration C_ℓ, the effective segregation coefficient, (k_{eff}), was derived for each impurity.[1-3] The most current values of the segregation coefficients are listed in Table 7.

The target, calculated and measured, concentrations of the intentionally added impurities are compiled in Sect. 4.7 of Ref. 3 and in Appendix III. There the target concentrations are derived by multiplying the melt concentration (based on atoms of melt and atoms of impurity element added) times the effective segregation coefficient. The calculated concentrations represent the product of measured melt concentration corrected for the amount of melt solidified and the effective segregation coefficient.

In addition to direct analysis of the added metal concentration, some effort also was expended to provide assurance that unintentionally added impurities were not present in doped and undoped ingots. The sensitivity of the SSMS measurements is inadequate to detect the majority of potential contaminants below the concentration of approximately 1.5×10^{14} atoms cm^{-3}, so NAA was used to examine 26 selected samples. Typical concentrations of all unintentionally added impurities (Table 3, Ref. 3, Vol. 1) are well below concentrations which would have any impact on solar cell performance.

*Neutron activation analysis was performed at General Activation Analysis, San Diego, CA, and Kraftwerk Union A.G., Erlangen, FDR.

3.4.1 Data Evaluation

In general, excellent agreement exists between target and calculated ingot impurity concentrations. A calculated value within ± 60 percent of the targeted value was considered sufficient to assure that the melt was properly doped. In most cases, the agreement was considerably better than this.

Target differences did occur for the impurities calcium, magnesium, sodium, zinc, and lead, which are volatilized from the melt as noted earlier. A discrepancy in nickel concentration for ingot W-006 was caused by a loss of dopant nickel powder during furnace evacuation. The differences in calculated and target values for ingot W132 are ascribed to the difficulty in measuring the small amount of tantalum present.

The measured impurity concentrations typically represent an average of several measurements; occasionally only a single data point was available. At least three SSMS measurements were made on each ingot having an impurity concentration above the detection limit of the SSMS. The sensitivity of the SSMS is inadequate to detect the majority of potential impurities below the concentration of approximately 1.5×10^{14} atoms/cm^3 (3 ppba). Measurement of nickel and cobalt in silicon is somewhat more complicated[3] and reliance on neutron activation analyses (NAA) was made in these cases.

Three impurities, niobium, zirconium, and gadolinium, have yet to be detected by SSMS or NAA, while tantalum, tungsten, cobalt, palladium, and gold have been detected in one ingot. Data for the elements are indicated as upper limits based on the detection limits of the SSMS or NAA methods.[3] Since zinc, sodium, calcium, and lead volatilize during growth, they have not been detected. Aluminum was measured by both SSMS and resistivity measurements since it is electrically active at room temperature. A higher aluminum concentration is measured by SSMS than electrical measurements.[1-3]

Besides the standard seed and analytical specimens, a few tang end slices also were analyzed. Samples taken from a region of good crystal structure, i.e., well in advance of apparent structural breakdown, produce excellent agreement with the seed end measurements. Tang end concentrations were always greater by from 25 percent to approximately 45 percent, as would be expected due to impurity segregation. The magnitude of difference depended on the location of the sample and the melt volume consumed. However, the closer the slices lie to the region where structural breakdown occurs, the nearer is the impurity concentration to that of the melt. Changes in concentration of 4 to 5 orders of magnitude within a few centimeters are common. Thus, great care must be taken to properly interpret any data gathered from tang end material.

3.4.2 Best Estimates of Impurity Concentrations

Table 8 sets forth our best estimates of the impurity concentration characteristic of each ingot grown. These values are based on the complete analytical data base available for each ingot. Also incorporated in this judgement is the degree of reliability in the effective segregation coefficients. It is this best estimated value which is used in all analyses drawn throughout the rest of the report.

Bearing in mind the limited data for tantalum, cobalt, gadolinium tungsten, palladium, and gold, we placed the following degrees of uncertainty on the best estimates listed in Table 8:

ELEMENT	(% UNCERTAINTY)
Ag	± 40
Al	± 40
Au	± 60
B	± 15
C	± 50
Ca	± 50, - 100
Co	± 70
Cu	± 40
Cr	± 35
Gd	± 50, - 100
Fe	± 35
Mg	+ 50, - 100
Mn	± 25
Mo	± 30
Nb	± 50, - 100
Ni	± 40
P	± 15
Pd	± 60
Sn	± 60
Ta	± 40
Ti	± 30
V	± 40
W	± 40
Zn	+ 50, - 100
Zr	+ 50, - 100

While the uncertainty in a few cases is larger than desired, we feel it is well within the bounds needed to identify the utility of solar grades of silicon. Extensive use of NAA would considerably improve the situation for impurities like Ta, Ti, V, Zr, Ni, and W.

TABLE 8 BEST ESTIMATE OF IMPURITY CONCENTRATIONS

Ingot Identification	Best Estimate of Impurity Conc. (10^{15} atoms/cm^3)
W-001-00-000	--
W-002-00-000	--
W-003-00-000	--
W-004-Cr-001	1.0
W-005-Mn-001	1.3
W-006-Ni-001	1.6
W-007-Cu-001	1.7
W-008-Ti-001	0.20
W-009-V-001	0.4
W-010-Ni-002	16
W-011-Zr-001	<0.0007
W-012-Cr-002	0.20
W-013-Mn-002	0.25
W-014-00-000	--
W-015-Zn-001	<0.001
W-016-Fe-001	0.9
W-017-Cu-002	19
W-018-Fe-002	1.7
W-019-Cu-003	0.4
W-020-00-000	--
W-021-Mg-001	0.003
W-022-00-000	--
W-023-00-000	--
W-024-Mg-002	0.032
W-025-00-000	--
W-026-Mn-003	0.012
W-027-Mn/Cu-001	1.3/1.7
W-028-Al-001	26
W-029-Cr-003	0.012
W-030-Cr/Cu-001	1.0/1.7

TABLE 8 BEST ESTIMATE OF IMPURITY CONCENTRATIONS (Cont.)

Ingot Identification	Best Estimate of Impurity Conc. (10^{15} atoms/cm^3)
W-031-Cr/Mn-001	1.0/1.3
W-032-Mg-003	0.32
W-033-Ti-002	0.002
W-034-00-000	--
W-035-V-002	0.004
W-036-Zr-002	<0.0014
W-037-Zr/Ti-001	<0.0007/0.22
W-038-Al-002	60
W-039-Ni-003	32.8
W-040-Cr/Ni-001	0.8/12.8
W-041-Ni/Cr/Cu-001	12.8/0.8 /1.7
W-042-Ti-003	0.04
W-043-Fe/Ti-001	0.56/0.033
W-044-Fe-003	0.017
W-045-Cr/Fe-Ti-001	0.65/0.43 /0.039
W-046-Fe/V-001	0.57/0.07
W-047-Cu/Ni/Zr-001	1.7/4.7/<0.00021
W-048-Ti-004	0.0002
W-049-V-003	0.0004
W-050-Ti/V-001	0.0002 /0.0004
W-051-Cu/Ti-001	1.7/0.20
W-052-Ni-004	33.6
W-053-Poly	--
W-054-00-000	--
W-055-Cu-004	0.05

TABLE 8 BEST ESTIMATE OF IMPURITY CONCENTRATIONS (Cont.)

Ingot Identification	Best Estimate of Impurity Conc. (10^{15} atoms/cm^3)
W-056-Cu-005	65
W-057-00-000	--
W-058-00-000	--
W-059-00-000	--
W-060-00-000	--
W-061-Cr/Ti-001	1.0/0.11
W-062-N/Cu-001	2.5
W-063-N/Cr-001	0.8
W-064-N/Mn-001	1.0
W-065-N/Ti-001	0.20
W-066-Ti-005	0.033
W-067-Cr/Mn/Ti-001	0.4 0.5 0.0033
W-068-Cr-004	1.0
W-069-Fe-004	1.0
W-070-Al-003	50
W-071-00-000	--
W-072-Cr-005	0.4
W-073-Cr/Mn/Ni/Ti/V-001	0.4 0.4 8.1 0.0024 0.004
W-074-Cr/Mn/Ni/Ti/V-002	0.08 0.08 2.0 0.00033 0.0006

TABLE 8 BEST ESTIMATE OF IMPURITY CONCENTRATIONS (Cont.)

Ingot Identification	Best Estimate of Impurity Conc. (10^{15} atoms/cm^3)
W-075-Ti/V-002	.056 0.1
W-076-Poly-2	--
W-077-Mo-001	0.0042
W-078-00-000	--
W-079-00-000	--
W-080-Ph-001	0.7
W-081-N/Ni-001	6.9
W-082-N/V-001	0.4
W-083-N/Fe-001	1.0
W-084-N/Al-001	50
W-085-N/Zr-001	<0.0007
W-086-C-001	200-400
W-087-Ca-001	?
W*-088-Cr-001	0.5
W*-089-Cu-001	2.0
W*-090-Mn-001	0.7
W-091-Cr/Mn-002	0.5/0.3
W-092-Ph-002	28
W-093-Mn-004	0.7
W-094-Mn-005/Poly	0.9
W-095-Mn-006(F)	1.0
W-096-Mn-007(S)	0.63
W-097-00-000	--
W-098-Mo-002	0.00092
W-099-Fz-001	--

TABLE 8 BEST ESTIMATE OF IMPURITY CONCENTRATIONS (Cont.)

Ingot Identification	Best Estimate of Impurity Conc. (10^{15} atoms/cm^3)
W-100-Cu/Ti-002	1.0/0.033
W-101-FZ-002	--
W-102-Ti-006/Poly	0.11
W*-103-Ti-001	0.167
W-104-Cu/Ti-003	2.0/0.14
W*-105-V-001	0.4
W-106-N/Al-002	10
W-107-FZ/Al-001	30
W-108-N/V-002	0.08
W-109-C-002	<20-140
W*-110-Fe-001	0.8
W-111-Cu/V-001	2.5/0.3
W-112-Ta-001	0.00083
W-113-FZ/Cr-001	0.8
W-114-00-200	--
W-115-N/Cu-002	10
W*-116-Ph-001	100
W-117-00-000	--
W-118-Ph-003	140
W-119-N/Fe-002	0.3
W-120-N/Cr-002	0.3
W-121-N/Ti-002	0.039
W-122-Ti-007 (F)	0.089
W-123-Ti-008 (S)	0.105

TABLE 8 BEST ESTIMATE OF IMPURITY CONCENTRATIONS (Cont.)

Ingot Identification	Best Estimate of Impurity Conc. (10^{15} atoms/cm^3)
W-124-Mo-003	0.000018
W-125-Mo-004	0.0003
W-126-Multi-001	See Data Sheet
W-127-FZ/Ti-001	0.039
W-128-Ta-002	0.000168
W-129-00-000 (7.6 cm)	NA
W-130-00-000 (7.6 cm)	NA
W-131-Mn-008 (7.6 cm)	0.55
W-132-Ta-003	0.000042
W-133-00-000	NA
W-134-Ti-009	0.03
W-135-Fe-005	0.78
W-136-Fe-006	0.24
W-137-Ti-010	0.21
W-138-Mo-005	0.001
W-139-Mo-006	0.0042
W-140-Ti-001 (7.6 cm)	0.18
W-141-Mo/Cu-001	0.004 /4.4
W*-142-00-000	NA
W*-143-Ti 002	0.20
W-144-Mo-001	0.004
W-145-W-001	0.00085
W-146-Co-001	3.0
W-147-N/Ni-002	1.6
W-148-N/Mn-002	0.60

TABLE 8 BEST ESTIMATE OF IMPURITY CONCENTRATIONS (Cont.)

Ingot Identification	Best Estimate of Impurity Concentration ($X10^{15}$ atoms/cm^3)
W-149-N/Fe-003	0.60
W-150-N/V-003	0.03
W**-151-00-000	NA
W**-152-Ti-001	0.21
W-153-N/Ti-003	0.013
W-154-N/Cr-003	0.5
W-155-N/Mo-001	0.001
W-156-N/Mo-002	0.004
W-157-N/Ti/V-001	0.08/0.12
W-158-N/Ti/V/Cr-001	0.05/0.05/0.55
W-159-N/Cr/Mn/Ti/V-001	0.35/0.36/0.02/0.02
W*-160-Ti-001	0.17
W**-161-Ti-002	0.03
W-162 Ni/Ti-001	4.0/0.16
W-163-Ni/V-001	4.0/0.44
W-164-Ni/Mo-001	4.0/0.004
W-165-Co-002	0.6
W-166-Fe-007	1.06
W-167-Nb-001	<0.01
W*-168-Ph-002	110+
W*-169-Ph-004	136+
W-170-Ph-005	150+
W-171-W-002	0.0015
W-172-Cu-006 (7.6 cm)	24.0
W-173-Fe-008 (7.6 cm)	0.51
W-174-Ta-004	0.00084
W-175-W-003	0.00027

TABLE 8 BEST ESTIMATE OF IMPURITY CONCENTRATIONS (Cont.)

Ingot Identification	Best Estimate of Impurity Concentrations ($X10^{15}$ atoms/cm^3)
W-176-00-000	NA
W-177-N/Cr/Mn-001	1.20/1.26
W-178-N/Mn/Ti-001	0.86/0.08
W*-179-Ph-006	NA
W*-180-Ti-001	0.13
W-181-Cr-006	1.04
W-182-Cr-007	0.45
W-183-Nb-002	<0.002
W-184-Pd-001	6.5
W-185-Cu/Ti-004	Cu: 1.2 Ti: 0.16
W-186-Co-003	0.054
W-187-Co-004	0.28
W-188-W-004	0.0002
W-189-Nb-003	<0.0003
W-190-Cu/Zr-001	Cu: 2.0 Zr: <0.0012
W-191-Cu/Ta-001	Cu: 2.0 Ta: 0.00068
W-192-Ag-001	2.20
W-193-Sn-001	4846
W-194-Ti-012	0.003
W-195-Ti/V/Mo-001	Ti: 0.003 V : 0.003 Mo: 0.0006
W-196-Ti/V-Mo/Ta-001	Ti: 0.003 V : 0.003 Mo: 0.0006 Ta: 0.0003

TABLE 8 BEST ESTIMATE OF IMPURITY CONCENTRATIONS (Cont.)

Ingot Identification	Best Estimate of Impurity Conc. ($\times 10^{15}$ ATOMS/CM^3)
W-197-Ti/V/Mo/Ta/Cu-001	Ti: 0.003 V : 0.003 Mo: 0.0006 Ta: 0.0003 Cu: 2.0
W-198-00-000	NA #
W-199-00-000	NA
W-200-V-004-Poly	0.38
W-201-Mo-007-Poly	0.003
W-202-Ti-013-Poly	0.018
W-203-V-005-Poly	0.05
W-204-Cr-008-Poly	0.82
W-205-Fe-009-Poly	0.61
W-206-V-006	0.026
W-207-Mo-008	0.002
W-208-Cr-009	0.19
W-209-Ti-014	0.02
W-210-Ti-015	0.10
W-211-Cu-007	1.8
W-212-Cu-008	12.5
W-213-Pb-001	<0.1
W-214-V-007-Poly	0.4
W-215-Mo-009-Poly	0.002
W-216-Cr-010-Poly	1.0
W-217-Ta-005	0.0003
W-218-Ta-006	0.0001
W-219-V-008	0.009

TABLE 8 BEST ESTIMATE OF IMPURITY CONCENTRATIONS (Cont.)

W-220-W-005	0.0007
W-221-Ni-005	8.2
W-222-Ag-002	4.6
W-223-Ni-006	1.1
W-224-HSC/DCS057	++
W-225-Mn-009	1.5
W-226-Mn-010	***
W-227-Cr-011-Poly	0.4
W-228-Gd-001	<0.4
W-229-Au-001	0.6
W-230-Al-003	120
W-231-Mn-011-Poly	0.23
W-232-N/Ti-001	0.01****
W-233-Cr-012	0.12
W-234-M0-010	0.0005
W-235-N/V-001	0.006****
W-236-N/Mo-001	0.003****
W-237-Cr-001	0.02****
W-238-Mn-001	1.0****

* Asterisk indicates low-resistivity p-type ingot ($\lesssim$ 1 ohm-cm)
** 30 ohm-cm o-type ingot
\+ Value based on resistivity measurement
\# Not applicable
++ No intentional impurity
*** Single growth prohibited due to excessive impurity doping for permanence studies
**** High-resistivity ingot, 30 ohm-cm

3.5 Model Analysis of Impurity Effects in p and n Solar Cells

During the course of this study, we have developed a first order model to predict solar cell performance as a function of the species and amounts of impurities present in devices made from contaminated silicon.[1,2] The model was later extended to synergic behavior, gettering and resistivity effects, and polycrystalline devices[3,19,20] so that it provides useful guidelines to those involved with the processing of silicon, the growth of crystals, or the fabrication of solar cells.

A detailed derivation of the model is available in reference 3, Vol. 2, or reference 19; an abbreviated version highlighting assumptions, basic equations for calculation, and a summary of pertinent experimental results is given here.

3.5.1 Model Assumptions

a. The performance of a solar cell can be modeled as a wide-base device consisting completely of a single-base region with uniform electrical properties and for which the basewidth exceeds the diffusion length.

b. The effect of impurities is exclusively that of reducing the carrier diffusion length in the effective base region.

c. The impurity-induced diffusion length reduction results either from carrier recombination via deep centers associated with the impurities or from carrier mobility loss due to ionized impurity scattering.

d. The number of electrically active centers is a species- and process-dependent linear function of the total metallurgical concentration of that impurity.

These assumptions imply the effective base diffusion length, L_n, is a characterizing parameter for the impurity effects. Since experience shows that the diffusion length, or equivalently the lifetime, is difficult and time consuming to measure accurately,[1,2] we therefore chose to model impurity effects as a function of the short-circuit current,

a more easily measured quantity and one which is directly related to the diffusion length. A list of symbols used in the model analysis appears in Table 9.

3.5.2 Relation of Short-Circuit Current to Diffusion Length

While numerical integration is necessary to solve the carrier transport equations for a real solar spectrum, a closed-form expression in which the distributed spectrum is represented by an equivalent monochromatic illumination, producing the same current on the cell, proves a good approximation.[3,19] For basewidths that are large compared to the diffusion length, L_n, and the absorption length, L_λ

$$I_{sc} \doteq \frac{q\, AN_\lambda\, (1-R_\lambda)}{\frac{L_\lambda}{L_n} + 1}. \tag{10}$$

Defining normalized variables

$$I_{sco} = I_{sc}\ \text{(baseline sample)}$$

$$I_n = \frac{I_{sc}\ \text{(impurity sample)}}{I_{sco}}$$

$$I_{n\infty} = \frac{I_{sc}(L_n = \infty)}{I_{sco}} = \frac{qAN_\lambda\, (1 - R_\lambda)}{I_{sco}}$$

transforms equation 10 to the convenient form:

$$I_n = I_{n\infty} \left[\frac{1}{\frac{L_\lambda}{L_n} + 1} \right]. \tag{11}$$

TABLE 9

LIST OF SYMBOLS USED IN THE IMPURITY MODEL DERIVATION

A	cell area, cm^2
I	solar cell terminal current, A
I_{sc}	short-circuit current, A
P	cell power, W
I_p	current at peak power point, A
V_p	voltage at peak power point, V
n	ideality factor
R_s, R_{sh}	series and shunt resistances, ohms
I_o	diode saturation current, A
V_T	kT/q, the thermal voltage V
I_λ	photocurrent for illumination with wavelength λ, A
L_λ	$1/\alpha_\lambda$, the absorption length at wavelength λ, cm
R_λ	reflection coefficient at wavelength λ
N_λ	number of photons at wavelength λ, $sec^{-1}\ cm^{-2}$
x	distance from front surface of cell, cm
L_n, L_p	effective electron diffusion length, p-base, n-base
L_{no}, L_{po}	diffusion lengths in baseline cells
I_{sco}	short-circuit current for baseline cells (no added impurities), A
I_n	I_{sc}/I_{sco}, normalized short-circuit current
$I_{n\infty}$	value of I_n which would result if L_n were infinite
V_{oco}	open-circuit voltage for baseline cells (no added impurities), V
V_n	V_{oc}/V_{oco}, normalized open-circuit voltage
V_{oc}	open-circuit voltage, volts
N_x, N_y, N_z	concentration of impurity species x, y and z, cm^{-3}
τ	minority-carrier lifetime
τ_x	minority-carrier lifetime due to impurity x
τ_o	minority-carrier lifetime in baseline devices
σ_x	recombination cross section for impurity x
v_{th}	thermal velocity
A_x	ratio of electrically active recombination centers to metallurgical concentration
k_x	$(\sigma_x v_{th} A_x)/D$
C_1	model constant
C_{2x}	model constant specific to impurity x
n_i	intrinsic carrier concentration, cm^{-3}
d, D_n, D_p	minority-carrier diffusivity, cm^2/sec
i	I/I_{sco}, normalized terminal current of the lighted solar cell at voltage V
v	V/V_{oco}, normalized terminal voltage at current I

$I_{n\infty}$ and L_λ are model constants depending only on device geometry (primarily cell thickness) and are found by a least squares fit to experimental data to be 1.11 and 19.2 μm, respectively. L_λ = 19.2 μm corresponds to a wavelength of 869 nm, plausibly near the center of the solar spectrum.

3.5.3 Impurity Dependent Diffusion Length

Following the development in references 3 and 19, we assume the diffusion length within the cells depends on the density of recombination centers N_T, which is proportional to the metallurgical (total) impurity concentration in the silicon, i.e., $N_T = A_x N_x$. Here, A_x is the electrically active impurity fraction.

For this case, it can be shown that the diffusion length in silicon containing metals x, y -- z, etc. is linked to that in uncontaminated baseline material (L_{no}) by the relation

$$1/L_n^2 = 1/L_{no}^2 + k_x N_x + k_y N_y + \text{----} + k_z N_z \qquad (12)$$

where $$k_x = \frac{\sigma_x V_{th} A_x}{D_n}.$$

By using equation (11), we transform (12) to

$$\left(\frac{In_\infty}{In} - 1\right)^2 = L_\lambda \left(1/L_{no}^2 + k_x N_x + k_y N_y + \text{---} + k_z N_z\right) \qquad (13)$$

If we define constants C_1 and C_{2x}, we find for <u>single</u> impurities a convenient form for calculation is

$$\left(\frac{I_{n\infty}}{I_n} - 1\right)^2 = C_1 + C_{2x} N_x = C_1 \left[1 + \frac{N_x}{N_{ox}}\right]. \qquad (14)$$

$N_{ox} = C_1/C_{2x}$ is defined as the threshold concentration for impurity x, above which cell performance is degraded. The values of C_1, C_{2x}, and N_{ox} obtained by a least squares fit to experimental data (reference 3 and Appendix IV) for impurity-doped solar cells are compiled in Tables 10 and 11. For an impurity concentration equal to N_{ox}, the short-circuit current is reduced about 4%.

3.5.4 Open-Circuit Voltage

Based on the "shifting approximation,"[21] the normalized open-circuit voltage is given by[3,19]

$$V_n = \frac{nV_T}{V_{oco}} \ln \left[\frac{I_{sc}}{I_o}\right]. \tag{15}$$

Eliminating L_n from equation 11, using the definition of I_o, and combining the result with equation 15 we find:

$$I_o = \frac{qA\, n_i^2\, D_n}{N_A} \frac{I_{n\infty}}{L_\lambda} \left[\frac{1}{I_n} - \frac{1}{I_{n\infty}}\right] \tag{16}$$

Combining equations 6 and 7 gives the desired relationship between V_n and I_n.

$$V_n = \frac{nV_T}{V_{oco}} \ell n \left[\frac{N_A L_\lambda\, I_{sco}}{qAn_i^2\, D_n\, I_{n\infty}}\right] + \frac{nV_T}{V_{oco}} \ell n \left[\frac{I_n}{\frac{1}{I_n} - \frac{1}{I_{n\infty}}}\right] \tag{17}$$

which may be written in the form:

$$V_n = \ell n \left[\frac{I_n}{\frac{1}{I_n} - \frac{1}{I_{n\infty}}}\right] + F. \tag{18}$$

A least squares fit of equation 18 to experimental data[3,19] yields E = 0.0472 and F = 0.8747.

TABLE 10

MODEL COEFFICIENTS FOR SINGLY DOPED, P-BASE SOLAR CELLS

IMPURITY	C_1	C_{2X}	N_{OX}
Aluminum	1.2 E-02	2.9 E-18	4.4 E+15
Chromium	9.2 E-03	6.7 E-17	1.3 E+14
Cobalt	1.2 E-02	1.0 E-17	1.1 E+15
Copper	1.2 E-02	3.0 E-20	4.1 E+17
Gold	1.21 E-02	1.1 E-15	1.1 E+13
Iron	1.2 E-02	4.7 E-17	2.5 E+14
Manganese	9.8 E-03	5.3 E-17	1.8 E+14
Molybdenum	1.3 E-02	2.0 E-14	6.0 E+11
Nickel	1.4 E-02	2.5 E-18	5.0 E+15
Niobium	1.2 E-02	7.4 E-15	1.6 E+12
Palladium	1.21 E-02	2.37 E-18	5.1 E+15
Phosphorous	1.1 E-02	6.8 E-21	1.7 E+18
Silver	1.21 E-02	1.46 E-18	8.3 E+15
Tantalum	1.2 E-02	5.1 E-14	2.3 E+11
Tin	1.21 E-02	6.37 E-23	1.9 E+20
Titanium	1.2 E-02	4.5 E-15	2.6 E+12
Tungsten	1.1 E-02	9.1 E-15	1.2 E+12
Vanadium	1.3 E-02	5.4 E-15	2.5 E+12
Zirconium	1.0 E-02	2.7 E-14	3.6 E+11

TABLE 11

MODEL COEFFICIENTS FOR SINGLY DOPED, N-BASE SOLAR CELLS*

IMPURITY	C_1	C_{2X}	N_{OX}
Aluminum	1.0 E-02	1.1 E-18	8.5 E+16
Chromium	1.0 E-02	8.7 E-17	1.2 E+14
Copper	1.1 E-02	1.3 E-19	8.0 E+16
Iron	1.0 E-02	5.7 E-17	1.8 E+14
Manganese	1.1 E-02	1.2 E-17	9.5 E+14
Titanium	1.3 E-02	3.6 E-16	3.7 E+13
Vanadium	1.3 E-02	3.3 E-16	4.1 E+13
Molybdenum	1.1 E-02	8.5 E-15	1.3 E+12

*Data for Ni does not fit a model based on lifetime reduction as the dominant impurity effect.

Direct calculation gives E = 0.0477 and F = 0.8740 where $N_A = 3.5 \times 10^{15}$ cm^{-3}, $D_n = 32$ cm^2/S, $L_\lambda = .0019$ cm, $I_{sco} = 0.0225$A, A = 1 cm^2, $V_{oco} = 0.556$V, $I_{n\infty}$ and L_λ are deduced from the experimental data, and the remaining values are measured. Note that the voltage behavior, unlike short-circuit current, is dependent on the base doping.

3.5.5 Efficiency Behavior

The final step -- to relate efficiency and short-circuit current -- is again facilitated by using the "shifting approximation"[21] to provide the illuminated voltage-current equation

$$I = I_{sc} - I_o \exp\left(\frac{V}{nV_T}\right). \tag{19}$$

Substituting for I_o from equation 16 and normalizing the voltages and currents gives:

$$i = I_n - \frac{qAn_i^2 D_n I_{n\infty}}{N_A L_\lambda I_{sco}} \left[\frac{1}{I_n} - \frac{1}{I_{n\infty}}\right] \exp\left[\frac{v\, V_{oco}}{nV_T}\right]. \tag{20}$$

Using the data given in Section 3.5.4, the coefficient of the second term is 9.58×10^{-9}. Applying the boundary constraint, that if I_n = 1 and i = 0 then v = 1, leads to a value for n = 1.0151 which agrees with the value obtained in the V_{oc} analysis.

The normalized peak power is obtained from the cell when v and i satisfy the relation:

$$\frac{dp}{dv} = \frac{d\,(iv)}{dv} = i + v\,\frac{di}{dv} = 0. \tag{21}$$

This combined with equation 11 becomes:

$$I_n - \left[\frac{qAn_i^2 D_n I_{n\infty}}{N_A L_\lambda I_{sco}} \left[\frac{1}{I_n} - \frac{1}{I_{n\infty}}\right] \exp\frac{v\, V_{oco}}{nV_T}\right]\left[1 + \frac{v\, V_{oco}}{nV_T}\right] = 0. \tag{22}$$

Numerically solving equation 22 for the peak power voltage, v_p, and equation 20 for i_p and I_n as a parameter provides the normalized efficiency where the zero subscripts denote baseline values.

$$\frac{\eta}{\eta_o} = \frac{i_p \, v_p}{i_{po} \, v_{po}} \tag{23}$$

The resulting curve of η/η_o as a function of I_n is in good agreement with experimental data.[3,19] As equation 22 has no closed-form solution, an empirical approximation was obtained.

$$\frac{\eta}{\eta_o} = 0.872 \; I_n^{1.128} + 0.128 \; I_n^{12} \tag{24}$$

Referring to the short-circuit current equation 14 , we observed that when an impurity reaches the threshold concentration (N_{ox}), the current (I_n) is reduced to 96 percent of its baseline value. Correspondingly, efficiency is reduced to 91.2 percent of its baseline value.

3.5.6 Single Impurity Behavior

The efficiency as a function of metal concentrations can now be calculated using equations 13 or 14, with the coefficients given in Table 10 or 11 to obtain I_n, and equation 24 then provides the efficiency. Nearly 240 impurity-containing ingots were processed into solar cells as described in reference 3. The data base, analyzed by the method described above, was used to compute the least squares coefficients listed in Table 10 and 11 and then to derive the curves depicted in Figures 9 and 10 for 4-cm p-base and 1.5 ohm-cm n-base devices, respectively. It is notable that n-base devices are generally less affected by several impurities than are the corresponding p-base devices.[3]

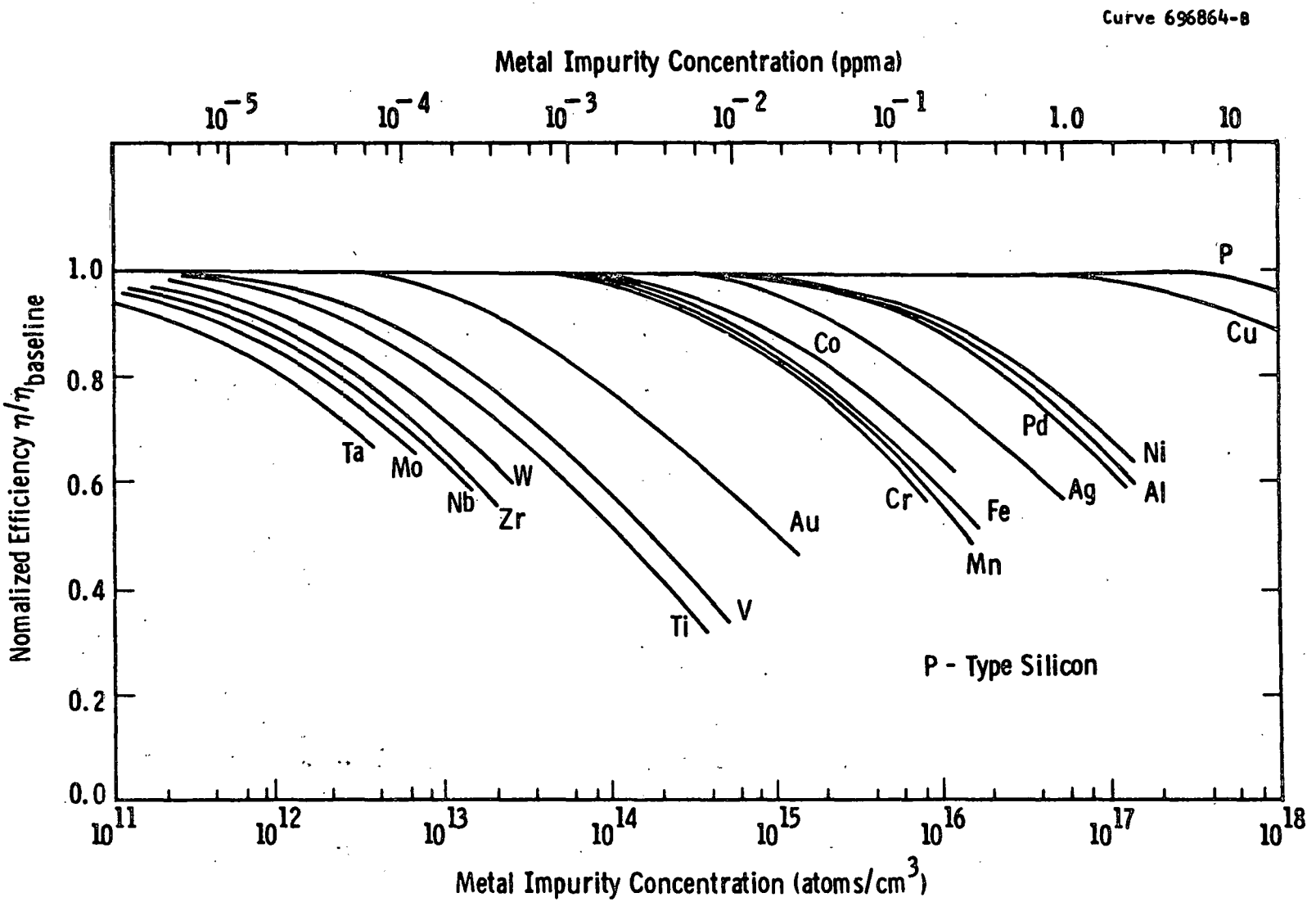

Figure 9 Model-derived curves for the normalized solar cell efficiency as a function of metal impurity content for devices made on 4 ohm-cm, p-type silicon (see reference 3 for solar cell data). Data for Ti and V overlay closely as do those for Pd and Ni. Curves are separated somewhat for clarity. The curve for Sn lies off scale to the right.

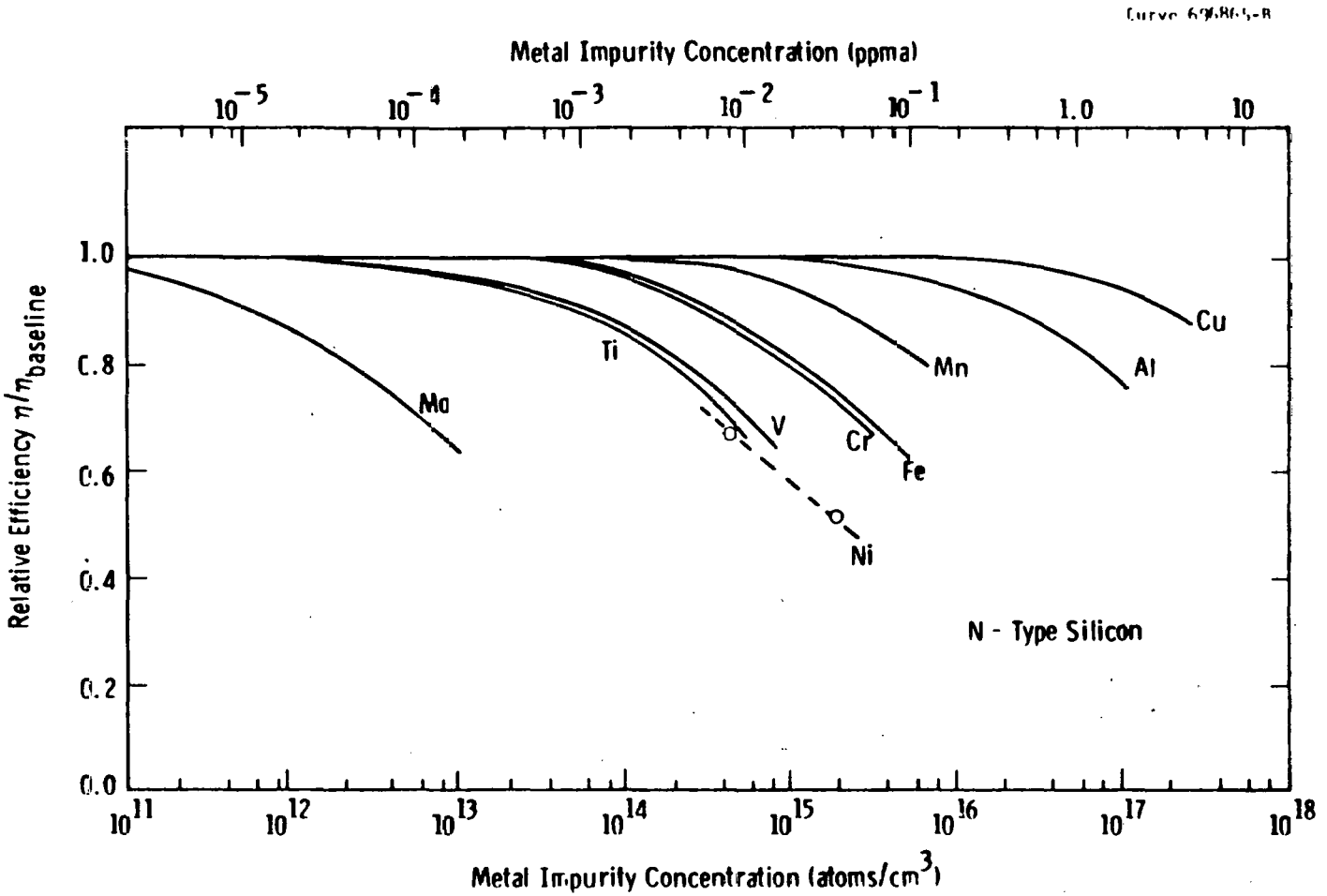

Figure 10 Model-derived curves illustrating the variation in normalized solar cell efficiency with impurity concentration for devices made on 1.5 ohm-cm, n-type silicon (see reference 3 for solar cell data)

Experimental data have been omitted for clarity from Figures 9 and 10, but the agreement with the model curves is quite good.[1-3,19] Notable exceptions are iron, copper, and nickel and to a lesser extent Co and Ag, which at their highest concentrations induce excessive junction shunting and space-charge region recombination.[22] These mechanisms were excluded from the model analysis because of their unpredictable behavior. An example of junction degradation by copper is shown in Figure 11. The dark IV data are shown as the two exponential components governing the diffusion current (upper right) and the junction space-charge current (bottom left).[22,23,24] The effects of series and shunt resistance have been removed.[25,26] It is apparent that the upper segment shifts little with increasing copper concentration reflecting negligible change in the base lifetime.

The shift of the lower segments, however, implies a considerable current increase which accounts for nearly all of the cell degradation. This excess junction current, a typical feature of I-V curves for Cu, Fe, Ni, and Co[3], is thought to be mainly due to a combination of nonlinear shunting and field emission associated with precipitates rather than simple recombination in the space charge layer.[2,22]

In contrast, the dissected dark IV data for titanium and other lifetime-killing impurities display a shift of the upper curves to the left with increasing metal concentration, a feature associated with reduced bulk lifetime,[22] viz. Figure 12. The depletion region component of the dark current, denoted by the lower segments, shows some increase with the higher Ti concentrations but remains negligible with respect to device performance. This is also characteristic of other impurities like W, Ta, Mo, Nb, Pd, Au, Cr, and Zr, which degrade cell efficiency by destroying bulk lifetime.

3.5.7 Multiple Impurity Results

Once the model constants for single impurities have been determined, the linearity of equation 13 permits us to calculate the expected performance of samples containing multiple impurities at various

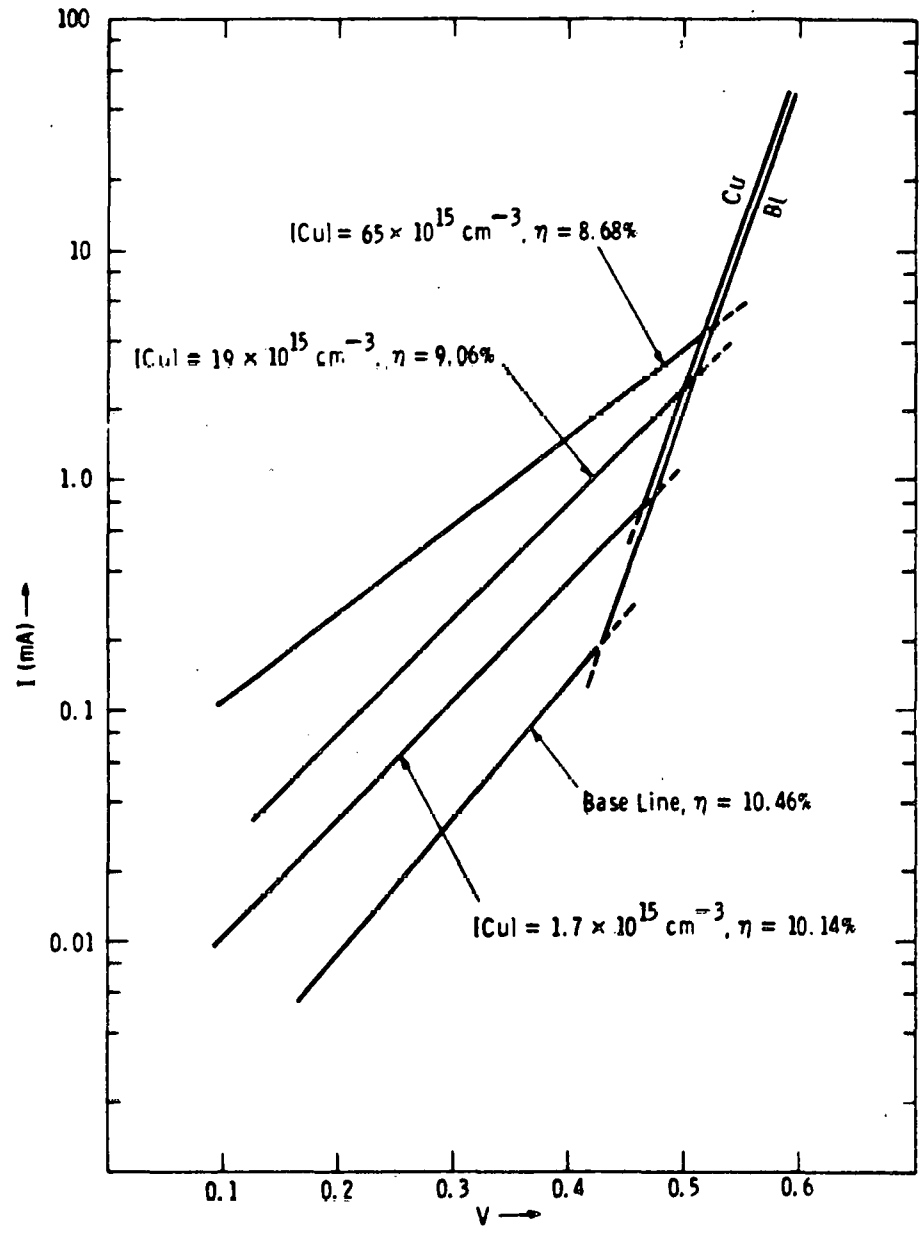

Figure 11 Transformed dark I-V curves for Cu-doped solar cells. As the Cu concentration increases, so does the junction depletion current (lower segment of curve). Cells doped with Ni, Co, Fe, and, to a lesser extent, Ag also show this behavior.

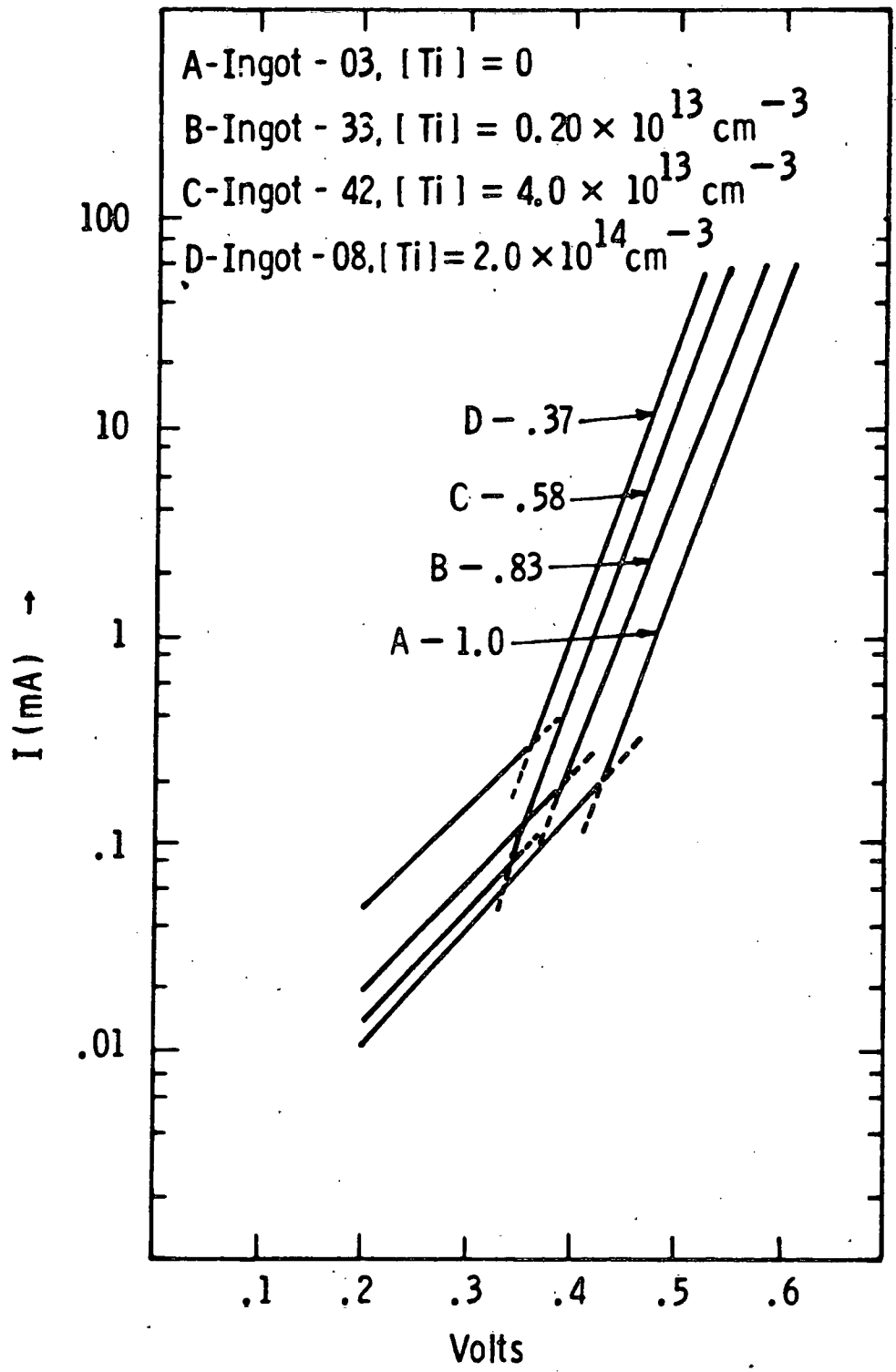

Figure 12 Transformed dark I-V curves for Ti-doped solar cells. As the Ti content increases, the bulk lifetime diminishes, as shown by the shift of the curve's upper segment.[2,11] This behavior is typical of lifetime-killing impurities such as Ti, V, Mo, N, Nb, Ta, Pd, Au, Zr, and Cr.

concentration levels. The calculation includes the assumption that the impurities act independently; thus, a comparison of calculated and experimental values permits assessment of any interactive effects. This comparison is shown in Figure 13 for a sampling of the multiply-doped devices we previously studied[3]; the ingots are identified in Table 12.

While these data suggest some anti-synergic behavior as evidenced by the calculated efficiency being larger than the measured value (the points lie below the unity slope correlation line), supplementary data obtained by the dark I-V analysis and deep-level transient spectroscopy (DLTS) have shown negligible impurity interactivity except for copper with titanium, vanadium, and zirconium.[3,19] The general downward displacement of the data is attributed either to junction degradation (precipitation) effects at higher total impurity concentrations which are not included in the calculations, or to inaccurate impurity concentration data. In the case of Ti, V, and Zr, the addition of copper results in a small improvement in cell performance. DLTS measurements (Appendix V) have in fact shown that the number of recombination centers due to these impurities is reduced by copper.[3] It is believed that the mobile copper atoms diffuse to the locations of the second metal species, where co-precipitation then electrically deactivates some of the Ti, V, or Zr (see also Sections 3.6 and 3.7) and are thus well described by the impurity-performance model.

3.5.8 Modeling Polycrystalline Behavior and Resistivity Effects

We have examined the effects of a number of impurities in samples with resistivities ranging from 0.2 to 30 ohm-cm and in polycrystalline material produced by Czochralski growth.[19]

A convenient way of presenting these results is by determining the impurity concentration threshold N_{ox} and comparing the experimental value to that deduced from the 4 ohm-cm single-crystal data. Using subscripts α and β to designate 4 ohm-cm p-base and the comparison sample data, respectively, we obtain from equations 11 and 14 the experimental threshold $N_{ox\beta}$. All currents are normalized with respect to the α baseline values

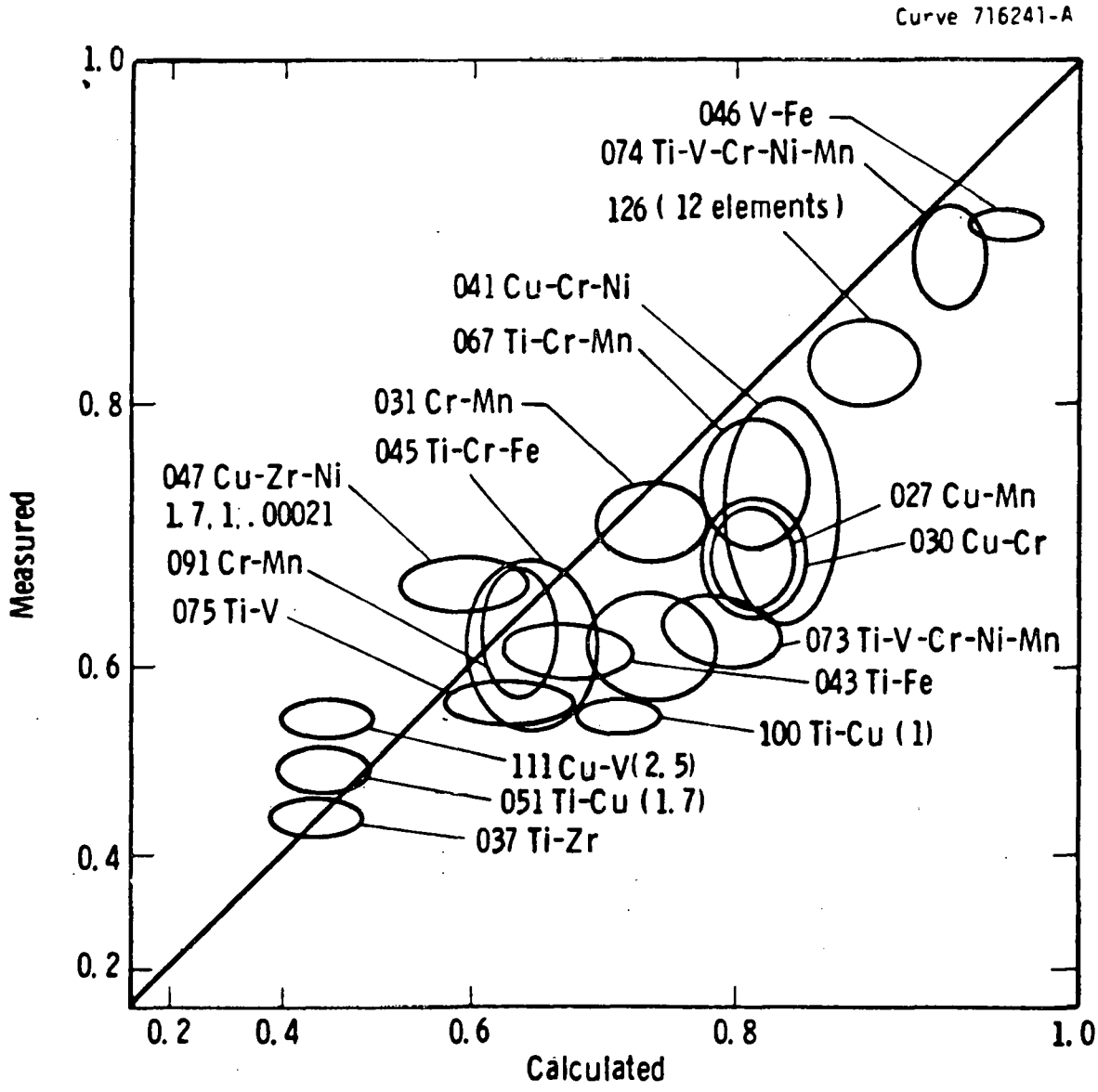

Figure 13 Normalized efficiencies for multiply-doped 4-ohm-cm p-base solar cells

TABLE 12

IMPURITY CONCENTRATIONS FOR MULTIPLY-DOPED INGOTS IN FIGURE 13
(10^{15} ATOMS CM^{-3})

Ingot No	Ti	Cu	V	Cr	Fe	Zr	Ni	Mn
027		1.7						1.3
030		1.7		1.0				
031				1.0				1.3
037	0.22					<0.0007		
041		1.7		0.8			2.1	
043	0.033				0.56			
045	0.039			0.65	0.43			
046			0.07		0.57			
047		1.7				<0.00021	1.0	
050	0.0002		0.0004					
051	0.20	1.7						
061	0.011			1.0				
067	0.0033			0.4				0.5
073	0.0024		0.004	0.4			2.0	0.4
074	0.00033		0.0006	0.08			0.5	0.08
091				0.5				0.3
100	0.033	1.0						
111		2.5	.3					
126	Al, 1.0; B 3.5; Cr .02; Cu .80; Fe .02, Mn .02; Mo .00015; Ni .80; P .9; Ti .0004; V.0004; Zr .0004							
75	.056		.1					
104	.14	2.0						
162	.2						1.21	
185	.15	1.2						

$$N_{ox\beta} = \frac{N_{x\beta}}{\left[\frac{(I_{n\infty}/I_{n\beta}) - 1}{(I_{n\infty}/I_{no\beta}) - 1}\right]^2 - 1}. \qquad (25)$$

$I_{n\beta}$ is the normalized short-circuit current in the cell containing impurity x at a concentration of $N_{x\beta}$. $I_{no\beta}$ is the current measured in β samples containing no added impurities.

If we assume the impurities behave identically in 4 ohm-cm p-base samples and in the β samples, we can deduce a value for $N_{ox\beta}$. After some manipulation of the equations, we obtain for the expected value of the degradation threshold

$$N_{ox\beta} = \frac{D_{n\beta}\,[(I_{n\infty}/I_{no\beta}) - 1]^2}{D_{n\alpha}C_{2x}}. \qquad (26)$$

Data expressed in this manner are shown in Figure 10 of reference 19. These data show that for most cases considered, the impurity degradation effects can be projected from the behavior in the 4 ohm-cm p-base devices.

For example, titanium in polycrystalline cells (ingot 102) acts almost identically as in single-crystal devices, a result which has been corroborated by DLTS measurements [3] (see section 3.8). The high- and low-resistivity data agree with the projection with low-resistivity devices being slightly less affected by impurities than are high-resistivity devices.[3,19]

3.6 Impurity Behavior in High-Efficiency Devices

The impurity performance model and corroborating experimental evidence provide a clear picture of the way in which contaminants in silicon impair the efficiency of conventional solar cells. However, as recent studies show,[27] solar cell efficiency has a major impact on overall PV system costs, so that improvements in processes and materials

to raise cell efficiency will be increasingly important considerations. For these reasons, we have examined the potential impact of silicon purity on high-efficiency solar cells.

3.6.1 Considerations for Efficiency Improvement

Our investigations of solar cell impurity effects have relied on a conventional device of rather conservative design. The fabrication technology was minimally complex[3] and optimized for reliability and repeatability rather than for cell efficiency. In the following discussion, we refer to these as "standard-efficiency" (SE) cells as distinguished from "high-efficiency" (HE) cells. SE baseline cells, i.e., containing no added impurities, have an AM1 efficiency of ∿14.5% with AR coatings. In the analytic model devised to relate the performance of the SE cells to their content of added impurities, the parameter obtained to characterize the impact of each impurity is its degradation threshold (N_{ox}), above which cell performance is significantly degraded (Section 3.5).

The relations between normalized short-circuit current, cell efficiency, and N_{ox} are given by equations 14 and 24. From the model derivation, it follows that the degradation threshold also can be expressed as

$$N_{ox} = D_{nb}/(L_{no}^2 V_{th} \sigma_x A_x) \qquad (27)$$

where the symbols are given in Table 9. Of these parameters, σ_x, the capture-cross section, and A_x, the electrically active impurity fraction, are direct properties of the specific impurities. L_{no} and possibly D_{nb} are indirectly affected by the type and amount of impurity.

Experimentally, the ohmic-back "standard-efficiency" (SE) cells used throughout the impurity effects study exhibit values of L_{no} from ∿140 to ∿180 μm and typically have a basewidth of ∿275 μm. Diffusion length data are obtained from measurements of the open-circuit voltage decay, short-circuit current, and from modelling analysis with results in good agreement. Diffusion lengths have also been determined

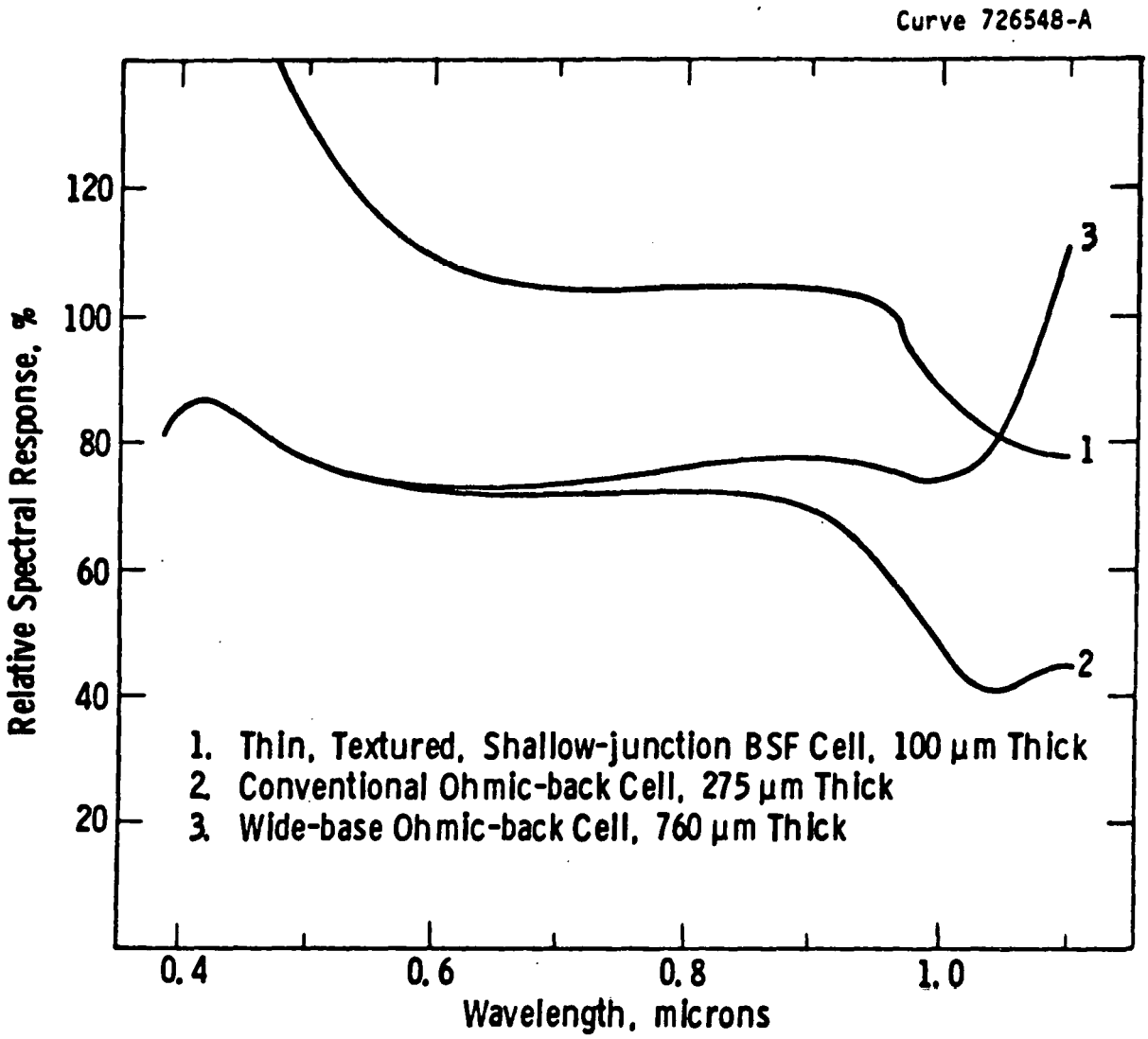

Figure 14 Measured spectral response for solar cells of three different designs

from spectral quantum efficiency measurements. The results are in qualitative agreement with the other methods but yield lower absolute values by a factor of 2 to 4. This discrepancy is probably a consequence of the extremely low injection levels used in measuring spectral response, since it is well known that minority-carrier lifetimes increase significantly at higher injection levels. Figure 14 illustrates typical measured spectral response curves for cells of three different designs, and Figure 15 shows the corresponding quantum efficiency curves. Diffusion lengths obtained from these data are: Device #1, L_{no} = 204 μm; Device #2, L_{no} = 100 μm; and Device #3, L_{no} = 315 μm. The other methods of measurement gave: Device #1, 400 μm; Device #2, 175 μm; and Device #3, 450 μm.

High-efficiency cell performance requires that the cell or its basewidth exceed the absorption length of the lowest energy photons within the absorption band of silicon. It is further necessary, in order to collect the generated carriers, that the diffusion length be substantially greater than the width of the device. These requirements can be satisfied only by proper design of the cell-doping profiles and contact geometry, the use of high-quality silicon, and careful processing to minimize introducing defects or contamination. Minimizing minority-carrier recombination at the surfaces and in the bulk is also necessary.

Surface recombination can be reduced by the use of back-surface fields and by passivation of the physical surfaces, e.g., with oxides. Bulk recombination, although somewhat process dependent, is primarily determined by the quality of the silicon crystal; that is, its impurity content and its defect structure. The defect structure is controlled by the crystal growth technique and can be reduced to levels of minor importance in crystals prepared by CZ, FZ, dendritic web, and some other methods. However, some casting and ribbon-growth methods result in significant twinning and randomly oriented grain boundaries as well as other defects in the silicon. These defects, with the exception of coherent twin boundaries, have been shown to have large recombination

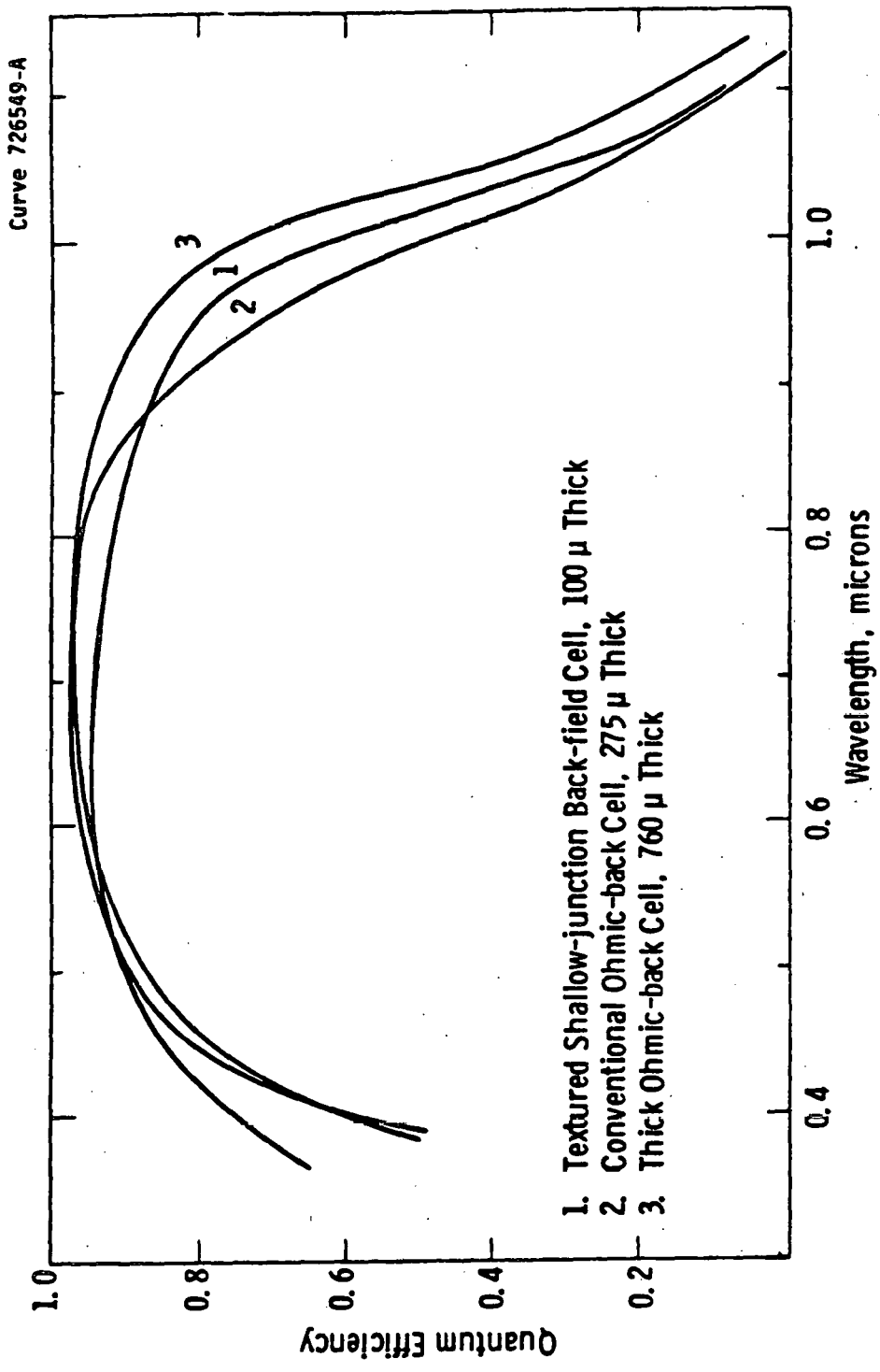

Figure 15 Quantum efficiency plots corresponding to the data of Figure 14

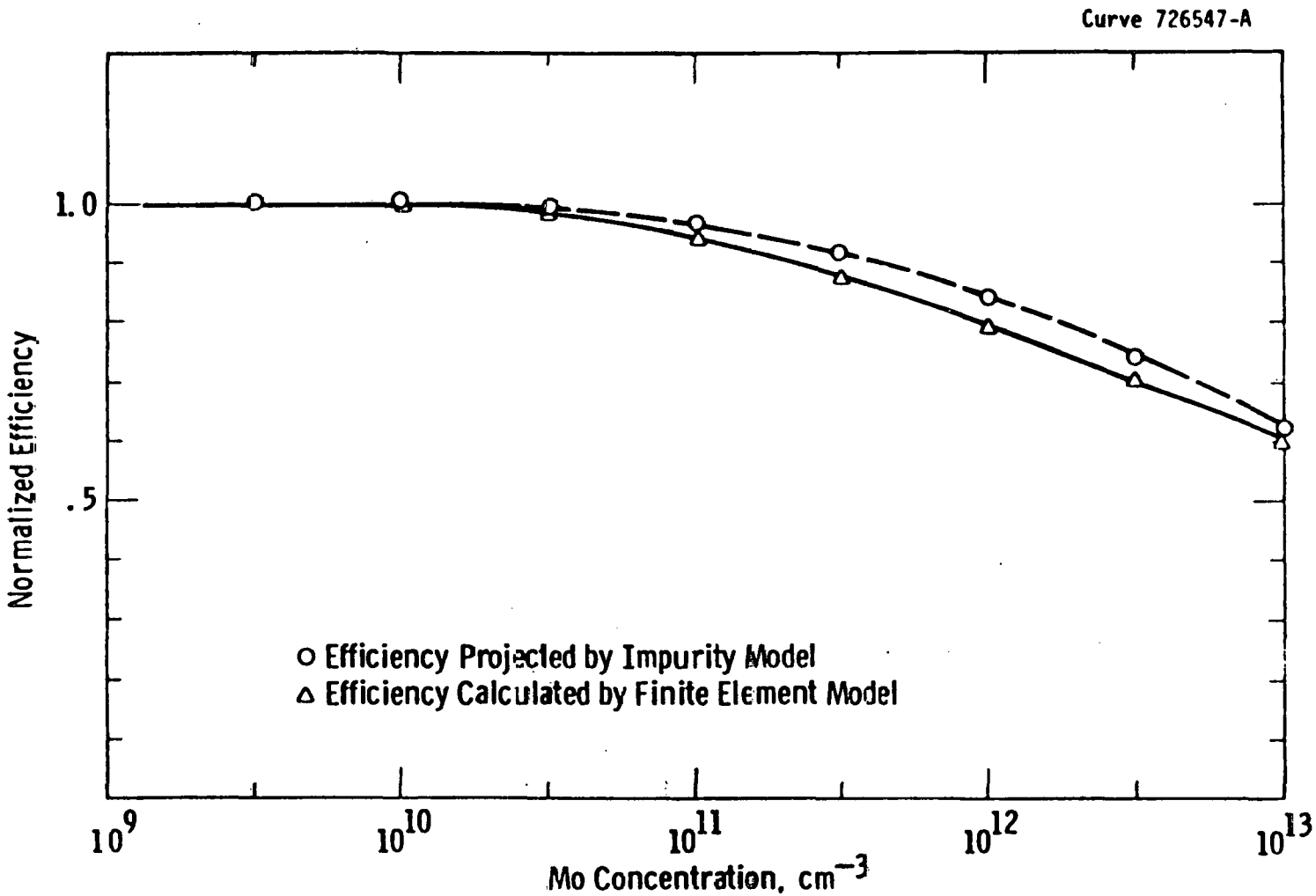

Figure 16 Calculated cell efficiency as a function of molybdenum concentration for a standard (SE) design cell (η = 14%, W_B = 275 μm)

activity even when impurities are not present. Thus, for a polycrystalline material to be a likely candidate for high-efficiency cells, it must have very large grain structure or consist primarily of grains bounded by coherent twins.

3.6.2 Modelling Impurity Impact on High-Efficiency Cells

Having identified a large effective diffusion length as a primary requirement for high efficiency, we can now examine the sensitivity of HE devices to impurities using the equations of the impurity model. If we assume that the constants C_1 and $I_{n\infty}$ (equation 14) are independent of cell design, then the model can predict the HE behavior from the data obtained with the SE devices by knowing the value of $I_{n\infty}$ required for a particular HE device. The design independence assumption is clearly questionable but, as we show later, it is approximately true in the range of impurity concentrations of interest.

Using equation 27 , we obtain an expression for the degradation threshold of an HE cell in terms of the value obtained for SE cells.

$$N_{ox}(HE) = N_{ox}(SE)\ [L_{no}(SE)/L_{no}(HE)]^2\ (D_{nb}(HE)/D_{nb}(SE)) \qquad (28)$$

Let us consider, for example, the effect of adding molybdenum to a wide-base HE cell, cell #3 in Figures 14 and 15 above. The degradation threshold for Mo in SE cells is $6\times10^{11}/cm^3$ and $L_{no}(SE) = 175\ \mu m$; the diffusion length in the wide-base HE cell, $L_{no}(HE) = 450\ \mu m$. These data in equation 28 imply that the degradation threshold for Mo will be reduced to $9\times10^{10}/cm^3$ for the wide-base HE devices. The model curves for SE cells containing Mo are shown in Figure 17, where $N_{ox}(moly) = 6\times10^{11}$. Figure 18 shows the efficiency curve for the HE device, where $N_{ox}(moly) = 9\times10^{10}$. By comparing the two figures, it can be seen that the curve has moved to the left for the HE device, indicating its approximately seven-fold higher sensitivity to the Mo concentration. A qualitatively similar behavior would be seen for other lifetime-destroying impurities.

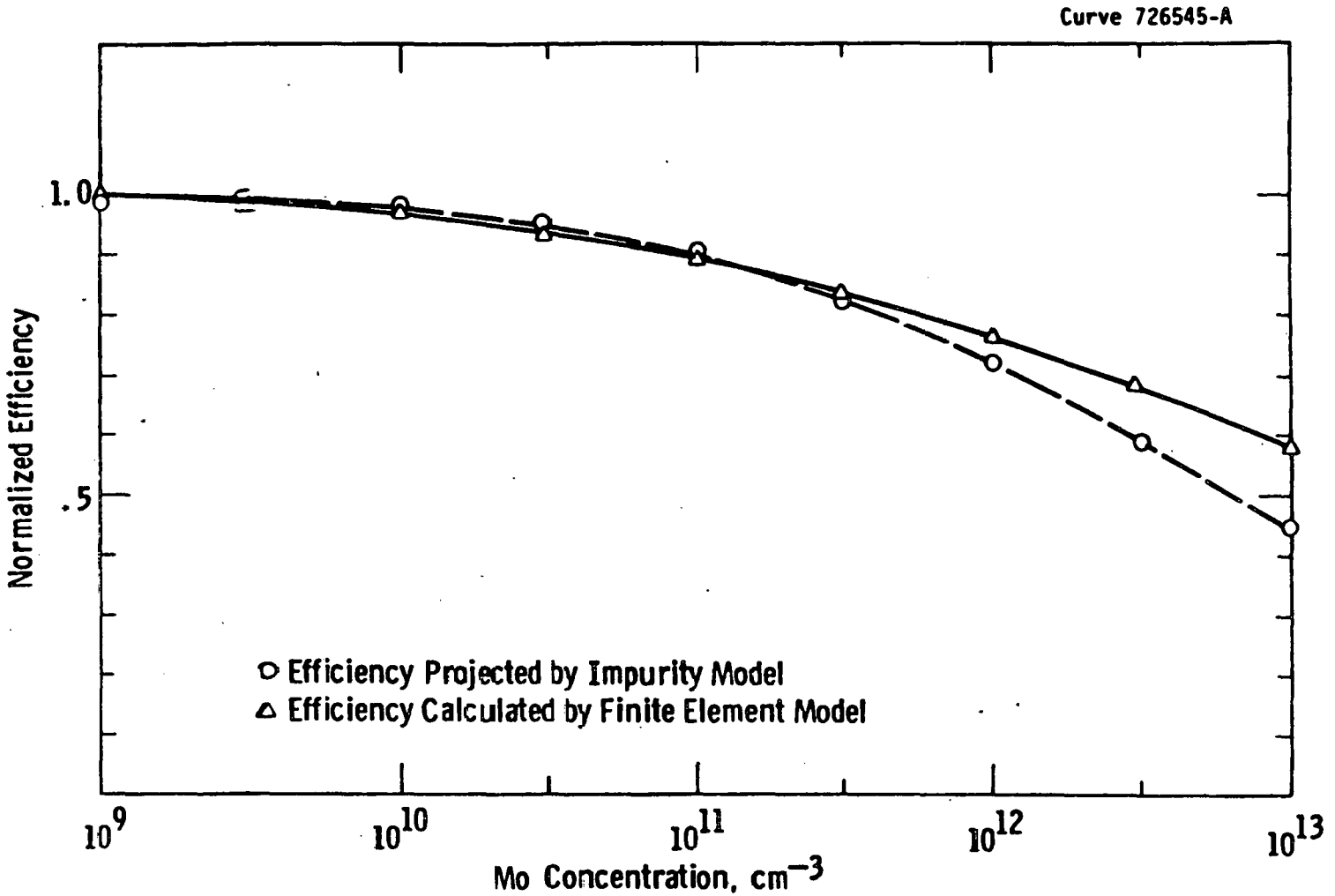

Figure 17 Calculated efficiency as a function of molybdenum concentration for a narrow-base, back-surface field HE cell (η = 15.35%, W_B = 150 μm)

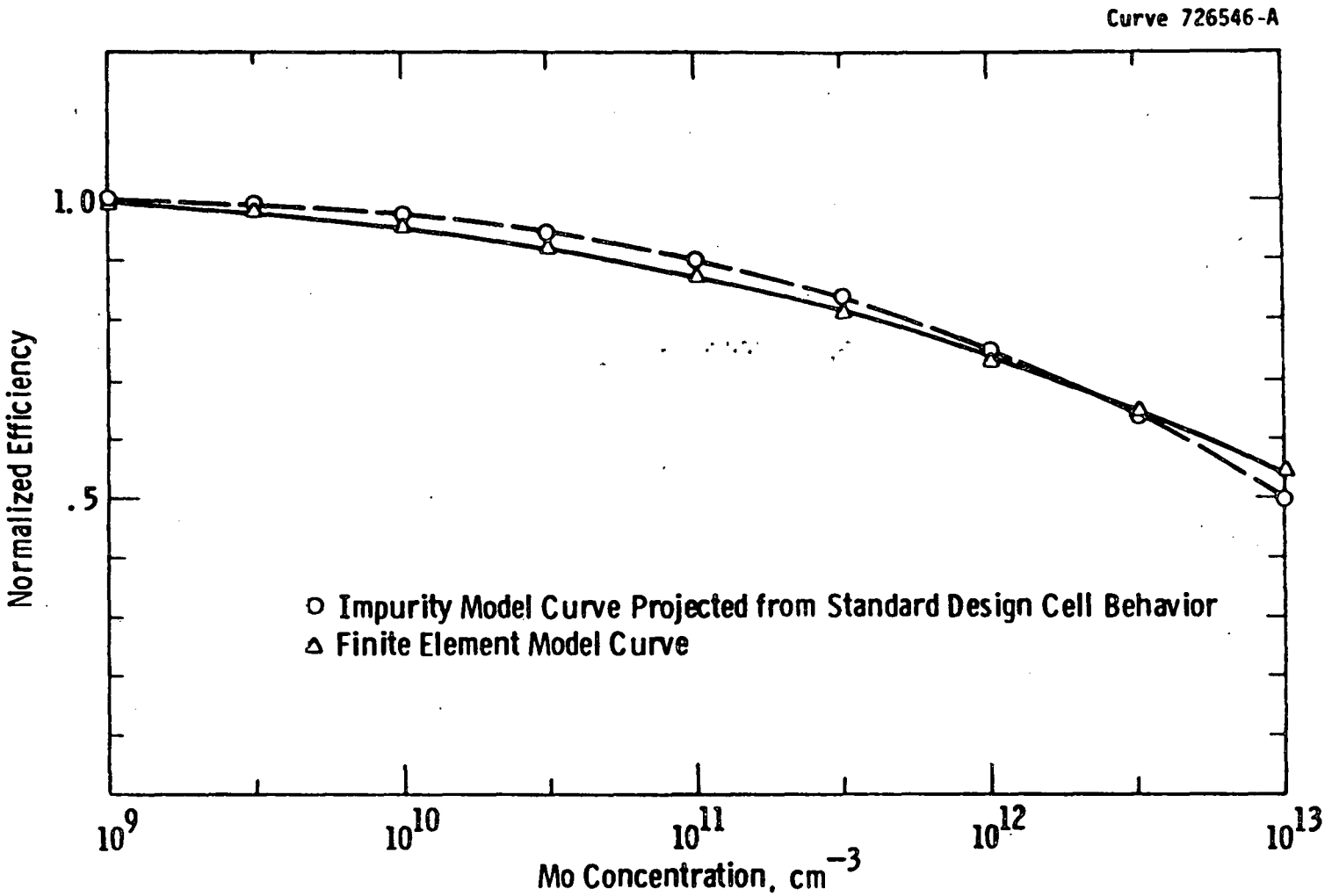

Figure 18 Calculated efficiency as a function of molybdenum concentration for a wide-base HE cell (η = 15.5%, W_B = 765 μm)

In order to test the validity of predictions of the analytic impurity model, we have developed a considerably more detailed, finite element model with which we can calculate cell performance for various spectra and operating conditions. The model is derived from Poisson's equation and the continuity equations for one dimension. In the derivation, we assume low-level injection, space-charge quasi-neutrality, and a steady-state analysis. For minority electrons in p-type material, Poisson's equation becomes

$$Jn = q\,\mu m(nE + V_T \frac{\partial n}{\partial x}) \tag{29}$$

and the continuity equation

$$\frac{\partial n}{\partial t} = 0 = G_n - U_n + \frac{\partial J_n}{q\partial x}. \tag{30}$$

See Table 9 for symbol definitions.
The generation term is given by:

$$G_n = \frac{N_\lambda}{L_\lambda} e^{-\frac{x}{L_\lambda}} \tag{31}$$

and the recombination by the Shockley, Read, Hall expression

$$U_n = \frac{n-n_o}{\tau_n} \tag{32}$$

For a sufficiently narrow region within the device, the coefficients of the coupled equations 29 and 30 will be constant, and a general analytic solution for the carrier concentration is obtained.

$$n_{(x)} = k_1 e^{AX} + k_2 e^{BX} + k_3 e^{CX} \tag{33}$$

where $A = \frac{\varepsilon}{2} - (1 + \varepsilon^2)^{\frac{1}{2}}$

$$B = \frac{\varepsilon}{2} + (1 + \varepsilon^2)^{\frac{1}{2}}$$

$$C = -L\ (1 + \varepsilon^2)^{\frac{1}{2}}$$

$$X = \frac{x}{L_n}$$

$$\varepsilon = \frac{E}{E_T} \qquad E_T = \frac{V_T}{L_n}$$

$$L = \frac{L_\lambda}{L_n} \qquad S_T = \frac{D}{L_n}$$

$$K_3 = N_\lambda \cdot K_3'$$

The minority-carrier current is given by:

$$Jn(x) = qS_T K_1 A e^{AX} + qS_T K_2 B e^{BX} + qS_T K_3 e^{CX} + qS_T e_n \tag{34}$$

The carrier concentration and the current must be continuous at the boundaries of each model element but are not known a priori. However, n and j are known at the surface of an element which is an exterior surface, e.g., a contact or at a surface bounding a junction space-charge region.

For a contact surface at Xs characterized by a surface recombination velocity, S_o we have

$$-\frac{dn}{dx} = S_o n_{(X_s)}.$$

At the edge of a space-charge region at X_j

$$n_{(X_j)} = n_{po} e^{\frac{qV}{kT}}$$

where V is the voltage across the junction and

$$-\frac{dn}{dx} = S_j N_{(xj)}$$

where S_j is a collection velocity, always of the order of 10^7 cm/sec.

These conditions are sufficient to determine the constants in equations 33 and 34 for an outer element. With this information, the boundary conditions are set at its inner surface and the next element can be solved. The successive transformations of $n(x)$ and $jn(x)$ across the elemental regions depend only on the material properties of the element (including those related to impurity type and concentration) and completely describe the performance of the device.

Using this more precise model, we have predicted the effect of molybdenum on the performance of SE cells and two types of HE cells. The results of these calculations are shown in Figure 16, 17, and 18, where they are compared with similar computations employing the simpler analytic model. The agreement with the impurity model predictions and with experimental data is also quite good in all three cases, at least for moderate Mo concentrations. At the highest concentrations, the impurity model predicts too great a performance loss, particularly for the narrow-base back-surface field device, the design details of which deviate most from the assumptions used in the impurity model derivation.

The agreement between the two model calculations (e.g., Figures 16-18) indicates that for most practical purposes the simple analytic expressions, equations 14 and 28, are suitable for determining the impurity behavior of high-efficiency solar cells. The necessary data are the values of N_{ox} for SE cells from the published data base and a value for the effective diffusion length in an uncontaminated HE cell of the required design.

3.6.3 Performance of Narrow-Base, Impurity-Doped Cells

Our calculations indicate that HE cells will be more sensitive to impurity degradation than are SE cells. That is, the degradation threshold (N_{OX}) for a given impurity will be smaller for HE cells than for SE cells. We expect this increased sensitivity to be observed for wide-base cells and for medium-base cells using back-surface fields and passivated surfaces. One way to reduce this sensitivity in HE cells is by making devices with narrow basewidths, although doing so may lower the short-circuit current and efficiency because of reduced spectral absorption. The performance tradeoff is small for basewidths down to approximately 100 μm and so such devices formed a basis for our experiments. The characteristics of our typical SE cell and the HE cells studied are given in Tables 13 and 14, respectively.

Data for two types of narrow-base cells are given in Tables 15 and 16. These devices have a basewidth of 100 μm and are expected to have reduced sensitivity to the impurity, i.e., a larger value of N_{OX}. The impurity in these samples is vanadium, which has a degradation threshold in SE cells of $N_{ox} = 2.5 \times 10^{12}$ cm^{-3}.

To analyze these vanadium-doped cells, equation 28 can be written

$$N_{OX}(HE) = N_{OX}(SE) \left[\frac{L_{no}(SE)}{L_{no}(HE)}\right]^2 \qquad (35)$$

The other parameters of equation 28 vanish because the base material is the same for both devices and we are considering the same impurity in both cases.

For ohmic back devices $L_{no}(SE) = 175$ μm, $L_{no}(HE) \simeq 140$ μm, and $N_{OX}(V) \triangleq 2.5 \times 10^{12}/cm^3$, so we find:

$$N_{OX(V)}(HE) = 3.91 \times 10^{12} \text{ cm}^{-3}$$

TABLE 13

PROPERTIES OF STANDARD-PROCESS CELLS

STANDARD-EFFICIENCY CELLS (SE)

P-Base: 3-5 ohm-cm (N_A 3.5 x $10^{15}/cm^3$)

Basewidth: $\sim$ 275 μm

Cell Area: 1.032 cm^2

Front Junction: Phosphorus Diffused, $X_j \doteq .3$ μm

Contact Grid: $\sim$ 5.3% coverage, Ti-Pd-Ag.

No AR coating

No BSF

Ohmic Back: Ti-Pd-Ag

TYPICAL PERFORMANCE ($\sim$AM1, 91.6mW/cm^2) (No AR coating)

J_{SC} = 21.8mA, V_{OC} = .556 Volts, FF = .78, EFF = 9.5%

Effective Base Diffusion Length $\doteq$ 175 μm

Effective Base Lifetime $\doteq$ 9 μs

TABLE 14

HIGH-EFFICIENCY CELL TYPES UNDER INVESTIGATION

Wide Base	1	$W_B \geq 750$ µm	No AR	Ohmic Back
	2		With AR*	
Medium Base	1	$W_B \doteq 275$ µm	With AR*	Ohmic Back
	2			Gridded Back - No passivation of back surface
	3			Gridded Back - with passivation
Narrow Base	1	$W_B \leq 150$ µm	No AR	Ohmic Back
	2			Gridded Back - No passivation of back surface
	3			" - with passivation
	4		With AR*	" "

Base material is P-type 3-5 ohm-cm ($N_A \doteq 3.5 \times 10^{15}/cm^3$)

Front junction is phosphorus diffused with $X_j = .25$ to $.35$ µm

*AR coating process includes passivation of exposed front surface

A second method of calculating the threshold utilitizes the effective diffusion lengths in the impurity-containing HE cells. We can relate the diffusion length to the lifetime:

$$L_n^2 = D_n \tau_n \tag{36}$$

and using Shockley-Reed recombination theory

$$\tau_n = \frac{1}{\sigma_x N_{th} N_T} \tag{37}$$

where N_T = the density of recombination centers.

We have shown in Section 3.5 for a given impurity x that $N_T = A_x N_x$ so that:

$$L_n^2 = \frac{D_n}{\sigma_x V_{th} N_x A_x} \tag{38}$$

Now substituting equation 36 in equation 27, we obtain:

$$N_{OX} = \left[\frac{L_n}{L_{no}}\right]^2 N_x \tag{39}$$

Using the diffusion length and impurity concentration data in Table 15, we get for Ingot W206V006:

$$N_{OX} = 5.40 \times 10^{12}/cm^3$$

and for W219V008:

$$N_{OX} = 4.68 \times 10^{12}/cm^3$$

The degradation threshold may be calculated a third way from the measured short-circuit current of cells containing a known impurity concentration. The relationship between these quantities is given by the impurity model equation[14] with the constants given in section 3.5.2.

$$\left(\frac{I_{n\infty}}{I_n} - 1\right)^2 = C_1\left(1 + \frac{N_x}{N_{ox}}\right)$$

All measured currents are normalized by the measured short-circuit current of baseline cells.

Solving equation 14 for N_{OX} gives:

$$N_{OX} = \frac{N_x}{\frac{1}{C_1}\left(\frac{I_{n\infty}}{I_n} - 1\right)^2 + 1} \qquad (40)$$

Using equation 40 and the data in Table 15, for cells from Ingot W206V006 we obtain:

$$N_{OX}(V) = 4.5 \times 10^{12}$$

and from Ingot W219V008:

$$N_{OX}(V) = 3.5 \times 10^{12}$$

The predicted and experimental values of the threshold are in fairly good agreement and confirm, as expected, that these thin base cells are less sensitive to impurity contamination.

Following the experiment of Table 15, the metal backs of these cells were photo-masked and etched so as to leave a back-contact grid--that is, leaving only about 5% of the cell back covered with metal and the remainder of the back surface being bare silicon. This has the effect of significantly reducing the effective surface-recombination velocity of the back. The metal-covered surface has an $S_o \doteq 10^6$ cm/s, while the bare silicon has $S_o \doteq 5 \times 10^3$ cm/s. Based on model calculations, a reduction in S_o should improve the effectiveness of the BSF and result in increased efficiency. This is borne out by the experimental data shown

TABLE 15

100 μm CELLS WITH BSF AND OHMIC BACKS, AVERAGED DATA

	J_{SC}	V_{OC}	FF	E_{FF}	L_n	I_n	N_x	N_{OX}	
W198 Baseline	21.00	.546	.755	9.46	140	1	0	3.91×10^{12}	(1)
W206V006	19.10	.528	.750	8.05	64	.909	2.5×10^{13}	5.4×10^{12}	(2)
								4.50×10^{12}	(3)
W219V008	20.48	.556	.750	9.03	101	.975	9×10^{12}	4.68×10^{12}	(2)
								3.51×10^{12}	(3)

Notes (1) predicted from baseline data using equation 4

(2) calculated from diffusion length data using equation 8

(3) calculated from short-circuit current data using equation 10

in Table 16. The baseline cell efficiencies increased approximately one percentage point, while the efficiencies of the vanadium-containing cells increased somewhat less.

Diffusion length data are not available for these cells, but values of N_{OX} are calculated from the short-circuit current data using equation 40. The results are shown in Table 16, with the values straddling the value obtained for SE cells. We know from the increased short circuit that these devices have longer effective diffusion lengths than those of Table 15; consequently, it should be expected that a smaller threshold concentration be observed. It should be noted that attrition due to breakage of the very fragile 100-μm thin cells left us a statistically small number of samples and thus larger uncertainty than in the previous experiment. Diffusion length data for these samples will be available soon and will help clarify the results.

The data from these experiments are in fairly good agreement with the analytic models and further confirm the usefulness of the impurity model equations to estimate the impact of impurities on HE cell performance.

3.7 Impurities in Polycrystalline Silicon

One way to reduce the cost of solar cells is to fabricate them on polycrystalline sheets made from cheaper, less pure "solar" grades of silicon. Relatively little is known about the interaction between grain boundaries and impurities and to what extent such coupled behavior degrades solar cell performance. Therefore, part of our study was divided to an investigation of impurity behavior in polycrystalline silicon.

Polycrystalline ingots, grown as described in Section 3.2, were doped with controlled additions of Mo, Ti, V, Cr, Fe, and Mn, respectively. A typical grain size of about 1 mm was achieved in these specimens. Impurity interaction with microstructural defects was investigated by DLTS measurements, dark and lighted I-V measurements on solar cells, spectral response determinations, and by optical photomicrography,

TABLE 16

100 μm CELLS WITH BSF AND GRIDDED BACK (See Text), AVERAGED DATA

	J_{SC}	V_{OC}	FF	E_{FF}	L_n	I_n	N_x	N_{OX}
W198 Baseline	21.80	.572	.772	10.51	-	1	0	-
W206V006	19.4	.540	.747	8.54	-	.88	2.6×10^{13}	3.9×10^{12} (2)
W219V008	20.02	.560	.773	9.42	-	.918	9×10^{12}	2×10^{12} (2)

Note (2) Calculated from I_n and N_x using equation 10

as described in Vol. 1 of reference 3. Data were also analyzed by comparison to impurity behavior in single crystal doped with the same impurities.

3.7.1 Experimental Observations

The macroscopic impacts of impurities and grain boundaries on solar cell performance can be visualized with the aid of the solar cell data, Table 17, and the spectral response curves depicted in Figures 19 to 24. The 10% uncoated efficiency of the uncontaminated single-crystal cells (equivalent to about 14% AM1 with common anti-reflective coatings) is reduced to 6.9% by the introduction of microstructured defects or grain boundaries into the crystals. Besides cell efficiency, short-circuit current (I_{SC}), open-circuit voltage (V_{OC}), fill factor (FF), and carrier lifetime (τ_{OCD}) are each depressed.

The addition of Mo, Ti, V, and Cr to single crystals causes a loss of cell performance primarily due to a reduction in minority-carrier lifetime. The addition of these same impurities to polycrystalline ingots produces somewhat smaller efficiencies compared to their counterpart single-crystal cells. The difference between the performance of the contaminated single-crystal and polycrystalline cells is a direct function of single-crystal cell efficiency. That is, the smaller the adverse effect of an impurity on the single-crystal cell efficiency, the more evident are the effects of grain boundaries.

For example, in the case of Ti-contaminated single-crystal ingots, the cell efficiencies are typically 4 to 6%, and the difference between single and polycrystalline cell performance is small. On the other hand, Mo- and Cr-contaminated single-crystal cell efficiencies are around 8%, but then counterpart polycrystalline cells are about 2% (absolute) less efficient.

These observations can be explained by the fact that grain boundaries by themselves degrade the carrier lifetime in the bulk silicon, viz. Figure 25 and Table 17. However, if the impurity is present in sufficient quantity to dominate the bulk lifetime (τ), then the grain boundary

Table 17

LIGHTED I-V DATA FROM SOLAR CELLS USED TO COMPARE IMPURITY BEHAVIOR IN SINGLE-CRYSTAL AND POLYCRYSTALLINE SILICON

Ingot ID	Impurity conc. (cm^{-3})	I_{SC} (mA)	V_{OC} (volts)	FF	η (%)	τ_{OCD} μsecs
0.02-Baseline	--	22.4	0.55	0.76	10	4.5
0.76-Poly Baseline	--	19.2	0.51	0.66	6.9	1.1
209-Ti	2.0×10^{13}	16.0	0.50	0.67	5.8	0.3
210-Ti	1.0×10^{14}	14.0	0.47	0.67	4.7	0.8
137-Ti	2.0×10^{14}	12.6	0.46	0.68	4.2	0.8
202-Ti-Poly	1.8×10^{13}	15.4	0.49	0.69	5.4	0.5
102-Ti-Poly	1.1×10^{14}	13.6	0.45	0.61	4.0	0.6
207-Mo	2.0×10^{12}	20.2	0.52	0.72	8.0	0.7
139-Mo	4.2×10^{12}	18.4	0.51	0.68	6.8	0.6
215-Mo-Poly	2.0×10^{12}	17.0	0.49	0.69	6.1	0.5
004-Cr	1.0×10^{15}	18.6	0.53	0.76	7.8	1.0
227-Cr-Poly*	4.5×10^{14}	16.0	0.47	0.66	5.3	0.4
206-V	2.6×10^{13}	18.6	0.51	0.71	7.1	0.5
203-V	5.0×10^{13}	17.3	0.50	0.71	6.4	0.5

*Mass spec analysis showed impurity concentration of 2.2×10^{15}.

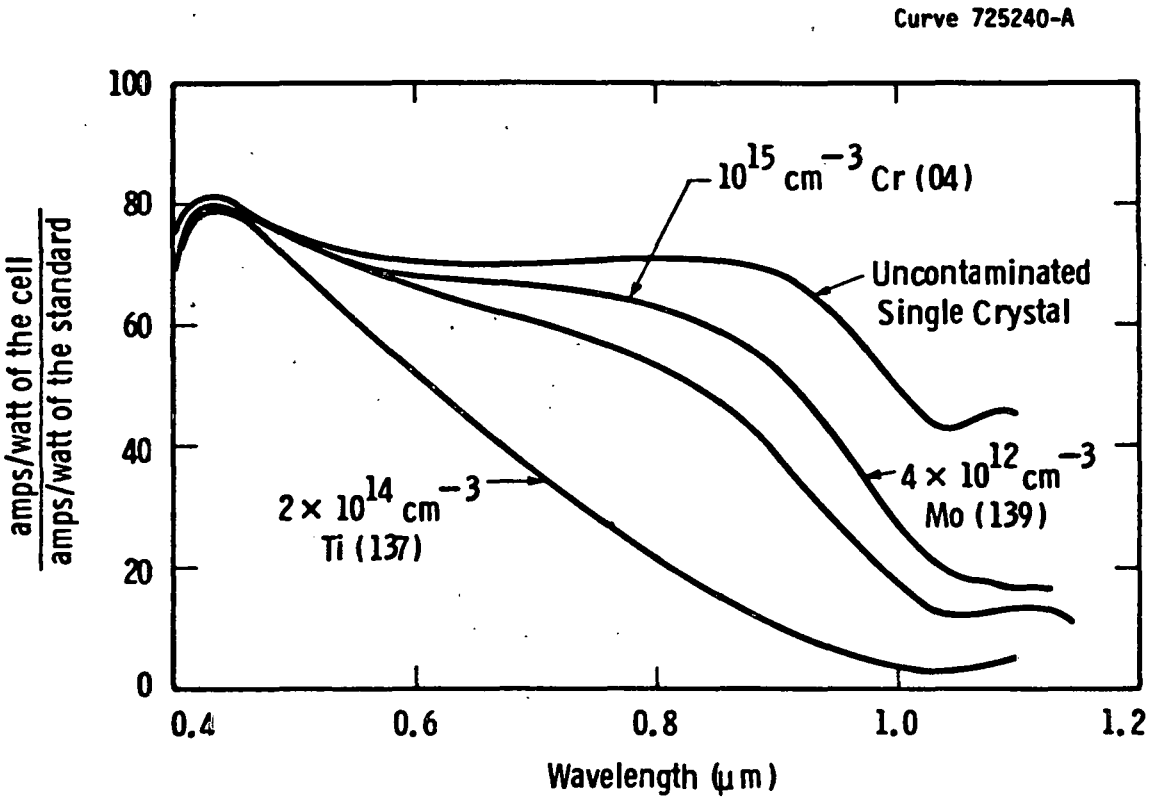

Figure 19 The effect of Cr, Mo, and Ti on the spectral response of single-crystal silicon solar cells

Curve 725239-A

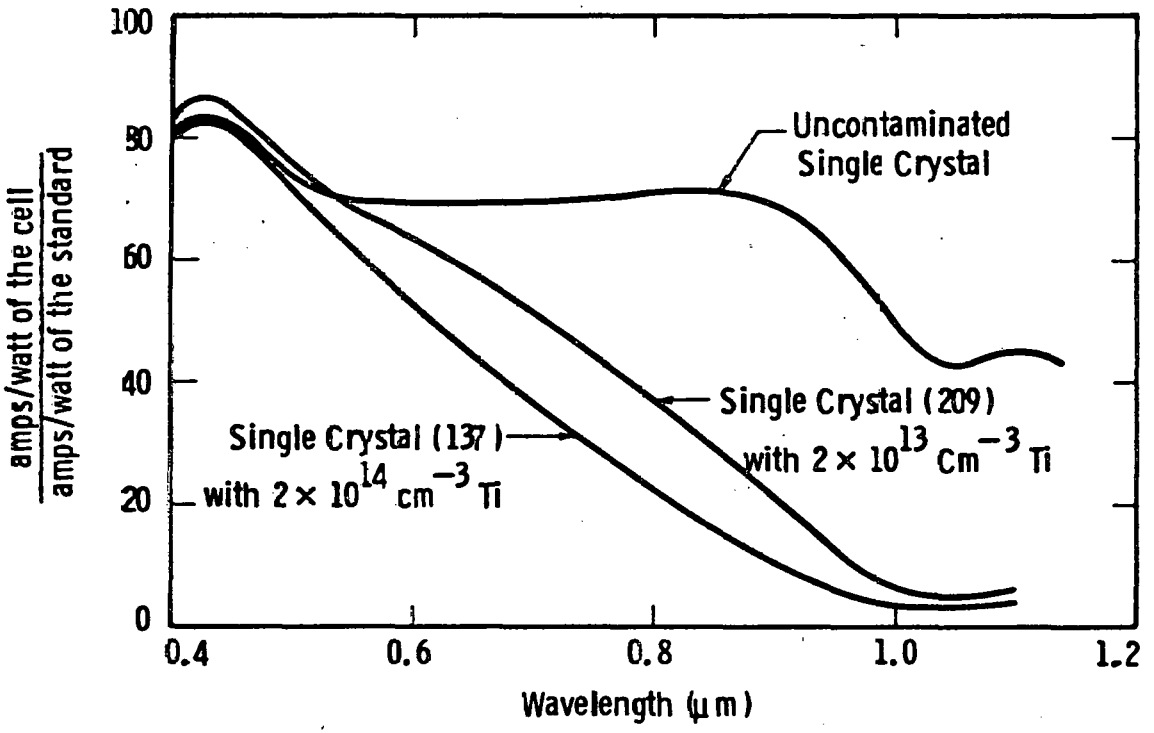

Figure 20 Change in the spectral response of single-crystal silicon solar cells with Ti impurity additions

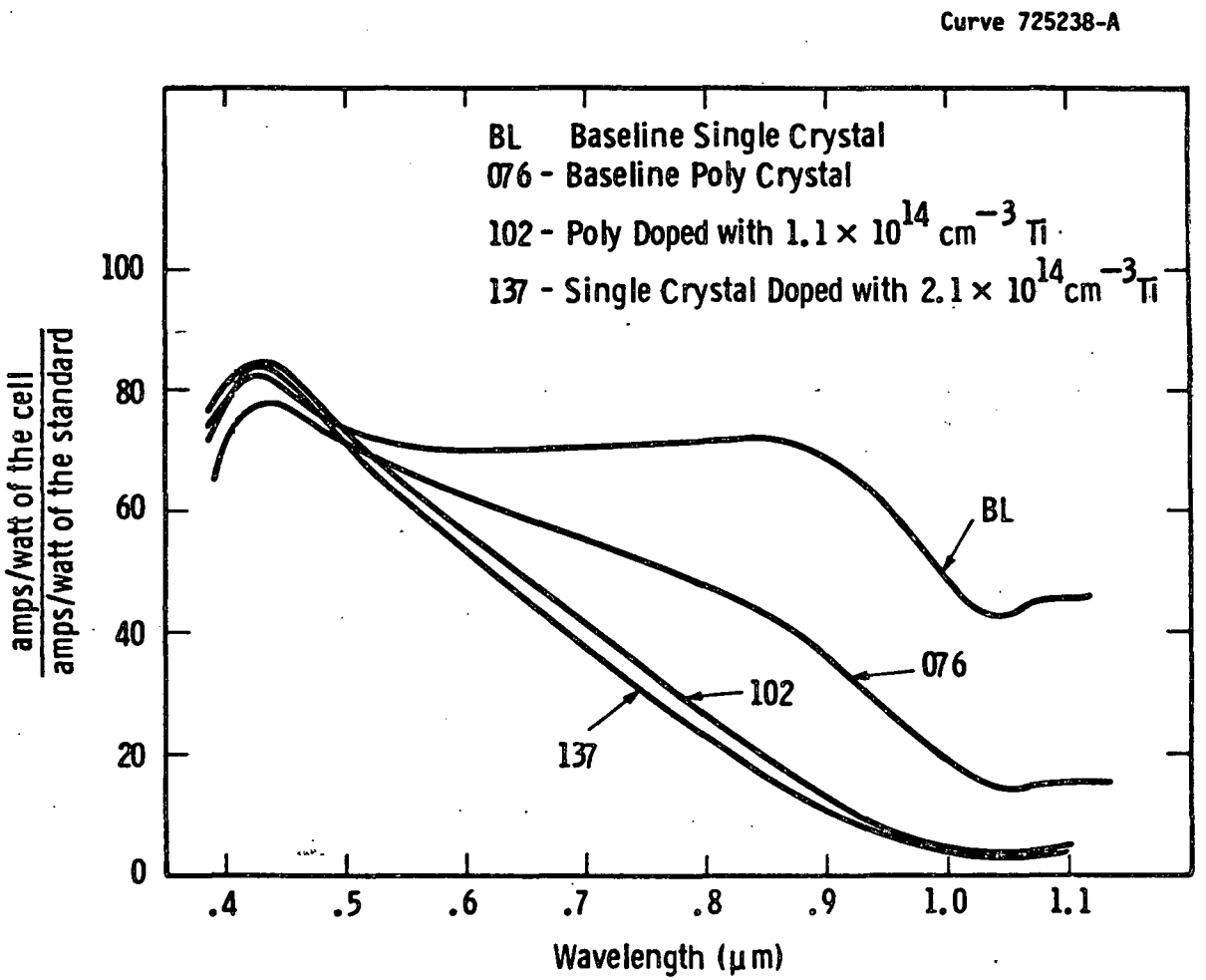

Figure 21 The effect of 1.2 x 10^{14} cm^{-3} Ti on the spectral response of silicon solar cells

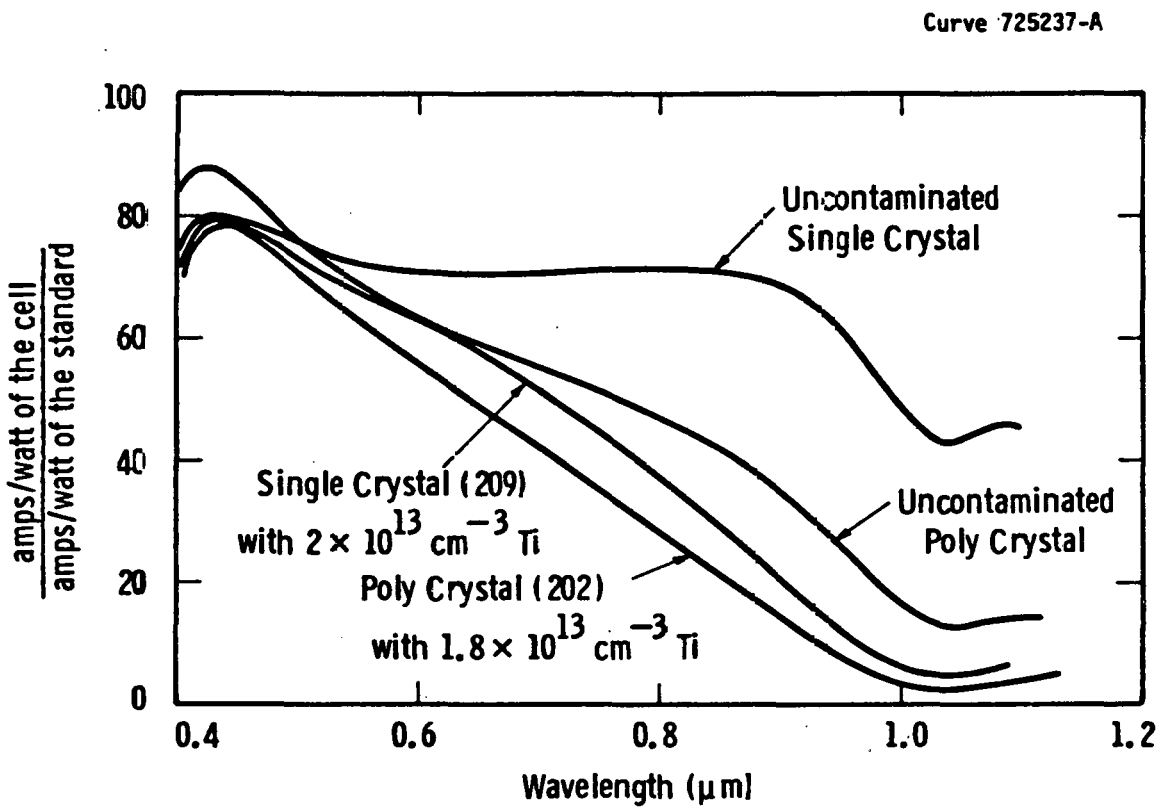

Figure 22 Effect of 2 x 10^{13} cm^{-3} Titanium in the spectral response of single and polycrystalline solar cells

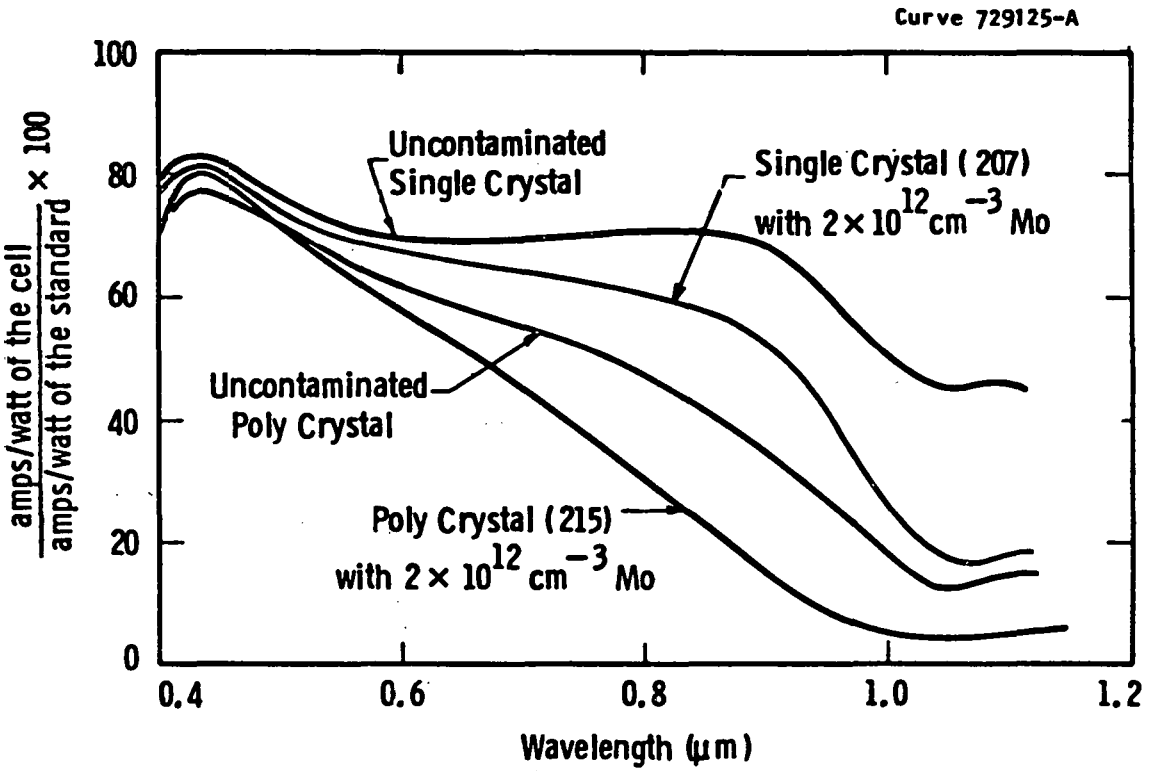

Figure 23 The effect of Molybdenum on the spectral response of single-crystal and polycrystalline silicon solar cells

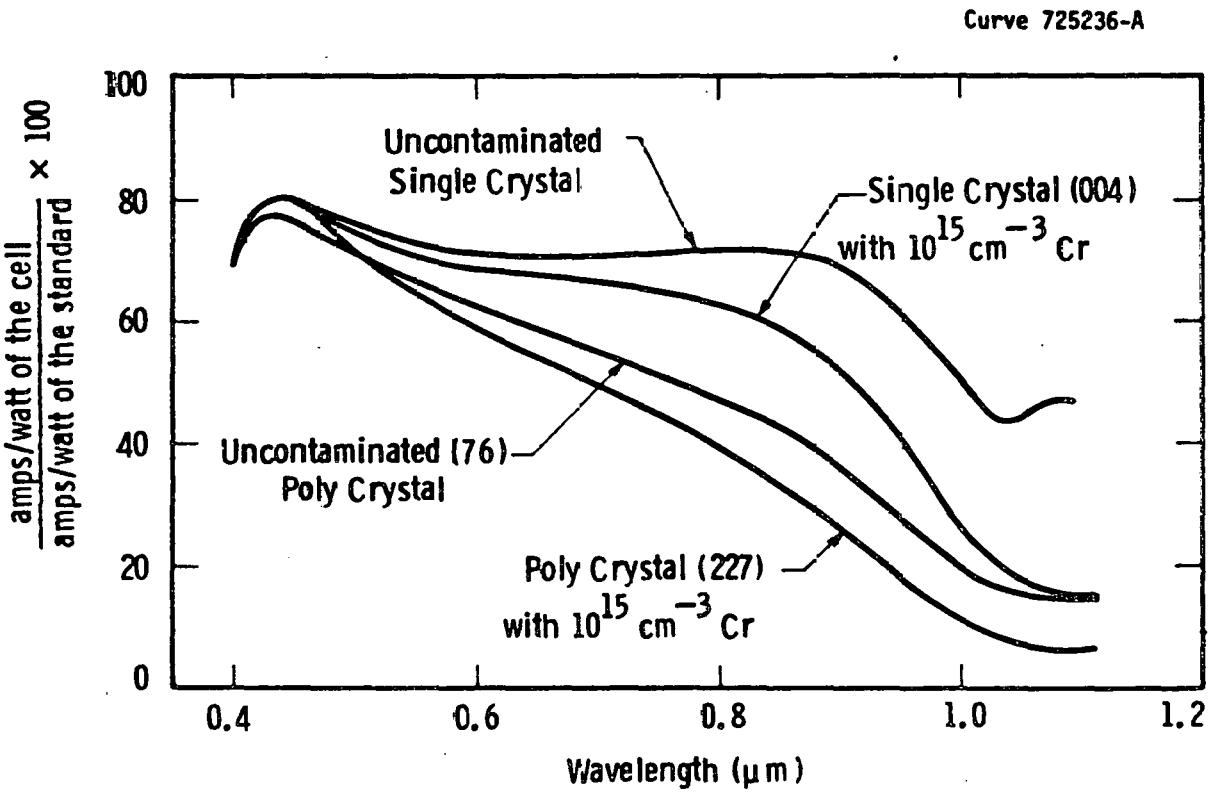

Figure 24 The effect of Cr on the spectral response of single and polycrystalline silicon solar cells

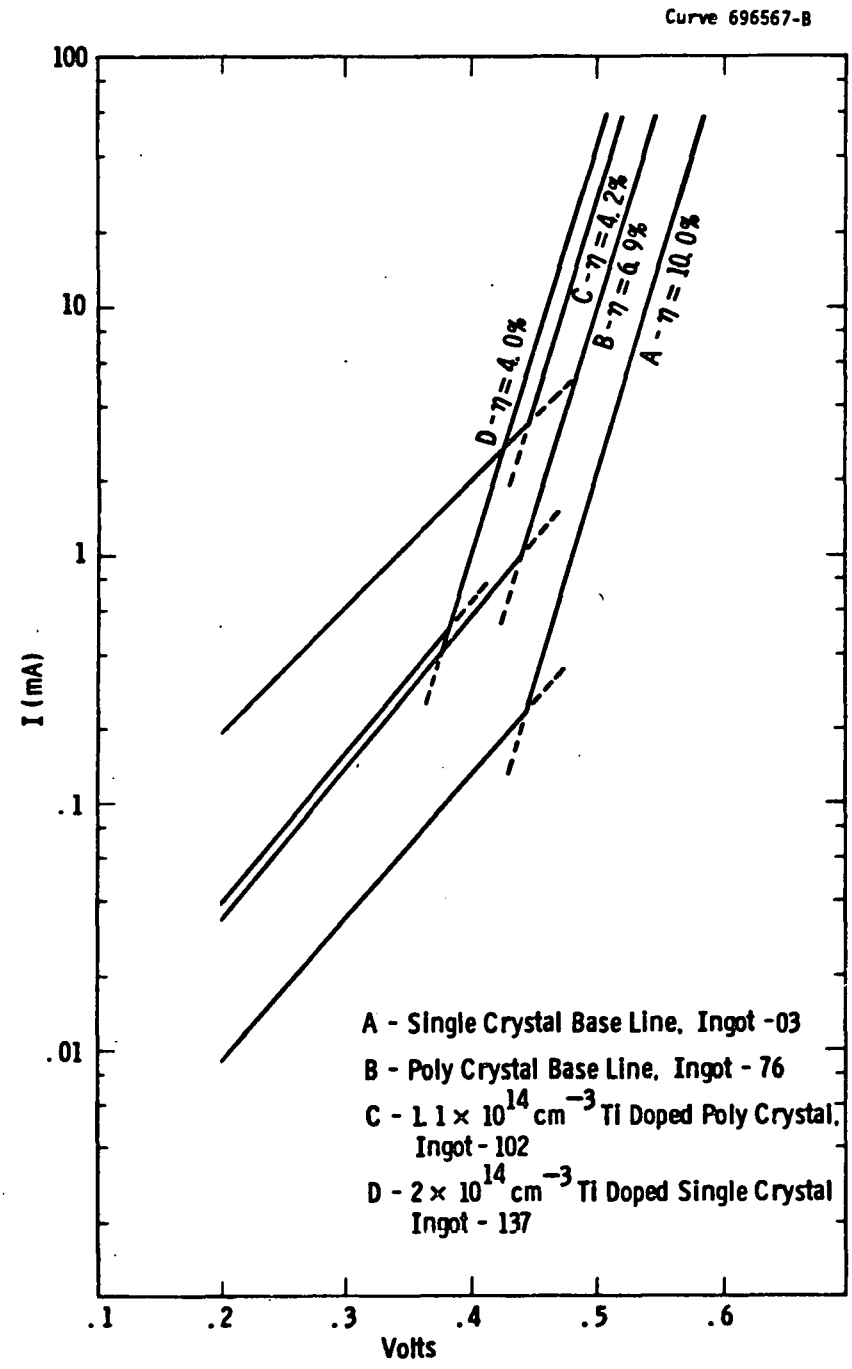

Figure 25 Transformed I-V curves for Ti-contaminated single and polycrystalline solar cells

effect is secondary because

$$\frac{1}{\tau} = \frac{1}{\tau_{impurity}} + \frac{1}{\tau_{microstructure}}$$

It is important to recognize that small additional variations can result if sufficient numbers of electrically active grain boundaries are present in the depletion region of the solar cell. There they can also degrade the cell performance by increasing the junction recombination current, as is clearly evident in Figure 25.

The spectral response from a large number of single-crystal and polycrystalline cells was measured[3] to gain better insight into the effects of impurities and grain boundaries on cell performance. Figure 19 illustrates the effects of 10^{15} cm^{-3} Cr, $4x10^{12}cm^{-3}$ Mo, and $2x10^{14}$ cm^{-3} Ti on the spectral response of single-crystal solar cells. (These concentrations typify the upper limits which can be incorporated during Czochralski growth of single-crystal silicon.) It is quite clear that the presence of impurities degrades the red response of all the solar cells. Since poor red response correlates well with low bulk lifetime, the spectral response data are consistent with our cell measurements and the OCD lifetime measurements. The addition of increasing amounts of impurity gradually impairs the red response or the carrier lifetime (Figure 20).

Figures 21 and 22 illustrate the spectral response of single-crystal and polycrystalline solar cells, with and without Ti. The presence of grain boundaries alone degrades the spectral response which again is consistent with the loss in cell efficiency (Table 1). The curves in Figure 21 and 22 also indicate that the performance differences between Ti-contaminated single and polycrystalline cells are small because Ti controls the cell efficiency. The differences in behavior become more apparent at smaller Ti concentration.

In Figure 23 we show the effect of Mo on the spectral response of single-crystal and polycrystalline solar cells. The data clearly indicate that the polycrystalline cell containing $\sim 2\times10^{12}$ cm^{-3} Mo exhibits degradation from grain boundaries as well as from the impurity because neither effect dominates the bulk lifetime.

In Figure 24 the spectral response data for uncontaminated, as well as Cr-doped, single-crystal and polycrystalline cells again illustrate how both grain boundaries and the impurity effect solar cell performance.

The I-V and spectral response data provide a phenomenological picture of how impurites and material substructure influence the overall properties of devices. However, these data give little insight into localized or small-scale changes in material and device characteristics. For that reason, we used DLTS measurements[3] on small diodes to evaluate variations of the electrically active impurity concentration within the grains of the polycrystalline material, and also near microstructural features such as twin and grain boundaries. (We define the electrically active concentration as the concentration of the trap with highest density and not necessarily the one controlling carrier lifetime.) In Table 18 are compiled the average values of the active impurity concentration measured on a variety of wafers and solar cells used in this study.

We find two Ti-induced recombination centers, E_V+0.30eV and E_C-0.26eV, in both single and polycrystalline cells. The E_V+0.30eV level was present both in the as-grown silicon and the wafers processed into cells. The E_C-0.26 eV is a minority-carrier trap and was detected by forward biasing the p-n junctions. There were only faint indications of levels due to the microstructural features themselves in the polycrystalline material, but the data were not sufficient or reproducible enough to measure the levels accurately.[3] The active Ti concentration in the as-grown wafers and cells is lower than that in the single crystals, consistent with the fact that less Ti was originally added to

the polycrystalline ingot. It is also clear from the data in Table 18 that the electrically active Ti in the as-grown ingots is only about 35% of the total Ti present. We have found similar behavior for other impurities.[3] A further reduction in active Ti concentration occurs due to phosphorus gettering near the junction when cells are made, so that less than a tenth of the metallurgical Ti remains electrically active there.[28]

The DLTS data for the Ti-contaminated polycrystalline material exhibits more scatter than that for the single crystal. The variation is caused by changes in Ti concentration in the vicinity of microstructural features like those illustrated in Figure 26, an optical photograph which typifies the many devices we examined by DLTS measurements. The corresponding electrically active Ti concentrations are also shown in the figure. In general, we find a small but measureable reduction in Ti concentration in the vicinity of meandering grain boundaries, e.g., like (a), while the active Ti concentration near straight-sided twin boundaries (d) or within the interior of a grain (b) are at or above the average value for all the diodes made on the cells. (Another Ti-doped polycrystalline ingot, 202, containing $\sim$ 5 times less Ti did not show appreciable reduction in active concentration at the grain boundaries, suggesting the same concentration dependence of impurity-grain boundary interaction.)

A combination of reflected-light micrograph and laser-scanned photoresponse micrograph of the same area, Figure 27, on Ti-doped polycrystalline reveals high-recombination rates at etched features which resemble grain boundaries (the thick dark strip is part of the contact grid). Straight-sided twins like those in the upper right corner of Figure 27 (a), however, do not show electrical activity. Similar results have been noted by other workers.[29]

In the case of Mo-doped silicon wafers, we found one deep level located at E_V+0.30eV. Unlike Ti, 100% of the metallurgically added Mo in the single crystal or polycrystalline silicon wafers is electrically

TABLE 18

AVERAGE IMPURITY CONCENTRATIONS IN SINGLE-CRYSTAL AND POLYCRYSTALLINE SILICON INGOTS AND CELLS

Ingot ID	Metallurgical Concentration cm^{-3}	Electrically Active Concentration in As-grown wafer cm^{-3}	Electrically Active Concentration in Solar cell (near junction) cm^{-3}
Ti-137-Single	2.0×10^{14}	$(8.0\pm1)\times10^{13}$ (40)	$(1.8\pm0.2)\times10^{13}$ (50)
Ti-210-Single	1.0×10^{14}	$(3.8\pm0.5)\times10^{13}$ (20)	$(4.0\pm0.5)\times10^{12}$ (10)
Ti-102-Poly	1.1×10^{14}	$(4.6\pm2)\times10^{13}$ (20)	$(6.0\pm2.0)\times10^{12}$ (32)
Cr-004-Single	1.0×10^{15}	$(1.5\pm0.5)\times10^{14}$ (20)	undetectable (30)
*Cr-227-Poly	4.5×10^{15}	$(8-2\bar{0}0)\times10^{12}$ (40)	undetectable (10)
V-206-single	2.6×10^{13}	$(6.5\pm0.5)\times10^{12}$ (10)	undetectable (10)
V-203-Poly	5×10^{13}	$(17\pm2)\times10^{12}$ (15)	undetectable (6)

*Mass Spec. Analysis Showed Impurity Concentration of 2.2×10^{15} cm^{-3}

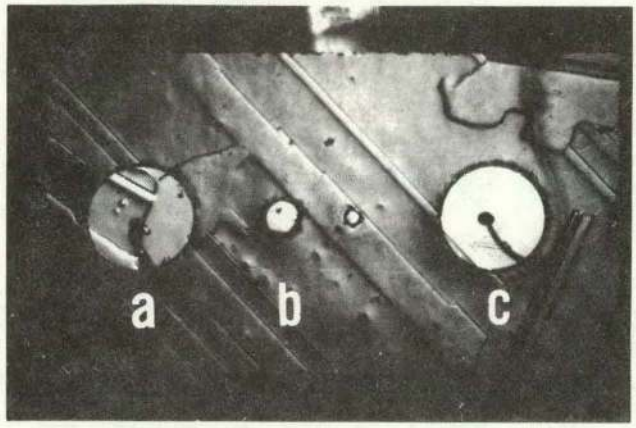

$a = 4.95 \times 10^{12} cm^{-3}$, $b = 8.1 \times 10^{12} cm^{-3}$, $c = 8.11 \times 10^{12} cm^{-3}$

30 mil

(a)

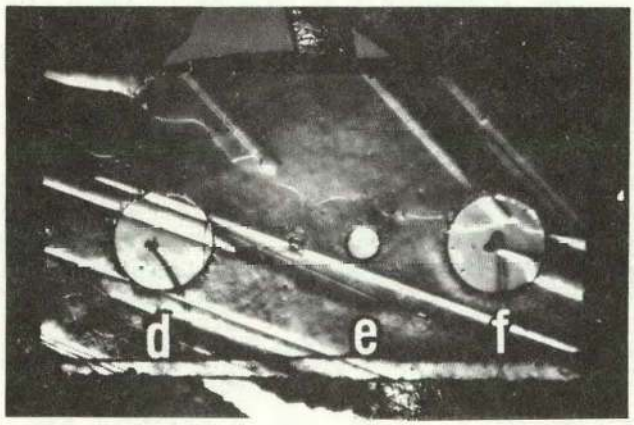

$d = 8.11 \times 10^{12} cm^{-3}$, $e = 6.56 \times 10^{12} cm^{-3}$, $f = 4.12 \times 10^{12} cm^{-3}$

(b)

Figure 26 Localized variation in the concentration of the Ti-induced E_V+0.30eV trap in the depletion region of the polycrystalline cell

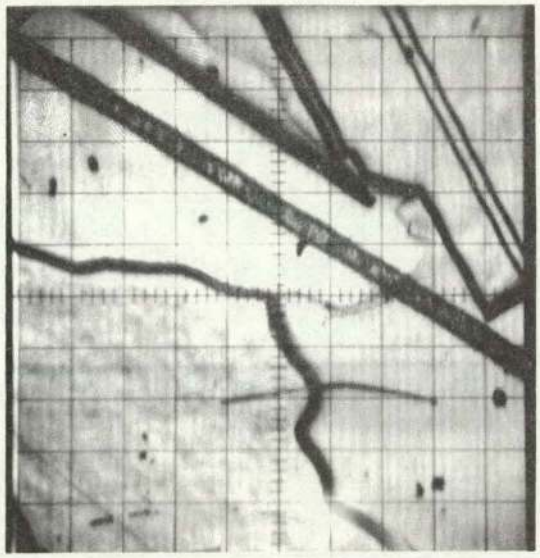

(a)

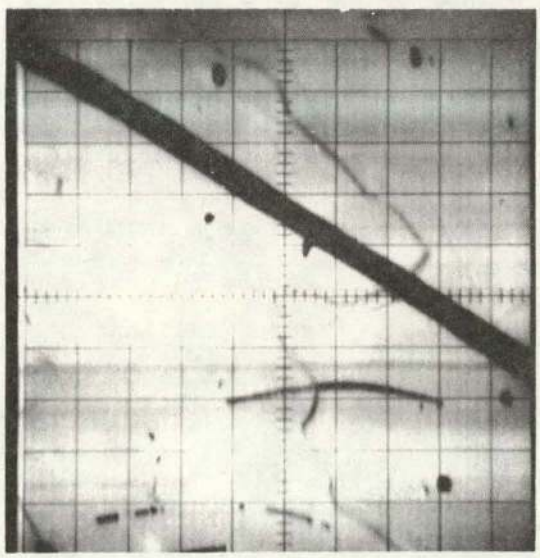

(b)

Figure 27 Magnified views of a) reflective-light micrograph of a region on the Ti-doped polycrystalline cell and b) laser-scanned photoresponse micrograph of the same cell area

active (Table 18). Even after solar cell fabrication , no change in the active Mo concentration was detected. The data in Table 18 indicate that there was no appreciable scatter and the active Mo concentration was nearly the same over 20 Schottky barrier diodes fabricated on a Mo-doped polycrystalline wafer. Figure 28 illustrates, for example, that the measured active Mo concentration was independent of the underlying microstructural features; presence of grain boundaries had no influence on the electrical activity of Mo.

From Table 18 we note that Vanadium in p-type silicon produces a deep level at E_V+0.42eV. Only about 28% of the metallurgical V is electrically active in the as-grown single-crystal and polycrystalline wafers. The scatter in active V concentration from place to place on a wafer was also small. Figure 29 shows that in a polycrystalline wafer containing $\sim 2\times10^{13}$ cm^{-3} V, the active V concentration remains nearly the same regardless of the presence of grain boundaries.

Cr grown into silicon causes two deep levels, at E_V+0.22eV and E_V+0.31eV. Only about 20% of the total Cr in the wafers is electrically active in single-crystal wafers. However, there is a very striking difference in the behavior of Cr compared to other impurities in polycrystalline silicon. Unlike Mo, V, and Ti, there is more than an order of magnitude variation in electrically active Cr with a polycrystalline wafer (Table 18). The highest concentration is nearly equal to what one would expect in a single crystal. Figure 30 illustrates that regions with high Cr concentration are free of grain boundaries, while the presence of a grain boundary significantly reduces the electrical activity of Cr. Straight-sided twins, Figure 30a, do not show any appreciable influence on the active Cr concentration, an observation consistent with results for other impurities.

3.7.2 Analysis of Impurity Behavior

Our data for uncontaminated polycrystalline silicon indicate that uncoated cell efficiency declines to $\sim$ 7% in material with 1-mm size grains from the 10% value characteristic of the baseline single-crystal

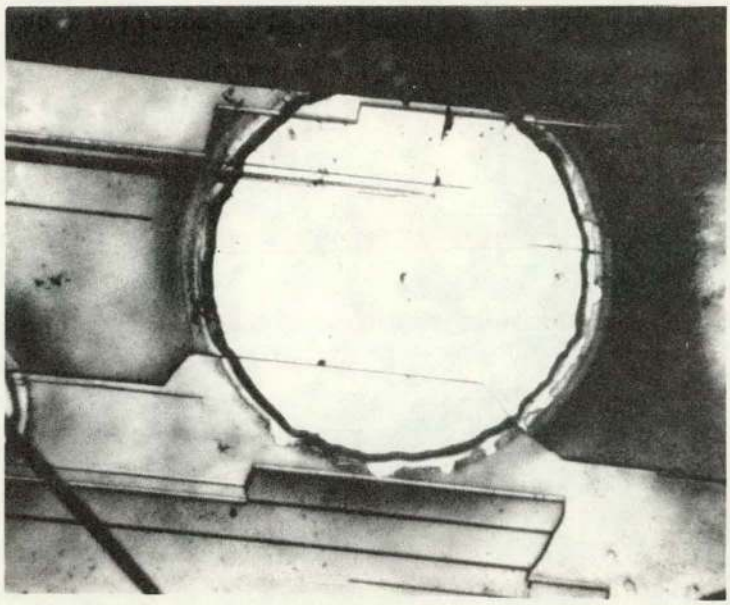

$[Mo^*] = 2.5 \times 10^{12}\ cm^{-3}$

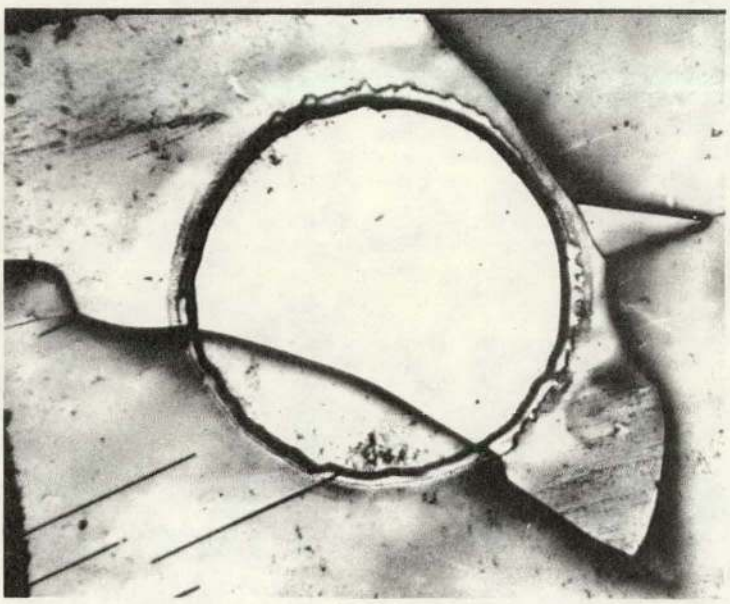

$[Mo^*] = 2.6 \times 10^{12}\ cm^{-3}$

30 mil

Figure 28 Optical micrographs and corresponding electrically active Mo concentration in regions of a polycrystalline wafer

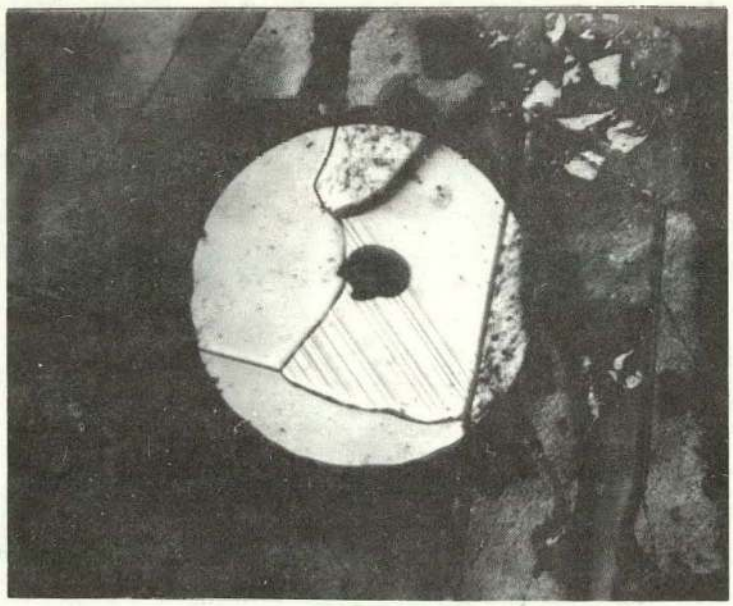

$[V^*] = 1.6 \times 1^{13}\ cm^{-3}$

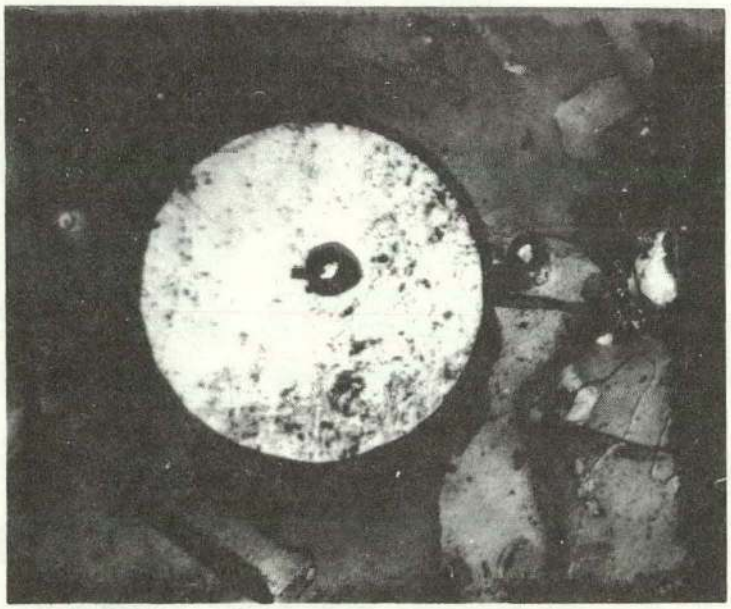

$[V^*] = 1.6 \times 10^{13}\ cm^{-3}$

30 mil

Figure 29 Optical micrographs and corresponding electrically active vanadium concentration in regions of a polycrystalline wafer

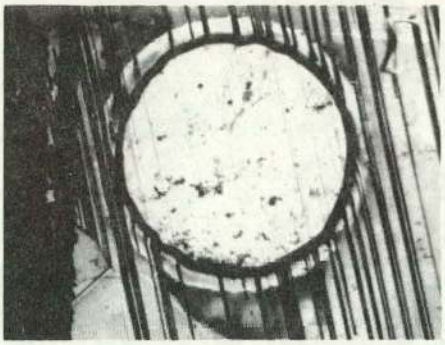

$[Cr^*] = 2.0 \times 10^{14}\ cm^{-3}$

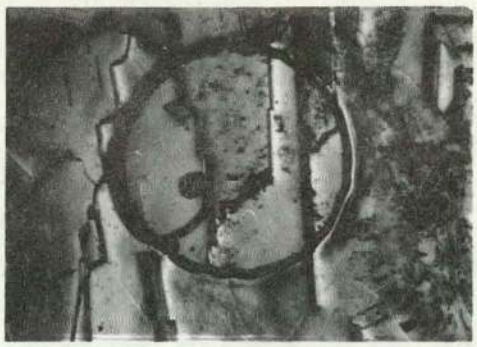

$[Cr^*] = 8.0 \times 10^{12}\ cm^{-3}$

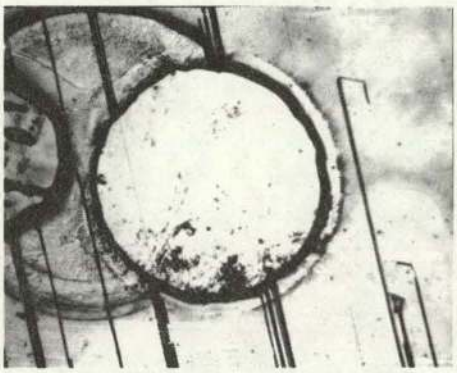

$[Cr^*] = 1.8 \times 10^{14}\ cm^{-3}$

$[Cr^*] = 1.7 \times 10^{13}\ cm^{-3}$

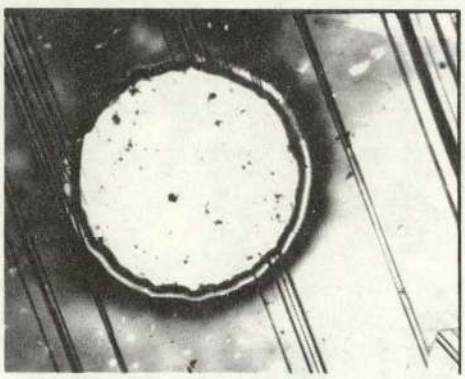

$[Cr^*] = 1.1 \times 10^{14}\ cm^{-3}$

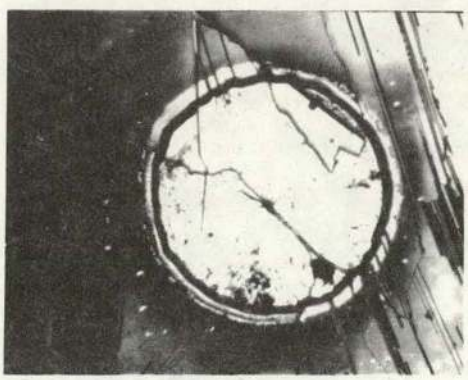

$[Cr^*] = 5.0 \times 10^{13}\ cm^{-3}$

30 mil

Figure 30 Optical photomicrographs and corresponding electrically active chromium concentrations from various regions of a polycrystalline wafer

devices. This efficiency value is well within the ranges found by others for solar cells made on polycrystalline silicon with comparably sized grains.[29-32] The dominant performance reduction mechanism is a decrease in the bulk lifetime, primarily due to carrier recombination at grain boundaries, e.g., Figure 27. The lower effective bulk lifetime in the polycrystalline material causes both short-circuit current and open-circuit voltage to drop (Table 17). Electrically active grain boundaries which penetrate the junction region also cause increases in junction recombination current so that fill factor also depreciates. Detailed I-V measurements, Figure 25, and spectral response curves, Figures 21 to 24, confirm this reduction in recombination lifetimes.

The addition of Mo, Ti, V, and Cr to single-crystal silicon produces a significant decrease in cell efficiency (Table 18 and Section 3.5). At metallurgical concentrations of 2×10^{14} cm^{-3} Ti (less than 10 ppba), 2×10^{12} cm^{-3} Mo, 2.6×10^{13} cm^{-3} V, and 1×10^{15} cm^{-3} Cr, the uncoated cell efficiencies are reduced from 10% to 4%, 8%, 7%, and 7.8%, respectively. The totality of our data make it very clear that this reduction in cell efficiency stems almost entirely from the loss in bulk lifetime by carrier recombination at deep levels introduced by these impurities. Indeed, from the impurity performance model (section 3.5), solar cell efficiency can be predicted from impurity concentration assuming an inverse proportionality between bulk lifetime and impurity content.

When impurities are incorporated into polycrystalline ingots, two independent sources of carrier-lifetime reduction coexist in the silicon: the impurity-induced traps and the grain boundaries themselves. The net carrier lifetime (τ) can be written as

$$\frac{1}{\tau} = \frac{1}{\tau_{\text{impurities}}} + \frac{1}{\tau_{\text{grainboundaries}}} \qquad (41)$$

If the impurity is severely detrimental and reduces the lifetime significantly compared to grain boundary recombination, then $\tau = \tau_{imp}$ and the effect of the grain boundary on cell performance will be negligible. On the other hand, if $\tau_{imp} \gtrsim \tau_{gb}$, then the influence of

grain boundary on the polycrystalline cell performance will be evident as well.

We, in fact, observe this in our cell data. When $2x10^{14}$ cm^{-3} Ti is added to single or polycrystalline material, uncoated cell efficiency is about 4% in both cases because τ is controlled by Ti impurity-recombination centers. However, data for Mo-, Cr-, and V-doped cells indicate that the single-crystal cell efficiency is close to that of the uncontaminated polycrystalline cells. Therefore, a further reduction in the cell performance was observed when the same amount of impurities were added to the polycrystalline material. These observations are consistent with the model described by equation 41 because cell efficiency is directly related to carrier lifetime. Spectral response data, Figures 21 to 24, also show that for Mo-, V-, and Cr-doped cells, the red response is decreased by both grain boundaries and impurities. In the case of Ti, the observed effect of the grain boundary in the polycrystalline cell is small, as expected (Figure 22).

The most direct evidence of impurity grain-boundary interaction is revealed by the optical photomicrographs and DLTS measurements (Figures 26, 28, 29, and 30). For impurities like Mo, which diffuse slowly in silicon, we found that the electrically active metal concentration was independent of the underlying microstructural features of the polycrystalline wafer (Figure 28), and was equal to that typical of doped single crystals. This indicates there is no measureable interaction between Mo and the grain boundaries. This is in striking contrast to the data for Cr, an element which diffuses rapidly in silicon In Figure 30, grain boundary free regions exhibit high Cr concentrations—nearly equal to what would be expected in a single crystal. However, regions of the wafers which contained grain boundaries exhibit a significant reduction in the Cr electrical activity. In some regions this reduction was more than an order of magnitude.

Qualitatively, the decrease in the active Cr concentration seems proportional to the volume of the specimen occupies by the grain boundaries. For Ti, the diffusion constant of which falls in between those of Mo and Cr (see Section 3.8), we observed a reduction of active Ti concentration by a factor of 1.5 to 2 in the regions of the specimen containing grain boundaries (Figure 26).

We conclude that the electrical activity of impurities decreases in the vicinity of grain boundaries, and that the magnitude of reduction in activity is a function of the diffusion constant of the impurity. These observations can be rationalized by the simple model depicted in Figure 31. At the solidification temperature, impurity concentration in the solid (C_s) is nearly uniform and equal to the product of impurity concentration in the liquid (C_ℓ) and the segregation coefficient of the impurity (k). The model assumes that the crystallographically disordered grain boundary regions act as effective sinks for impurities. As the crystal cools from the growth temperature, impurities will tend to diffuse from grain interiors toward the boundaries. There the impurities precipitate and become electrically inactive.

The result of this process is the observed decrease in electrically active impurity concentration (conversely, an increase in metallurgical impurity concentration) at the grain boundary that is depicted in Figure 31. Since in the bulk crystal the active impurity concentration is a fixed fraction of metallurgical concentration,[3] a loss of electrical activity will be observed near the grain boundary, and this loss will be a direct function of the diffusion constant of the impurity.

It is reasonable to assume that the process of deactivation begins in the solid because the liquid diffusion constants of most impurities in silicon are similar (Section 3.3) and quite large ($\sim 10^{-4}$ cm^2/sec) compared to values in the solid. For these reasons, if melt and grain boundary interaction were responsible for deactivation, we would have observed a similar decrease in electrical activity for all the impurities, regardless of their diffusion constant in the solid.

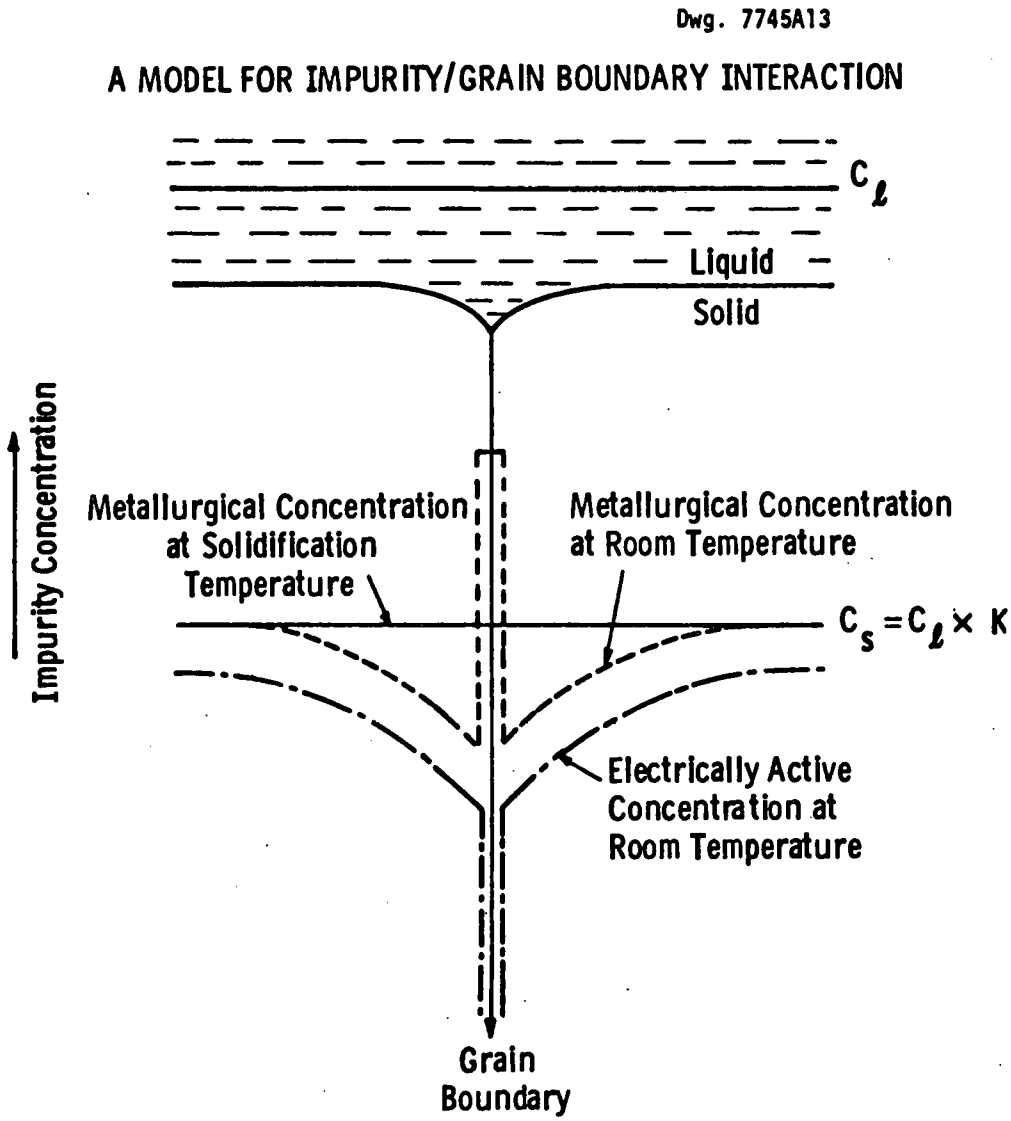

Figure 31 Model of impurity/grain boundary interaction in which the electrical activity of a species is reduced in the vicinity of the boundary

3.8 The Impact of Thermochemical Processing on Impurity-Doped Silicon and Solar Cells

In the preceding sections of this report we described the effects of various impurities on solar cell performance and developed models to predict the degradation due to specific impurities. These analyses showed that the dominant effect of most impurities is to reduce carrier lifetime in bulk silicon, although a few other impurities, notably Cu and Fe, cause an increase in excess junction current.

In the section to follow we report how various thermochemical processes performed after crystal growth can alter the distribution and chemical state of the impurities in silicon and thus change significantly the nature or magnitude of an impurity's impact on solar cell performance.

The processes we investigated were:

(a) various types of gettering,

(b) ion implantation of junctions, and

(c) simple heat treatments.

Based on our results, a model of the processing effects was then developed.

3.8.1 Gettering of Impurities in Silicon

Several processes today are in common use within the semiconductor industry to improve performance by gettering impurities and crystal defects out of the active volume of semiconductor devices. In our investigation, the effects of $POCl_3$ gettering, HCl gettering, mechanically induced damage gettering, and ion-implantation gettering have been evaluated.

3.8.1.1 Background

We previously reported in detail[3] the changes in efficiency of Ti-, Mo-, Fe-, and Cr-doped solar cells subjected to HCl, $POCl_3$, and damage treatments. Briefly, we found that for $POCl_3$ treatments in the temperature range 950 to 1100°C:

1. increasing the gettering temperature generally causes an increase in solar cell efficiency;
2. the cell performance of Mo-doped silicon was improved little, if at all;
3. the cell performance of Ti-doped silicon improved considerably, but extended times or high temperatures would be necessary to raise the efficiency to a value comparable to that of the uncontaminated baseline cells;
4. the cell efficiency of Cr- and Fe-doped silicon was improved relative to that of the baseline cells;
5. except for the Cr-doped silicon, the cell efficiency improvement could be interpreted as due to a single, thermally activated mechanism.

For HCℓ gettering between 1000 and 1100°C, it was found that:

1. HCℓ is as effective as $POCℓ_3$ in gettering Fe and Cr;
2. HCℓ was somewhat more effective than $POCℓ_3$ in gettering Ti;
3. HCℓ, like $POCℓ_3$, is <u>not</u> effective in gettering Mo;
4. since $POCℓ_3$ gettering produces a region of heavy phosphorus doping which must be removed for solar cell fabrication, HCℓ gettering is more attractive as a practical process.

We also found that impurity-doped silicon gettered simultaneously by HCℓ and mechanical lapping damage was not measureably different from silicon gettered by HCℓ alone.

The mechanism of gettering appears to be thermally activated diffusion of the impurity species to the silicon surface where electrical deactivation of the impurity-induced recombination centers takes place. During out-diffusion, a concentration profile is formed in the wafer. Typical impurity profiles, Figure 32, measured by DLTS on step-etched wafers[3] illustrate that an 825°C, 50-min $POCℓ_3$ or HCℓ gettering (1) has

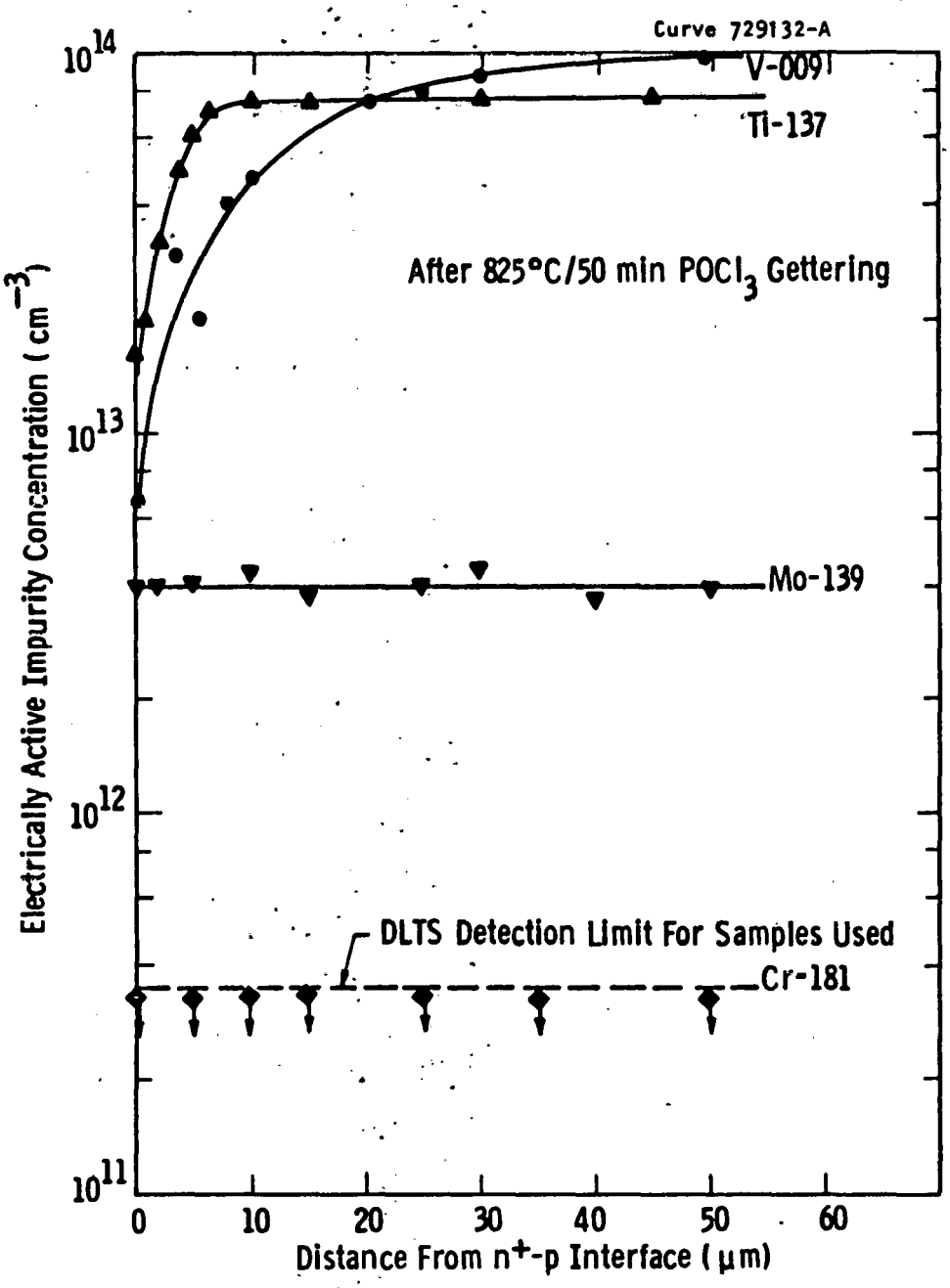

Figure 32 Electrically active impurity profiles for several species after an 832°C, 50-min $POC\ell_3$ treatment

no effect on the active Mo concentration, (2) produces a concentration profile in the first 10 μm near the silicon surface for Ti or V, and (3) significantly reduces the active Cr concentration (it falls below the DLTS detection limit). The shapes of the profiles are species and treatment dependent.

Since these initial results, we have extended our studies to (1) measure the activation energy for Ti gettering, (2) evaluate gettering of polycrystalline material, (3) examine the gettering behavior of copper, and (4) test the effectiveness of argon ion implant damage as a gettering mechanism.

3.8.1.2 Thermal Activation of Impurity Gettering

Following an examination of the concentration dependence of Ti gettering which we find to be small, we have measured the activation energy of Ti out-diffusion from silicon. These experiments are reviewed below.

Our earlier studies of Ti gettering employed Ingot W137, which contained a metallurgical concentration of 2×10^{14} cm^{-3} Ti (8×10^{13} cm^{-3} electrically active Ti). More recent results are based on data from Ingot W123, containing 1×10^{14} cm^{-3} total Ti ($\sim 3.8 \times 10^{13}$ cm^{-3} electrically active Ti). In Figure 33 we compare the profiles of electrically active Ti produced by an 825°C/50 min. $POCl_3$ heat treatment of wafers from each ingot. The data indicate that following gettering the active Ti concentration of Ingot 151 returns to the initial bulk value within 10 μm of the surface. However, the active Ti concentration for ingot W123 does not recover to its initial value within the bulk; instead it saturates substrates at a concentration about a factor of two lower. Since there could be an experimental error of about a factor of two variation in metallurgical Ti concentration from seed and tang ends, it is difficult to determine whether this effect at lower Ti concentration is real.

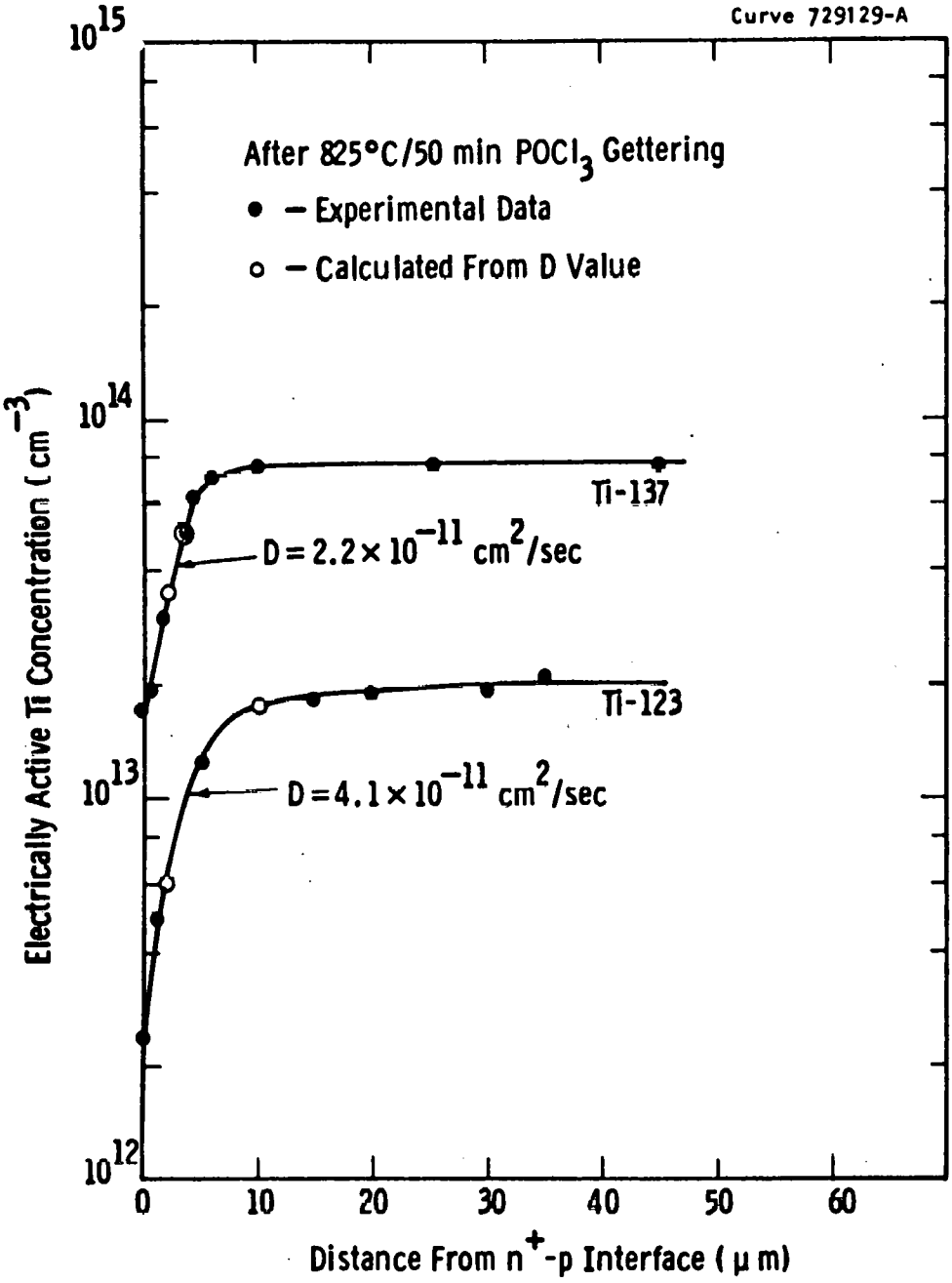

Figure 33 Electrically active impurity profile formed by an 825°C $POC\ell_3$ gettering of Ti wafers

Qualitatively, the two profiles in Figure 33 are very similar; to evaluate quantitatively the difference in the profiles, we fit the experimental data to a model which assumes that diffusion of Ti out of the specimen to the wafer surface prevails during gettering. This model, described in detail earlier,[3] uses a one dimensional diffusion equation to describe the diffusion process:

$$\frac{\partial N(x,t)}{\partial t} = D \frac{\partial^2 N(x,t)}{\partial x^2} \qquad (42)$$

The equation has a general solution given by

$$N(x,t) = (A \sin \alpha n + B \cos \alpha x) \exp (-\alpha^2 Dt) \qquad (43)$$

where $N(x,t)$ is the impurity concentration as a function of distance from the center of the wafer and t is the time of the gettering process. D is the diffusion constant for the impurity in solid silicon. It was previously shown that, with appropriate boundary conditions, two solutions for this equation can be derived. Both solutions are infinite series; the solution chosen for computation is that which converges more rapidly for specific values of D and t. N_o, the experimentally determined saturation value of the impurity concentration after gettering, and N_s, the impurity concentration at the surface, are used as two boundary conditions to obtain a numerical value of the diffusion constant.

In Figure 33 the open circles denote the calculated data fit to this out-diffusion model. Clearly, agreement with experiment is very good. The value of D equal to 2.2×10^{-11} cm^2/sec for Ti-137 Ingot and $4.1 \times 10^{-11} cm^2/sec$ for Ingot 123 provided the best fits to the data. Within the accuracy of experiments these are reasonably close, suggesting that out-diffusion process is not appreciably influenced by the initial impurity concentration in the bulk.

If the observed Ti profiles form by a diffusion mechanism, then we expect the process to be thermally activated and the temperature dependence of the diffusion constant to be described by an equation of the form

$$D = D_o \exp(-E/kT) \qquad (44)$$

where E is the activation energy.

We systematically evaluated the Ti concentration profiles formed in wafers subjected to $POCl_2$ gettering for 50 min at various temperatures in the range 825 to 1100°C. Again, the concentration profiles of electrically active Ti are determined by first removing the n^+ layer from each wafer and then etching steps into the silicon followed by DLTS measurement on a Schottky barrier diode fabricated on each step. The fit of this data, Figure 34, to the out-diffusion model gives diffusion constants of 4.1×10^{-11} cm^2/sec, $1.8\times10^{-10} cm^2/sec$, and 1.4×10^{-9} cm^2/sec at 825°C, 900°C, and 1100°C, respectively.

An Arrhenius plot of the diffusion constant as a function of 1000/T, Figure 35, has a slope of 8.33 which is equal to $\frac{E}{2.3\times1000\times K}$ from equation 44. This gives an activation energy E = 1.66eV. Substituting this value of E in equation 44 gives $D_o = 1.2\times10^{-3}$ cm^2/sec. Equation 44 for Ti impurity can then be rewritten as

$$D = 1.2\times10^{-3} \exp(-1.66eV/kT)\, cm^2/sec. \qquad (45)$$

Boldgrev et al.[33] found the activation energy for Ti diffusion to be 1.5eV and $D_o = 2\times10^{-5}$ cm^2/sec by diffusing a radioactive isotope of Ti into silicon. Our activation energy is in good agreement with Boldgrev's value. However, D_o differs by almost two orders of magnitude, a feature we have as yet not explained but which may be related to differences in experimental conditions.

The facts that (a) Ti profiles fit the out-diffusion equation very well, (b) diffusion constants at various temperatures follow the first order diffusion equation $D = D_o \exp(-E/kT)$, and (c) the activation energy agrees fairly well with the literature's values all support our initial hypothesis that the gettering mechanism of grown-in impurities, particularly Ti, is diffusion limited. The results further indicate that, in principle, silicon can be doped with Ti by diffusion in the temperature range 1000-1250°C with diffusion annealing periods of the order of 100 hrs.

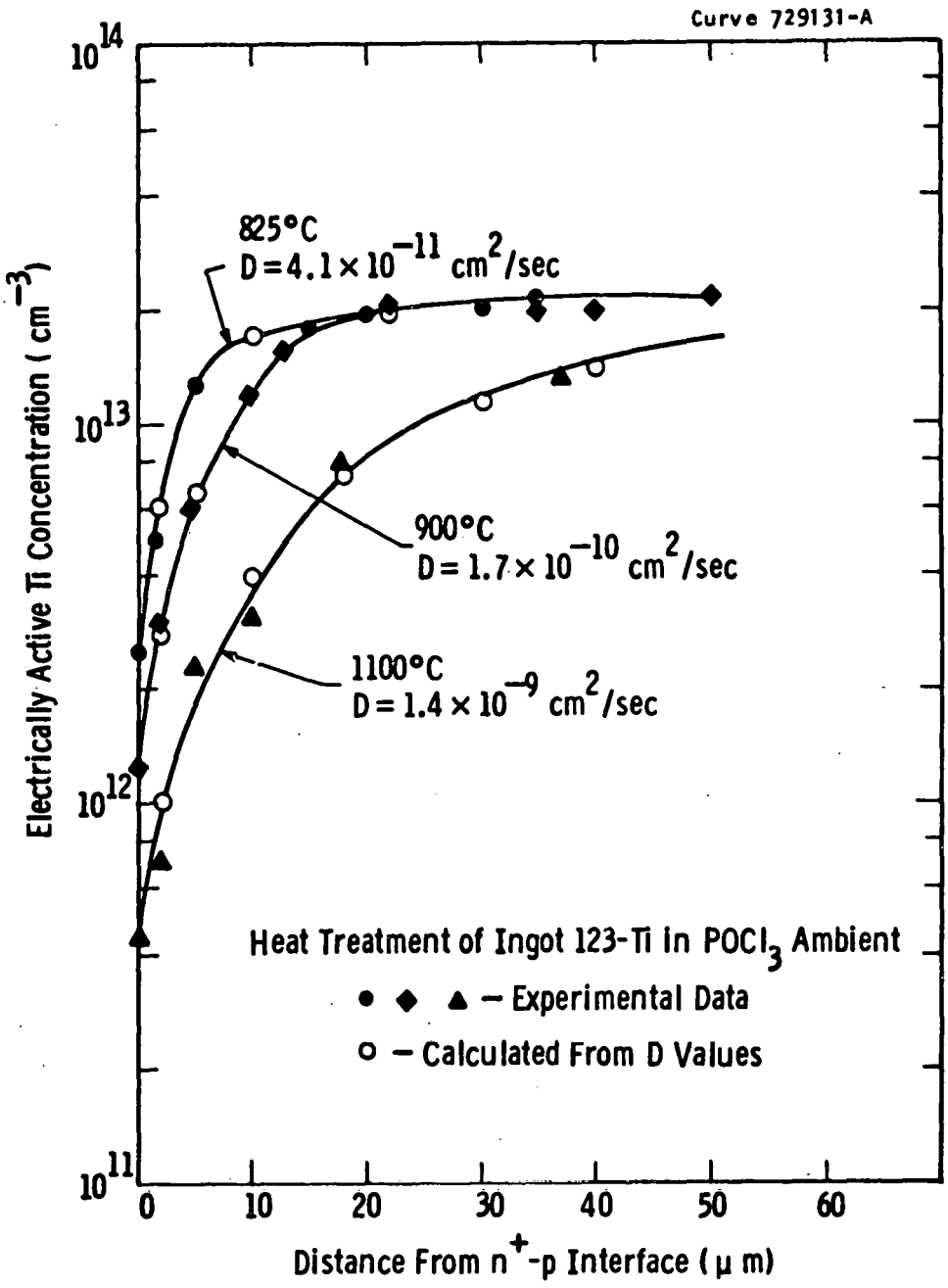

Figure 34 Electrically active Ti concentration profiles following 50-min $POCl_3$ gettering at several temperatures

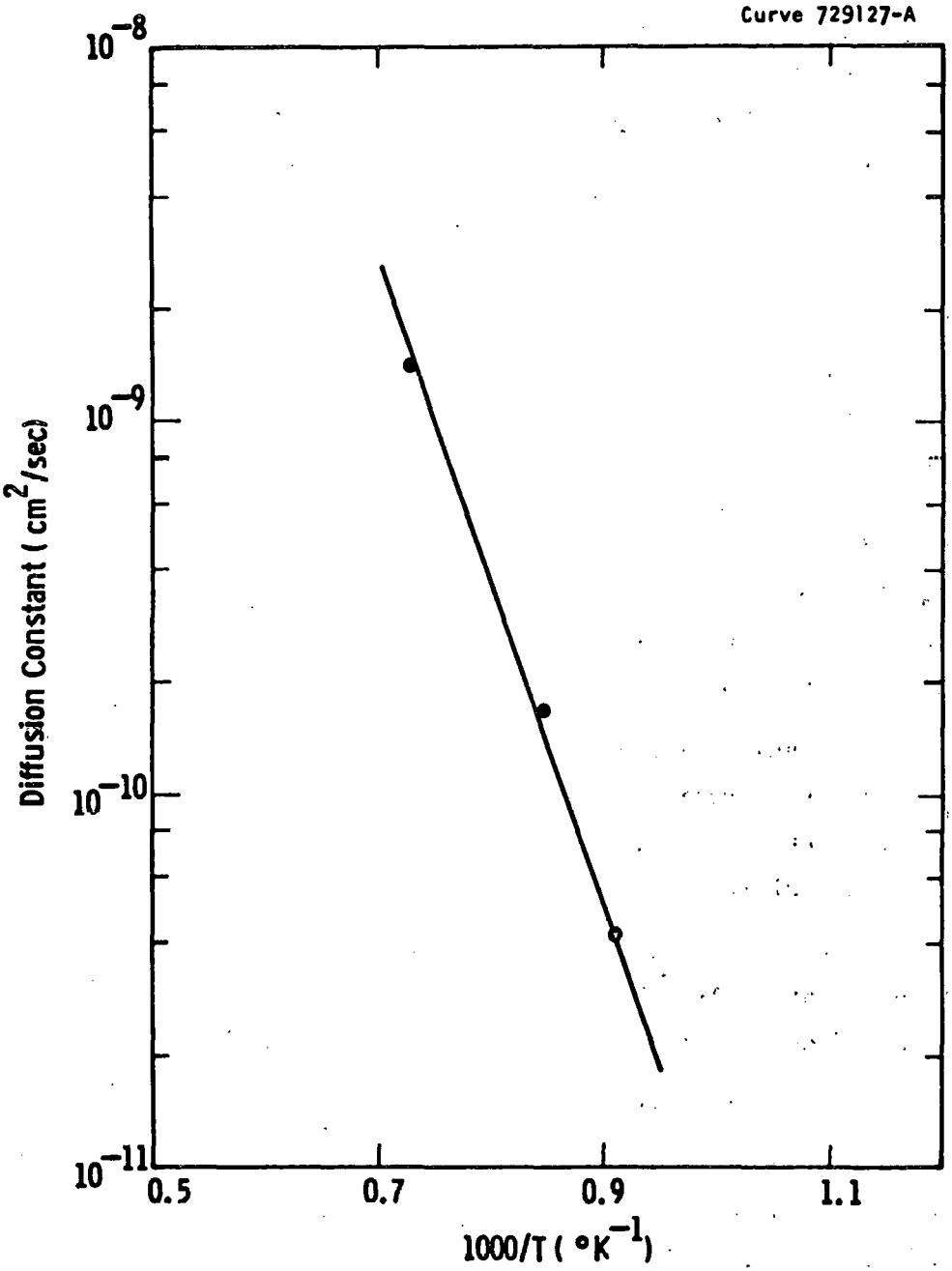

Figure 35 Variation of Ti diffusion constant with inverse temperature

3.8.1.3 Gettering of Polycrystalline Silicon

Recently, our studies of HCℓ and $POCℓ_3$ gettering have been extended to impurity-doped polycrystalline silicon. In general, the results conform very closely to those for the same impurities in single-crystal silicon (reference 3, vol. 2), although cell efficiencies are further impacted by the presence of grain boundaries in the devices.

The effects of $POCℓ_3$ gettering for periods of one hour at temperatures of 950°, 1000°, and 1100°C are illustrated in Figure 36. The data indicate that titanium and vanadium indeed can be gettered from polycrystalline silicon, resulting in an increase in cell efficiency. However, the efficiency of cells made with polycrystalline material will still be low relative to single-crystal material. As noted above, molybdenum diffuses only very slowly in silicon; this property is reflected in the data of Figure 36, where it is apparent that molybdenum is not gettered to any observable extent from polycrystalline silicon under these test conditions.

The results of HCℓ gettering for one hour at 1000° or 1100°C, respectively, is illustrated in Figure 37. Again, the more rapidly diffusing elements titanium and vanadium are effectively gettered from polycrystalline silicon, while slower diffusing molybdenum is not.

Clearly, while gettering can raise the efficiency of polycrystalline solar cells, the absolute efficiency values still remain well below those of comparable single-crystal devices.

3.8.1.4 Gettering by Ion Implant Damage

We found previously that damage gettering by a lapped surface on the back side of solar cell wafers was not effective in enhancing the effect of HCℓ gettering.[3] Because the damage induced by back-surface lapping is both difficult to quantify and to reproduce accurately, a more easily controlled damage method, back-surface ion-implant damage, was chosen for further investigation.

Curve 726580-A

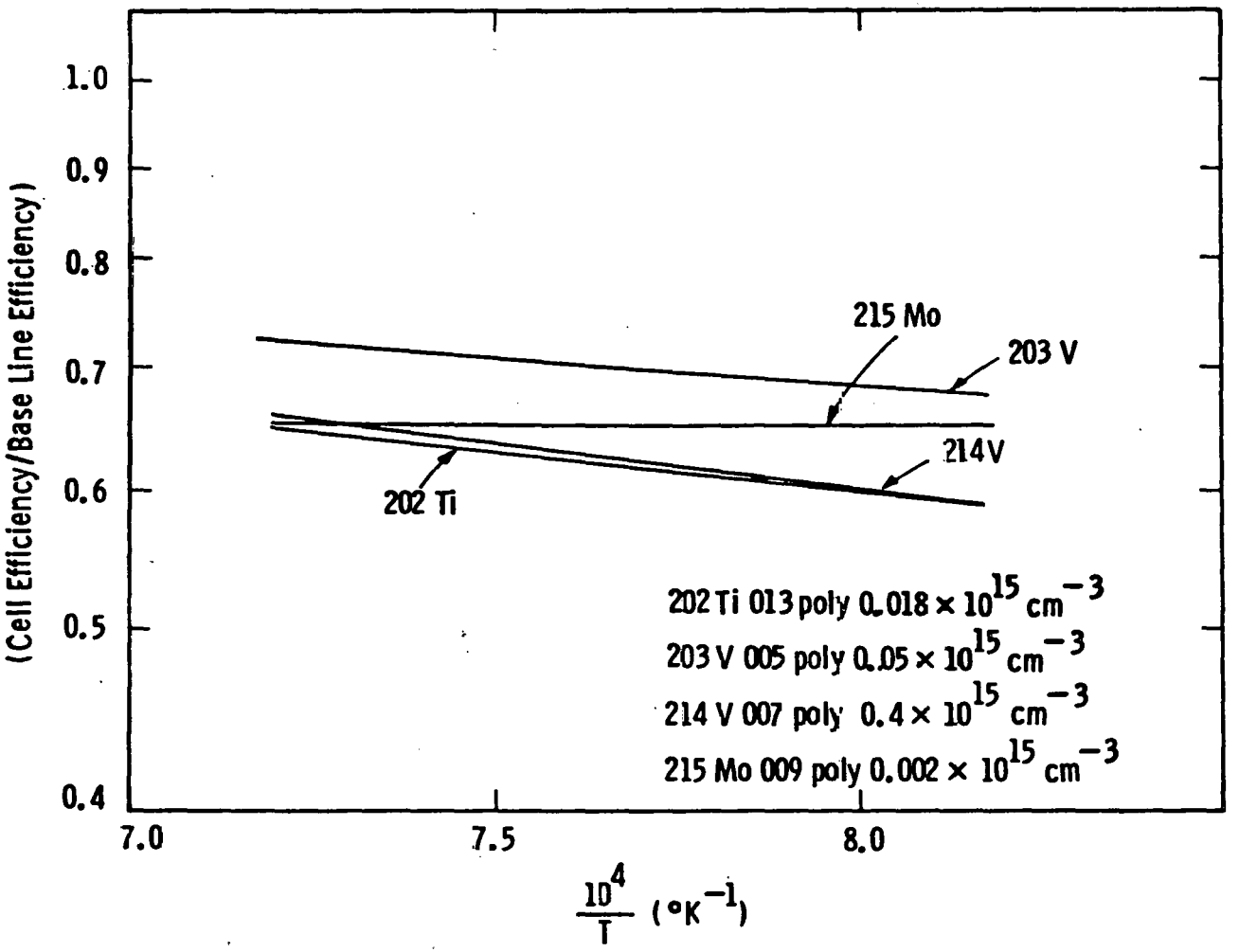

Figure 36 Gettering of titanium, vanadium, and molybdenum from Polycrystalline Silicon by $POCl_3$ treatment at 940, 1000, and 1100°C

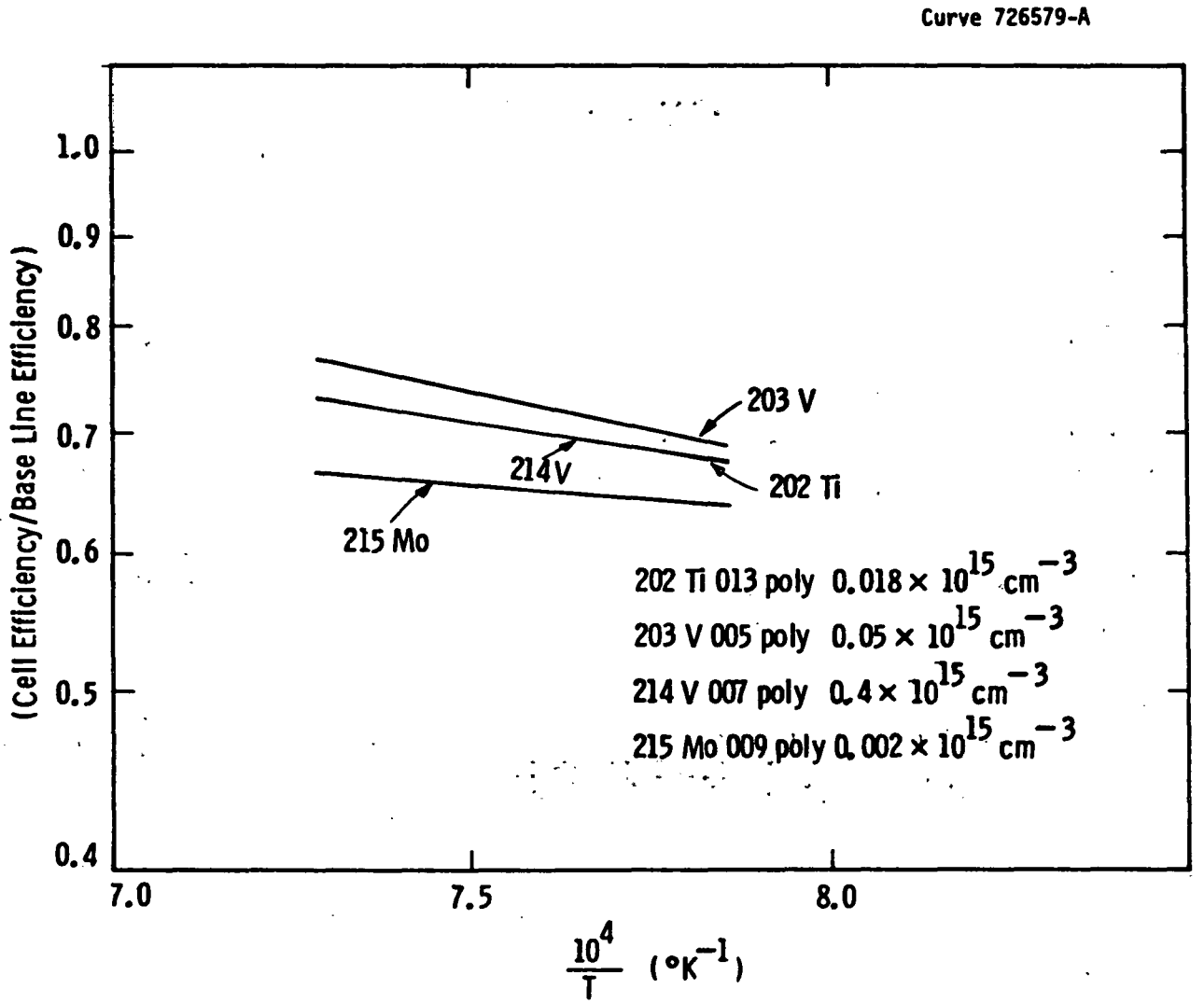

Figure 37 Gettering of titanium, vanadium, and molybdenum from polycrystalline silicon by HCℓ treatment at 1000 and 1100°C

Two impurities, copper and titanium, representative of fast and slowly diffusing elements in silicon, were made the test vehicles for these studies. Wafers containing the two impurities were damaged on their back sides by argon ion implantation. The ions were implanted at 100 keV to a dose level of 1×10^{15} cm^{-2}. Some wafers were simply annealed at 1100°C in nitrogen to assess the gettering capability of back-surface damage alone; others were further gettered with HCℓ at 1000°C and 1100°C, or with $POCℓ_3$ at 950°C, 1000°C, and 1100°C. Gettering times were always for one hour. Following the thermochemical gettering step, the HCℓ-gettered wafers and the "damage only"-gettered wafers were processed to remove surface oxides. The $POCℓ_3$-gettered wafers were chemically etched to remove the phosphorus-doped surfaces formed during the gettering process. All wafers were then processed to form solar cells according to our standard process sequence.[3] The results of the experiment are depicted in Figures 38 through 41.

Copper diffuses rapidly through silicon.[3] In solar cells its primary effect, unlike that of most heavy metals, is to cause efficiency degradation by increasing junction leakage rather than by reducing minority-carrier lifetime. The mechanism by which this degradation takes place is believed to be the precipitation of copper atoms at defect sites within the silicon, causing electric field concentrations in the junction region and occasionally shunting the junction with low-resistance paths.[1-3] Thus, the effects of any high-temperature treatment of copper-containing silicon can be expected to be complex.

Figures 38 and 39 illustrate that copper-containing silicon as grown can be fabricated into solar cells the efficiencies of which are very close to those of devices fabricated on pure silicon. A high-temperature process, such as ion damage gettering alone, decreases cell efficiency perhaps because it permits more copper precipitation to take place, while the ion-damaged region is not very effective in removing copper atoms from the junction region.

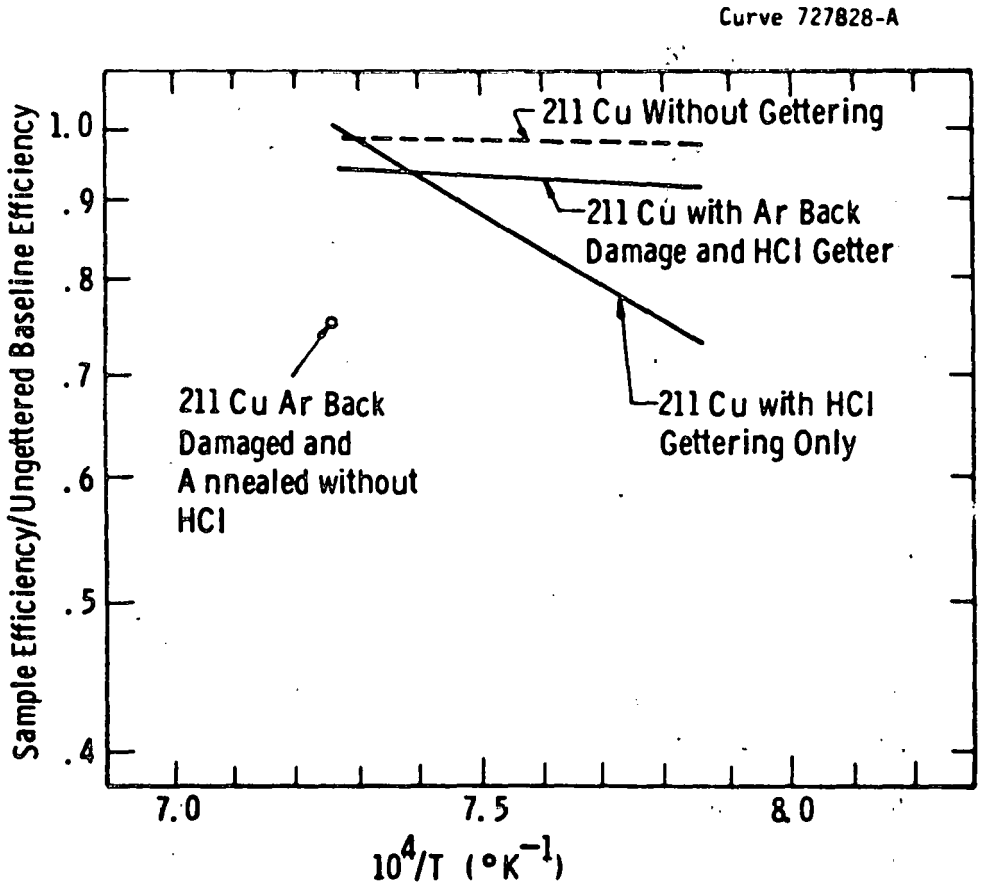

Figure 38 Effects of HCℓ and ion-implant damage gettering on solar cell material containing copper

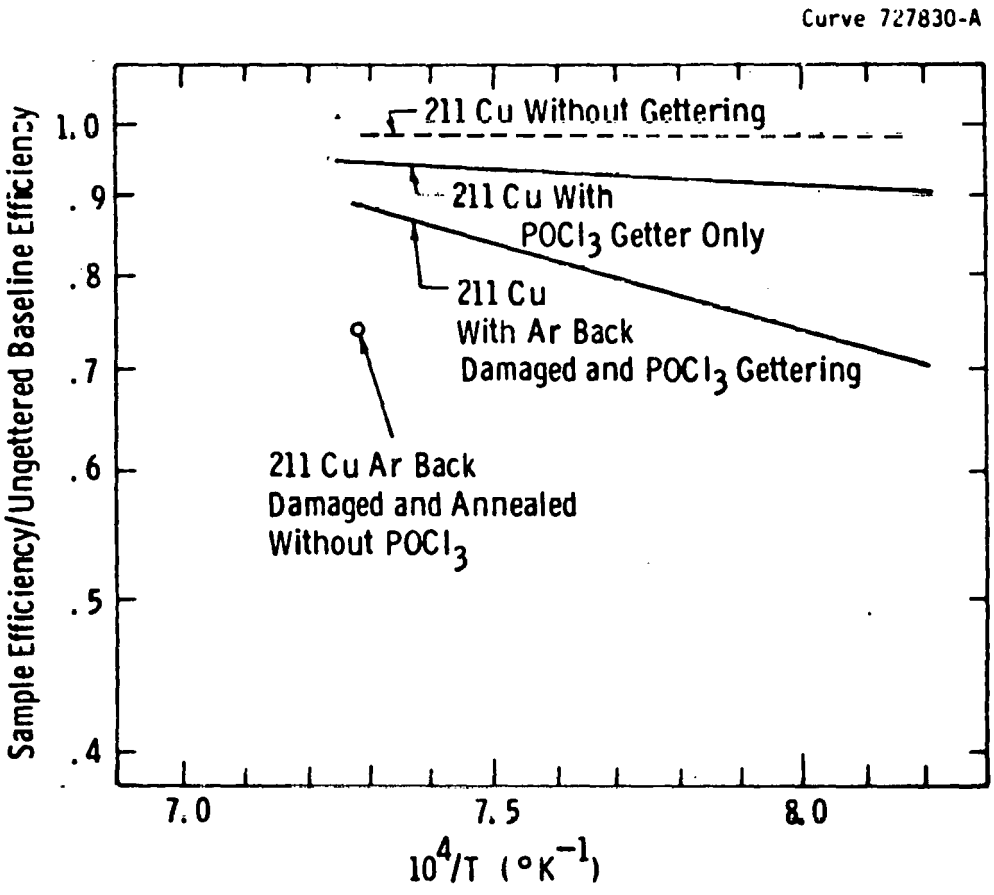

Figure 39 Effects of $POC\ell_3$ and ion-implant damage gettering on solar cell material containing copper

$POCl_3$ or HCl gettering, either by themselves or in combination with ion damage gettering, are more effective in raising cell efficiency than is ion damage gettering alone, but on the basis of our data it is doubtful that any of these gettering processes can produce better material than the original as-grown silicon.

As we pointed out earlier in this section, titanium diffuses fairly slowly through silicon. Its presence in silicon causes minority-carrier traps which reduce the lifetime in both n and p-type material. The data in Figures 40 and 41 show that ion damage gettering by itself is effective in raising the efficiencies of titanium-containing silicon solar cells. They also show that the improvement due to ion damage gettering is small in comparison to what can be achieved with HCl or $POCl_3$ gettering.

The data presented here show that, at least for copper and titanium impurities in silicon, ion-implant damage gettering is not as effective for improving solar cell efficiency as are the HCl or $POCl_3$ treatments we have previously studied. In the case of copper, high-temperature processing appears to degrade the material; the original quality of the material can be regained only by prolonged gettering at high temperature.

In contrast to the results for Cu, all of the treatments improved the efficiencies of the Ti-doped cells compared to the ungettered condition. Based on these and earlier results our conclusions are:

(1) $POCl_3$ and HCl gettering raise the solar cell efficiency by 1 to 1.5% (absolute) compared to the ungettered case; the improvement is greatest at the highest gettering temperature, 1100°C.

(2) The combined treatments, Ar damage plus HCl or $POCl_3$, also improve cell efficiency but not as much as HCl or $POCl_3$ alone.

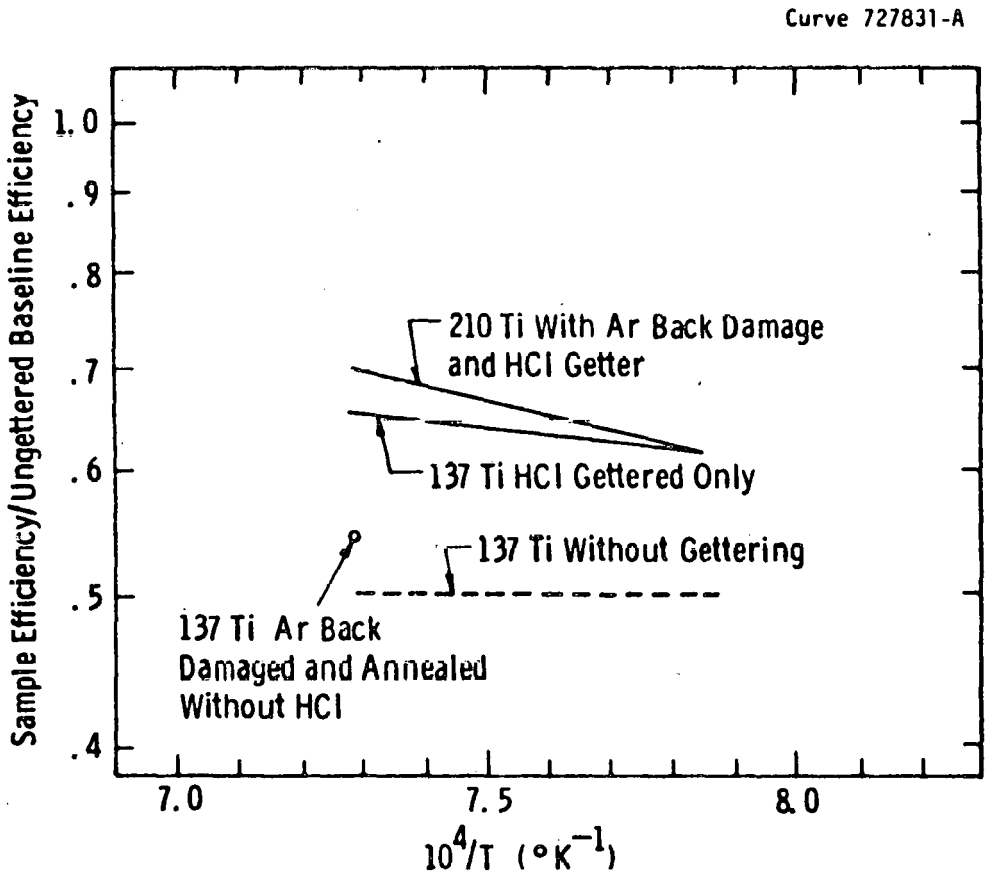

Figure 40 Effects of HCℓ and ion-implant damage gettering on solar cell material containing titanium

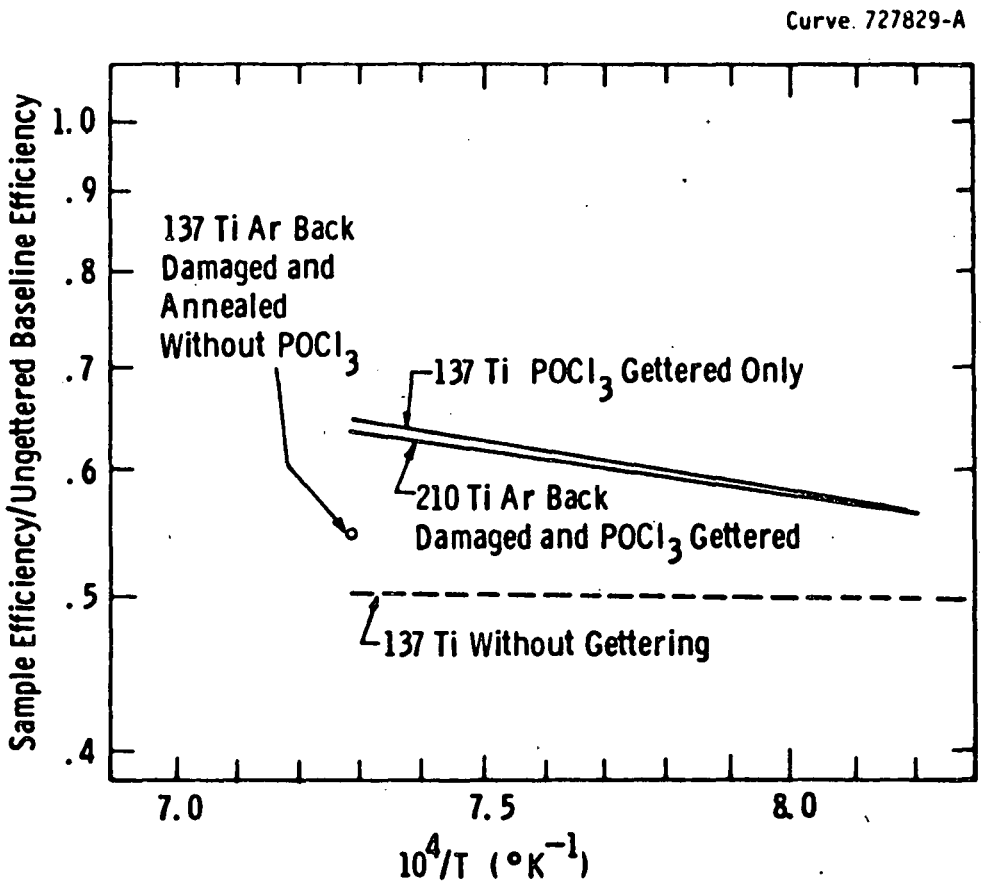

Figure 41 Effects of $POC\ell_3$ and ion-implant damage gettering on solar cell material containing titanium

(3) Ar damage plus annealing at 1100°C (no $POCl_3$ or HCl) produces a small but real improvement in cell efficiency compared to the untreated devices.

(4) The HCl-based treatments appear more effective overall than those employing $POCl_3$.

3.8.2 Ion Implantation Junction Formation in Impurity-Doped Cells

Some studies have concluded that solar cell junction formation by ion implantation may offer significant cost savings over diffusion processes.[34] Since it has been shown that high-temperature processes (and particularly $POCl_3$ gettering) affect the efficiency of impurity-containing cells, it is important to evaluate separately the influence of impurities in cells fabricated without a conventional $POCl_3$ junction-forming diffusion.

In this investigation, wafers from six impurity-doped ingots as well as wafers from a baseline ingot were ion implanted with phosphorus for comparison with similar wafers in which the front junctions were formed by $POCl_3$ diffusion. The experimental ingots are listed in Table 19.

With the cooperation of JPL staff, wafers were implanted at the Motorola facility with non-mass-analyzed phosphorus. Target parameters for this process were a fluence of 2×10^{15} atoms/cm^2 at 10 keV. The wafers were implanted at an angle 10° off the <111> crystal axis.

After implantation, the wafers were annealed in nitrogen for 30 min. each at 550, 850, and 550°C, a sequence previously shown effective for activating the dopant. Following the anneal, the measured sheet resistivity of the n^+ layer was approximately 60 ohms per square, a value similar to that obtained in our normal diffusion sequence.[1]

Experimental cells were fabricated by our standard process (except for junction diffusion) including mechanical lapping of the back surface. Measured efficiencies of the ion-implanted cells are compared to those of diffused cells in Table 20. In each case, in order to

TABLE 19

INGOTS USED IN IMPLANTED JUNCTION EXPERIMENTS

INGOT ID	IMPURITY	BULK IMPURITY CONCENTRATION (10^{15} cm^{-3})
W016	Fe	0.4
W068	Cr	1.0
W135	Fe	0.78
W198	Baseline	-
W209	Ti	0.02
W210	Ti	0.10
W211	Cu	1.8

Table 20

COMPARISON OF THE EFFICIENCIES OF ION-IMPLANTED CELLS TO THOSE OF DIFFUSED CELLS

Ingot ID	Ion Implanted			Diffused		
	η Avg.	Std. Dev.	% of Diffused Baseline	η Avg.	Std. Dev.	% of Diffused Baseline
016 Fe	8.34	0.65	87.3	9.08	0.78	86.4
068 Cr	6.80	0.29	71.2	7.91	0.33	77.8
135 Fe	5.82	1.22	61.0	7.76	0.18	78.7
198 Base	9.17	0.61	96.0	9.55	0.10	100
209 Ti	4.69	0.58	49.1	5.65	0.27	56.9
210 Ti	4.38	0.23	45.9	4.68	0.21	50.1
211 Cu	8.60	0.52	90.1	9.55	0.28	99.3

eliminate any influence due to processing variables, a comparison is made between impurity-doped cells and baseline cells which were processed at the same time.

Inspection of the data shown in Table 20 indicates that, except for the more highly doped Fe material, the cell efficiencies achieved by ion implantation are slightly lower than those achieved by comparable cells with diffused junctions. This relationship is illustrated in Figure 42.

These data may be interpreted as showing that some impurites are gettered during the $POC\ell_3$ junction diffusion process and that no such gettering accompanies the ion implantation and anneal sequence. On the other hand, the data may merely indicate that the ion implantation and anneal conditions have not yet been optimized for solar cell junction formation in contaminated silicon. However, the performance differences found in our preliminary studies warrant further examination of this question.

3.8.3 Response of Impurities to Heat Treatment

In order to distinguish whether the impurity response to $POC\ell_3$ and $HC\ell$ gettering were primarily temperature dependent or ambient dependent, we heat treated the metal-contaminated wafers in N_2 at 825°C for 50 min without any $POC\ell_3$ or $HC\ell$. After heat treatment, DLTS measurements were performed as before to determine the active impurity concentration profiles.

The results of this experiment are shown in Figure 43. The electrically active concentration in ingots W077Mo, W123Ti, and W181Cr prior to heat treatment was $4x10^{12}$ cm^{-3}, $4x10^{13}$ cm^{-3}, and $1x10^{14}$ cm^{-3}, respectively. As observed in the case of $POC\ell_3$ gettering, the N_2 heat treatment produces a profile-like distribution for Ti, the Cr concentration is reduced below the DLTS detection limit, and there is no appreciable change in the initial Mo concentration or distribution. It is not yet clear why the N_2 treatment promotes a gettering-like behavior. One possible source for gettering could be residual surface damage. Although the wafers were chemically polished and with no intentional

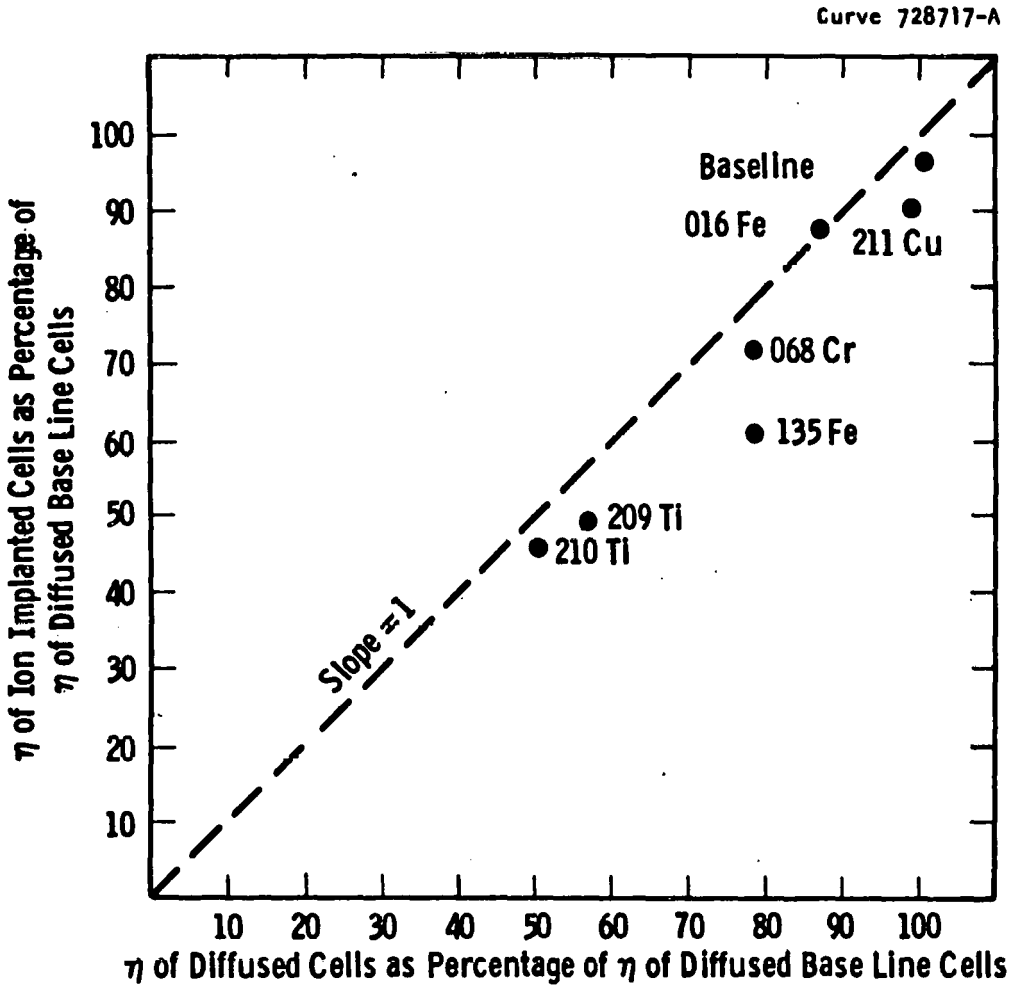

Figure 42 Relationship between the relative efficiencies of impurity-doped cells the front junctions of which were fabricated by phosphorus ion implant and phosphorus diffusion

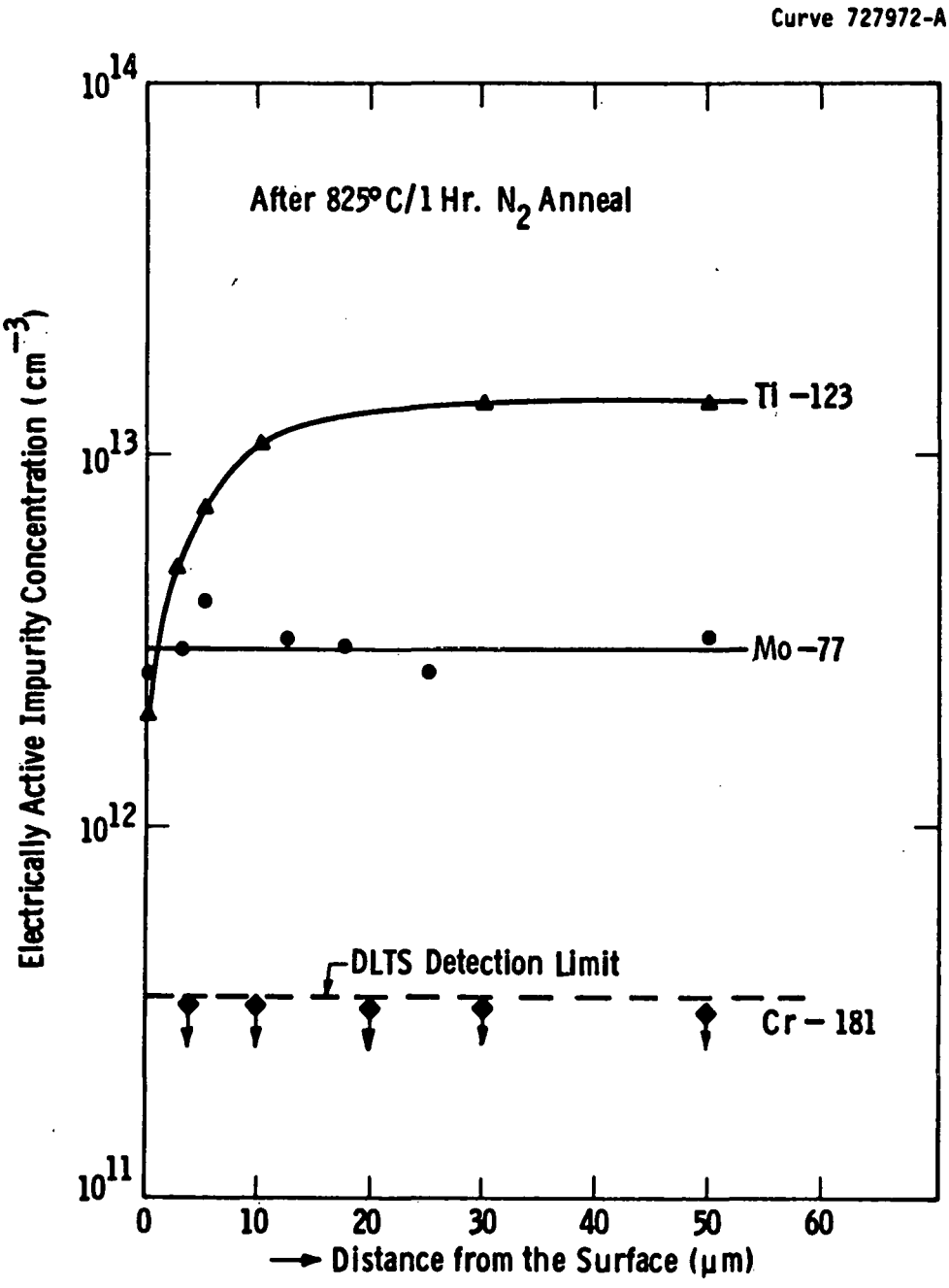

Figure 43 Change in electrically active impurity concentration after an 825°C/1-hour N_2 anneal

damage, the surface may not be completely damage-free and could provide a sink for impurities when the impurities reach surface sites, possibly by vacancy-aided diffusion, and they are no longer electrically active. It is not clear how N_2 could react (as the Cℓ in $POCℓ_3$ or HCℓ does) with the impurities on the surface to reduce the surface concentration and to produce a concentration gradient. (Contamination of N_2 by a reactive species like O_2 is a possibility, albeit an unlikely one.)

In order to compare the extent of gettering due to the $POCℓ_3$, HCℓ, and N_2 heat treatments, we have replotted in Figure 44 the respective Ti impurity profiles produced after an 1100°C/50-min heat treatment in each ambient. It is striking to note that within experimental error, each ambient produces the same gettering response, i.e., there is no difference in the Ti concentration profile with ambient condition. This indicates that it is the treatment temperature and not the chemical species in the gas phase which determines the profile, a fact consistent with our hypothesis that gettering of impurities in silicon is a diffusion-limited process. As long as there is an appreciable sink for impurites at the wafer surface ($POCℓ_3$, HCℓ, N_2, or surface damage), one should observe the same profile if bulk impurity atoms migrate to the surface by a diffusion process because the rate of diffusion depends only on temperature and not the ambient.

The ambient conditions may influence the surface concentration but if the surface concentration is at least half an order of magnitude below the bulk concentration, then its influence on the profile in the bulk becomes negligible. This is evident from the data in Table 21. Here we have calculated the Ti concentration at a location 4 μm below the silicon surface as a function of surface concentration. The diffusion conditions used for these calculations were 50 min. at 825°C, and the bulk impurity concentration was assumed to be $7.6 \times 10^{13} cm^{-3}$ (Ingot Ti-137). The calculations clearly indicate that even when the surface concentration is varied from 0 to 10^{12} cm^{-3}, the concentration at a 4-μm depth remains about 5.1×10^{13} cm^{-3}. If surface concentration is raised to 5×10^{13} cm^{-3}, there is only a very slight increase in the concentration at 4 μm to 5.0×10^{13} cm^{-3}.

TABLE 21

CALCULATED Ti CONCENTRATION 4 μm BELOW THE n+p INTERFACE AFTER 825°C/50 MIN $POCl_3$ TREATMENT WHEN THE Ti CONCENTRATION AT THE n+p INTERFACE IS VARIED.

In this out-diffusion model, calculations of bulk Ti concentration are assumed to be 7.6×10^{13} cm^{-3} and $D = 2.2 \times 10^{-11}$ cm^2/sec.

Ti Concentration at n+-p interface (cm^{-3})	Ti Concentration 4 μm below the n+-p Interface (cm^{-3})
0	5.07×10^{13}
10^{12}	5.10×10^{13}
10^{13}	5.40×10^{13}
5×10^{13}	6.0×10^{13}

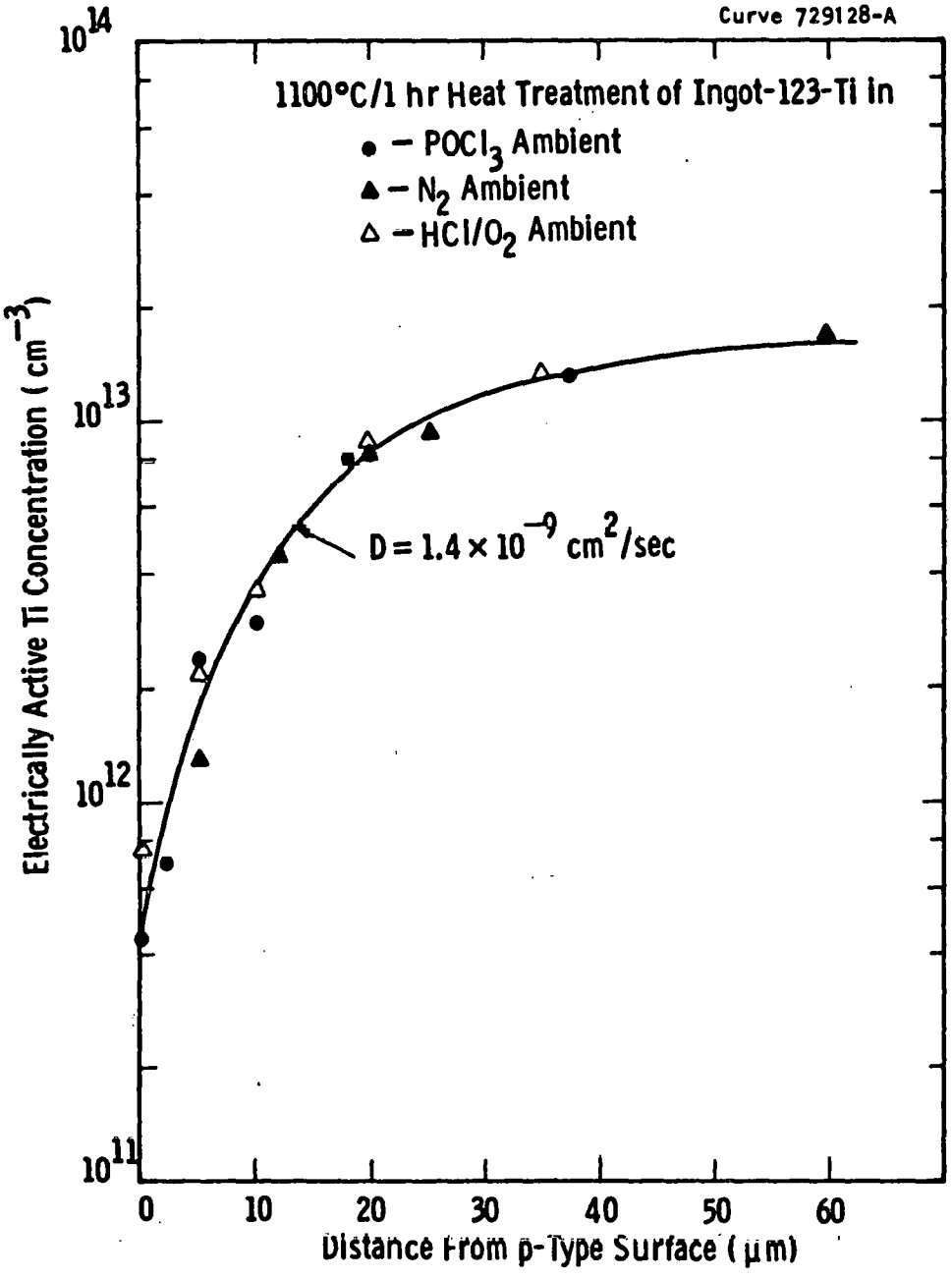

Figure 44 Electrically active Ti profile produced after an 1100°C treatment in various ambients

The data in Figure 44 indeed show that the surface concentration in all three ambients, $POCl_3$, HCl, and N_2, was more than an order of magnitude below the bulk concentration and this is why all three profiles are similar. For these conditions only the temperature and bulk concentration govern the impurity concentration profile.

Heat treatment of Cr-doped silicon above 800°C in $POCl_3$, HCl, or N_2 results in a substantial loss of Cr activity, e.g., Figure 32 (in all cases the active Cr concentration falls below the DLTS detection limit of $\sim 3.5 \times 10^{11}$ cm^{-3}). Thus, to obtain diffusion data for Cr in silicon, we heat treated the Cr-doped wafers at much lower temperatures, 100-600°C in a N_2 ambient. The treatment time was one hour in all cases. Following heat treatment, 30-mil diameter Schottky barrier diodes were fabricated to detect the active Cr at the wafer surface via DLTS. The results of these experiments are illustrated in Figure 45. Even after the 100°C treatment, we detect about a factor of 5 loss in the electrical activity of Cr at the surface. After the 400°C treatment a reduction of two orders of magnitude in electrical activity was observed.

In common with the $POCl_3$ gettering experiments, nearly a complete loss of Cr electrical activity occurs after a 600°C heat treatment. These data, therefore, also suggest that the loss of Cr electrical activity during $POCl_3$ gettering is primarily an effect of thermal treatment, not the particular chemical ambient.

To gain a clearer idea of the mechanism by which the loss of electrical activity occurs, we determined the active Cr concentration profile in the silicon following a 300°C N_2 treatment. Figure 46 illustrates the formation of an impurity profile during the treatment. The Cr concentration profile extends through the first 50 μm of the surface region suggesting that, like Ti, the decrease or loss of electrical activity in the bulk after heat treatment occurs by out-diffusion of the metal impurity toward the surface, and not by precipitation or mechanisms which would reduce the electrical activity uniformly throughout the bulk.

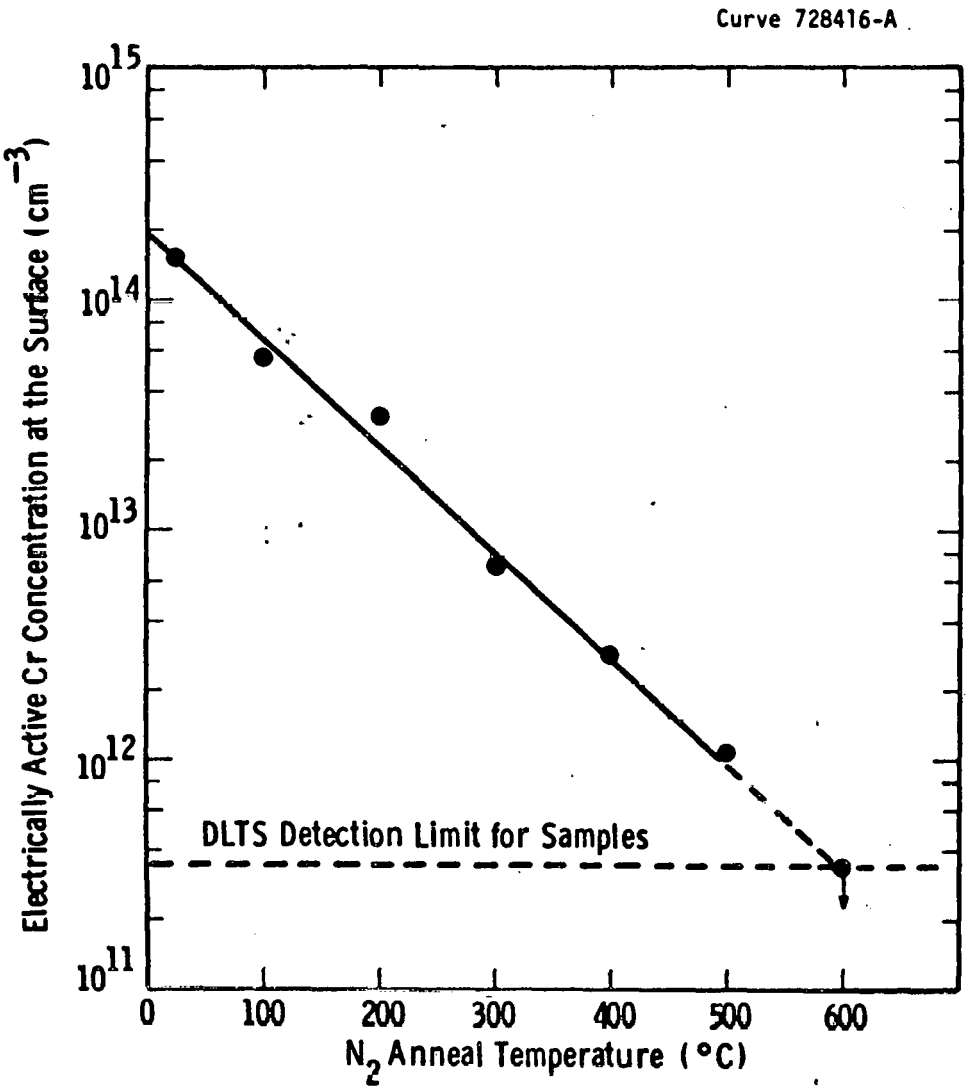

Figure 45 Variation in electrically active Cr concentration at the wafer surface as a function of N_2 treatment temperature

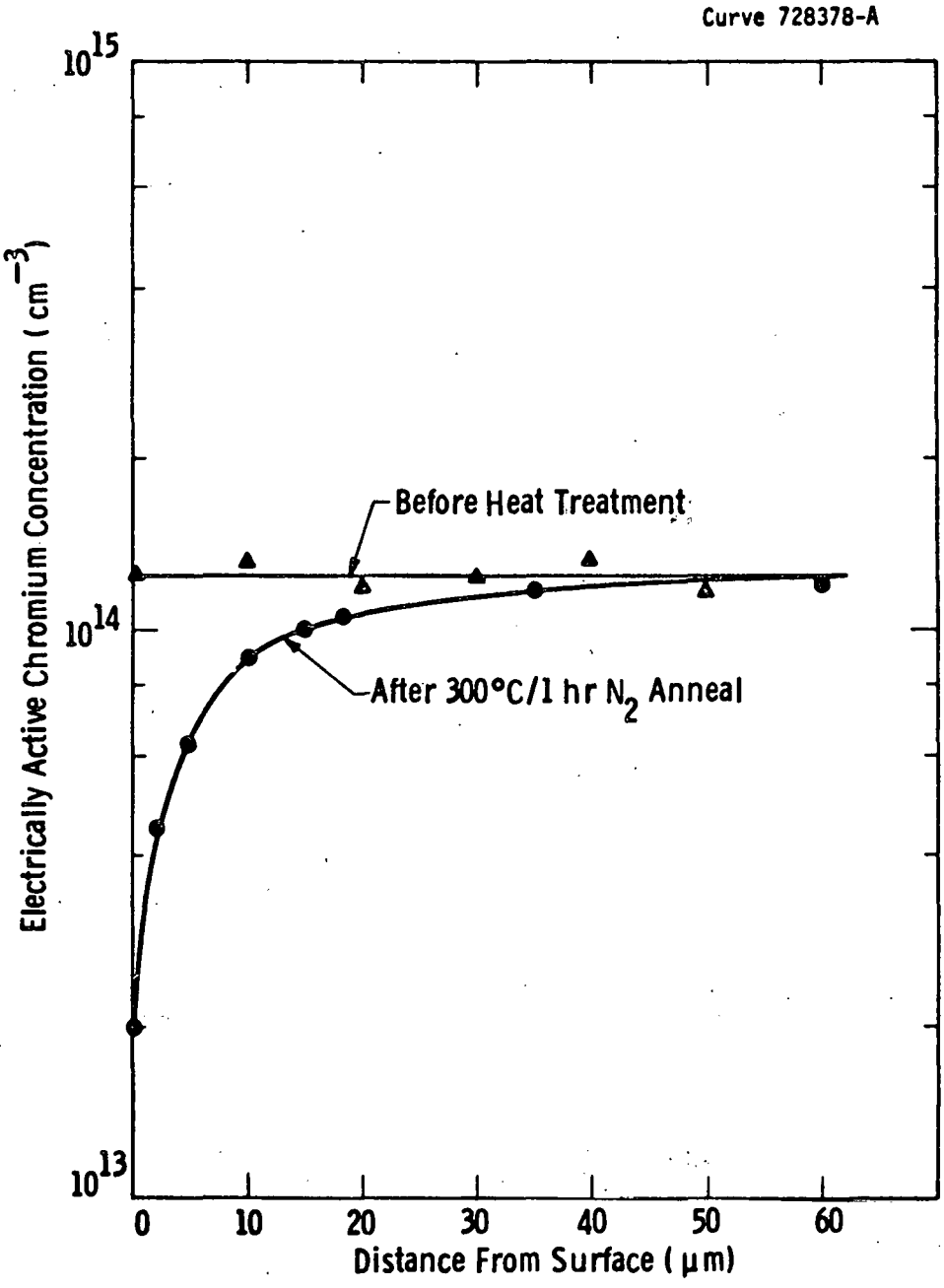

Figure 46 Variation in electrically active Cr concentration with depth in a silicon wafer treated at 300°C in N_2

The data in Figure 46 were also fitted to our out-diffusion model and give excellent agreement with the experimental data when a diffusion constant of 1.33×10^{-10} cm^2/sec is chosen. We obtain a similar diffusion constant for Ti at 900°C, which confirms our belief that Cr is a very rapidly diffusing species compared to Ti.

3.8.4 Summary

Overall, our data indicate that gettering and thermal treatments predominantly affect the distribution and concentration of electrically active impurities via a diffusion-limited process in the silicon wafer. Impurities which degrade cell performance via lifetime reduction and which diffuse rapidly in silicon (e.g., Fe or Cr) can be successfully gettered with significant improvements in cell performance. Elements which diffuse slowly (Ti, V) can be thermally deactivated with an improvement in cell efficiency, but not in a practical time-temperature process regime. For the most slowly diffusing species (Mo), no change in active-impurity concentration or distribution was observed at the highest temperatures tested (1250°C). If a suitable surface impurity sink is provided, thermal treatments alone apparently induce gettering. Damage—mechanically induced or by argon ion implant — gives little advantage over the thermochemical treatments ($HC\ell$, $POC\ell_3$) themselves. Impurity-doped solar cells fabricated by phosphorus implant produce efficiencies somewhat lower than similar cells the front junctions of which were diffused.

3.9 Permanence of Impurity Effects

3.9.1 Background

Solar cell modules for terrestrial applications must have useful lives of 20 years or longer. The data in Section 3.5 outline the immediate effects of metallic impurities upon solar cell efficiency; in this section we consider the effects of representative impurities upon long-term solar cell operation, a knowledge of which is important in defining the utility of devices made from less-pure "solar grade" silicon.

Since it is intended to project behavior over periods of time which are extremely long compared to practical testing times, an accelerated aging technique is required. In our investigation, elevated temperature was used as the accelerating mechanism. The response to elevated temperature aging was modelled, and extrapolations were made to determine useful lifetimes at practical operating temperatures. In a separate set of experiments, electrical bias was also examined for its impact on impurity behavior.

The impurities chosen for this study represent elements which may be present in partially refined silicon (iron, copper, titanium, and molybdenum); elements which may be used in the construction of high-temperature processing equipment (molybdenum and niobium); and elements which may be used as electrical contacts and electrodes on solar cells (chromium, copper, silver, and nickel). Previous studies[22,23] have shown that these elements affect solar cell performance in different ways. Slowly diffusing elements like titanium and molybdenum affect cell performance predominantly through the formation of deep-level traps which reduce minority-carrier lifetime,[28] as does niobium, which has a very low solubility in silicon. Copper, a rapidly diffusing impurity, primarily affects the junction recombination current. Nickel, chromium, silver, and iron degrade both lifetime and junction properties to different degrees depending upon processing history and metal concentration.

3.9.2 Accelerated Aging Studies

Impurity-doped silicon wafers were junction diffused with $POCl_3$ at 850°C and were then aged at temperatures from 400 to 800°C for periods of time varying from ten minutes to 200 hours. After the aging period, solar cell fabrication was completed with cell-area definition and contact metallization.

Our standard cell design[3] was used for this investigation since simplicity, reproducibility, and insensitivity to minor process variations are important to yield reliable data.

Examples of the changes in cell efficiency observed at a single temperature and increasing time are illustrated in Figure 47 for several impurities.

We have assumed that in the initial stages, the cell performance change at a given temperature is linear with time, and that the degradation mechanism, being thermally activated, can be represented by the following relationship

$$\frac{1}{\eta_o}\frac{d\eta}{dt} = A \exp\ (-E_a/kT). \qquad (46)$$

$\frac{1}{\eta_o}\frac{d\eta}{dt}$ is the rate of change of efficiency normalized to the initial efficiency, A is a constant for a particular impurity, E_a is the activation energy of the process, k is Boltzmann's constant, and T is the Kelvin temperature. Measurement of $\frac{1}{\eta}\frac{d\eta}{dt}$ at various temperatures allows the determination of A and E_a so that expected behavior can be extrapolated to other temperatures and a "time to failure" can be predicted for any given temperature.

Experimentally determined values of A and Ea are given in Table 22. We have arbitrarily defined "time to failure" to be the time during which cell efficiency will decrease to nine-tenths of the original efficiency. Figure 48 shows predicted times to failure as a function of temperature. The shaded area in the figure is of practical importance. It includes temperatures up to 150°C and times up to 20 years. Time to failure for only a few elements fall in this region of the plot.

Results for copper and iron do not appear in Table 22 and Figure 48 because the aging studies showed that their effects are complex at the aging temperatures, and their behavior cannot be predicted on the basis of a single, thermally activated mechanism.

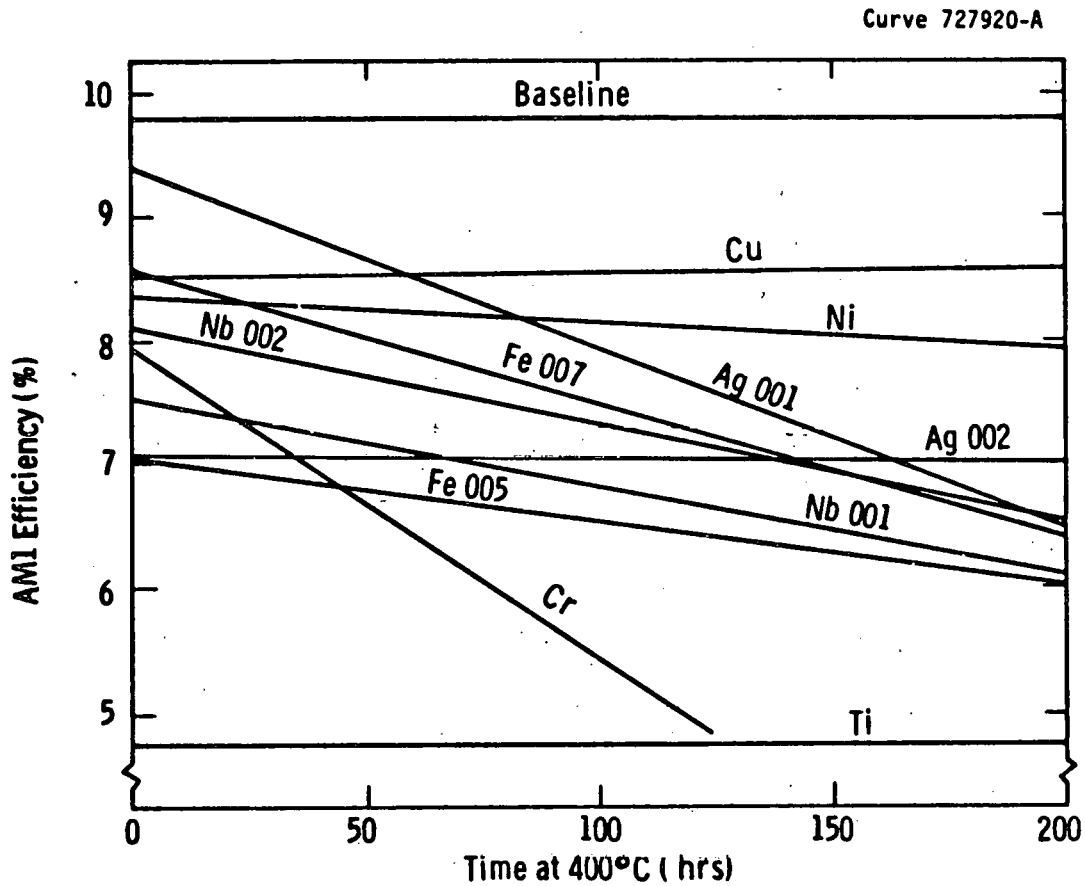

Figure 47 Effects of impurities and high-temperature aging upon the efficiency of solar cells

TABLE 22

CALCULATED PARAMETERS FOR $\frac{1}{\eta_o}\frac{d\eta}{dt} = A \exp(-E_a/kT)$

INGOT ID	IMPURITY CONCENTRATION (10^{15} cm^{-3})	η_o (%)	A (hr^{-1})	E_a (eV)
097-00	None	9.85	-3.58	1.35
072-Cr	0.4	7.93	-51.9	0.58
077-Mo	0.0042	7.30	-9.8×10^{6}	1.98
123-Ti	0.105	4.78	-4.0×10^{14}	3.97
135-Fe	0.78	7.76	---	---
166-Fe	1.06	8.41	---	---
167-Nb	<0.044	7.52	-450	0.79
183-Nb	<0.009	8.16	-310	0.77
192-Ag	2.20	9.30	-25.6	0.59
222-Ag	4.6	8.54	-14.9	0.63
211-Cu	1.0	8.54	---	---
221-Ni	8.2	8.38	-28.5	0.67

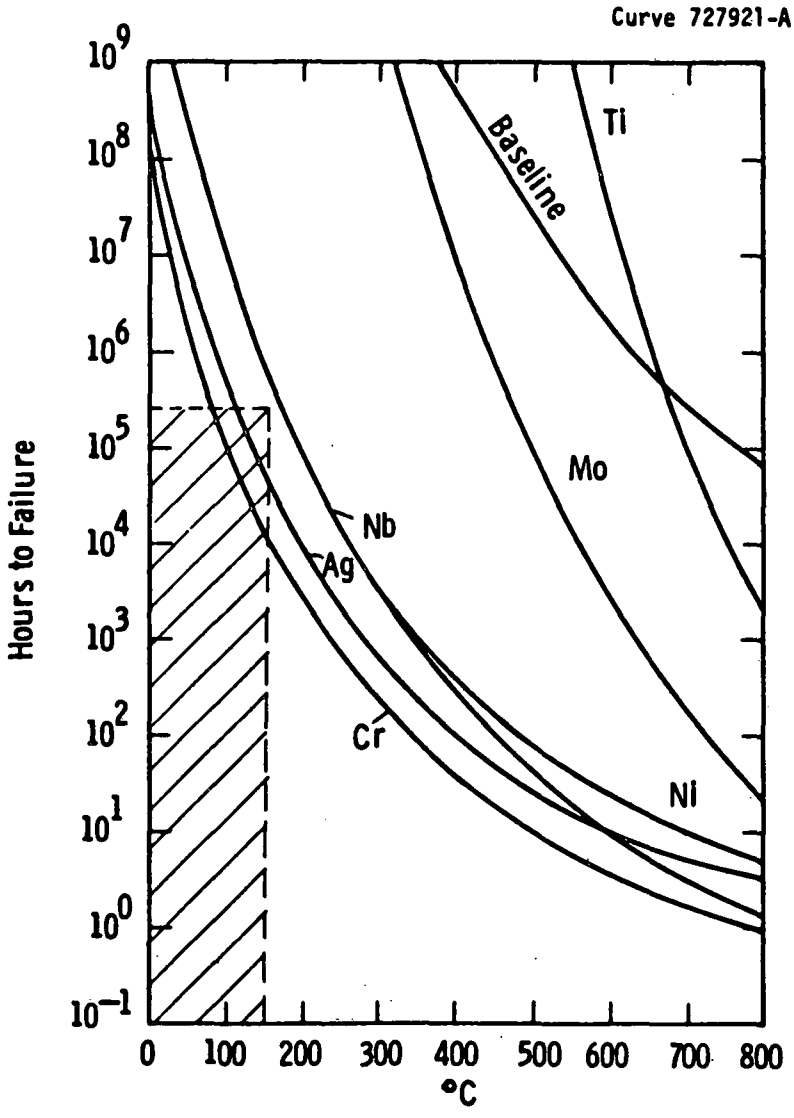

Figure 48 Predicted time to failure for solar cells containing various impurities, as a function of temperature

This phenomenological description of aging behavior can be interpreted and generalized by considering that the properties of silicon solar cells can be altered by the presence of metallic impurites in any of several ways. Electrically active impurities may form centers which reduce the minority-carrier diffusion length either by increasing the recombination rate or by reducing the minority-carrier diffusivity. Additionally, impurities may induce degradation at the contact interface or in the metallic contact itself. They may cause series or shunt resistance effects or may form precipitates and other junction defect phenomena which can cause excess current leakage.[22]

Impurity-induced carrier-trapping centers can be measured and characterized by deep-level transient spectroscopy (DLTS) measurements.[35] These measurements, made on as-grown silicon and upon silicon which has been aged at high temperature, can be used to quantify the trap-induced degradation mechanism. Junction degradation and shunt and series resistance effects can be detected by detailed dark and lighted current voltage measurements.

Much, but not all, of the observed behavior can be explained on the basis of the following model. During Czochralski ingot growth, the crystal cools rapidly enough to quench some impurity atoms in solid solution at a concentration higher than the equilibrium room-temperature value. The individual atoms in solution are electrically active as deep-level traps; those atoms which precipitate to form a second phase may not be active as traps, but when the precipitate is formed in the junction depletion region, the junction properties of the solar cell can be degraded.

Slowly diffusing elements such as molybdenum will be loss likely to agglomerate into precipitates during crystal cooling and the concentration of deep-level traps will be nearly equal to the metallurgical concentration of the metal. Rapidly diffusing elements such as chromium will be more likely to diffuse to precipitation sites and very few atoms will remain as deep-level centers (see section 3.7); therefore, the deep-level concentration will be much less than the metallurgical concentration.

During solar cell aging, the material continues to approach its equilibrium state as the concentration of deep levels associated with individual atoms decreases while the number and size of second-phase precipitates increases. The decrease in trap concentration will be pronounced for a rapidly diffusing element (such as chromium) and slight for a slowly diffusing element (such as molybdenum).

We hypothesize that the disappearance of deep levels is accompanied by an increase in the number and size of metallic precipitates. These precipitates, when they occur in or near the junction depletion region, will degrade the junction properties of the cell, resulting in increased junction generation current and reduced fill factors, effects which were observed in the aging studies.

The model implies that as a result of the decrease in trap concentration, the minority-carrier lifetime and the short-circuit current should increase with aging. This effect was not observed in the aging studies. Another phenomenon, perhaps involving complexing between metallic impurities and other residual impurities or defects to form new carrier recombination sites, may be involved. A few recent DLTS measurements appear to support this conjecture (Table 23).

We conclude from the results of these aging studies that the long-term degradation of solar cells by most heavy-metal impurities is not significant for ordinary cell-operating temperatures. The immediate effects of these impurities upon solar cell efficiency will be more important in the economics of photovoltaic energy production. The effects of a few metals, notably chromium and silver, may be detectable over the expected 20-year module lifetime. Since these metals have been considered for use as contacts and electrodes, their effects may be important.

From the data of this study, we were not able to predict the long-term effects of iron and copper, elements which have been found to reduce solar cell efficiency by degradation of the junction properties. These effects are complex and were not amenable to extrapolation from simple temperature-accelerated aging data.

TABLE 23

EFFECT OF ONE-HOUR, 850°C HIGH-TEMPERATURE AGING ON DEEP-LEVEL TRAP CONCENTRATION NEAR THE SILICON SURFACE

		CONCENTRATION (cm^{-3})	
Ingot	Metallurgical	Traps before aging	Traps after aging
077-Mo	4.2×10^{12}	4.2×10^{12}	4.0×10^{12}
123-Ti	1.0×10^{14}	4.0×10^{13}	2.0×10^{12}
181-Cr	1.0×10^{15}	2.5×10^{12}	not detectable

The mechanism by which impurity elements can degrade solar cells is postulated to be the precipitation of impurites from supersaturated solid solution. The net effect of the disappearance of trapping centers associated with individual atoms and the growth of second-phase precipitates in the junction region is to decrease cell efficiency. Because rapidly diffusing impurities are able to reach precipitation sites readily, they degrade solar cell efficiency more rapidly than do slowly diffusing impurities.

3.9.3 Electrical Bias Effects

The accelerated high-temperature aging of impurity-doped cells did not include the investigation of any effects which might be due to interactions between impurities and electric fields in operating solar cells. Electric fields are known to affect the behavior of some carrier traps. These effects, where they exist, are reflected in the measurement of cell parameters under light and dark conditions. Long-term interactions between impurities and electric fields are not well known and, if they exist, must be determined empirically.

Fabricated cells representing eight impurity-doped ingots and a baseline ingot were individually contacted in a test fixture. A constant current power supply was used to forward bias these cells with a current density of 30 mA/cm^2 (the approximate current density which would result from one sun illumination). The biased cells were placed in an environmental chamber and subjected to an elevated temperature for 100 hours. The cells were then retested, the chamber temperature was increased, and the bias stress was repeated. Test temperatures were kept relatively low to prevent parameter changes due to contact metal sintering or reaction with silicon.

The ingots tested in this manner are listed in Table 24. The measured average relative efficiency of the baseline cells after 100 hours bias aging at temperatures of 125, 135, 145, 155, 165, 175, 185, 195, 205, 225, 245, 265, and 280°C are illustrated in Figure 49. The results for the impurity-doped cells, normalized to the baseline behavior, are shown in Figures 50-57.

TABLE 24

SILICON INGOTS FOR ELECTRICAL BIAS SOLAR CELL TESTING

Ingot No.	Impurity
W-198-00-000 Baseline	None
W 166-Fe-007	Fe 1.06×10^{15}
W-167-Nb-001	Nb $<0.044 \times 10^{15}$
W-192-Ag-001	Ag 2.20×10^{15}
W-181-Cr-006	Cr 1.04×10^{15}
W-016-Fe-001	Fe 0.4×10^{15}
W-056-Cu-005	Cu 65×10^{15}
W-183-Nb-002	Nb $<0.009 \times 10^{15}$
*W-123-Ti-008	Ti 0.105×10^{15}

*These cells were broken after the 225° test.

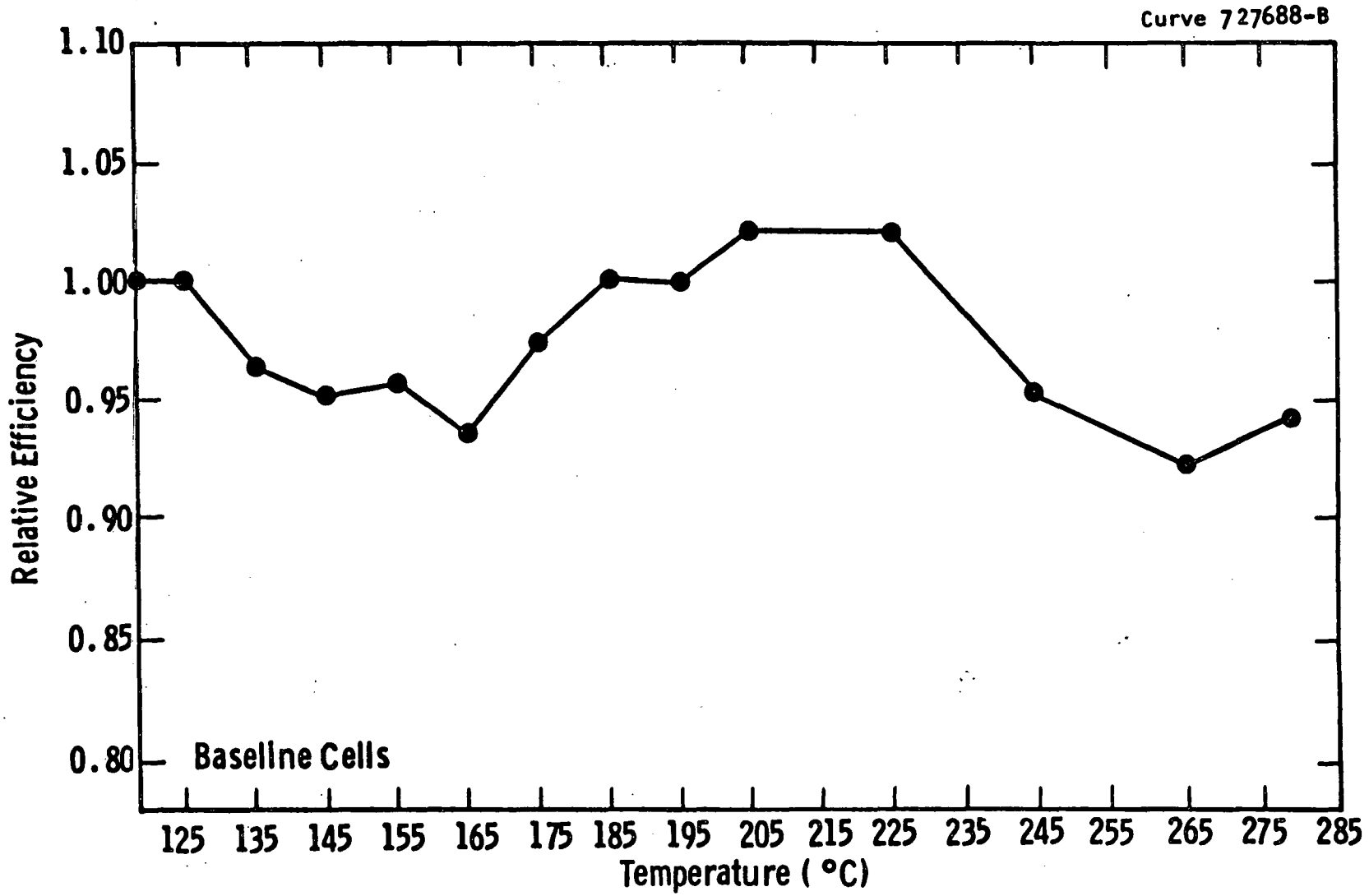

Figure 49 Baseline cell efficiency as a function of bias test temperature

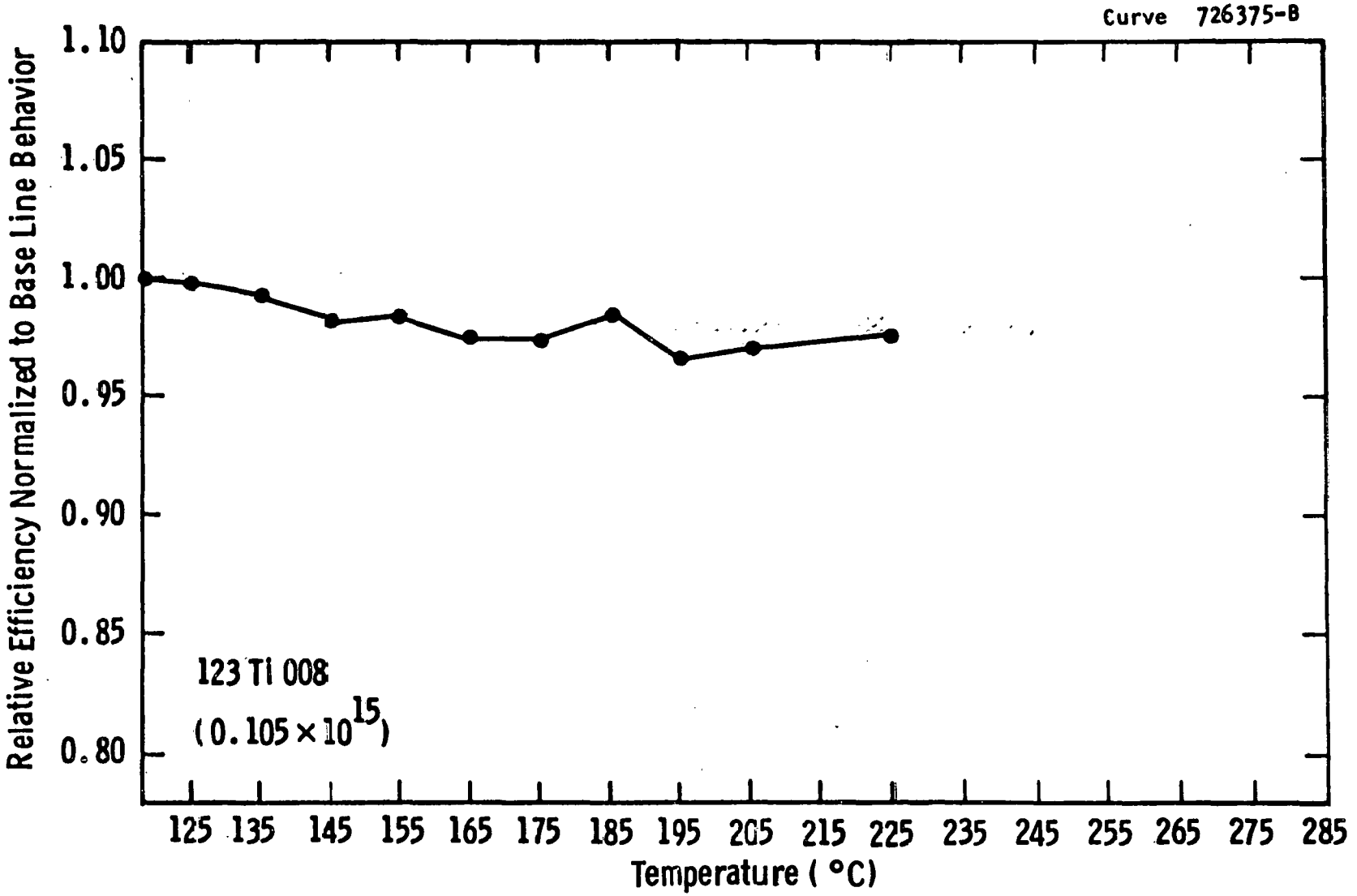

Figure 50 Ti cell efficiency as a function of bias test temperature

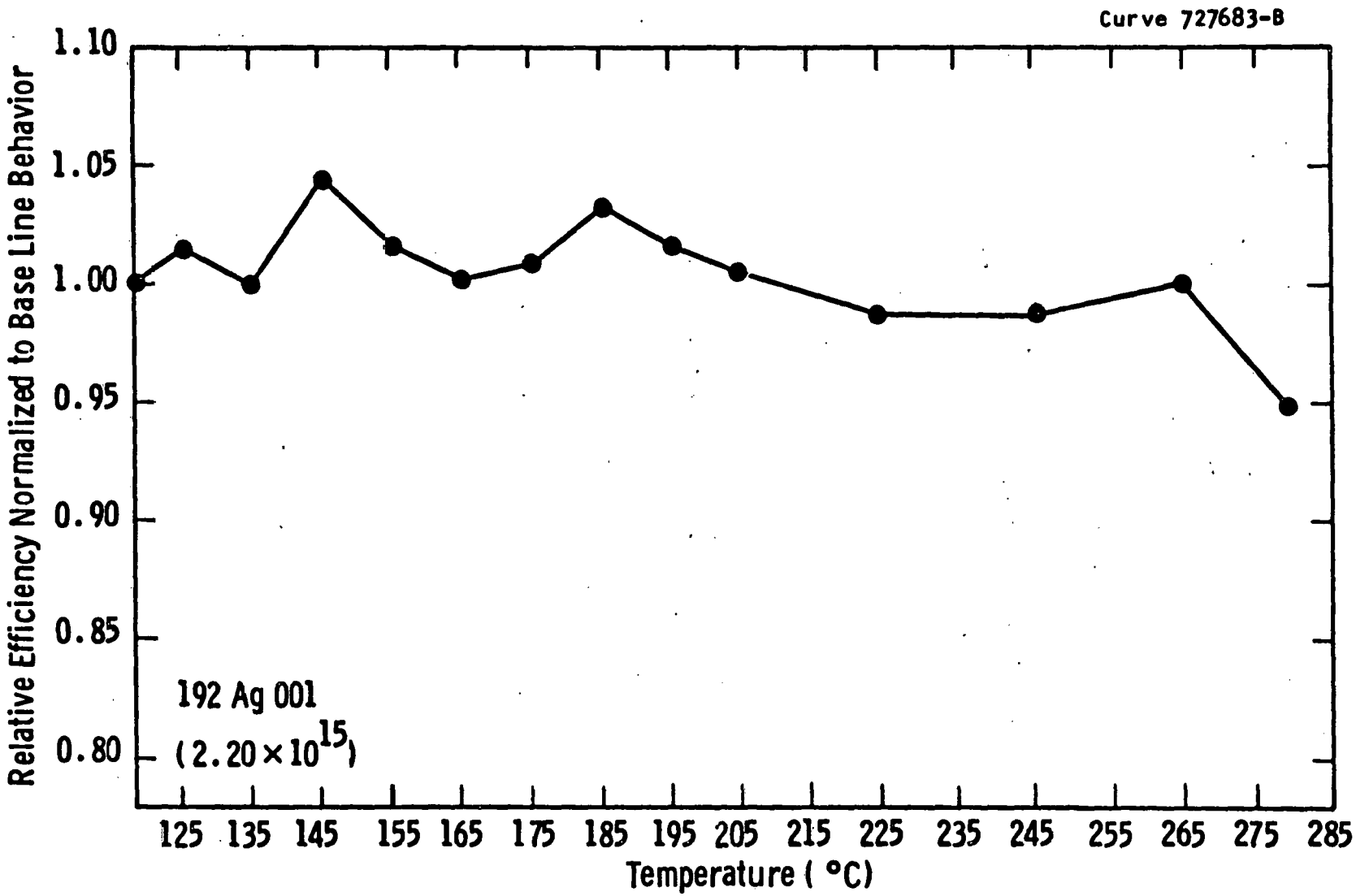

Figure 51 Ag-doped cell efficiency as a function of bias test temperature

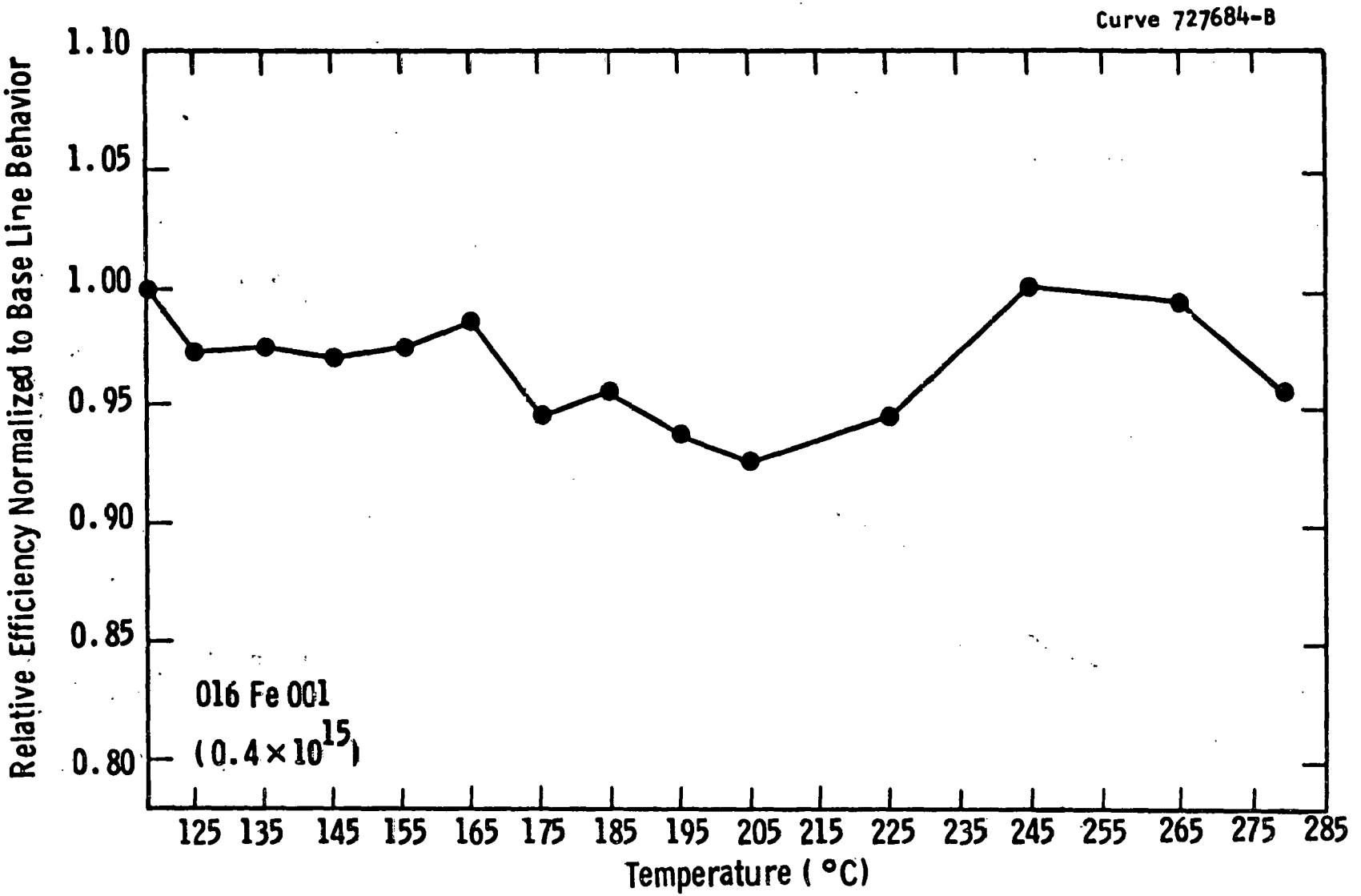

Figure 52 Fe-doped cell efficiency as a function of bias test temperature Ingot 016Fe001

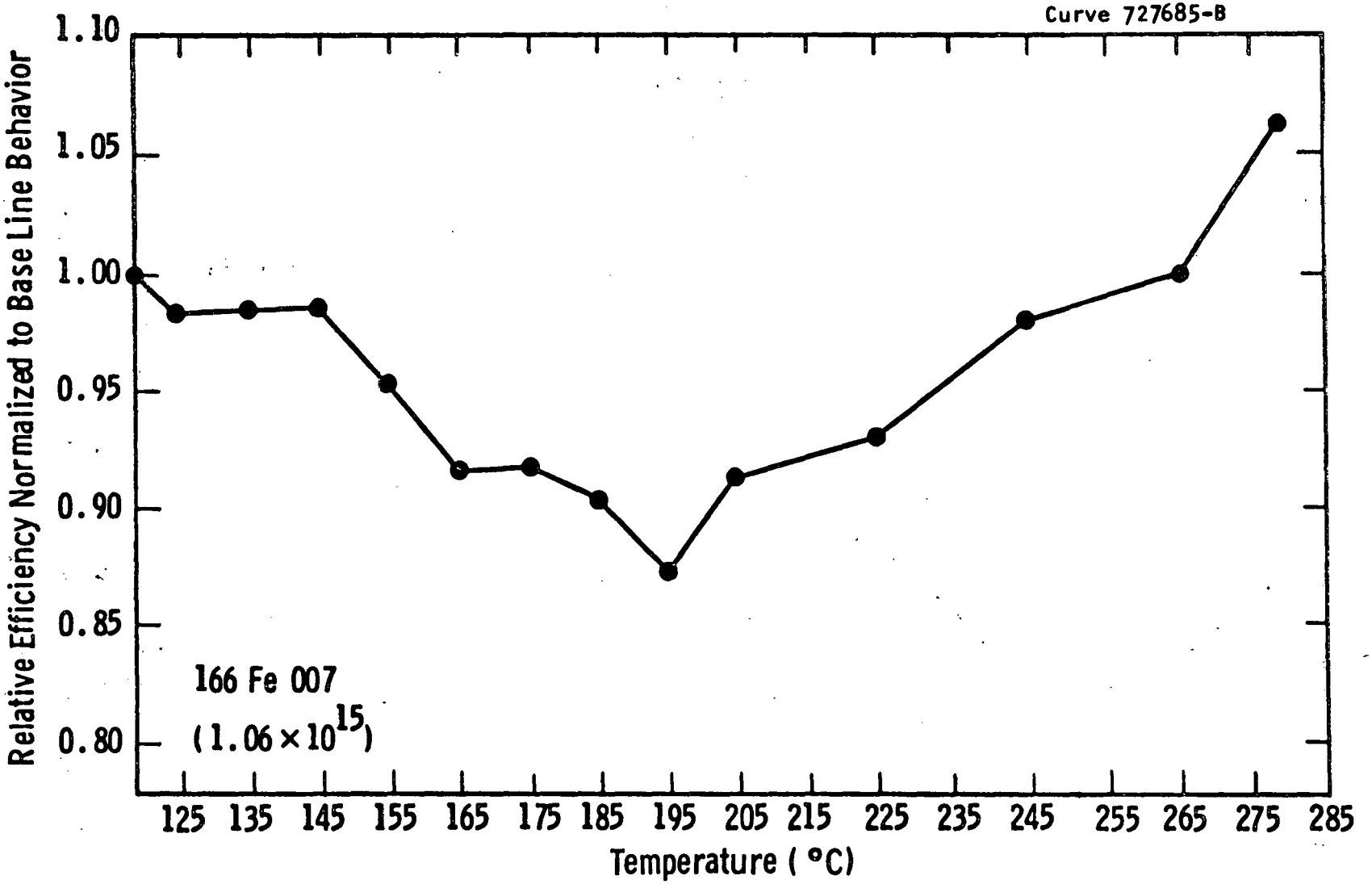

Figure 53 Fe-doped cell efficiency as a function of bias test temperature Ingot 166Fe007

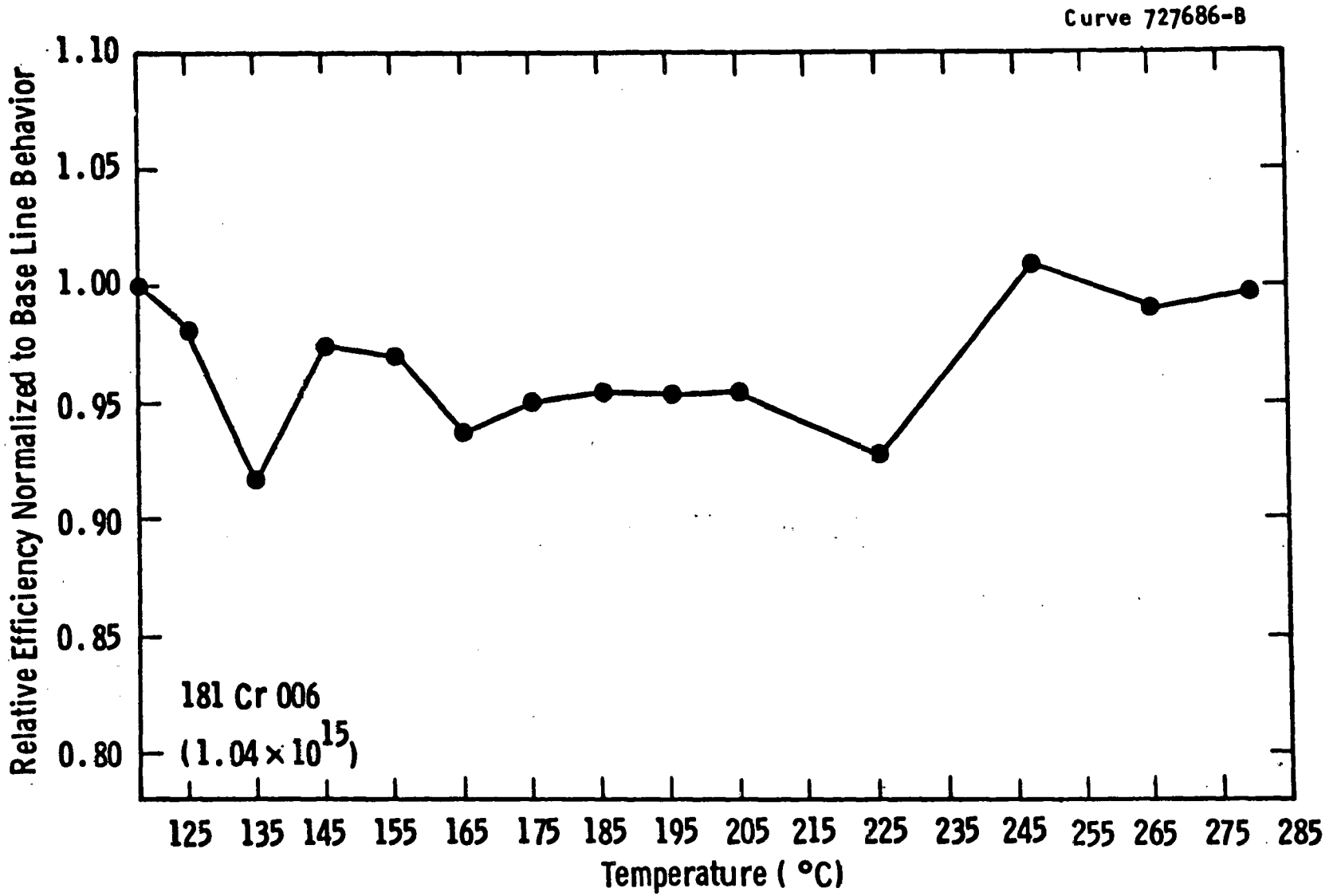

Figure 54 Cr-doped cell efficiency as a function of bias test temperature

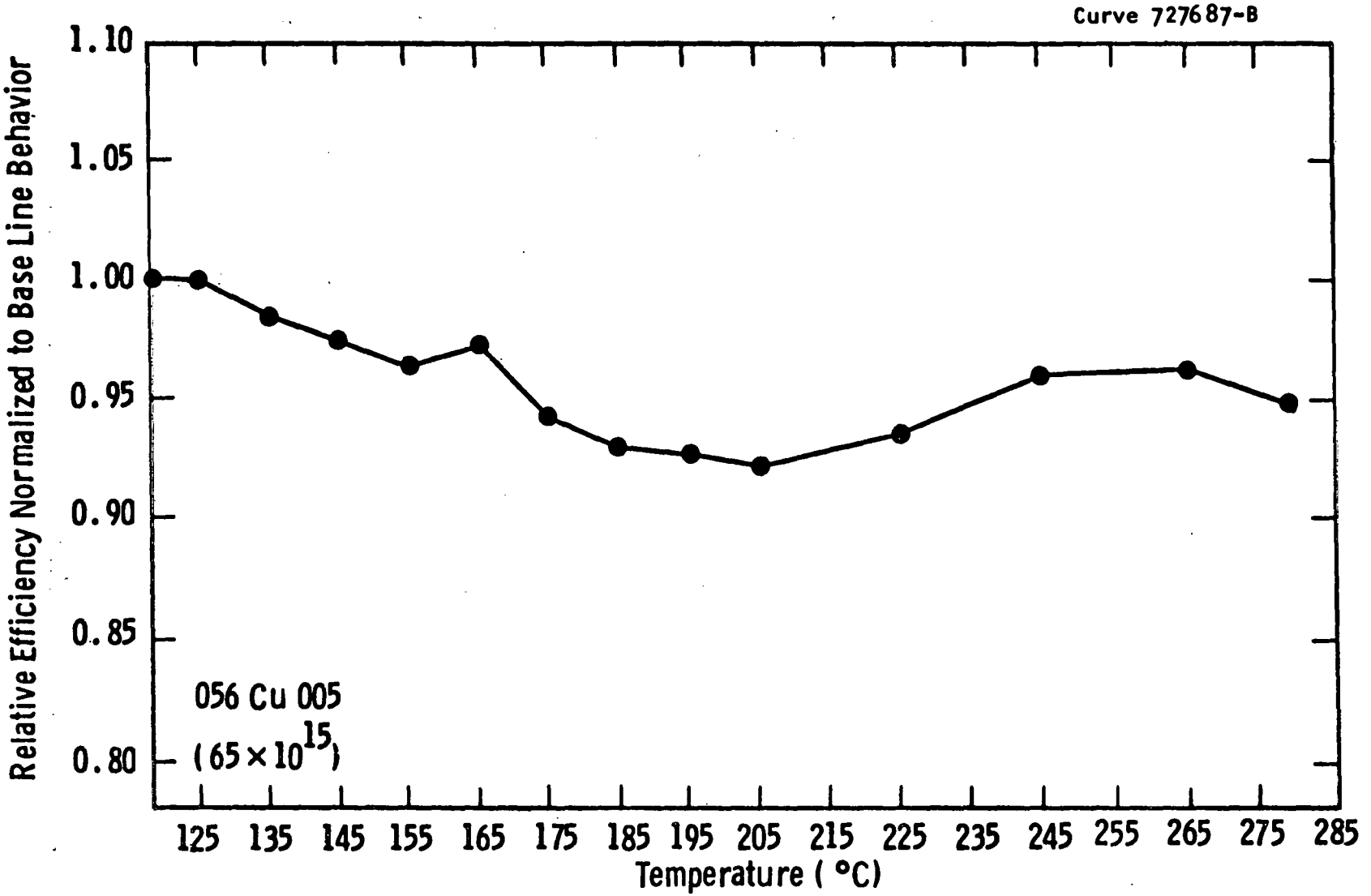

Figure 55 Cu-doped cell efficiency as a function of bias test temperature

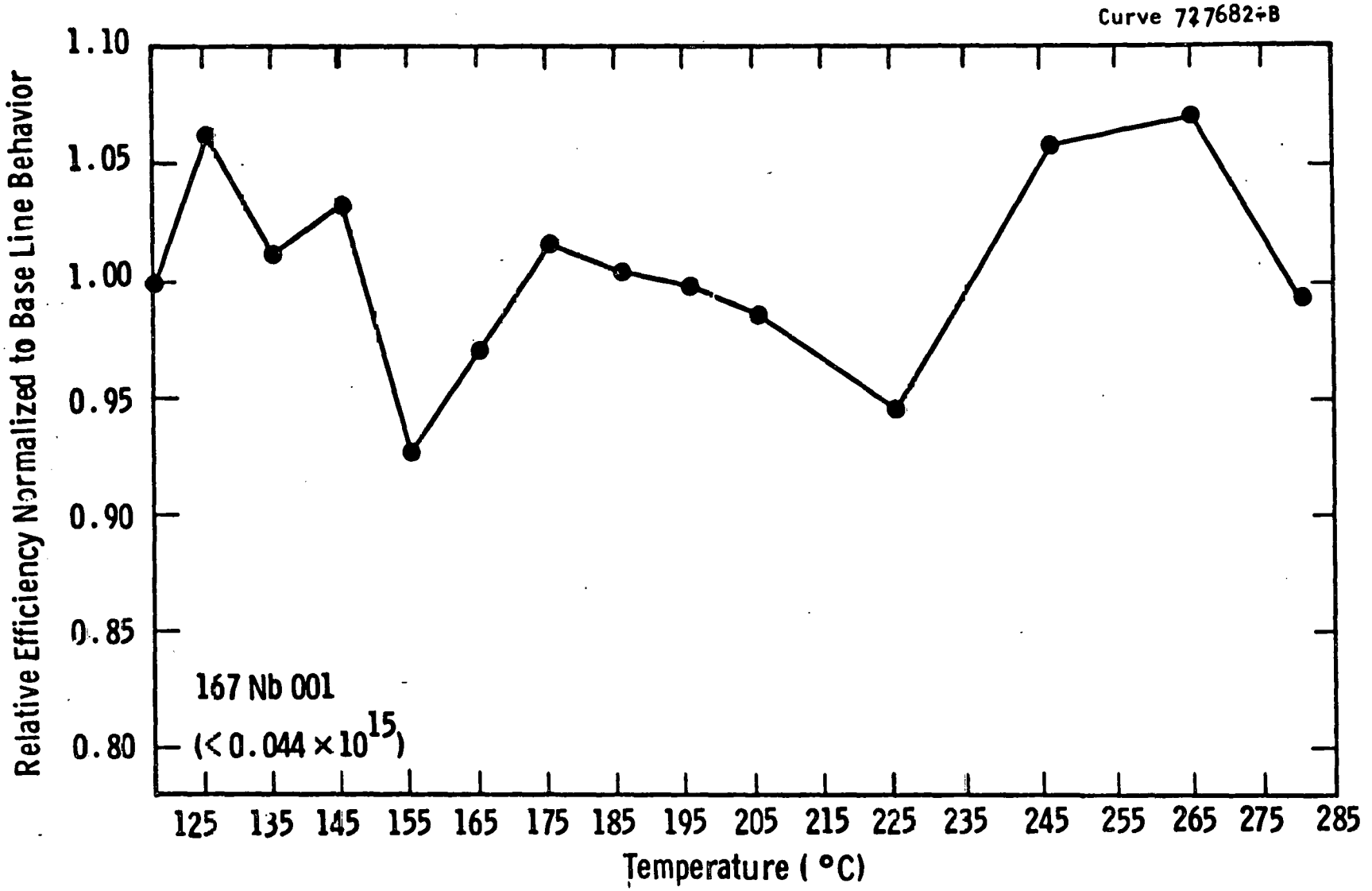

Figure 56 Nb-doped cell efficiency as a function of bias test temperature Ingot 167Nb001

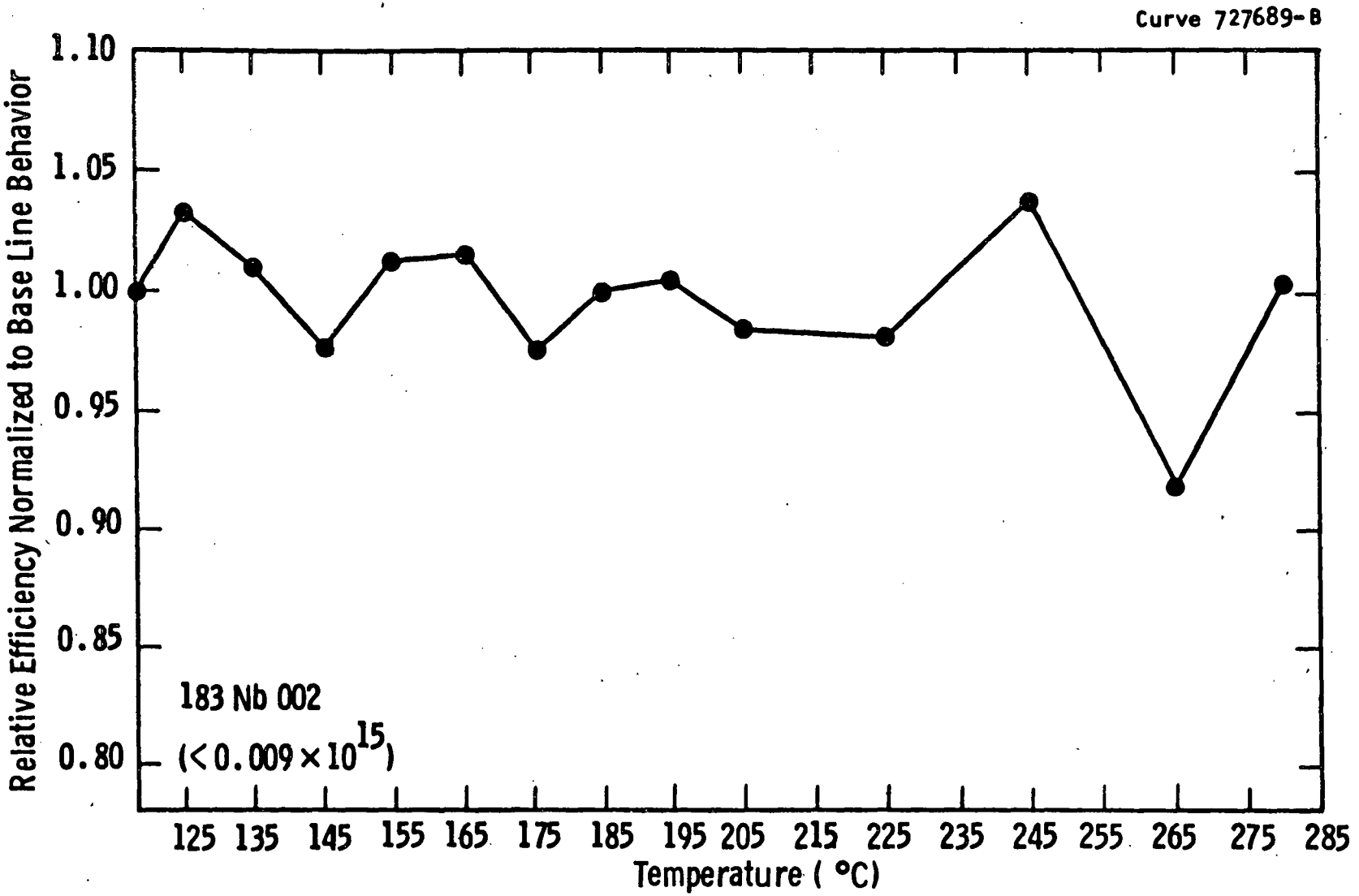

Figure 57 Nb-doped cell efficiency as a function of bias test temperature Ingot 183Nb002

These data show no systematic effect that can be attributed to a thermally activated interaction between impurities and the electric field up to 280°C, the limiting temperature of the environmental test chamber. During these experiments, average efficiencies did not deviate more than 10% from the initial efficiency. The slight variations which were observed can be ascribed to contact annealing effects and measurement errors.

In the temperature range investigated, the data do not show evidence that a thermally activated mechanism controls the effects of interaction between impurities and electric field. It is possible, however, to make a worst case interpretation of the data so that a projection of low-temperature behavior can be calculated.

For this investigation, we define the worst case as follows:

(1) A 10% reduction in efficiency occurs during 100 hours of operation at 280°C;

(2) the activation energy of the thermally activated process is small, say 0.58eV, the smallest activation energy measured in the high-temperature aging studies.

The temperature dependence of the degradation rate would be described by

$$\frac{1}{\eta_o}\frac{d\eta}{dt} = -A \exp\ (-Ea/kT)$$

where η_o is the initial cell efficiency, $\frac{d\eta}{dt}$ is the rate of efficiency degradation, E_a is the activation energy, k is Boltzmann's constant, T is the Kelvin temperature, and A is a constant. For the postulated worst case then, A = 192 hr^{-1} and E_a = 0.58eV. The normalized rate of cell degradation at 60°C would then be

$$\frac{1}{\eta_o}\frac{d\eta}{dt} = -192 \exp\ (-0.58eV/8.62x10^{-5}X333)$$

$= 3.2 \times 10^{-7}\ hr^{-1}$ and the time required for a 10% cell degradation at 60°C would be 3.1×10^{5} hours or 35 years. This worst case analysis predicts that, since no significant cell degradation was observed in this experiment, it can be safely assumed that no more than minimal effects would be observed during the 20-year expected life of a photovoltaic panel containing cells made from impurity-containing silicon.

3.9.4 Summary

Neither the high temperature aging studies nor the low temperature electrical bias tests reveal major long-term impacts that can be attributed to impurity aging effects within a 20-year module lifetime. Rapidly diffusing species like Ag and Cr may degrade cell performance to some extent over the projected 20-year module lifetime and should be examined in further detail.

3.10 Evaluation of Experimental Silicon Materials

Techniques such as precision chemical analysis, impurity-cell performance modeling, detailed I-V measurement, and deep-level spectroscopy, which we developed or employed extensively (on this program) provide powerful tools to evaluate experimental silicon materials as they are developed, to identify critical impurities which may enter the process stream, and to suggest remedial action to the producer. Thus, one activity during the latter part of the program was the evaluation of silicon produced by other contractors of the LSA project. As of this writing, two such materials were studied -- silicon produced from dichlorosilane by Hemlock Semiconductor Corporation and silicon produced from silicon tetrachloride by Battelle Laboratories.

3.10.1 Hemlock Silicon

Under JPL Contract 955533, Hemlock Semiconductor Corporation is developing a potentially cheaper, high-purity polycrystalline feedstock.[36] In this process, trichlorosilane is chemically redistributed to form dichlorosilane (DCS). The DCS subsequently is decomposed to silicon by chemical vapor deposition and deposited in the form of a cylindrical rod.

The projected advantages of the DCS process over conventional methods include higher conversion efficiencies and deposition rates while using less energy and expendable materials. The material is expected to resemble semiconductor-grade silicon in form and purity, but at much lower cost.

A bar of DCS silicon from the Hemlock experimental reactor was grown into a Czochralski crystal using the same furnace and growth conditions previously employed throughout this program (Section 3.2.1). The ingot is designated W224-HSC/DSC-057 as noted in Table 8 and Appendix III. The melt was doped to produce a nominal ingot resistivity of 1.5 ohm-cm, slightly lower than the 4 to 6 ohm-cm typical of other ingots we have studied.

Twenty-five wafers from ingot W224 were fabricated into solar cells, along with five 4 ohm-cm baseline wafers from ingot W198. The standard process sequence we use includes an 825°C phosphorus diffusion to form an n+p cell. This typically produces uncoated devices with AM1 conversion efficiencies in the 9 to 10% range (12.7 to 14.3% with antireflective coatings) for 4 ohm-cm material.[3]

In the first process run, cells from ingot W224 exhibited an uncoated efficiency of 9.13 $\pm$ 0.75% (~12.8% coated) compared to 9.28 $\pm$ 0.25% for the baseline devices (the scatter for all the data in this run is higher than we usually observe and some evidence for impairment of junction quality was noted). The individual uncoated cell efficiencies for ingot W224 ranged from a high of 10.11% (14.2% coated) to a low of 7.9% (11.1% coated), although the majority of the cell efficiencies clustered around 9%. As expected from the lower resistivity of ingot W224, the solar cells made on the DCS material exhibited higher open-circuit voltages (average 0.571 mV) than those made on the baseline silicon (average 0.556 mV). A second process run produced essentially similar I-V parameters.

Gold-Ti-Si Schottky barrier diodes also were fabricated on representative wafers from ingot W224 to facilitate deep-level transient spectroscopy measurement. No deep levels were found in the DCS material, in keeping with its expected high purity and the fact that any metals present in the starting material would be segregated during crystal growth. The sensitivity of the DLTS method is about 10^{12} trapping centers per cubic centimeter at 1.5 ohm-cm resistivity.

In general then, we conclude that the silicon produced by the Hemlock Semiconductor dichlorosilane process is comparable in behavior to our standard Czochralski material made by trichlorosilane decomposition.

3.10.2 Battelle Silicon

Earlier in the program, samples of a fine granular silicon produced at the Battelle Memorial Institute[37] under JPL Contract 933645 were provided to us for evaluation. The Battelle process utilizes the reduction of silicon tetrachloride by zinc by a fluidized-bed technique; as a result, prior chemical analyses of lot 3364-38-97 (from which our samples came) had established the presence of about 0.2% Zn in the silicon.

Thus we first fired the material at 1290°C, confirming by weight loss and x-ray diffraction measurements that most of the Zn was driven off. Since the circuit of silicon was limited, web growth, rather than Czochralski pulling, was employed to get crystals. Silicon web crystals were successfully pulled, indicating the silicon's suitability for crystal growth.[8] The web was grown at 1.6cm/min with a melt undercooling of about 3°C. The change weight was 100 grams of silicon to which 2.3×10^{15} atoms cm^{-3} of boron were added as an intentional dopant. The target resistivity was nominally 9 Ω-cm.

The resulting web crystals had a resistivity of 0.25 ohm-cm indicating that some p-type impurity (probably zinc) was initally present. Nevertheless, the resulting solar cells, fabricated from crystal W180-1 and W180-3 had efficiencies of 8.9% and 9.0% respectively without AR coating (estimated to be 12.6% and 12.8% had AR coatings been applied). Two deep levels, E_V+0.3eV and E_C-0.55eV, were detected by DLTS, and apparently correspond to reported levels for elemental Zn.

Clearly, efficient solar cells can be made from the Battelle Silicon, but reduction of the Zn content would reduce potentially troublesome deep levels and also facilitate the crystal-growth process by eliminating evolution of the metal into the growth system.

4. IMPURITY CORRELATIONS

In many cases, hard experimental data on impurity behavior in silicon are unavailable to project expected impurity segregation or device performance. For this reason, guidelines or empirical rules of thumb are useful.

Figure 58 illustrates how the segregation coefficient depends both on the bond radius of the various impurities and also on the electronic shell structure of the individual atoms. Such size and valence effects have been predicted in semiquantitative fashion by Wieser,[38] who based his analysis on the strain and bond-energy effects attending the insertion of a foreign atom in the silicon lattice. The segregation data presented in the figure were obtained from the present work supplemented by information from Wolf[39] and Trumbore[40] for impurities we did not examine. The bond radii data are from Pauling.[41] Extrapolation and interpolation of the curves between data points provides approximate segregation coefficients for cases where no data exist.

Figure 60 illustrates the dependency of impurity properties on position in the periodic table. The vertical height of the inverted pyramids corresponds on a logarithmic scale to the value of the degradation threshold (N_{ox}) for each of the impurities. Those impurities displaying taller pyramids can be tolerated at high concentrations, while only minute concentrations of the short ones are tolerable without cell performance loss. The thresholds for oxygen and carbon are minimum values representing the highest concentrations achieved. The value of N_{ox} for silicon is shown as 5×10^{22} cm^{-3}, its theoretical density. The general sloping of the thresholds from upper right to lower left indicates a corresponding increase in the effective recombination cross sections, which lacks theoretical explanation at this time. This trend can be used to estimate the performance degradation to be expected for impurities falling at intermediate positions.

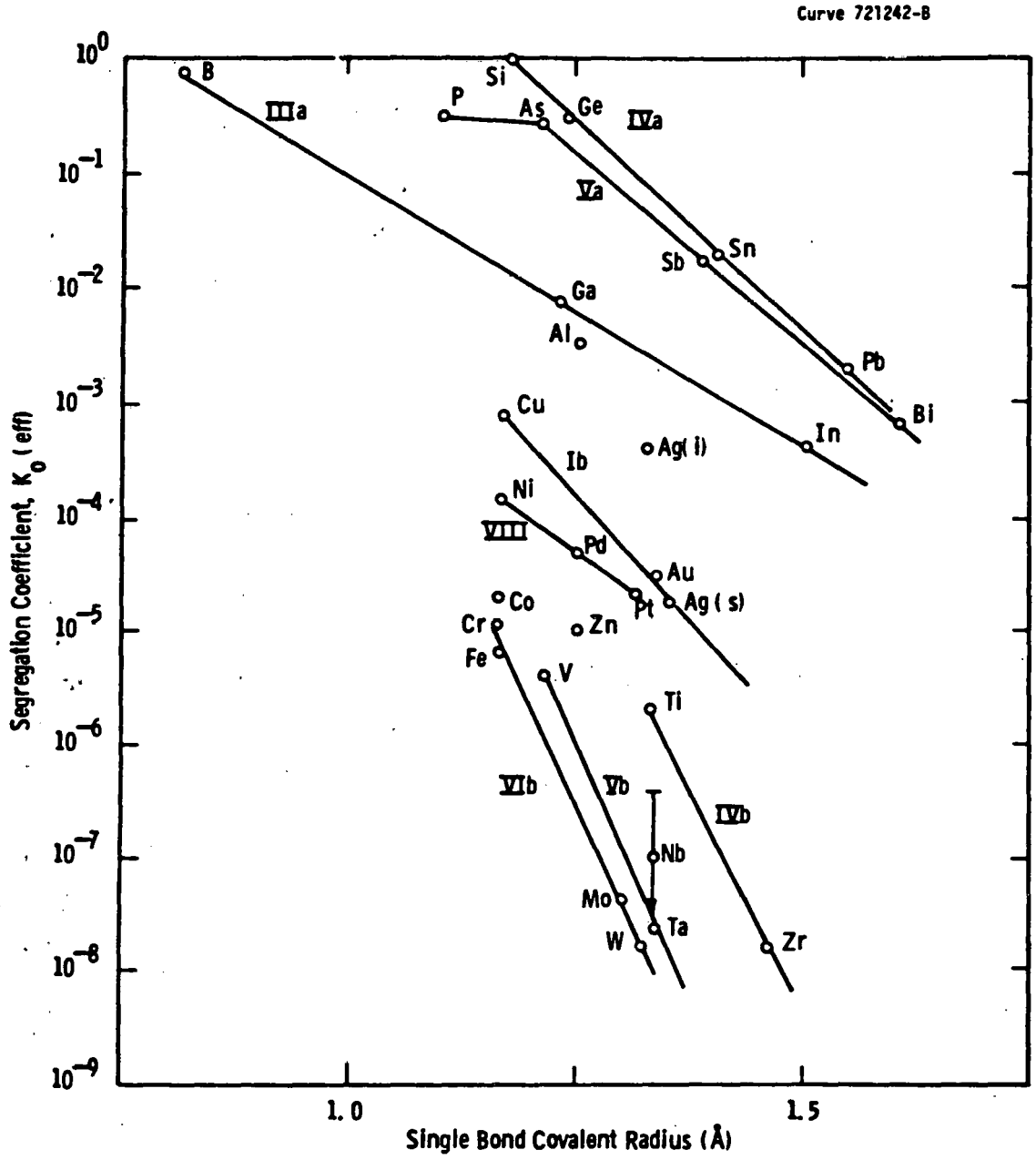

Figure 58 Variation of segregation coefficient with impurity bond radius

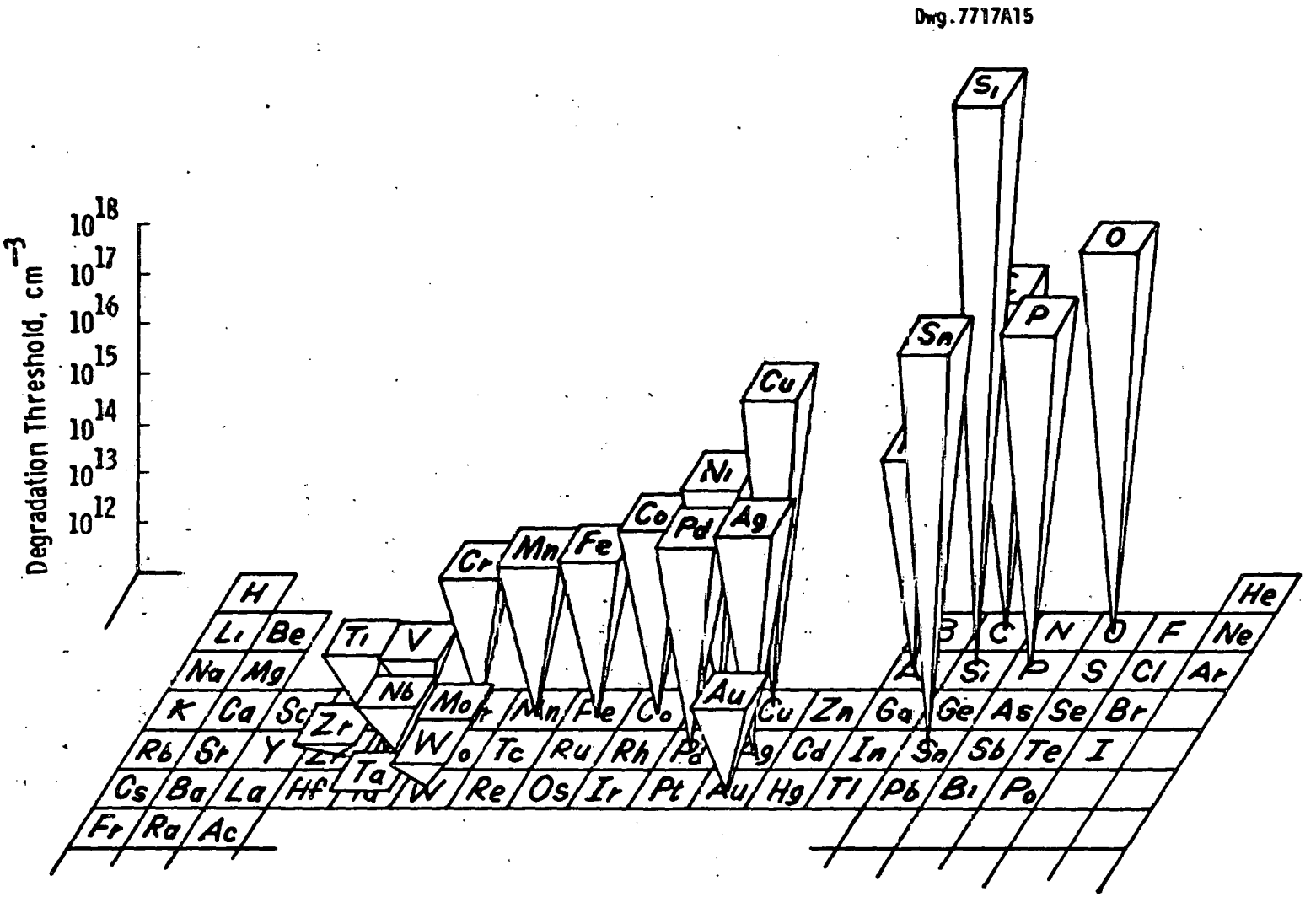

Figure 59 The periodic behavior of the threshold concentration for solar cell performance loss

5. IMPURITY TOLERANCE IN SOLAR GRADES OF SILICON

To reduce significantly the cost of photovoltaic power, silicon much cheaper than now available must be provided for crystal growth and subsequent solar cell fabrication. That material, termed Solar Grade silicon, may contain contaminants at levels higher than is common or acceptable for current semiconductor-grade feedstock. The dominant impacts of these contaminants are device performance degradation and reduced crystal-growth yield (via structural breakdown). The degree of acceptability of a solar-grade feedstock thus depends on the growth technique, as well as the cell fabrication processes involved.[1-3] We have identified specific tradeoffs between feedstock purity and the methods used to transform the silicon into its end-product solar cells. Using the common Czochralski growth technique as an illustration, we review here a method for estimating tolerable impurity ranges in silicon. The approach is a general one and has been applied to other crystal production processes as well.[3]

The data in Table 25 (derived from the updated cell performance and analytic results in Sections 3.4 and 3.5) illustrate that efficiency degradation depends on the impurity species and also that the tolerable feedstock impurity level is a function of the amount of crystal pulled and the melt replenishment strategy adopted. When a relative efficiency equal to 90% of the uncontaminated baseline cells ($\eta = 0.9\ \eta_o$) is acceptable, the feedstock impurity concentration ranges from about 10^{17} to nearly 10^{20} cm^{-3} (~ 1 to 1000 ppm) for a <u>single</u>-charge Czochralski growth operation in which about 90% of the melt is converted to crystal. Elements like Nb, Ti, and V fall at the low end of the tolerable range, Cu at the upper end, and Co, Cr, and Fe at intermediate positions. When five melt recharges are employed — a situation probably necessary to assure process economy — the tolerable impurity concentrations are reduced

Table 25

TOLERABLE FEEDSTOCK IMPURITY CONCENTRATIONS TO ACHIEVE CELL EFFICIENCY 90% OF BASELINE UNCONTAMINATED DEVICES

Impurity	One Pull		Five Sequential Replenishments	
	atoms cm^{-3}	ppma	atoms cm^{-3}	ppma
Cu	$1.0(10^{20})$	2000	$2.2(10^{19})$	434
Pd	$3.6(10^{19})$	720	$7.9(10^{18})$	158
Ag	$1.8(10^{19})$	360	$4.0(10^{18})$	80
Fe	$9.3(10^{18})$	186	$2.0(10^{18})$	40
W	$8.8(10^{18})$	176	$1.9(10^{18})$	38
Zr	$< 5.0(10^{18})$	< 100	$< 1.1(10^{18})$	< 22
Co	$4.6(10^{18})$	92	$1.0(10^{18})$	20
Mn	$3.8(10^{18})$	76	$8.3(10^{17})$	17
Cr	$3.6(10^{18})$	72	$7.8(10^{17})$	16
Ta	$1.05(10^{18})$	21	$2.3(10^{17})$	4.6
Mo	$9.6(10^{17})$	19	$2.1(10^{17})$	4.1
P	$5.7(10^{17})$	11.4	$1.2(10^{17})$	2.5
Au	$2.0(10^{17})$	4.0	$4.4(10^{16})$	0.9
Nb	$< 1.4(10^{17})$	< 2.8	$< 3.0(10^{16})$	< 0.61
Ti	$1.3(10^{17})$	2.6	$2.8(10^{16})$	0.56
V	$1.1(10^{17})$	2.2	$2.4(10^{16})$	0.48
Al	$3.3(10^{16})$	0.7	$7.2(10^{15})$	0.15

by about a factor of five[2] compared to the single ingot growth case. Continuous rather than sequential replenishment is advantageous: tolerable impurity concentrations can be as high as a factor of ten greater when continuous replenishment is employed rather than growing an equivalent amount of crystal by sequential replenishment (Figure 60).

If, on the other hand, we set the acceptable cell efficiency higher, say 0.95 η_o, then the values of feedstock impurity concentration suggested in Table 25, must be reduced — in this example by a factor of 3 to 4, depending on the impurity. Fortunately, many of the impurities which degrade cell performance most severely also have small segregation coefficients. For example, when the degradation threshold concentration (N_{ox}) derived in Section 3.5 is plotted against effective segregation coefficient, Figure 61, it is apparent that the two parameters are correlated; those impurities which are most damaging to cell performance, i.e., that have small values of N_{ox}, are also most difficult to incorporate during the growth of a silicon crystal. Nature in effect has provided a helping hand since the feedstock, or melt concentration, of the worst impurities can be fairly large without significant effect on solar cell performance. If, however, k_{eff} is large for all impurities, as is probably the case with EFG ribbon growth, then tolerable feedstock impurity concentrations like those in Table 25 would be considerably smaller.

The second major negative impact of impurities, structural breakdown during crystal growth, is governed by the <u>total</u> impurity content of the feedstock rather than by the species present. For Czochralski growth, the critical liquid-impurity content C_ℓ^* at which structural breakdown occurs is given by equation 6 of Section 3.2.

$$C_\ell^* = -\frac{D}{m}\left[\frac{A}{r^{1/2}V} - B\right] e^{-130V}$$

Here, D is the liquid-diffusion coefficient, m the liquidus slope, r the crystal radius (cm), and V the growth velocity (cm/sec).

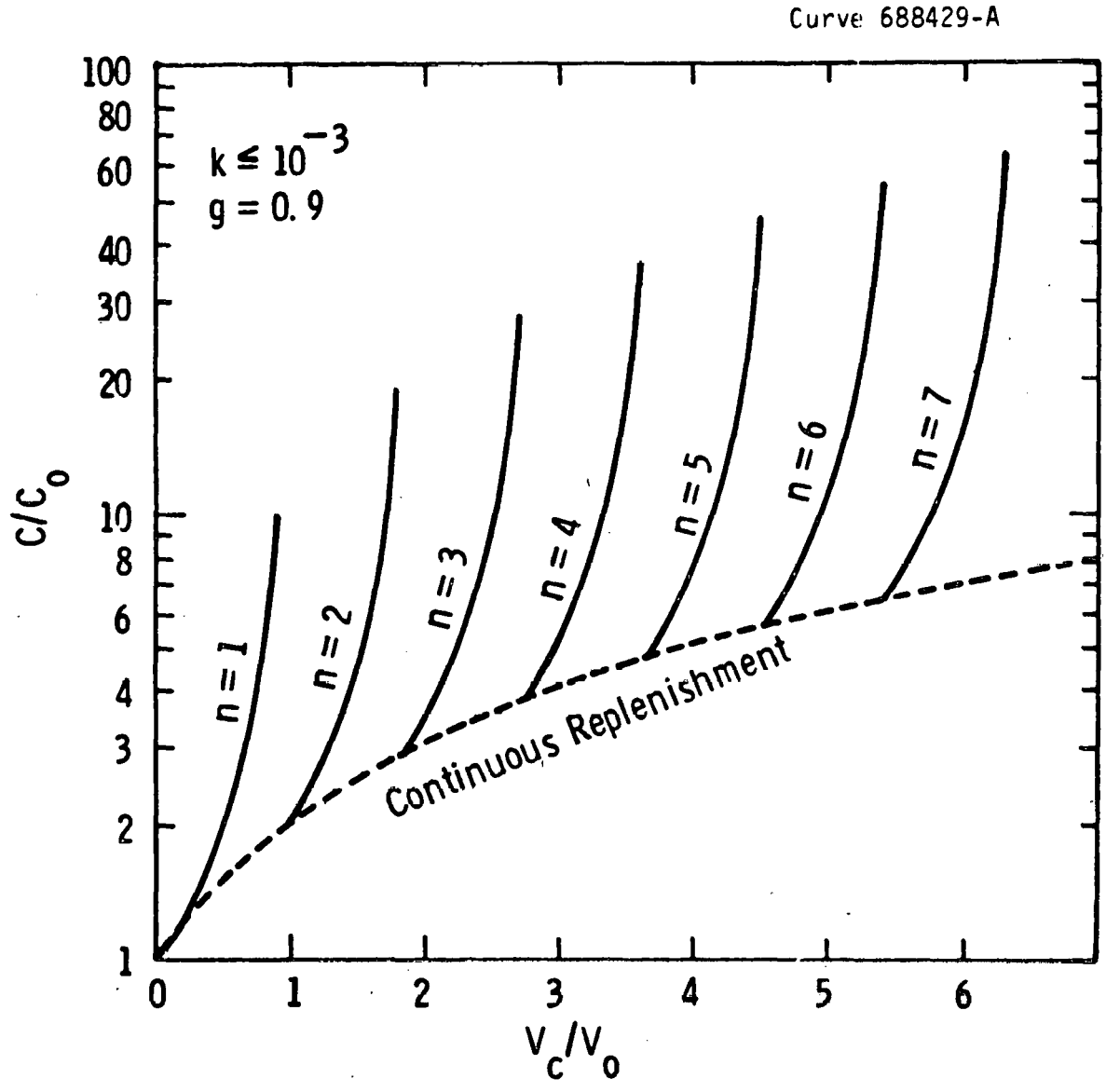

Figure 60 Solute build-up in the liquid (or crystal) as a function of the volume of crystal grown for sequential (solid) or continuous (dashed) melt replenishment

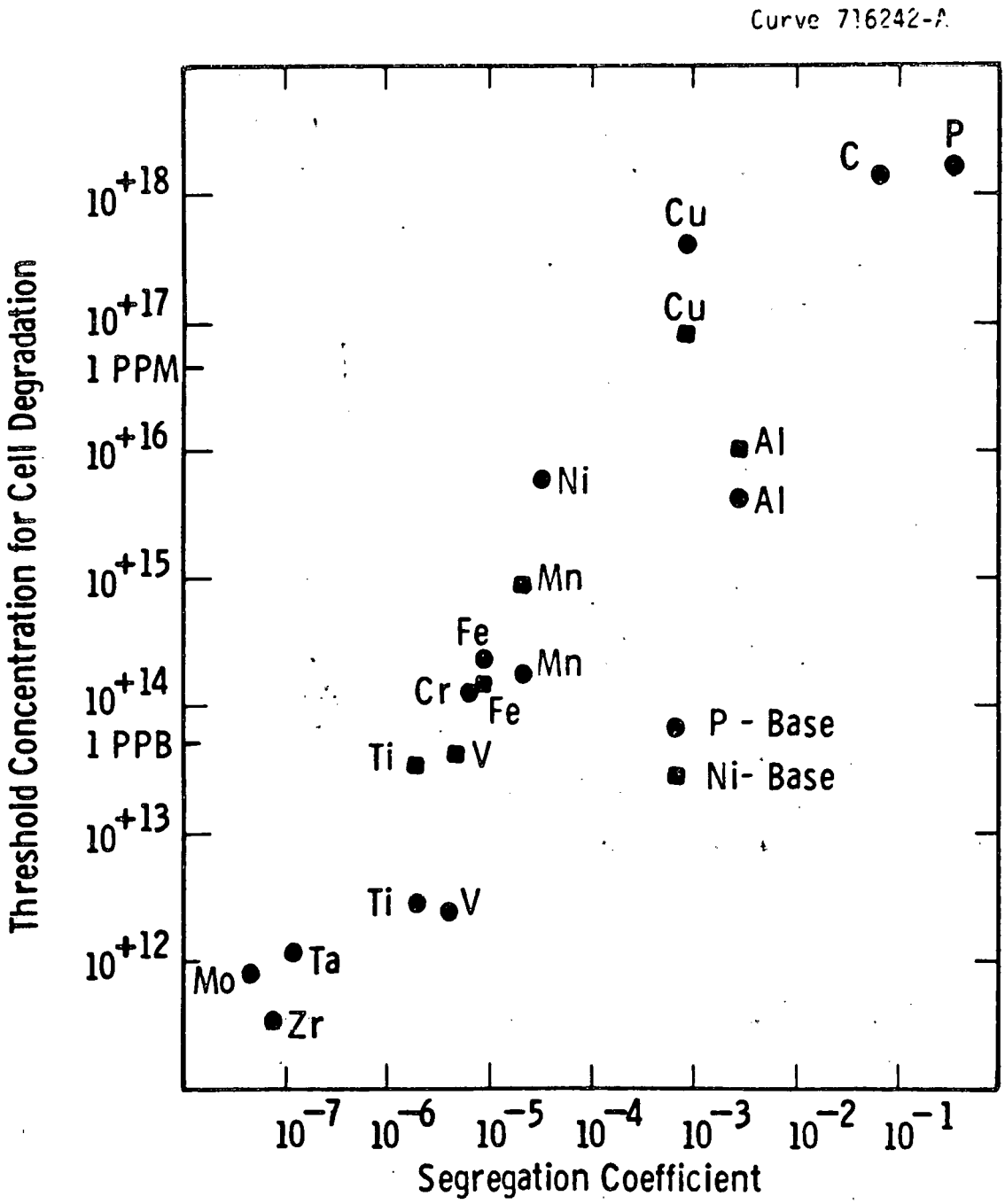

Figure 61 Observed correlation between threshold degradation concentration (N_{ox}) for cell performance loss and segregation coefficient for crystal growth.

When the impurity concentration in the liquid exceeds C_ℓ^*, the planar freezing front degenerates to a cellular morphology entrapping second-phase inclusions like those pictured in Figures 1 through 6; ingot structure transforms from single crystal to arrays of twins and grain boundaries.

By means of equation 6 and the constants given in Section 3.2, we computed the values of C_ℓ^* for a variety of growth velocities and ingot diameters likely to be encountered in practice. The calculated and measured critical-breakdown concentrations typically fall in the low- to mid-10^{20} cm^{-3} (few thousand ppma) range for our experiments (Section 3.2). Since these values represent the point at which structural degradation initiates, the feedstock concentrations corresponding to one Czochralski pull would be about one-tenth these values (~ 200 to 500 ppma). For five recharges the tolerable levels would be about one-fiftieth of these values.

As ingot sizes and pull rates scale up from the 7.6 cm and 7 cm/hr. range common now to 15-cm diameter and 10-cm/hr. rates, the impurity concentration at which structural breakdown occurs will also diminish as indicated in Table 26. When this happens, breakdown rather than cell efficiency will probably set the upper limit on acceptable impurity concentrations.

The analysis for Czochralski growth is only an example. (A similar analysis of silicon web growth has been made.[2]) The analysis, however, serves to show where tradeoffs exist between feedstock purity and other processing costs. The data indicate target impurity ranges in which solar-grade feedstocks must probably lie if they are to be at all useful: for the least harmful impurities, concentrations in the 20- to 100-ppma range will be the maximum likely; for others, like Ti and V, the acceptable levels will be nearly two orders of magnitude less than these if melt replenishment is to be employed effectively. Our data indicate that for a few impurities, these restrictions might be relaxed somewhat by the choice of an n-base rather than p-base device (Section 3.5). This advantage probably is outweighed by the difficulty in controlling base resistivity

Table 26

VARIATION IN CRITICAL-BREAKDOWN CONCENTRATION (cm^{-3}) WITH GROWTH RATE AND INGOT DIAMETER

Growth Velocity (cm/hr)	Ingot Diameter (cm)				
	3.1	7.6	10	12.5	15
3	7.9×10^{20}	$4.8(10^{20})$	$4.1(10^{20})$	$3.6(10^{20})$	$3.2(10^{20})$
6	3.2×10^{20}	$1.9(10^{20})$	$1.6(10^{20})$	$1.3(10^{20})$	$1.1(10^{19})$
8	2.1×10^{20}*	$1.2(10^{20})$	$9.4(10^{19})$	$7.8(10^{19})$	$6.7(10^{19})$
10	1.5×10^{20}	$7.6(10^{19})$	$6.0(10^{19})$	$4.8(10^{19})$	$3.9(10^{19})$

*Size and pullspeed typical of most test ingots used on this program.

with phosphorus as the electrically active dopant, due to the large segregation coefficient for this impurity.

By using the same methodologies we have developed for tradeoffs analysis, we can also project the efficiency of solar cells when the feedstock purity and process history are specified. A model of this kind described earlier[2] provides several benefits. For example, it can be used to estimate the impact of specific species (in a feedstock containing several impurities) on cell efficiency, thus providing a "figure of merit" for the product of a given refining scheme. A manufacturer could, for example, evaluate alternative refining and design strategies or raw material specifications in a cost effective manner. Comparison of crystal growth and replenishment strategies can be evaluated for different types of solar grade silicon without recourse to expensive experimental reduction to practice. Finally, with an expanded data base on thermal treatment effects, the role of such processes as gettering can be factored into the analysis.

6. CONCLUSIONS

The objective of this program has been the investigation of the effects of impurities, processing, and impurity process interactions on terrestrial silicon solar cells. During the investigation, now successfully finished, we have studied how metallic impurities, both singly and in combinations, impact the performance of silicon solar cells. Czochralski, float zone, and polycrystal ingots as well as silicon web crystals were grown with controlled additions of secondary impurities. The primary electrical dopants were boron and phosphorous. The metal elements were selected because of their occurrence in silicon raw materials, possible introduction during subsequent processing, or because they were common construction materials for process equipment or the cells themselves. The metals included Ag, Au, Al, C, Ca, Cr, Co, Cu, Fe, Gd, Mg, Mn, Nb, Ni, Pd, Sn, Ta, Ti, V, W, Zn, and Zr. Impurity concentrations were in the range of 10^{11} to 10^{18} cm^{-3}.

All silicon ingots were grown under controlled and carefully monitored conditions from high-purity charge and dopant material to minimize unintentional contamination. Following growth, each crystal was characterized by chemical, microstructural, electrical, and solar cell tests to provide a detailed and internally consistent description of the relationships between silicon impurity concentration and solar cell performance. Analysis of vacuum-cast melt samples provided an accurate determination of the melt impurity concentration at the completion of crystal growth. Melt concentrations coupled with reliable effective segregation coefficients in turn were used to calculate ingot impurity concentrations, which were in excellent agreement with the ingot impurity concentrations measured directly by spark source mass spectroscopy and neutron activation analyses. Deep-level spectroscopy measurements used to measure impurity concentrations at levels below detectability of the other

techniques (see Appendix V) also show very good correlation with calculated ingot impurity concentrations.

Solar cells made using a conventional diffusion process optimized for repeatability and reliability were used to evaluate the impact of impurities. For the majority of contaminants, impurity-induced performance loss was due to a reduction of the base diffusion length. From these observations, we formulated an analytical model which predicts cell performance as a function of metal impurity concentration. The calculated performance parameters agree well with measured values except for the impurities Cu, Ni, and Fe, which at high concentrations degrade the cell performance substantially by means of junction mechanisms. The model has been used successfully to predict the behavior of solar cells bearing as many as 11 impurities. The concentration of recombination centers identified by deep-level transient spectroscopy not only correlates directly with the concentration of metallurgically added impurity, but also with solar cell performance.

Extension of the impurity performance model to high-efficiency solar cells indicates, in general, that such devices will be more sensitive to impurities than are their more conventional counterparts. This increased impurity sensitivity will be exhibited in widebase cells and medium-base cells with back-surface fields or passivated surfaces, but can be significantly reduced by making cells with narrow (~ 100 μm) basewidths.

The effects of impurities in n-base and p-base devices differ in degree but can be described by the same modelling analysis. Some of the more deleterious impurities in p-base devices produce significantly less performance reduction in n-base silicon. For example, nearly ten times more Ti is acceptable in n-type silicon to produce the same cell efficiency as in a similarly contaminated p-base device.

When the model-calculated and measured cell performance for multiple impurities are compared, there is limited indication of interaction between impurities. For example, copper improves the efficiency of

Ti- and V-doped cells, although the effect is small. Apparently, Cu diffuses to and combines with the second transition metal to reduce its electrical activity. Precipitated impurities have little or no effect on carrier-transport properties in the low-field base region of the solar cell, but do affect cell performance when they occur in or near the high-field junction region.

The major direct impacts of less pure solar-grade material are device performance reduction and diminished crystal-growth yields. The degree of acceptability of solar-grade feedstock depends on the growth technique, melt replenishment strategy, and solar cell processes involved. Both the Czochralski and silicon web techniques are somewhat "tolerant" of feedstock impurities since most of the contaminants are rejected to the melt during growth. The degree of tolerance is species sensitive. Elements like V impair cell efficiency considerably more than do Cu or Sn. For example, in a one-pass Czochralski operation, only about 2 ppma Ti would be acceptable to produce cells 90% as efficient as baseline devices, while nearly 2000 ppm of Cu could be present in the feedstock. The higher the efficiency required, the lower must be the impurity concentration of the feedstock. Because impurities concentrate in the liquid during growth, feedstock contaminants must be several times lower in concentration than suggested above when melt replenishment is employed. Continuous replenishment has the advantage over the sequential recharge method because higher feedstock impurity levels can be tolerated.

When ingot diameters reach the projected 12- to 15-cm size required to produce economically viable photovoltaic systems, structural breakdown due to constitutional supercooling of the melt will probably control the maximum allowable impurity concentration in polysilicon feedstock. Breakdown concentrations calculated from theory agree well with experimental data; a more extensive data base would be valuable. High concentrations of impurities such as Zn, Pb, Ca, Mg, or Na, which evaporate at the melting temperature of silicon, probably will not be acceptable in polycrystalline feedstock material because they can contaminate crystal growth equipment.

We found that the electrical activity of impurities decreases due to precipitation in the vicinity of the grain boundaries in polycrystalline material. The magnitude of the reduction is directly related to the impurity diffusion coefficient in silicon. More than a ten-fold reduction in activity occurs for Cr, a rapidly diffusing species, while no change in activity occurs for Mo, which diffuses so slowly that few atoms reach the grain boundaries during the time it takes an ingot to cool from the growth temperature. Ti and V represent intermediate cases. Within the grains, the electrical activity of impurities correlates well with that observed in single crystals.

Thermochemical processing, using HCℓ or $POCℓ_3$ to getter impurities, can produce absolute efficiency improvements of 1 to 2% in cell performance for the longest times and highest temperatures we studied. Cu-, Cr-, Fe-, and Ti-doped wafers respond to the gettering treatment while Mo-doped silicon does not. Gettering appears to be a diffusion-controlled process in which impurities migrate to the wafer surface and are electrically deactivated, thus raising cell performance. During the thermal treatment, a concentration profile of the electrically active species is formed. Cr, which diffuses rapidly, shows the greatest response to gettering or thermal treatment. In contrast, Mo diffuses little, even at 1200°C, and no cell performance improvement occurs. Gettering of impurity-doped polycrystalline silicon produces qualitatively similar results, although cell efficiencies remain low due to the presence of grain boundaries.

Solar cells with phosphorous ion-implanted junctions fabricated on impurity-doped wafers exhibit lower efficiencies than diffused junction cells made from the same wafers. The effect may be due to the lack of gettering available during the implant process or because the activation anneal sequence is not optimum for impurity-containing base material.

Of the several impurities subjected to accelerated high-temperature aging, only Cr and Ag show possible aging effects within the projected 2-year module lifetimes. Further detailed examination of those species' behavior may be warranted. No systematic impurity effects

attributable to electric field effects up to temperatures as high as 280°C were found. A worse-case analysis indicates a 10% depreciation in cell efficiency could occur in 35 years for impurities with the smallest activation energies.

7. PROGRAM STATUS

All tasks of the program have been successfully completed.

8. REFERENCES

1. R. H. Hopkins, et al., 5th Quarterly Report and Summary, Silicon Materials Task, DOE/JPL-954331-77/1 (January 1977).

2. R. H. Hopkins, et al., 11th Quarterly Report and Summary, Silicon Materials Task, DOE/JPL-954331-78/3 (July 1978).

3. R. H. Hopkins, et al., 17th Quarterly Report and Summary, Vols. 1 and 2, Silicon Material Task, DOE/JPL-954331-80/9 (January 1980).

4. Silicon Data Sheets, October 1969, AD 698-342.

5. Silicon Semiconductor Technology, W. R. Runyun, McGraw-Hill, NY, p. 58,59 (1965).

6. Mass Spectrometer Type MS-7 Performance Characteristics, Associated Electrical Industries Ltd.

7. General Activation Analysis Data Sheet "Multi-Element Survey Analysis of Silicon," General Activation Analysis, Inc., San Diego, CA.

8. C. S. Duncan, et al., Annual Report, Silicon Web Process Development, DOE/JPL-954654-78/2 (April 1978).

9. See for example, J. Colby, Computer Program for Quantitative Microprobe Analysis, Bell Telephone Laboratories (1973).

10. W. G. Moffat, Binary Phase Diagram Handbook, General Electric Corp. Schenectady, NY (1976).

11. M. Hansen and K. Anderko, Constitution of Binary Alloys, McGraw-Hill, NY (1958).

12. F. A. Shunk, Constitution of Binary Alloys (Second Supplement), McGraw-Hill, NY (1969).

13. R. H. Hopkins, et al., J. Crystal Growth 42 493 (1977).

14. D. T. J. Hurle, Solid State Electronics 3, 37 (1961).

15. T. F. Gizek J. Appl. Physics 47, 440 (1976).

16. C. D. Thurmond and M. Kowalchik, Bell Syst. Tech. Journal 35, 444 (1964).

17. H. Kodera, Japanese J. of Appl. Physics 2, 212 (1963).

18. T. G. Digges and R. Shima, J. Crystal Growth 50, 865 (1980).

19. J. R. Davis, et al., IEEE Transactions on Electron Devices, ED-27, 677 (1980).

20. A. Rohatgi, et al., IEEE Transactions on Electron Devices, ED 28, 103 (1981).

21. F. A. Lindholm, IEEE Transactions on Electron Devices, ED-26, 165 (1979).

22. J. R. Davis, Proc. 13th IEEE PVSC (IEEE, NY), 490 (1978).

23. A. Rohatgi et al., "Effect of Titanium, Copper and Iron on Silicon Solar Cells," J. Sol. State Electronics, 23 415 (1980).

24. A. Neugroschel, F. Lindholm and C. T. Sah, "A Method for Determining the Emitter and Base Lifetime in p-n Junction Diodes," IEEE Trans. on Electron Devices, ED-24, 662 (1977).

25. R. J. Stirn, "Junction Characteristics of Silicon Solar Cells," Proc. 9th Photovoltaic Specialists Conf. IEEE, NY 72 (1972).

26. M. Wolfe, H. Rauschenbach, "Series Resistance Effects on Solar Cell Measurements," Solar Cells, edited by C. E. Backus, IEEE Press, New York, p. 89 (1976).

27. P. F. Pittman, et al., Proceedings of 12th DVSC, IEEE,NY (1976).

28. A. Rohatgi et al., Proc. of 14th IEEE Photovoltaic Specialists Conf., p. 908 (January 1980).

29. R. V. Ravi et al. in Proc. 12th IEEE Photovoltaic Specialists Conf, p. 280 (1976).

30. H. Fisher and Pschunder, Proc. 12th IEEE Photovoltaic Specialists Conf, p. 280 (1976).

31. T. Lindmayer, Proc. 13th IEEE Photovoltaic Specialists Conf., p. 1096 (1978).

32. A. B. Kuper, Proc. 13th IEEE Photovoltaic Specialists Conf., p. 1090 (1978).

33. V. P. Boldyrev et al., Sov. Phys. Semicond. Vol. 11, No. 6, p. 709 (June 1977).

34. A. R. Kirkpatrick, Proceedings of 14th PVSC, IEEE, NY 820 (1980).

35. G. L. Miller et al., Ann. Rev. Material Science, p. 377 (1977).

36. K. Sharp et al., 2nd Qu. Report, Silicon Materials Task, DOE/JPL 955533-79/1 May (1980).

37. M. F. Browning, et al., Proceedings of 12th PVSC, IEEE, NY 130 (1976).

38. K. Wieser, J. Phys. Chem. Solids, 7, 118 (1958).

39. H. A. Wolf, Silicon Semiconductor Data, Pergamon Press (1969).

40. F. Trumbore, Bell System Tech. Journal, 39 205 (1960).

41. L. Pauling, Nature of the Chemical Bond, Ed 3, Cornell University Press, Ithaca, NY (1960).

42. A. G. Milnes, Deep Impurities in Semiconductors, NY, Wiley Interscience (1973).

43. J. W. Chen and A. G. Milnes, Appl. Rev. Material Science, 10, 157 (1980).

9. APPENDICES

Listed in the following appendices are data for all Phase IV Ingots (W198 to W238). Data for ingots W001 through W197 can be found in reference 3, Volumes 1 and 2.

APPENDIX I

Summary of Phase IV Ingot Electrical and Defect Characteristics

Ingot Identification	TGT Resistivity (ohm-cm)	Actual Resistivity (ohm-cm)	Etch Pit Density* (#/cm^2)
W-197-Ti/V/Mo/Ta/Cu-001	4.0 (B)	4.0-3.4	0-2K
W-198-00-000	4.0	4.1-3.9	0-3K
W-199-00-000	4.0	3.7-3.5	1-5K
W-200-V-004/Poly	4.0	3.6-2.3	NA^{+++}
W-201-Mo-007/Poly	4.0	3.8-2.3	NA
W-202-Ti-013/Poly	4.0	5.3-3.9	NA
W-203-V-005/Poly	4.0	4.4-3.8	NA
W-204-Cr-008/Poly	4.0	4.7-4.3	NA
W-205-Fe-009/Poly	4.0	4.0-3.2	NA
W-206-V-006	4.0	3.7-3.6	0-5K
W-207-Mo-008	4.0	3.8-3.5	0-15K
W-208-Cr-009	4.0	3.7-3.5	0-15K
W-209-Ti-014	4.0	4.0-3.3	0-10K
W-210-Ti-015	4.0	4.0-3.5	0-5K
W-211-Cu-007	4.0	4.0-3.1	0-5K
W-212-Cu-008	4.0	3.9-3.3	5-20K
W-213-Pb-001	4.0	3.3-2.7	10-20K
W-214-V-007-Poly	4.0	3.8-3.1	NA

Ingot Identification	TGT Resistivity (ohm-cm)	Actual Resistivity (ohm-cm)	Etch Pit Density* (#/cm^2)
W-215-Mo-009-Poly	4.0	3.8-1.7	NA
W-216-Cr-010-Poly	4.0	7.6-2.9	NA
W-217-Ta-005	4.0	3.5-3.0	0-10K
W-218-Ta-006	4.0	3.7-3.2	0-5K
W-219-V-008	4.0	3.6-3.3	0-5K
W-220-W-005	4.0	3.7-3.2	0-20K
W-221-Ni-005	4.0	3.5-3.1	0K
W-222-Ag-002	4.0	5.8-5.7	0-Gross Lineage
W-223-Ni-006	4.0	3.6-3.1	0-5K
W-224-HSC/DCS057	1.0	1.4-1.2	5-20K
W-225-Mn-009	4.0	5.5-3.5	0-5K
W-226-Mn-010	4.0	++++	++++
W-227-Cr-011-Poly	4.0	3.9-3.5	NA
W-228-Gd-001	4.0	5.4-5.1	0-Gross Lineage
W-229-Au-001	4.0	4.3-4.2	0-30K
W-230-Al-003	1.5	1.5-0.5	0-20K
W-231-Mn-011-Poly	4.0	4.4-3.1	NA
W-232-N/Ti-001	30	31-23	0-20K
W-233-Cr-012	4.0	4.1-3.7	0-5K
W-234-Mo-010	4.0	4.1-3.8	0-5K
W-235-N/V-001	30	33.5-23.0	0-5K
W-236-N/Mo-001	30	34.4-28.3	0-20K
W-237-Cr-001	30	24.0-17.4	0-5K
W-238-Mn-001	30	50-23	0-5K

*The first figure is etch pit density of the seed; second figure etch pit density of extreme tang end of ingot. The first value shown is indicative of dislocation density in slices used for cell fabrication. Structural degradation commonly occurs at the tang end of the most heavily doped ingots due to constitutional supercooling.

APPENDIX II

Ingot Carbon and Oxygen Concentrations of Selected Phase IV Ingots

Ingot Identification	Carbon Concentration ($X10^{16}$ atoms/cm^3)	Oxygen Concentration ($X10^{16}$ atoms/cm^3)
W-175-W-003	10	158
W-177-N/Cr/Mn-001	8	150
W*-179-Ph-006	***	***
W-181-Cr-006	8	119
W-183-Nb-002	6	35
W-185-Cu/Ti-004	5	39
W-187-Co/-004	20	164
W-189-Nb-003	13	138
W-191-Cu/Ta-001	12	110
W-193-Sn-001	9.4	200
W-195-Ti/V/Mo-001	32	110
W-197-Ti/V/Mo/Ta/Cu-001	15	130
W-201-Mo-007-Poly	7.0	61
W-203-V-005-Poly	12	59
W-205-Fe-009-Poly	8.0	34
W-207-Mo-008	5.4	43
W-209-Ti-014	6.4	61
W-211-Cu-007	6.0	57
W-213-Pb-001	8.0	57
W-215-Mo-009-Poly	10.0	56
W-217-Ta-005	12.0	50
W-219-V-008	25.0	43
W-221-Ni-005	10.0	53
W-223-Ni-006	20.0	77
W-225-Mn-009	4.0	58
W-227-Cr-011-Poly	16.0	82
W-229-Au-001	7.3	80
W-231-Mn-011-Poly	13.0	38
W-233-Cr-012	9.0	45
W**-235-N/V-001	12.0	50
W**-237-Cr-001	8.0	55

* Low-resisitivity ingot

** High-resistivity ingot

*** Due to free carrier-absorption, infrared methods cannot be used for carbon and oxygen determination in this sample.

APPENDIX III

Ingot Impurity Concentration for Phase IV Ingots

Ingot Identification	Target Concentration 10^{15}atoms/cm^3	Calculated Concentration 10^{15}atoms/cm^3	Measured Concentration 10^{15}atoms/cm^3
W-198-00-000	None	N/A	None
W-199-00-000	None	N/A	None
W-200-V-004-Poly	0.4	0.38	18.5[s]
W-201-Mo-007-Poly	0.005	0.003	77[s]
W-202-Ti-013-Poly	0.02	0.018	<0.25
W-203-V-005-Poly	0.04	0.053	<0.15
W-204-Cr-008-Poly	1.0	0.82	1322[s]
W-205-Fe-009-Poly	0.5	0.61	<1.5
W-206-V-006	0.02	0.026	<0.15
W-207-Mo-008	0.002	0.002	<0.5
W-208-Cr-009	0.2	0.19	0.6
W-209-Ti-014	0.02	0.024	<0.25
W-210-Ti-015	0.08	0.10	<0.25
W-211-Cu-007	1.0	1.0	2.6
W-212-Cu-008	10	12.5	27
W-213-Pb-001	Max. Conc.	Non Detectable	<0.10[x]
W-214-V-007-Poly	0.20	0.30	0.55[t]
W-215-Mo-009-Poly	0.0025	0.002	<0.5[t]
W-216-Cr-010-Poly	1.1	0.64	2.2[t]
W-217-Ta-005	0.00015	0.0003	<0.5
W-218-Ta-006	0.000065	0.0001	<0.5
W-219-V-008	0.007	0.009	<0.15
W-220-W-005	0.0008	0.0007	<0.15

APPENDIX III (Cont.

Ingot Identification	Target Concentration 10^{15} atoms/cm^3	Calculated Concentration 10^{15} atoms/cm^3	Measured Concentration 10^{15} atoms/cm^3
W-221-Ni-005	10	8.2	<1.5
W-222-Ag-002	4.5	3.2	6.0
W-223-Ni-006	1.0	1.1	<1.5
W-224-HSC/DCS057	NA[y]	None	<0.2[y]
W-225-Mn-009	1.0	1.5	5.5
W-226-Mn-010	4.0	u	u
W-227-Cr-011-Poly	0.55	0.43	2.2
W-228-Gd-001	<0.2	###	<0.2 (<0.07)[+]
W-229-Au-001	0.6	0.6	0.55
W-230-Al-003	120	64	120
W-231-Mn-011	0.25	0.23	0.75
W-232-N/Ti-001	0.02	0.01	<0.25[v]
W-233-Cr-012	0.11	0.12	0.2
W-23-Mo-010	0.0007	0.00051	<0.5
W-235-N/V-001	0.006	0.008	<0.15[v]
W-236-N/Mo-001	0.003	0.002	<0.5[v]
W-237-Cr-001[++]	0.02	0.017	<0.15[v]
W-238-Mn-001[++]	0.80	1.0	3.5[v]

++ 30 ohm-cm p-type ingot.

+ Value in parenthesis based on Neutron Activation Analysis. Value without parentheses based on SSMS.

s Ingots contain metal-rich inclusions due to constitutional supercooling.

t Ingots regrown to remove metal-rich inclusions due to constitutional supercooling.

x Pb dopant vaporized on two separate ingot growths.

y No intentional impurity.

u Single growth prohibited due to excessive impurity doping for permanence studies.

Atomic absorption analysis of ingot melt sample showed 2.8% Gd by weight of sample.

v High-resistivity ingot, 30 ohm-cm.

APPENDIX IV

Solar Cell I-V Characteristics of Phase IV Ingots

More than 11,000 devices have been evaluated during the program. The large amount of data gathered has necessitated the use of a computer for data storage, reduction, and analysis. A data base system was developed which contains the measured cell data and ingot analysis along with necessary sample and run identifiers. Sufficient coding is provided to permit addressing data by content or by location. An editing program also was developed so data can be modified, corrected, or edited.[3]

Data sheets for each Phase IV impurity-doped ingot have been printed from the data base and are tabulated in the following pages. Data for ingots W001 to W197, Phases I to III, appear in Table 16 in reference 3, volume 1.

SOL17 6 /19/81

00220 W198 AND W199 BASELINES W133 00 000
SOL17 6 /19/81 AMI: PO=91.60MW/CM^2 NO AR COATING

ID	ISC	VOC	IP	LOG(IO)	N	R	FF	Eff	OCD	PCDa	PCDb
2R*	21.90	.563	19.91	-6.780	1.84	-.74	.748	9.75	.00	.00	.00
1B	22.20	.559	20.39	-7.620	1.56	-.00	.751	9.86	3.64	.00	.00
2B	22.40	.563	20.88	-8.821	1.31	.09	.777	10.36	4.55	.00	.00
3B	22.60	.561	21.06	-8.768	1.32	.05	.777	10.42	4.55	.00	.00
4B	22.70	.562	21.08	-8.512	1.37	.12	.770	10.38	4.55	.00	.00
5B	22.60	.560	21.05	-8.755	1.32	.05	.777	10.40	4.55	.00	.00
6B	22.90	.561	21.07	-7.648	1.56	-.19	.759	10.31	4.56	.00	.00
1981	22.70	.558	20.93	-7.848	1.50	-.06	.759	10.17	3.64	.00	.00
1982	23.00	.558	21.22	-7.890	1.49	-.05	.760	10.32	4.29	.00	.00
1983	22.90	.560	21.12	-7.858	1.50	-.09	.761	10.32	4.94	.00	.00
1984	22.50	.556	20.87	-8.361	1.38	.05	.768	10.17	4.16	.00	.00
1985	22.50	.556	20.95	-8.765	1.30	.12	.775	10.25	4.55	.00	.00
1991	22.50	.557	20.63	-7.362	1.63	-.40	.757	10.04	3.25	.00	.00
1992	22.30	.561	20.81	-8.930	1.29	.05	.781	10.33	4.60	.00	.00
1993	22.40	.559	20.69	-7.949	1.48	-.15	.765	10.13	4.42	.00	.00
1994	22.60	.559	20.87	-7.966	1.48	-.10	.764	10.21	4.16	.00	.00
1995	22.60	.561	20.97	-8.356	1.40	-.03	.771	10.34	4.16	.00	.00
AVERAGES: 00220 BASELINE W133 00 000											
	22.57	.561	20.92	-8.354	1.41	.02	.768	10.29	4.40	.00	.00
STD	.22	.001	.25	.518	.11	.10	.010	.20	.34	*	*
00220 W198 AND W199 BASELINES											
	22.60	.559	20.91	-8.128	1.45	-.07	.766	10.23	4.22	.00	.00
STD	.21	.002	.17	.448	.10	.14	.007	.10	.46	*	*
PERCENT OF BASELINE											
	100.1	99.6	99.9	102.7	103	*****	99.7	99.4	95.8	*****	*****
STD%	1.9	.5	2.0	11.7	16	*****	2.3	2.9	18.6	*****	*****

00417 W202TI013 POLY W198 00 000
SOL17 6 /19/81 AM1: PO=91.60MW/CM^2 NO AR COATING

ID	ISC	VOC	IP	LOG(IO)	N	R	FF	Eff	OCD	PCDa	PCDb
2R*	21.90	.555	19.91	-6.839	1.79	-.54	.744	9.56	.00	.00	.00
1B	22.10	.552	20.69	-9.433	1.19	.37	.779	10.05	4.55	.00	.00
2B	22.10	.550	20.32	-7.647	1.53	-.14	.756	9.72	4.55	.00	.00
3B	21.80	.548	20.13	-7.975	1.45	-.05	.762	9.63	3.90	.00	.00
4B	21.90	.546	19.80	-6.497	1.89	-.79	.740	9.35	3.25	.00	.00
5B	21.60	.550	19.93	-7.937	1.46	-.06	.761	9.56	4.16	.00	.00
1C	15.30	.488	13.72	-6.703	1.67	.45	.705	5.56	.46	.00	.00
2C	15.40	.488	13.81	-6.706	1.67	.50	.703	5.59	.52	.00	.00
3C	15.20	.484	13.54	-6.400	1.76	.26	.697	5.43	.52	.00	.00
4C	15.10	.485	13.51	-6.533	1.72	.22	.704	5.45	.39	.00	.00
5C	15.40	.484	13.59	-6.090	1.89	.36	.682	5.37	.39	.00	.00
6C	15.60	.482	13.82	-6.222	1.82	.43	.686	5.45	.39	.00	.00
7C	16.00	.489	14.32	-6.554	1.72	.30	.703	5.82	.52	.00	.00
8C	15.10	.481	13.43	-6.298	1.79	.13	.696	5.35	.52	.00	.00
9C	15.40	.486	13.75	-6.513	1.73	.38	.699	5.53	.52	.00	.00
10C	15.40	.483	13.77	-6.646	1.67	.64	.697	5.49	.52	.00	.00
1S	15.30	.504	13.57	-6.764	1.70	2.21	.664	5.42	.52	.00	.00
2S	15.10	.485	13.54	-6.729	1.65	.54	.703	5.44	.40	.00	.00
3S	15.60	.489	13.96	-6.493	1.74	.06	.707	5.70	.65	.00	.00
4S	15.40	.485	13.61	-6.056	1.91	-.00	.689	5.44	.52	.00	.00
5S	15.30	.483	13.59	-6.271	1.81	.21	.693	5.42	.52	.00	.00
6S	15.60	.484	13.76	-6.006	1.93	.07	.685	5.47	.39	.00	.00
1T	15.20	.489	13.52	-6.224	1.85	-.17	.701	5.51	.52	.00	.00
2T	15.40	.488	13.68	-6.235	1.84	.08	.695	5.52	.52	.00	.00
3T	15.50	.487	13.75	-6.244	1.83	.26	.691	5.52	.39	.00	.00
4T	15.40	.478	13.12	-4.959	2.54	-1.01	.651	5.07	.39	.00	.00
5T	15.50	.487	13.58	-5.692	2.10	-.44	.682	5.45	.52	.00	.00
AVERAGES: 00417 BASELINE W198 00 000											
	21.90	.549	20.17	-7.898	1.50	-.13	.760	9.66	4.08	.00	.00
STD	.19	.002	.31	.937	.22	.37	.013	.23	.48	*	*
00417 W202TI013 POLY											
	15.39	.486	13.66	-6.302	1.83	.26	.692	5.48	.48	.00	.00
STD	.20	.005	.22	.404	.19	.56	.013	.14	.07	*	*
PERCENT OF BASELINE											
	70.3	88.5	67.7	120.2	121	394.6	91.1	56.7	11.8	*****	*****
STD%	1.6	1.2	2.2	15.2	33	*****	3.3	2.8	3.3	*****	*****

00418 W203V005 POLY W198 00 000
SOL17 6 /19/81 AM1: PO=91.60MW/CM^2 NO AR COATING

ID	ISC	VOC	IP	LOG(IO)	N	R	FF	Eff	OCD	PCDa	PCDb
2R*	21.90	.552	19.70	-6.188	2.04	-1.12	.737	9.43	.00	.00	.00
1B	21.50	.547	19.57	-6.999	1.71	-.33	.742	9.23	3.90	.00	.00
2B	21.60	.547	19.94	-8.008	1.44	.03	.760	9.50	3.90	.00	.00
3B	21.60	.547	19.91	-7.915	1.46	.05	.757	9.46	3.64	.00	.00
4B	22.00	.547	20.07	-7.143	1.67	-.24	.745	9.48	3.90	.00	.00
1C	17.10	.495	15.27	-6.314	1.82	-.17	.707	6.33	.52	.00	.00
2C	17.10	.495	15.25	-6.298	1.82	-.01	.702	6.28	.52	.00	.00
3C	17.10	.495	15.25	-6.298	1.82	-.01	.702	6.28	.65	.00	.00
4C	17.20	.498	15.41	-6.436	1.78	-.20	.713	6.46	.65	.00	.00
5C	17.60	.496	15.74	-6.495	1.75	.31	.701	6.47	.52	.00	.00
6C	17.40	.495	15.48	-6.221	1.85	-.03	.700	6.37	.52	.00	.00
7C	17.30	.496	15.50	-6.443	1.77	-.13	.712	6.46	.52	.00	.00
8C	17.30	.491	15.43	-6.287	1.81	-.06	.703	6.32	.52	.00	.00
9C	17.30	.495	15.52	-6.490	1.75	-.17	.714	6.47	.52	.00	.00
10C	17.30	.490	15.48	-6.424	1.76	-.01	.707	6.34	.52	.00	.00
11C	17.40	.495	15.77	-7.080	1.55	.26	.724	6.59	.52	.00	.00
1S	17.50	.493	15.54	-5.956	1.96	-.77	.708	6.46	.52	.00	.00
2S	17.20	.491	15.39	-6.406	1.77	-.08	.709	6.33	.52	.00	.00
3S	17.10	.493	15.34	-6.512	1.74	-.05	.712	6.35	.52	.00	.00
4S	17.50	.493	15.46	-6.010	1.94	.08	.687	6.27	.52	.00	.00
5S	17.20	.489	15.15	-5.787	2.03	-.47	.691	6.15	.52	.00	.00
6S	17.40	.490	15.35	-5.815	2.02	-.52	.694	6.26	.52	.00	.00
1T	17.50	.497	15.62	-6.243	1.85	-.33	.709	6.52	.52	.00	.00
2T	17.40	.496	15.66	-6.665	1.69	.02	.716	6.53	.52	.00	.00
3T	17.40	.495	15.40	-5.966	1.97	-.30	.696	6.34	.52	.00	.00
4T	17.40	.491	15.44	-6.029	1.92	-.37	.700	6.33	.52	.00	.00
5T	17.20	.493	15.37	-6.373	1.79	-.04	.706	6.33	.52	.00	.00
6T	17.50	.493	15.63	-6.304	1.81	-.23	.709	6.47	.52	.00	.00
AVERAGES: 00418 BASELINE W198 00 000											
	21.68	.547	19.87	-7.516	1.57	-.12	.751	9.42	3.84	.00	.00
STD	.19	.000	.18	.449	.12	.17	.008	.11	.11	*	*
00418 W203V005 POLY											
	17.32	.494	15.45	-6.298	1.82	-.14	.705	6.38	.53	.00	.00
STD	.15	.002	.16	.282	.11	.24	.008	.10	.04	*	*
PERCENT OF BASELINE											
	79.9	90.3	77.8	116.2	116	85.3	93.9	67.8	13.9	*****	*****
STD%	1.4	.4	1.5	9.0	16	606.2	2.1	1.9	1.4	*****	*****

00930 W205FE009 (5E14) W199 00 000
SOL18 6 /19/81 AM1: PO=91.60MW/CM^2 NO AR COATING

ID	ISC	VOC	IP	LOG(IO)	N	R	FF	Eff	OCD	PCDa	PCDb
3R*	22.10	.546	19.62	-5.701	2.25	-1.15	.716	9.14	.00	.00	.00
1B.*	21.40	.543	18.69	-5.108	2.64	-1.95	.704	8.65	2.34	.00	.00
2B.*	21.30	.541	18.65	-5.123	2.62	-2.17	.711	8.67	2.86	.00	.00
3B.*	21.70	.538	18.87	-5.026	2.67	-1.75	.694	8.57	2.21	.00	.00
4B.*	21.70	.538	18.26	-4.236	3.49	-3.06	.667	8.24	2.08	.00	.00
5B*	21.40	.525	17.91	-4.334	3.29	-1.92	.644	7.65	1.04	.00	.00
3C	17.50	.476	14.59	-4.577	2.82	-.77	.623	5.49	.24	.00	.00
4C	18.00	.494	15.30	-4.786	2.71	-1.29	.654	6.15	.40	.00	.00
5C*	16.00	.385	9.67	-10.590	.73	17.49	.311	2.03	.09	.00	.00
6C	16.80	.477	14.44	-5.201	2.33	-.40	.656	5.56	.33	.00	.00
7C	18.00	.490	15.14	-4.538	2.93	-1.76	.646	6.03	.30	.00	.00
8C	16.80	.487	14.90	-6.030	1.91	-.33	.699	6.05	.40	.00	.00
10C*	15.70	.442	13.86	-8.001	1.19	5.11	.609	4.47	.13	.00	.00
1S	17.00	.486	14.77	-5.303	2.30	-1.06	.680	5.94	.30	.00	.00
2S	16.90	.479	14.43	-4.984	2.49	-.84	.653	5.59	.30	.00	.00
3S	17.50	.490	15.08	-5.050	2.49	-1.32	.672	6.09	.30	.00	.00
4S	17.10	.484	14.68	-5.047	2.46	-1.03	.663	5.80	.26	.00	.00
5S	18.00	.490	15.51	-5.088	2.45	-1.07	.669	6.24	.30	.00	.00
6S	18.40	.496	15.54	-4.569	2.92	-1.89	.654	6.31	.50	.00	.00

AVERAGES: 00930 BASELINE W199 00 000
NO BASELINE

	00930 W205FE009 (5E14)										
	17.45	.486	14.94	-5.016	2.53	-1.07	.661	5.93	.33	.00	.00
STD	.55	.006	.38	.407	.29	.47	.019	.27	.07	*	*

00422 W206V006 W198 00 000
SOL17 6 /19/81 AM1: PO=91.60MW/CM^2 NO AR COATING

ID	ISC	VOC	IP	LOG(IO)	N	R	FF	Eff	OCD	PCDa	PCDb
2R*	21.90	.554	20.04	-7.275	1.65	-.34	.752	9.65	.00	.00	.00
1B	21.70	.549	19.67	-6.647	1.84	-.69	.742	9.35	3.64	.00	.00
2B	21.40	.546	19.26	-6.304	1.97	-.83	.732	9.05	3.00	.00	.00
3B.*	21.40	.546	19.05	-5.791	2.21	-1.24	.722	8.92	2.86	.00	.00
4B	21.40	.548	19.40	-6.627	1.85	-.80	.744	9.23	3.12	.00	.00
5B	21.50	.545	19.32	-6.181	2.02	-1.03	.734	9.09	3.00	.00	.00
1C.*	18.00	.503	15.09	-4.254	3.35	-3.56	.664	6.35	.39	.00	.00
2C	18.00	.502	15.45	-4.856	2.70	-1.91	.675	6.45	.39	.00	.00
3C	18.30	.507	16.02	-5.326	2.36	-1.60	.699	6.86	.39	.00	.00
4C	18.10	.504	15.87	-5.450	2.27	-1.25	.696	6.72	.39	.00	.00
5C	18.60	.510	16.58	-6.004	1.99	-.95	.718	7.20	.40	.00	.00
6C	18.30	.506	16.33	-6.087	1.94	-.80	.717	7.02	.40	.00	.00
7C	18.10	.503	15.95	-5.655	2.15	-.96	.700	6.74	.40	.00	.00
8C	18.60	.506	16.54	-5.921	2.02	-.92	.713	7.10	.40	.00	.00
9C	18.50	.508	16.59	-6.239	1.88	-.82	.725	7.20	.50	.00	.00
10C	18.80	.507	16.70	-5.874	2.04	-.97	.713	7.19	.40	.00	.00
1S	19.20	.516	17.19	-6.157	1.94	-.84	.723	7.57	.65	.00	.00
2S	19.00	.513	17.22	-6.761	1.70	-.56	.738	7.61	.52	.00	.00
3S	18.90	.508	16.60	-5.495	2.25	-1.14	.698	7.09	.40	.00	.00
4S	18.60	.509	16.64	-6.171	1.91	-.77	.720	7.21	.40	.00	.00
5S	18.50	.500	15.71	-4.740	2.78	-1.37	.654	6.40	.40	.00	.00
6S	18.30	.502	16.04	-5.441	2.26	-1.22	.696	6.76	.40	.00	.00
1T	18.70	.512	16.79	-6.306	1.87	-.79	.727	7.36	.52	.00	.00
2T	18.50	.507	16.42	-5.867	2.05	-.87	.709	7.03	.39	.00	.00
3T	20.10	.515	17.46	-5.118	2.51	-1.42	.687	7.52	.50	.00	.00
4T	18.80	.510	16.98	-6.641	1.73	-.45	.731	7.41	.52	.00	.00
5T	18.90	.509	16.90	-6.193	1.90	-.62	.718	7.30	.52	.00	.00
6T	18.70	.502	16.16	-5.050	2.52	-1.43	.679	6.74	.39	.00	.00
AVERAGES: 00422 BASELINE W198 00 000											
	21.50	.547	19.41	-6.440	1.92	-.84	.738	9.18	3.19	.00	.00
STD	.12	.002	.16	.202	.08	.12	.005	.12	.26	*	*
00422 W206V006											
	18.64	.507	16.48	-5.779	2.13	-1.03	.706	7.07	.44	.00	.00
STD	.45	.004	.51	.547	.30	.36	.020	.34	.07	*	*
PERCENT OF BASELINE											
	86.7	92.8	84.9	110.3	111	76.4	95.7	77.0	13.9	*****	*****
STD%	2.6	1.0	3.3	11.6	20	67.1	3.4	4.7	3.5	*****	*****

00423 W207M0008 W198 00 000
SOL17 6 /19/81 AM1: PO=91.60MW/CM^2 NO AR COATING

ID	ISC	VOC	IP	LOG(IO)	N	R	FF	Eff	OCD	PCDa	PCDb
2R*	21.90	.556	19.84	-6.586	1.89	-.79	.743	9.56	.00	.00	.00
1B	22.70	.550	20.72	-7.236	1.64	.00	.740	9.77	3.64	.00	.00
2B	22.10	.552	20.45	-8.214	1.41	.10	.763	9.84	3.90	.00	.00
3B	22.80	.552	20.92	-7.449	1.59	-.23	.754	10.04	4.29	.00	.00
4B	22.50	.552	20.51	-7.166	1.67	-.02	.738	9.70	3.64	.00	.00
1C	19.90	.524	17.70	-5.938	2.07	-.73	.711	7.84	.65	.00	.00
2C	19.80	.525	17.97	-7.065	1.64	.17	.727	8.00	.65	.00	.00
3C	19.80	.524	17.77	-6.280	1.91	-.68	.724	7.95	.78	.00	.00
4C	20.20	.516	17.48	-5.055	2.56	-1.33	.680	7.50	.40	.00	.00
5C	19.90	.519	17.52	-5.561	2.25	-1.01	.700	7.65	.65	.00	.00
6C	19.90	.518	17.59	-5.740	2.14	-.71	.701	7.64	.55	.00	.00
7C	20.30	.522	18.08	-5.948	2.05	-.83	.715	8.01	.78	.00	.00
8C	20.40	.523	18.07	-5.675	2.19	-1.17	.712	8.03	.78	.00	.00
9C	20.20	.523	17.98	-5.905	2.08	-.92	.716	8.00	.78	.00	.00
1S	20.50	.523	18.02	-5.436	2.33	-1.25	.702	7.96	.65	.00	.00
2S	20.70	.525	18.50	-6.009	2.03	-.96	.723	8.31	.80	.00	.00
3S	20.70	.525	18.68	-6.497	1.82	-.64	.733	8.43	.78	.00	.00
4S	20.60	.526	18.65	-6.663	1.77	-.56	.737	8.44	.91	.00	.00
5S	20.50	.523	18.37	-6.108	1.98	-1.01	.728	8.26	.78	.00	.00
1T	20.20	.523	18.20	-6.387	1.86	-.80	.733	8.19	.78	.00	.00
2T	20.10	.520	17.90	-5.900	2.07	-1.02	.718	7.94	.65	.00	.00
3T	20.20	.520	17.97	-5.881	2.08	-.92	.715	7.94	.65	.00	.00
4T	20.40	.521	18.31	-6.315	1.88	-.54	.723	8.12	.65	.00	.00
5T	20.20	.518	17.40	-4.883	2.71	-1.69	.678	7.51	.52	.00	.00
AVERAGES: 00423 BASELINE W198 00 000											
	22.53	.552	20.65	-7.516	1.58	-.04	.749	9.84	3.87	.00	.00
STD	.27	.001	.18	.416	.10	.12	.010	.13	.27	*	*
00423 W207M0008											
	20.24	.522	18.01	-5.960	2.07	-.87	.715	7.98	.69	.00	.00
STD	.28	.003	.37	.513	.25	.37	.016	.27	.12	*	*
PERCENT OF BASELINE											
	89.8	94.7	87.2	120.7	132	*****	95.4	81.2	17.9	*****	*****
STD%	2.3	.7	2.6	11.6	26	*****	3.5	3.8	4.5	*****	*****

00424 W208CR009 (6E14) W198 00 000
SOL17 6 /19/81 AM1: PO=91.60MW/CM^2 NO AR COATING

ID	ISC	VOC	IP	LOG(IO)	N	R	FF	Eff	OCD	PCDa	PCDb
2R*	21.90	.553	19.93	-6.937	1.75	-.46	.745	9.54	.00	.00	.00
1B	22.00	.553	20.40	-8.301	1.39	-.03	.770	9.90	4.29	.00	.00
2B	21.90	.553	20.25	-8.134	1.43	.02	.764	9.78	4.03	.00	.00
3B.*	22.10	.546	19.38	-5.254	2.53	-1.60	.705	9.00	3.00	.00	.00
1C	20.10	.530	17.53	-5.126	2.58	-1.89	.700	7.88	.78	.00	.00
2C	19.80	.528	17.48	-5.496	2.33	-1.63	.714	7.89	.78	.00	.00
3C	20.60	.541	18.78	-7.022	1.69	-.55	.749	8.83	1.70	.00	.00
4C	19.70	.525	17.41	-5.645	2.23	-1.17	.708	7.75	.78	.00	.00
5C	20.90	.529	17.78	-4.495	3.14	-2.56	.674	7.89	.91	.00	.00
6C	20.70	.532	17.64	-4.523	3.13	-2.65	.678	7.90	.78	.00	.00
7C	20.30	.532	17.95	-5.535	2.31	-1.59	.716	8.18	1.10	.00	.00
8C	20.20	.538	18.33	-6.711	1.79	-.82	.746	8.57	1.43	.00	.00
9C	19.90	.466	15.64	-3.987	3.40	.17	.552	5.41	.20	.00	.00
1S	19.80	.527	17.02	-4.733	2.91	-2.45	.686	7.57	.78	.00	.00
2S	20.70	.539	18.60	-6.253	1.97	-.85	.730	8.61	1.43	.00	.00
3S	19.70	.525	17.54	-5.988	2.05	-.75	.713	7.80	.65	.00	.00
4S	19.80	.529	17.76	-6.123	2.00	-1.15	.731	8.10	.91	.00	.00
1T	20.60	.539	18.52	-6.269	1.96	-.87	.731	8.58	1.30	.00	.00
2T	20.00	.532	18.06	-6.509	1.85	-.76	.736	8.28	.91	.00	.00
3T	20.70	.536	18.25	-5.516	2.34	-1.26	.706	8.29	1.04	.00	.00
4T	20.30	.533	18.09	-5.934	2.10	-.94	.717	8.21	1.04	.00	.00
5T	20.30	.532	18.47	-6.988	1.68	-.39	.743	8.48	1.04	.00	.00
AVERAGES: 00424 BASELINE W198 00 000											
	21.95	.553	20.33	-8.218	1.41	-.01	.767	9.84	4.16	.00	.00
STD	.05	.000	.07	.084	.02	.03	.003	.06	.13	*	*
00424 W208CR009 (6E14)											
	20.23	.529	17.83	-5.714	2.30	-1.23	.707	8.01	.98	.00	.00
STD	.39	.016	.70	.855	.51	.75	.043	.72	.33	*	*
PERCENT OF BASELINE											
	92.2	95.6	87.7	130.5	163	*****	92.2	81.4	23.5	*****	*****
STD%	2.0	2.9	3.8	11.2	39	*****	6.0	7.8	9.0	*****	*****

00513 W209TI014 (2.5E14) W198 00 000
SOL17 6 /19/81 AM1: PO=91.60MW/CM^2 NO AR COATING

ID	ISC	VOC	IP	LOG(IO)	N	R	FF	Eff	OCD	PCDa	PCDb
2R*	21.90	.554	19.67	-6.137	2.07	-1.07	.733	9.41	.00	.00	.00
1B.*	22.20	.545	19.75	-5.965	2.11	-.50	.708	9.06	3.25	.00	.00
2B*	22.80	.549	19.20	-4.545	3.16	-1.06	.641	8.48	3.12	.00	.00
3B	22.70	.547	21.01	-8.391	1.35	.45	.755	9.91	3.64	.00	.00
4B	22.90	.552	21.34	-9.080	1.24	.62	.763	10.21	4.55	.00	.00
5B	22.80	.546	20.63	-6.653	1.82	-.36	.733	9.65	3.12	.00	.00
1C	16.00	.498	13.87	-5.382	2.32	-.61	.670	5.65	.21	.00	.00
2C	16.30	.488	13.95	-5.120	2.45	-.45	.651	5.48	.26	.00	.00
3C	16.50	.497	14.25	-5.295	2.36	-.49	.663	5.75	.33	.00	.00
4C	15.90	.493	13.02	-4.512	3.03	.03	.594	4.93	.26	.00	.00
5C	16.20	.485	13.76	-4.962	2.55	-.52	.642	5.33	.20	.00	.00
6C	16.10	.494	14.04	-5.580	2.18	-.27	.673	5.66	.33	.00	.00
7C	15.70	.495	13.73	-5.587	2.19	-.65	.682	5.60	1.56	.00	.00
8C	16.40	.493	14.22	-5.497	2.22	.00	.662	5.66	.26	.00	.00
9C	16.40	.500	14.65	-6.518	1.76	.41	.699	6.06	.30	.00	.00
10C	16.40	.494	14.23	-5.425	2.27	-.40	.668	5.73	.27	.00	.00
12C	16.10	.491	13.99	-5.571	2.17	.04	.665	5.56	.26	.00	.00
1S	15.80	.498	13.69	-5.311	2.37	-.99	.674	5.61	.26	.00	.00
2S	15.80	.501	14.19	-6.887	1.65	.89	.700	5.86	.26	.00	.00
3S	15.60	.499	13.99	-6.688	1.71	.42	.705	5.80	.30	.00	.00
4S	16.10	.494	13.66	-4.747	2.79	-1.79	.655	5.51	.20	.00	.00
5S	16.30	.503	14.43	-5.984	2.00	-.44	.698	6.05	.20	.00	.00
1T	15.50	.489	13.29	-5.248	2.38	-.09	.649	5.20	.20	.00	.00
2T	15.90	.500	14.28	-6.717	1.70	.30	.709	5.96	.26	.00	.00
3T	15.70	.501	14.06	-6.527	1.77	.11	.707	5.88	.26	.00	.00
4T	16.00	.497	14.00	-5.685	2.13	-.24	.678	5.70	.26	.00	.00
5T	15.70	.499	14.09	-6.674	1.71	.29	.708	5.86	.33	.00	.00
6T	15.90	.490	13.56	-5.010	2.55	-.77	.650	5.36	.26	.00	.00
AVERAGES: 00513 BASELINE W198 00 000											
	22.80	.548	20.99	-8.041	1.47	.24	.750	9.92	3.77	.00	.00
STD	.08	.003	.29	1.021	.25	.43	.013	.23	.59	*	*
00513 W209TI014 (2.5E14)											
	16.01	.495	13.95	-5.679	2.19	-.24	.673	5.65	.32	.00	.00
STD	.28	.005	.36	.683	.36	.56	.027	.27	.27	*	*
PERCENT OF BASELINE											
	70.2	90.3	66.5	129.4	149	*****	89.7	56.9	8.5	*****	*****
STD%	1.5	1.3	2.7	18.5	54	845.5	5.2	4.1	9.7	*****	*****

00527 W211CU007 (2.6E15) W198 00 000
SOL17 6 /19/81 AM1: PO=91.60MW/CM^2 NO AR COATING

ID	ISC	VOC	IP	LOG(IO)	N	R	FF	Eff	OCD	PCDa	PCDb
3R*	22.10	.555	19.90	-6.290	2.00	-.92	.735	9.54	.00	.00	.00
1B	21.70	.553	19.99	-7.759	1.52	-.17	.760	9.64	3.25	.00	.00
2B	21.70	.553	19.99	-7.759	1.52	-.17	.760	9.64	2.73	.00	.00
3B	22.10	.556	20.09	-7.035	1.73	.02	.733	9.52	3.90	.00	.00
4B	21.90	.551	20.04	-7.174	1.67	-.55	.756	9.64	2.60	.00	.00
5B.*	21.70	.549	19.38	-5.856	2.19	-1.34	.729	9.18	2.86	.00	.00
1C	21.80	.560	20.22	-8.419	1.38	.11	.767	9.91	4.16	.00	.00
2C	21.70	.557	19.93	-7.518	1.59	-.31	.758	9.69	3.64	.00	.00
3C	21.60	.557	20.02	-8.189	1.43	-.23	.773	9.84	3.90	.00	.00
4C	21.60	.553	19.84	-7.426	1.60	-.58	.764	9.65	3.90	.00	.00
5C	21.70	.551	19.90	-7.350	1.62	-.51	.760	9.60	3.90	.00	.00
6C	21.40	.555	19.68	-7.510	1.59	-.53	.764	9.60	3.12	.00	.00
7C	21.50	.553	19.61	-6.913	1.76	-.85	.756	9.50	3.64	.00	.00
8C	21.70	.552	19.19	-5.456	2.43	-1.75	.720	9.12	3.00	.00	.00
9C	21.70	.556	20.02	-7.763	1.52	-.39	.768	9.79	4.55	.00	.00
1S	21.30	.550	19.19	-6.310	1.98	-1.00	.737	9.14	2.60	.00	.00
2S	21.50	.549	19.51	-6.663	1.84	-.85	.747	9.33	2.60	.00	.00
3S	21.70	.552	19.82	-7.183	1.67	-.33	.748	9.48	3.25	.00	.00
4S	21.40	.549	19.58	-7.155	1.67	-.63	.757	9.40	2.60	.00	.00
5S	21.40	.547	19.35	-6.432	1.92	-1.05	.744	9.22	2.60	.00	.00
6S	21.50	.546	19.12	-5.660	2.28	-1.61	.726	9.02	2.34	.00	.00
1T	21.80	.554	20.07	-7.726	1.53	-.20	.760	9.71	4.29	.00	.00
2T	21.40	.551	19.36	-6.520	1.90	-.83	.741	9.23	2.86	.00	.00
3T	21.90	.553	20.06	-7.235	1.66	-.57	.758	9.71	3.25	.00	.00
4T	22.30	.551	20.66	-8.153	1.42	-.23	.773	10.04	3.90	.00	.00
5T	21.70	.551	19.86	-7.240	1.65	-.46	.755	9.54	3.25	.00	.00
6T	22.20	.553	20.51	-7.959	1.47	-.20	.767	9.96	4.55	.00	.00
AVERAGES: 00527 BASELINE W198 00 000											
	21.85	.553	20.02	-7.432	1.61	-.22	.752	9.61	3.12	.00	.00
STD	.17	.002	.04	.331	.09	.21	.011	.05	.51	*	*
00527 W211CU007 (2.6E15)											
	21.66	.552	19.79	-7.180	1.71	-.62	.754	9.55	3.42	.00	.00
STD	.25	.003	.41	.770	.27	.45	.014	.28	.67	*	*
PERCENT OF BASELINE											
	99.1	99.8	98.8	103.4	106	-83.9	100.3	99.3	109.7	*****	*****
STD%	1.9	.9	2.2	15.1	24	674.2	3.4	3.5	43.0	*****	*****

00514 W210TI015 (2.5E14) W198 00 000
SOL17 6 /19/81 AM1: PO=91.60MW/CM^2 NO AR COATING

ID	ISC	VOC	IP	LOG(IO)	N	R	FF	Eff	OCD	PCDa	PCDb
2R*	21.90	.550	19.50	-6.334	1.97	.55	.690	8.79	.00	.00	.00
1B.*	21.90	.535	18.64	-4.660	2.98	-1.47	.660	8.18	1.82	.00	.00
2B	21.70	.544	19.51	-6.374	1.93	-.49	.725	9.05	3.64	.00	.00
3B.*	22.00	.539	18.97	-4.863	2.81	-1.65	.681	8.54	2.34	.00	.00
4B*	13.80	.468	11.98	-5.652	2.06	.32	.660	4.51	.33	.00	.00
5B	22.00	.547	20.38	-8.438	1.35	.40	.758	9.64	4.16	.00	.00
1C	13.90	.471	12.19	-5.792	2.00	-.37	.683	4.73	.39	.00	.00
2C	13.70	.474	12.22	-6.541	1.69	.51	.696	4.78	.50	.00	.00
3C	14.20	.477	12.54	-6.101	1.87	.18	.685	4.91	.52	.00	.00
4C	14.20	.477	12.62	-6.357	1.77	.36	.692	4.96	.40	.00	.00
5C	14.20	.475	12.42	-5.833	1.99	.21	.672	4.79	.30	.00	.00
6C	13.90	.474	12.32	-6.258	1.80	.33	.689	4.80	.52	.00	.00
1S	13.90	.474	12.16	-5.873	1.97	.42	.669	4.66	.39	.00	.00
2S	14.10	.464	11.95	-5.040	2.43	-.27	.637	4.40	.30	.00	.00
3S	13.90	.469	12.00	-5.528	2.13	.30	.653	4.51	.40	.00	.00
4S	14.50	.481	12.74	-6.118	1.88	.93	.669	4.93	.33	.00	.00
5S	14.20	.469	12.17	-5.240	2.31	-.33	.651	4.58	.40	.00	.00
6S	14.10	.467	11.93	-4.979	2.49	-.46	.636	4.43	.40	.00	.00
1T	14.10	.478	12.38	-6.007	1.92	.57	.672	4.79	.26	.00	.00
2T	13.30	.472	11.77	-6.334	1.77	.84	.680	4.51	.40	.00	.00
3T	13.90	.478	12.41	-6.605	1.68	.67	.695	4.88	.52	.00	.00
4T	13.70	.463	11.51	-4.936	2.52	-.05	.623	4.18	.30	.00	.00
5T	14.10	.473	12.28	-5.757	2.02	.40	.664	4.68	.26	.00	.00
AVERAGES: 00514 BASELINE W198 00 000											
	21.85	.546	19.94	-7.406	1.64	-.04	.741	9.35	3.90	.00	.00
STD	.15	.002	.43	1.032	.29	.44	.017	.30	.26	*	*
00514 W210TI015 (2.5E14)											
	13.99	.473	12.21	-5.841	2.01	.25	.669	4.68	.39	.00	.00
STD	.26	.005	.30	.520	.26	.41	.021	.21	.09	*	*
PERCENT OF BASELINE											
	64.0	86.7	61.2	121.1	123	770.6	90.2	50.1	9.9	*****	*****
STD%	1.6	1.1	2.9	19.0	41	*****	5.0	3.9	3.0	*****	*****

00623 W212CU008 (8.05E16) W198 00 000
SOL17 6 /19/81 AM1: PO=91.60MW/CM^2 NO AR COATING

ID	ISC	VOC	IP	LOG(IO)	N	R	FF	Eff	OCD	PCDa	PCDb
3R*	22.10	.559	19.51	-5.446	2.46	-1.59	.715	9.34	.00	.00	.00
1B	22.10	.554	20.24	-7.387	1.61	-.19	.750	9.72	4.29	.00	.00
2B	21.80	.552	19.85	-6.968	1.74	-.43	.745	9.48	3.64	.00	.00
3B	21.70	.555	19.99	-7.722	1.53	-.27	.762	9.71	4.55	.00	.00
4B	22.20	.552	20.08	-6.570	1.88	-.59	.736	9.54	3.64	.00	.00
5B	22.30	.551	20.26	-6.839	1.77	-.44	.741	9.63	3.64	.00	.00
1C	21.60	.551	19.23	-5.733	2.26	-1.46	.725	9.13	2.21	.00	.00
2C	21.50	.547	18.86	-5.242	2.56	-1.80	.708	8.81	1.82	.00	.00
3C	21.60	.549	19.48	-6.349	1.96	-.92	.737	9.25	2.47	.00	.00
4C	22.00	.549	19.89	-6.470	1.91	-.84	.740	9.46	2.60	.00	.00
5C	21.50	.548	19.57	-6.967	1.73	-.43	.744	9.27	2.21	.00	.00
6C	21.80	.550	20.00	-7.434	1.59	-.36	.757	9.60	3.00	.00	.00
7C	21.90	.550	20.04	-7.217	1.65	-.45	.754	9.60	3.00	.00	.00
8C	22.00	.552	19.73	-6.057	2.10	-1.13	.732	9.40	3.38	.00	.00
9C	22.10	.553	20.35	-7.732	1.52	-.15	.759	9.81	3.38	.00	.00
10C	21.70	.549	19.71	-6.770	1.80	-.65	.745	9.38	2.47	.00	.00
1S	21.80	.548	19.52	-6.240	2.00	-.38	.716	9.04	3.00	.00	.00
2S	22.40	.550	19.94	-5.892	2.17	-.79	.714	9.31	3.00	.00	.00
3S	22.00	.550	20.11	-7.201	1.66	-.37	.751	9.60	3.00	.00	.00
4S	22.30	.555	20.58	-8.031	1.45	.16	.756	9.90	3.90	.00	.00
5S	22.10	.551	20.34	-7.710	1.52	-.15	.758	9.77	3.38	.00	.00
6S	22.40	.551	20.47	-7.249	1.64	-.17	.746	9.74	3.51	.00	.00
1T	21.50	.550	18.78	-5.098	2.68	-1.97	.704	8.80	2.34	.00	.00
2T	21.20	.548	19.15	-6.421	1.93	-1.00	.742	9.11	2.34	.00	.00
3T	21.60	.552	19.95	-7.943	1.47	-.17	.765	9.65	3.12	.00	.00
4T	21.50	.549	19.57	-6.895	1.75	-.62	.748	9.34	2.34	.00	.00
5T	21.60	.551	19.81	-7.380	1.61	-.45	.758	9.55	3.00	.00	.00
6T	21.80	.550	19.74	-6.620	1.85	-.66	.740	9.38	3.00	.00	.00
AVERAGES: 00623 BASELINE W198 00 000											
	22.02	.553	20.08	-7.097	1.71	-.38	.747	9.62	3.95	.00	.00
STD	.23	.001	.16	.409	.12	.14	.009	.09	.39	*	*
00623 W212CU008 (8.05E16)											
	21.81	.550	19.77	-6.757	1.85	-.67	.741	9.40	2.84	.00	.00
STD	.31	.002	.47	.810	.33	.53	.017	.30	.51	*	*
PERCENT OF BASELINE											
	99.1	99.5	98.4	104.8	109	24.9	99.2	97.8	71.9	*****	*****
STD%	2.5	.6	3.1	17.6	28	252.6	3.5	4.1	21.2	*****	*****

00818 W213PB001 [NON DETECTABLE] W199 00 000
SOL18 6 /19/81 AM1: PO=91.60MW/CM^2 NO AR COATING

ID	ISC	VOC	IP	LOG(IO)	N	R	FF	Eff	OCD	PCDa	PCDb
3R*	22.10	.547	19.62	-5.678	2.27	-1.25	.718	9.18	.00	.00	.00
1B	21.70	.549	20.27	-9.144	1.23	.29	.777	9.78	4.16	.00	.00
2B	22.00	.548	20.42	-8.442	1.35	.04	.770	9.82	4.42	.00	.00
3B	22.10	.551	20.21	-7.197	1.66	-.38	.751	9.67	4.16	.00	.00
4B	22.00	.550	19.98	-6.739	1.81	-.69	.745	9.54	3.90	.00	.00
5B.*	22.20	.547	19.37	-5.079	2.67	-1.82	.701	9.00	3.12	.00	.00
1C	21.90	.551	19.95	-6.891	1.76	-.69	.751	9.58	3.64	.00	.00
2C	21.90	.543	19.34	-5.506	2.36	-1.34	.711	8.95	2.34	.00	.00
3C	22.20	.549	20.38	-7.461	1.58	-.35	.758	9.77	3.64	.00	.00
4C	22.20	.548	19.57	-5.379	2.46	-1.63	.714	9.18	3.12	.00	.00
5C	22.00	.552	20.09	-7.076	1.70	-.55	.753	9.67	3.64	.00	.00
6C	22.00	.551	19.81	-6.307	1.98	-.87	.735	9.42	3.51	.00	.00
7C	21.60	.546	19.14	-5.643	2.29	-1.26	.715	8.92	2.73	.00	.00
8C	22.20	.544	19.16	-4.811	2.88	-2.00	.688	8.78	2.34	.00	.00
9C	22.20	.550	20.20	-6.864	1.76	-.55	.746	9.63	4.16	.00	.00
10C	22.00	.548	20.26	-7.706	1.51	-.27	.762	9.72	3.64	.00	.00
11C	22.00	.548	19.98	-6.816	1.77	-.48	.742	9.45	3.12	.00	.00
1S	22.00	.551	20.03	-6.967	1.73	-.40	.744	9.54	4.16	.00	.00
2S	21.90	.549	20.37	-8.623	1.32	.01	.775	9.86	3.64	.00	.00
3S	21.90	.547	20.22	-7.922	1.46	-.19	.765	9.69	3.64	.00	.00
4S	22.10	.550	19.94	-6.346	1.96	-.94	.739	9.50	3.77	.00	.00
5S	21.80	.549	20.12	-7.920	1.47	-.15	.764	9.67	4.03	.00	.00
6S	21.60	.545	20.01	-8.224	1.39	-.05	.768	9.56	3.12	.00	.00
1T	22.40	.550	20.43	-7.007	1.71	-.48	.749	9.75	3.64	.00	.00
2T	22.00	.549	20.01	-6.798	1.78	-.71	.748	9.56	3.64	.00	.00
3T	22.10	.550	20.27	-7.360	1.61	-.43	.758	9.74	3.90	.00	.00
4T	21.70	.533	17.81	-4.065	3.71	-2.07	.622	7.61	1.04	.00	.00
5T	21.90	.548	19.94	-6.863	1.76	-.69	.750	9.52	3.90	.00	.00
AVERAGES: 00818 BASELINE W199 00 000											
	21.95	.550	20.22	-7.880	1.51	-.18	.761	9.70	4.16	.00	.00
STD	.15	.001	.16	.959	.23	.38	.013	.11	.18	*	*
00818 W213PB001 [NON DETECTABLE]											
	21.98	.548	19.87	-6.752	1.91	-.73	.739	9.41	3.38	.00	.00
STD.	.19	.004	.57	1.097	.54	.58	.033	.48	.71	*	*
PERCENT OF BASELINE											
	100.1	99.7	98.3	114.3	126	*****	97.1	97.0	81.3	*****	*****
STD%	1.6	.9	3.6	26.0	61	*****	6.0	6.1	21.5	*****	*****

00624 W214V006 (5.5E14) W198 00 000
SOL17 6 /19/81 AM1: PO=91.60MW/CM^2 NO AR COATING

ID	ISC	VOC	IP	LOG(IO)	N	R	FF	Eff	OCD	PCDa	PCDb
3R*	22.10	.559	19.57	-5.576	2.38	-1.39	.716	9.35	.00	.00	.00
2B	21.70	.553	19.87	-7.260	1.65	-.46	.755	9.58	3.64	.00	.00
3B	22.40	.554	20.85	-8.814	1.29	.30	.770	10.10	4.16	.00	.00
4B	22.00	.553	20.29	-7.829	1.50	-.17	.762	9.81	4.00	.00	.00
5B	22.70	.552	21.08	-8.549	1.34	.20	.767	10.17	4.00	.00	.00
1C	15.20	.488	13.69	-6.931	1.59	.55	.710	5.57	.50	.00	.00
2C	17.60	.502	15.82	-6.643	1.72	.13	.712	6.65	.52	.00	.00
3C	15.40	.487	13.78	-6.433	1.76	-.20	.710	5.63	.46	.00	.00
4C	15.40	.481	13.79	-6.486	1.72	-.08	.710	5.56	.39	.00	.00
5C	15.20	.484	13.43	-5.963	1.95	-.34	.693	5.39	.33	.00	.00
6C	15.60	.484	13.85	-6.108	1.88	-.31	.699	5.59	.42	.00	.00
7C	15.30	.480	13.66	-6.423	1.74	.10	.702	5.45	.46	.00	.00
8C	15.30	.480	13.66	-6.423	1.74	.10	.702	5.45	.39	.00	.00
9C	15.50	.486	13.86	-6.455	1.75	-.01	.707	5.63	.52	.00	.00
10C	15.50	.481	13.90	-6.549	1.70	-.07	.712	5.61	.39	.00	.00
2S	15.20	.483	13.57	-6.370	1.77	-.14	.706	5.48	.33	.00	.00
3S	15.60	.489	13.99	-6.568	1.72	.03	.710	5.73	.40	.00	.00
4S	20.40	.503	18.11	-6.060	1.92	-.07	.697	7.56	.40	.00	.00
5S	15.60	.486	13.95	-6.464	1.74	.06	.705	5.66	.65	.00	.00
1T	15.10	.484	13.44	-6.301	1.80	.01	.699	5.41	.39	.00	.00
2T	15.40	.485	13.64	-6.074	1.90	-.18	.694	5.49	.39	.00	.00
3T	15.70	.487	14.11	-6.722	1.65	.24	.711	5.75	.39	.00	.00
4T	15.30	.482	13.61	-6.320	1.79	.17	.696	5.43	.52	.00	.00
AVERAGES: 00624 BASELINE W198 00 000											
	22.20	.553	20.52	-8.113	1.44	-.03	.764	9.91	3.95	.00	.00
STD	.38	.001	.48	.610	.14	.30	.006	.23	.19	*	*
00624 W214V006 (5.5E14)											
	15.79	.486	14.10	-6.405	1.77	.00	.704	5.72	.44	.00	.00
STD	1.24	.006	1.10	.239	.09	.20	.006	.52	.08	*	*
PERCENT OF BASELINE											
	71.1	87.9	68.7	121.1	123	201.5	92.2	57.7	11.0	*****	*****
STD%	6.9	1.3	7.1	9.1	19	*****	1.5	6.8	2.6	*****	*****

00625 W215M0009 (2E12) POLY W198 00 000
SOL17 6 /19/81 AM1: PO=91.60MW/CM^2 NO AR COATING

ID	ISC	VOC	IP	LOG(IO)	N	R	FF	Eff	OCD	PCDa	PCDb
3R*	22.10	.556	19.69	-5.790	2.25	-1.27	.724	9.40	.00	.00	.00
1B	21.70	.553	19.33	-6.125	2.07	-.15	.704	8.93	3.25	.00	.00
2B.*	21.70	.546	18.93	-5.123	2.64	-1.68	.698	8.74	2.34	.00	.00
3B	21.60	.547	19.64	-6.879	1.75	-.48	.743	9.29	2.86	.00	.00
4B	21.60	.548	19.79	-7.367	1.61	-.33	.754	9.44	3.00	.00	.00
1C	20.10	.502	17.52	-5.478	2.22	-.24	.673	7.19	.39	.00	.00
2C.*	12.20	.344	7.93	-6.241	1.33	15.36	.351	1.56	.00	.00	.00
3C.*	17.40	.497	14.46	-4.169	3.44	-3.54	.650	5.95	.40	.00	.00
4C	17.70	.496	15.56	-5.660	2.12	-.70	.692	6.42	.40	.00	.00
5C.*	14.10	.469	11.26	-3.762	4.09	-5.47	.613	4.29	.33	.00	.00
6C	17.70	.501	15.83	-6.245	1.86	-.53	.715	6.71	.52	.00	.00
7C	15.10	.482	13.39	-6.053	1.90	-.47	.700	5.39	.46	.00	.00
8C	17.20	.498	15.22	-5.847	2.04	-.75	.702	6.36	.46	.00	.00
10C	15.10	.485	13.46	-6.314	1.80	-.20	.705	5.46	.65	.00	.00
11C	19.70	.493	15.69	-3.916	3.72	-1.25	.579	5.95	.26	.00	.00
1S	17.20	.496	15.36	-6.281	1.83	-.25	.708	6.39	.52	.00	.00
2S	15.40	.483	13.58	-5.813	2.02	-.69	.695	5.46	.52	.00	.00
3S	17.40	.499	15.28	-5.577	2.18	-1.00	.695	6.38	.52	.00	.00
4S	14.80	.485	13.28	-6.606	1.70	-.07	.713	5.41	.30	.00	.00
>ALL TANG SAMPLES HAVE ZERO OUTPUT											
AVERAGES: 00625 BASELINE W198 00 000											
	21.63	.549	19.59	-6.791	1.81	-.32	.734	9.22	3.04	.00	.00
STD	.05	.003	.19	.511	.19	.13	.022	.21	.16	*	*
00625 W215M0009 (2E12) POLY											
	17.04	.493	14.92	-5.799	2.13	-.56	.689	6.10	.45	.00	.00
STD	1.72	.007	1.28	.683	.53	.35	.036	.58	.11	*	*
PERCENT OF BASELINE											
	78.8	89.7	76.2	114.6	118	26.1	93.9	66.2	15.0	*****	*****
STD%	8.2	1.7	7.3	17.2	45	224.8	7.9	8.0	4.5	*****	*****

00701 W216CR009 (2.2E15) POLY W198 00 000
SOL17 6 /19/81 AM1: PO=91.60MW/CM^2 NO AR COATING

ID	ISC	VOC	IP	LOG(IO)	N	R	FF	Eff	OCD	PCDa	PCDb
3R*	22.10	.561	19.64	-5.705	2.31	-1.33	.721	9.45	.00	.00	.00
1B.*	22.50	.555	19.55	-5.374	2.49	-.11	.666	8.80	3.00	.00	.00
2B*	21.60	.543	18.40	-5.234	2.54	1.00	.625	7.75	1.43	.00	.00
3B.*	21.80	.544	19.24	-5.825	2.18	-.13	.689	8.65	1.82	.00	.00
4B*	22.20	.553	18.62	-5.315	2.52	2.47	.587	7.63	2.34	.00	.00
5B.*	22.50	.544	19.48	-5.056	2.67	-1.07	.677	8.77	1.56	.00	.00
1C.*	13.20	.214	9.96	-11.781	.36	8.62	.405	1.21	.00	.00	.00
2C.*	15.90	.467	11.74	-3.556	4.42	-.46	.503	3.95	.00	.00	.00
3C.*	12.50	.150	8.89	-8.267	.39	6.30	.385	.76	.00	.00	.00
5C*	15.40	.281	10.65	-6.019	1.12	8.54	.384	1.76	.00	.00	.00
6C.*	15.60	.425	10.98	-4.323	2.82	7.36	.422	2.96	.00	.00	.00
7C.*	16.60	.422	11.69	-3.958	3.23	5.12	.434	3.21	.00	.00	.00
8C.*	15.00	.362	10.20	-5.498	1.65	10.91	.379	2.18	.00	.00	.00
9C.*	16.60	.378	11.09	-4.760	2.12	9.29	.379	2.51	.00	.00	.00
11C.*	13.70	.304	10.54	-7.215	.95	8.79	.443	1.95	.00	.00	.00
12C.*	16.20	.224	12.14	-6.026	.88	5.08	.437	1.68	.00	.00	.00
1S	18.60	.491	14.76	-3.975	3.65	-.79	.571	5.51	.00	.00	.00
3S.*	11.40	.404	6.81	-8.267	1.07	24.78	.311	1.51	.00	.00	.00
4T.*	14.00	.288	10.08	-7.805	.81	10.27	.394	1.68	.00	.00	.00

AVERAGES: 00701 BASELINE W198 00 000
NO BASELINE

00701 W216CR009 (2.2E15) POLY											
	18.60	.491	14.76	-3.975	3.65	-.79	.571	5.51	.00	.00	.00
STD	.00	.000	.00	.000	.00	.00	.000	.00	.00	*	*

00725 W217TA005 (3E11) W198 00 000
SOL17 6 /22/81 AM1: PO=91.60MW/CM^2 NO AR COATING

ID	ISC	VOC	IP	LOG(IO)	N	R	FF	Eff	OCD	PCDa	PCDb
3R*	22.10	.561	19.35	-5.072	2.74	-2.33	.714	9.36	.00	.00	.00
1B	22.30	.560	19.79	-5.629	2.35	-1.42	.720	9.51	3.64	.00	.00
2B	22.10	.552	18.86	-4.516	3.22	-2.54	.679	8.76	2.60	.00	.00
3B*	22.00	.541	18.35	-4.269	3.46	-2.00	.642	8.08	1.30	.00	.00
4B	22.30	.555	19.39	-5.009	2.76	-1.81	.695	9.10	3.00	.00	.00
5B*	21.90	.550	18.94	-5.143	2.64	-.68	.669	8.53	2.08	.00	.00
1C	21.10	.538	17.43	-4.405	3.29	-.54	.611	7.33	.56	.00	.00
2C	21.30	.553	18.83	-5.589	2.36	-1.22	.710	8.84	2.08	.00	.00
3C	21.20	.524	17.60	-4.662	2.93	.47	.603	7.09	.39	.00	.00
4C	21.20	.549	18.51	-5.295	2.53	-1.05	.688	8.47	1.69	.00	.00
5C	21.10	.536	17.88	-4.729	2.93	-.86	.645	7.72	.78	.00	.00
6C	21.10	.531	17.86	-4.821	2.82	-.78	.635	7.53	.65	.00	.00
7C	20.80	.549	18.28	-5.522	2.39	-.86	.694	8.39	1.69	.00	.00
8C	21.10	.541	17.91	-4.632	3.06	-1.54	.656	7.92	1.17	.00	.00
9C	21.10	.531	17.55	-4.400	3.25	-1.10	.626	7.41	.60	.00	.00
10C	21.10	.553	18.56	-5.409	2.47	-1.40	.704	8.69	2.21	.00	.00
11C	21.30	.543	18.16	-4.725	2.97	-1.40	.660	8.08	1.20	.00	.00
1S	21.50	.552	18.85	-5.307	2.53	-1.42	.700	8.79	1.82	.00	.00
2S	21.00	.552	18.61	-5.664	2.31	-1.25	.714	8.75	1.95	.00	.00
3S	21.10	.555	18.89	-6.135	2.08	-.73	.721	8.93	2.08	.00	.00
4S	21.40	.548	18.46	-4.890	2.84	-1.72	.682	8.46	1.69	.00	.00
5S	21.30	.548	18.44	-4.955	2.79	-1.73	.686	8.47	1.69	.00	.00
1T	21.40	.546	18.42	-4.887	2.83	-1.50	.675	8.34	1.17	.00	.00
2T	21.30	.544	18.35	-4.932	2.79	-1.38	.675	8.27	1.20	.00	.00
3T	21.60	.553	18.98	-5.545	2.38	-.66	.691	8.73	1.82	.00	.00
4T	21.30	.552	18.90	-5.719	2.28	-1.13	.714	8.88	1.82	.00	.00
5T	21.40	.539	18.23	-4.708	2.96	-1.40	.660	8.05	.78	.00	.00
AVERAGES: 00/25 BASELINE W198 00 000											
	22.23	.556	19.35	-5.051	2.78	-1.92	.698	9.12	3.08	.00	.00
STD	.10	.003	.38	.455	.36	.47	.017	.31	.43	*	*
00725 W217TA005 (3E11)											
	21.22	.545	18.32	-5.092	2.70	-1.08	.674	8.24	1.38	.00	.00
STD	.18	.008	.45	.468	.33	.51	.034	.54	.56	*	*
PERCENT OF BASELINE											
	95.5	98.0	94.7	99.2	97	143.8	96.5	90.4	44.9	*****	*****
STD%	1.2	2.1	4.3	19.2	26	46.7	7.3	9.2	27.0	*****	*****

00703 W218TA006 (1E11) W198 00 000
SOL17 6 /19/81 AM1: PO=91.60MW/CM^2 NO AR COATING

ID	ISC	VOC	IP	LOG(IO)	N	R	FF	Eff	OCD	PCDa	PCDb
3R*	22.10	.555	19.59	-5.619	2.34	-1.31	.716	9.29	.00	.00	.00
1B.*	21.40	.553	19.82	-9.356	1.20	2.04	.722	9.04	4.42	.00	.00
2B.*	21.40	.539	18.28	-4.748	2.92	-1.47	.665	8.11	1.43	.00	.00
3B	21.90	.550	19.76	-6.537	1.88	-.44	.730	9.29	4.29	.00	.00
4B*	21.90	.550	19.76	-6.537	1.88	-.44	.730	9.29	4.29	.00	.00
5B.*	21.90	.538	18.26	-4.244	3.48	-2.14	.643	8.01	1.69	.00	.00
1C	21.20	.540	17.15	-3.891	4.06	-2.42	.609	7.37	1.56	.00	.00
2C	20.20	.529	17.46	-5.759	2.17	1.60	.634	7.17	.91	.00	.00
3C	21.40	.549	18.20	-4.456	3.29	-2.75	.676	8.40	2.60	.00	.00
4C	21.40	.537	17.37	-3.946	3.94	-2.15	.610	7.41	1.30	.00	.00
5C	20.80	.532	16.90	-4.215	3.51	-.48	.592	6.93	1.17	.00	.00
6C	21.50	.538	18.17	-4.543	3.12	-1.57	.652	7.97	1.43	.00	.00
7C	21.30	.537	17.62	-4.119	3.66	-2.42	.635	7.68	1.50	.00	.00
8C	20.90	.526	17.16	-4.342	3.30	-.46	.603	7.01	1.04	.00	.00
9C	21.50	.550	19.16	-5.937	2.15	-.81	.715	8.94	3.00	.00	.00
10C	19.30	.548	17.08	-6.468	1.93	1.61	.666	7.45	2.21	.00	.00
11C.*	21.50	.546	17.78	-3.940	4.01	-3.78	.652	8.09	1.95	.00	.00
1S	21.30	.546	17.92	-4.880	2.84	.50	.618	7.60	1.82	.00	.00
2S	21.50	.543	18.67	-5.126	2.62	-1.20	.683	8.43	2.08	.00	.00
4S	21.50	.552	19.70	-7.469	1.59	-.10	.749	9.41	3.25	.00	.00
5S	21.70	.551	19.91	-7.518	1.57	-.17	.753	9.52	3.25	.00	.00
1T	21.40	.536	18.01	-4.482	3.18	-1.58	.647	7.85	1.17	.00	.00
2T	21.50	.526	17.87	-4.406	3.21	-.92	.623	7.45	.78	.00	.00
3T	21.90	.548	19.67	-6.334	1.96	-.47	.723	9.17	2.99	.00	.00
4T	21.60	.553	19.90	-7.897	1.48	.13	.754	9.52	3.25	.00	.00
5T	21.60	.541	18.50	-5.094	2.64	-.01	.646	7.98	1.69	.00	.00
6T	21.20	.529	17.51	-4.229	3.46	-1.56	.623	7.39	.91	.00	.00
AVERAGES: 00703 BASELINE W198 00 000											
	21.90	.550	19.76	-6.537	1.88	-.44	.730	9.29	4.29	.00	.00
STD	.00	.000	.00	.000	.00	.00	.000	.00	.00	*	*
00703 W218TA006 (1E11)											
	21.24	.541	18.20	-5.255	2.78	-.76	.661	8.03	1.90	.00	.00
STD	.57	.009	.97	1.242	.79	1.20	.051	.84	.85	*	*
PERCENT OF BASELINE											
	97.0	98.3	92.1	119.6	148	25.4	90.5	86.4	44.2	*****	*****
STD%	2.6	1.6	4.9	19.0	42	275.1	7.0	9.0	19.8	*****	*****

00724 W219V008 (9E12) W198 00 000
SOL18 6 /19/81 AM1: PO=91.60MW/CM^2 NO AR COATING

ID	ISC	VOC	IP	LOG(IO)	N	R	FF	Eff	OCD	PCDa	PCDb
3R*	21.90	.559	19.32	-5.429	2.48	-1.57	.713	9.23	.00	.00	.00
1B	20.90	.559	19.10	-7.056	1.74	-.80	.758	9.36	4.42	.00	.00
2B.*	20.40	.555	18.02	-5.441	2.47	-1.96	.720	8.62	3.51	.00	.00
3B	20.90	.558	19.23	-7.614	1.57	-.36	.761	9.39	4.16	.00	.00
4B	20.50	.556	18.42	-6.494	1.93	-.13	.716	8.64	3.90	.00	.00
1C	18.10	.529	16.23	-6.243	1.96	-.94	.726	7.35	.65	.00	.00
2C	18.10	.528	16.34	-6.518	1.85	-.91	.737	7.45	.65	.00	.00
3C	18.20	.527	16.35	-6.285	1.94	-1.00	.730	7.40	.65	.00	.00
4C	17.70	.531	16.57	-9.602	1.13	.59	.776	7.72	.78	.00	.00
5C	18.30	.527	16.46	-6.399	1.89	-.76	.728	7.43	.65	.00	.00
6C	18.20	.529	16.19	-5.924	2.11	-1.08	.715	7.28	.65	.00	.00
7C	18.70	.532	16.86	-6.485	1.87	-.79	.733	7.72	.85	.00	.00
8C	18.70	.530	16.92	-6.686	1.79	-.61	.736	7.71	.78	.00	.00
9C	18.50	.529	16.77	-6.702	1.78	-.83	.743	7.69	.78	.00	.00
10C	18.50	.525	16.17	-5.328	2.44	-1.43	.694	7.13	.52	.00	.00
11C	18.50	.525	16.30	-5.577	2.28	-1.24	.703	7.22	.52	.00	.00
12C	18.10	.519	15.78	-5.319	2.42	-1.20	.686	6.82	.40	.00	.00
1S	18.20	.528	16.28	-6.132	2.01	-1.00	.723	7.35	.72	.00	.00
2S	18.40	.529	16.56	-6.410	1.89	-.80	.730	7.51	.78	.00	.00
3S	18.40	.526	16.39	-5.996	2.06	-.95	.716	7.33	.65	.00	.00
4S	18.60	.528	16.76	-6.413	1.88	-.95	.735	7.63	.78	.00	.00
5S	18.50	.529	16.80	-6.854	1.73	-.63	.742	7.68	.78	.00	.00
6S	18.50	.528	16.74	-6.715	1.77	-.57	.736	7.60	.78	.00	.00
1T	17.80	.529	15.87	-5.920	2.12	-1.47	.724	7.21	.60	.00	.00
2T	18.30	.530	16.37	-6.079	2.04	-1.19	.726	7.45	.60	.00	.00
3T	18.30	.530	16.42	-6.198	1.98	-1.14	.730	7.49	.60	.00	.00
4T	18.50	.531	16.81	-6.919	1.71	-.51	.741	7.70	.65	.00	.00
5T	18.20	.532	16.58	-7.018	1.68	-.65	.748	7.66	.78	.00	.00
6T	18.30	.530	16.42	-6.198	1.98	-1.14	.730	7.49	.78	.00	.00
AVERAGES: 00724 BASELINE W198 00 000											
	20.77	.558	18.92	-7.055	1.75	-.43	.745	9.13	4.16	.00	.00
STD	.19	.001	.35	.457	.15	.28	.020	.35	.21	*	*
00724 W219V008 (9E12)											
	18.32	.528	16.46	-6.413	1.93	-.88	.729	7.46	.68	.00	.00
STD	.24	.003	.29	.799	.26	.40	.018	.22	.11	*	*
PERCENT OF BASELINE											
	88.2	94.7	87.0	109.1	110	-5.1	97.8	81.7	16.4	*****	*****
STD%	2.0	.7	3.2	17.9	25	286.0	5.1	5.6	3.5	*****	*****

00725 W220W005 (8E11) W198 00 000
SOL18 6 /19/81 AM1: PO=91.60MW/CM^2 NO AR COATING

ID	ISC	VOC	IP	LOG(IO)	N	R	FF	Eff	OCD	PCDa	PCDb
3R*	22.10	.556	19.62	-5.699	2.30	-1.23	.718	9.33	.00	.00	.00
1B	21.40	.555	19.62	-7.344	1.63	-.44	.757	9.50	4.16	.00	.00
2B.*	21.40	.551	19.10	-5.865	2.19	-1.28	.726	9.05	3.51	.00	.00
3B	21.20	.553	19.28	-6.848	1.79	-.66	.747	9.26	3.90	.00	.00
4B.*	21.20	.551	18.83	-5.664	2.31	-1.51	.722	8.92	3.12	.00	.00
5B	21.20	.553	19.30	-7.560	1.57	1.04	.715	8.87	3.64	.00	.00
1C	20.50	.541	18.66	-6.901	1.73	-.62	.747	8.76	1.82	.00	.00
2C	20.80	.544	18.75	-6.426	1.92	-.68	.731	8.75	1.69	.00	.00
3C	20.40	.541	18.61	-7.078	1.68	-.46	.748	8.73	2.60	.00	.00
4C	20.30	.541	18.30	-6.358	1.94	-.97	.737	8.55	1.95	.00	.00
5C	20.20	.541	18.16	-6.252	1.98	-1.03	.734	8.48	1.82	.00	.00
6C	20.20	.542	18.67	-8.096	1.41	-.04	.764	8.84	2.08	.00	.00
7C	20.00	.538	18.05	-6.510	1.87	-.71	.734	8.36	1.56	.00	.00
8C	20.70	.541	18.74	-6.655	1.82	-.59	.737	8.73	2.08	.00	.00
9C	20.70	.542	19.03	-7.630	1.52	-.21	.757	8.98	2.86	.00	.00
10C	20.40	.525	17.53	-4.883	2.75	-1.44	.671	7.60	.78	.00	.00
1S	20.70	.543	18.87	-7.078	1.68	-.38	.746	8.86	2.34	.00	.00
2S	20.50	.537	18.17	-5.690	2.24	-1.23	.714	8.31	1.56	.00	.00
3S	20.50	.540	18.81	-7.580	1.53	-.06	.751	8.79	2.34	.00	.00
4S	20.80	.538	18.72	-6.334	1.93	-.78	.731	8.65	1.69	.00	.00
1T	20.40	.539	18.15	-5.803	2.19	-1.29	.721	8.39	1.30	.00	.00
2T	20.40	.539	18.34	-6.205	1.99	-1.10	.734	8.54	1.69	.00	.00
3T	20.50	.535	17.82	-4.974	2.72	-2.21	.699	8.11	1.04	.00	.00
4T	20.40	.543	18.59	-6.969	1.72	-.67	.751	8.79	1.95	.00	.00
5T	20.50	.543	18.85	-7.562	1.54	-.42	.762	8.97	1.95	.00	.00
6T	20.80	.543	19.02	-7.326	1.61	-.17	.747	8.92	2.08	.00	.00
AVERAGES: 00725 BASELINE W198 00 000											
	21.27	.554	19.40	-7.251	1.66	-.02	.740	9.21	3.90	.00	.00
STD	.09	.001	.15	.298	.09	.76	.018	.26	.21	*	*
00725 W220W005 (8E11)											
	20.49	.540	18.49	-6.616	1.89	-.75	.736	8.61	1.86	.00	.00
STD	.21	.004	.40	.834	.35	.52	.021	.32	.48	*	*
PERCENT OF BASELINE											
	96.3	97.5	95.3	108.8	114	*****	99.5	93.4	47.7	*****	*****
STD%	1.4	.9	2.8	15.7	29	*****	5.3	6.3	15.6	*****	*****

00728 W221NI005 (10E15) W198 00 000
SOL18 6 /19/81 AM1: PO=91.60MW/CM^2 NO AR COATING

ID	ISC	VOC	IP	LOG(IO)	N	R	FF	Eff	OCD	PCDa	PCDb
3R*	22.10	.553	19.62	-5.656	2.31	-1.37	.720	9.31	.00	.00	.00
1B	20.90	.549	18.92	-7.163	1.67	.83	.710	8.62	3.12	.00	.00
2B	20.80	.545	18.43	-6.027	2.10	.09	.691	8.28	2.60	.00	.00
3B.*	21.10	.550	19.20	-7.836	1.49	1.66	.703	8.63	4.03	.00	.00
4B	21.40	.550	19.54	-7.885	1.48	1.31	.715	8.90	3.90	.00	.00
5B	21.00	.549	19.35	-8.440	1.36	1.16	.733	8.94	3.90	.00	.00
1C	20.40	.545	17.91	-5.592	2.33	-.50	.687	8.08	2.34	.00	.00
2C	20.50	.542	17.49	-4.796	2.91	-1.21	.658	7.73	1.30	.00	.00
3C	20.40	.541	16.91	-4.664	3.04	.55	.601	7.02	1.56	.00	.00
4C	20.10	.546	17.68	-5.726	2.26	-.26	.686	7.97	2.73	.00	.00
5C	20.30	.542	17.41	-4.959	2.77	-.95	.662	7.70	2.08	.00	.00
6C	20.40	.540	17.42	-5.036	2.70	-.15	.645	7.51	1.95	.00	.00
7C	20.40	.547	18.34	-6.513	1.89	-.10	.717	8.46	3.00	.00	.00
8C	21.10	.542	18.25	-5.380	2.44	.23	.655	7.92	2.34	.00	.00
9C	20.80	.543	18.16	-5.398	2.44	-.70	.683	8.16	2.34	.00	.00
10C	21.10	.542	18.49	-5.618	2.30	-.15	.679	8.21	2.34	.00	.00
11C	20.60	.539	17.78	-5.233	2.54	-.24	.660	7.75	1.82	.00	.00
1S	20.40	.546	17.77	-5.505	2.39	-.03	.669	7.88	2.60	.00	.00
2S	20.70	.548	18.18	-5.562	2.36	-.65	.690	8.28	3.00	.00	.00
3S	20.80	.549	19.01	-7.725	1.52	.87	.725	8.76	3.90	.00	.00
4S	20.60	.548	18.53	-6.616	1.86	.14	.713	8.51	3.51	.00	.00
5S	20.50	.548	18.70	-7.582	1.55	.81	.723	8.59	2.21	.00	.00
6S	20.40	.544	17.98	-5.751	2.24	-.36	.691	8.11	2.60	.00	.00
1T	20.20	.555	18.42	-7.384	1.63	.39	.731	8.67	3.64	.00	.00
2T	20.50	.555	18.87	-7.978	1.47	.36	.748	9.00	3.90	.00	.00
3T	20.40	.550	18.52	-7.200	1.67	.52	.721	8.56	3.25	.00	.00
4T	20.60	.547	18.34	-6.088	2.08	-.26	.704	8.39	2.47	.00	.00
5T	20.40	.549	18.06	-5.795	2.23	-.66	.702	8.31	2.73	.00	.00
6T	20.70	.549	18.60	-6.494	1.91	-.10	.716	8.60	3.12	.00	.00
AVERAGES: 00728 BASELINE W198 00 000											
	21.03	.548	19.06	-7.379	1.65	.85	.712	8.68	3.38	.00	.00
STD	.23	.002	.43	.902	.28	.47	.015	.26	.55	*	*
00728 W221NI005 (10E15)											
	20.53	.546	18.12	-6.026	2.20	-.11	.690	8.18	2.64	.00	.00
STD	.24	.004	.51	.959	.44	.53	.033	.45	.69	*	*
PERCENT OF BASELINE											
	97.7	99.6	95.1	118.3	133	-12.7	96.8	94.2	78.1	*****	*****
STD%	2.2	1.1	4.9	24.6	54	104.2	6.8	8.2	36.3	*****	*****

01003 W222AG002 (6E15) W199 00 000
SOL18 6 /19/81 AM1: PO=91.60MW/CM^2 NO AR COATING

ID	ISC	VOC	IP	LOG(IO)	N	R	FF	Eff	OCD	PCDa	PCDb
3R*	22.10	.552	19.78	-6.007	2.12	-1.03	.727	9.38	.00	.00	.00
1B.*	22.30	.551	19.72	-5.570	2.35	-1.19	.710	9.23	3.51	.00	.00
2B	22.10	.552	20.42	-8.099	1.43	.12	.759	9.80	4.55	.00	.00
3B	22.10	.552	20.37	-7.913	1.47	.04	.757	9.77	4.42	.00	.00
1C	21.10	.530	18.93	-6.225	1.95	-.67	.724	8.56	2.21	.00	.00
2C	22.00	.552	20.33	-8.066	1.44	.01	.762	9.79	4.29	.00	.00
3C	21.40	.527	18.68	-5.188	2.50	-1.47	.696	8.30	1.82	.00	.00
4C	21.10	.526	18.65	-5.636	2.22	-1.02	.707	8.30	1.56	.00	.00
5C	21.10	.525	18.27	-4.913	2.71	-1.95	.691	8.10	1.56	.00	.00
6C	21.40	.529	19.22	-6.297	1.91	-.57	.724	8.67	2.34	.00	.00
7C	21.50	.527	19.25	-6.155	1.96	-.64	.721	8.64	1.95	.00	.00
8C	20.70	.519	18.37	-5.781	2.12	-.97	.712	8.09	1.04	.00	.00
9C	21.50	.528	19.14	-5.902	2.08	-.81	.715	8.58	2.34	.00	.00
10C	19.80	.508	17.04	-4.903	2.65	-1.58	.676	7.19	.65	.00	.00
11C	21.30	.525	19.51	-7.659	1.46	.42	.737	8.72	2.08	.00	.00
12C	21.70	.528	19.91	-7.768	1.44	.44	.739	8.96	2.34	.00	.00
1S	21.20	.525	19.13	-6.681	1.75	-.04	.722	8.49	1.69	.00	.00
2S	21.10	.529	19.43	-7.920	1.41	.22	.751	8.86	1.82	.00	.00
3S	21.40	.528	19.76	-8.392	1.31	.71	.746	8.91	2.34	.00	.00
4S	21.20	.531	19.54	-8.114	1.38	.47	.747	8.90	2.34	.00	.00
5S	21.10	.524	18.80	-5.964	2.04	-.71	.714	8.34	1.56	.00	.00
6S	21.20	.522	18.94	-6.105	1.97	-.54	.715	8.37	1.56	.00	.00
1T	20.40	.522	17.91	-5.325	2.40	-1.58	.705	7.94	1.04	.00	.00
2T	20.70	.520	18.65	-6.539	1.79	-.26	.723	8.23	1.17	.00	.00
3T	20.20	.513	17.55	-5.187	2.45	-1.08	.681	7.47	.78	.00	.00
4T	20.40	.512	17.72	-5.079	2.52	-1.52	.688	7.60	.78	.00	.00
5T	20.20	.519	18.08	-6.142	1.95	-.74	.721	8.00	1.04	.00	.00
6T	20.00	.510	17.56	-5.437	2.28	-1.19	.699	7.54	.78	.00	.00
AVERAGES: 01003 BASELINE W199 00 000											
	22.10	.552	20.40	-8.006	1.45	.08	.758	9.78	4.49	.00	.00
STD	.00	.000	.02	.093	.02	.04	.001	.01	.06	*	*
	01003 W222AG002 (6E15)										
	20.99	.524	18.76	-6.307	1.99	-.63	.717	8.36	1.71	.00	.00
STD	.55	.009	.81	1.084	.42	.73	.022	.56	.78	*	*
PERCENT OF BASELINE											
	95.0	95.0	92.0	121.2	137	*****	94.6	85.4	38.2	*****	*****
STD%	2.5	1.6	4.1	14.6	31	*****	3.0	5.8	18.2	*****	*****

00819 W223NI006 (1.1E15) W198 00 000
SOL18 6 /19/81 AM1: PO=91.60MW/CM^2 NO AR COATING

ID	ISC	VOC	IP	LOG(IO)	N	R	FF	Eff	OCD	PCDa	PCDb
3R*	22.10	.552	19.76	-5.969	2.14	-1.04	.725	9.36	.00	.00	.00
1B.*	21.40	.544	18.69	-5.198	2.58	-1.53	.697	8.58	2.86	.00	.00
2B*	21.40	.468	16.65	-4.065	3.26	1.29	.530	5.62	.26	.00	.00
3B.*	22.30	.542	19.47	-5.132	2.60	-1.63	.699	8.94	2.47	.00	.00
1C	21.70	.525	18.28	-4.593	2.99	-.96	.640	7.71	.91	.00	.00
2C	21.90	.551	19.97	-6.971	1.73	-.61	.751	9.58	3.64	.00	.00
3C	22.10	.547	19.84	-6.165	2.03	-.90	.730	9.33	3.00	.00	.00
4C	22.00	.542	19.05	-4.959	2.74	-1.60	.686	8.65	2.21	.00	.00
5C	21.90	.548	20.10	-7.477	1.57	-.30	.757	9.60	3.77	.00	.00
6C	21.90	.520	18.00	-4.147	3.49	-1.54	.618	7.45	.78	.00	.00
7C	21.80	.528	18.35	-4.432	3.18	-1.77	.650	7.92	1.17	.00	.00
8C.*	21.90	.515	17.14	-3.669	4.27	-1.58	.566	6.75	.45	.00	.00
9C	21.70	.530	17.99	-4.163	3.54	-2.17	.636	7.73	1.04	.00	.00
10C	21.80	.526	18.34	-4.435	3.17	-1.67	.648	7.86	.90	.00	.00
1S	21.90	.550	19.29	-5.520	2.38	-1.01	.701	8.93	3.00	.00	.00
2S	21.70	.519	17.96	-4.378	3.19	-.72	.616	7.33	.65	.00	.00
3S	21.40	.520	17.75	-4.383	3.20	-.90	.620	7.30	.65	.00	.00
4S	22.00	.547	19.41	-5.461	2.40	-1.44	.712	9.06	3.00	.00	.00
5S	21.90	.539	19.00	-4.976	2.71	-1.73	.691	8.62	2.21	.00	.00
6S	21.60	.544	19.14	-5.583	2.32	-1.50	.719	8.94	2.34	.00	.00
1T	21.70	.529	17.63	-3.947	3.87	-2.10	.611	7.42	.91	.00	.00
2T	21.40	.483	17.04	-4.088	3.33	.18	.564	6.16	.26	.00	.00
3T	21.90	.538	18.93	-4.897	2.78	-1.72	.685	8.54	1.82	.00	.00

AVERAGES: 00819 BASELINE W198 00 000
NO BASELINE
00819 W223NI006 (1.1E15)

	21.79	.533	18.67	-5.032	2.81	-1.25	.669	8.23	1.79	.00	.00
STD	.19	.016	.85	.976	.62	.61	.052	.91	1.10	*	*

00804 W224HSC/DCS057 W198 00 000
SOL18 6 /22/81 AM1: PO=91.60MW/CM^2 NO AR COATING

ID	ISC	VOC	IP	LOG(IO)	N	R	FF	Eff	OCD	PCDa	PCDb
3R*	22.10	.560	19.51	-5.447	2.47	-1.55	.714	9.34	.00	.00	.00
1B	21.30	.559	19.55	-7.520	1.60	-.25	.756	9.52	4.29	.00	.00
2B*	21.00	.547	18.03	-4.720	3.00	-2.19	.681	8.27	2.34	.00	.00
3B	21.20	.549	18.10	-4.613	3.12	-2.24	.674	8.30	2.34	.00	.00
4B	21.10	.555	18.87	-5.938	2.18	-1.35	.731	9.05	3.64	.00	.00
5B	21.10	.550	18.58	-5.345	2.50	-1.81	.713	8.75	2.34	.00	.00
1C	20.90	.579	18.98	-6.770	1.90	-.72	.745	9.53	3.00	.00	.00
2C	21.00	.543	17.05	-4.167	3.64	-.72	.594	7.16	.42	.00	.00
3C	21.10	.568	18.17	-4.805	3.03	-2.10	.683	8.66	1.82	.00	.00
4C	21.40	.576	19.32	-6.402	2.03	-.98	.739	9.64	3.00	.00	.00
5C	21.00	.569	17.84	-4.427	3.46	-3.07	.677	8.56	1.82	.00	.00
6C	21.10	.552	17.76	-4.594	3.16	-1.03	.639	7.87	.72	.00	.00
7C	21.10	.565	18.21	-4.864	2.96	-2.03	.686	8.65	1.56	.00	.00
8C	21.20	.574	18.90	-5.830	2.31	-1.36	.725	9.32	2.34	.00	.00
9C	21.10	.573	18.71	-5.640	2.41	-1.47	.718	9.17	2.34	.00	.00
10C	21.30	.574	19.06	-6.000	2.22	-1.22	.729	9.42	2.60	.00	.00
11C	21.30	.576	19.36	-6.815	1.87	-.70	.746	9.68	3.00	.00	.00
1S	20.80	.577	18.71	-6.217	2.13	-1.22	.737	9.36	2.34	.00	.00
2S	21.20	.582	19.84	-9.547	1.23	.59	.775	10.11	3.90	.00	.00
3S	21.30	.579	19.52	-7.303	1.72	-.55	.758	9.88	2.86	.00	.00
4S	21.20	.578	19.44	-7.334	1.71	-.55	.759	9.83	3.00	.00	.00
5S	20.70	.574	18.19	-5.338	2.62	-1.77	.708	8.89	1.95	.00	.00
6S	21.00	.570	18.40	-5.298	2.63	-1.57	.701	8.87	1.82	.00	.00
1T	21.10	.583	19.27	-6.996	1.83	-.93	.759	9.87	3.64	.00	.00
2T	21.10	.571	18.29	-4.974	2.89	-1.90	.690	8.79	1.82	.00	.00
3T	21.10	.578	19.00	-6.183	2.14	-1.43	.742	9.58	3.00	.00	.00
4T	21.20	.581	19.53	-7.597	1.64	-.62	.769	10.01	3.64	.00	.00
5T	20.80	.548	17.62	-4.711	3.02	-1.00	.646	7.79	.65	.00	.00
6T	21.20	.568	18.47	-5.146	2.73	-1.60	.693	8.83	1.69	.00	.00
AVERAGES: 00804 BASELINE W198 00 000											
	21.18	.553	18.78	-5.854	2.35	-1.42	.718	8.90	3.15	.00	.00
STD	.08	.004	.53	1.070	.55	.74	.030	.44	.84	*	*
00804 W224HSC/DCS057											
	21.10	.571	18.68	-5.955	2.40	-1.21	.714	9.11	2.30	.00	.00
STD	.17	.010	.70	1.253	.62	.71	.045	.75	.93	*	*
PERCENT OF BASELINE											
	99.6	103.2	99.5	98.3	102	114.3	99.3	102.3	73.0	*****	*****
STD%	1.2	2.6	6.6	43.9	57	121.1	10.6	13.9	56.8	*****	*****

00820 W225MN009 (5.5E15) W199 00 000
SOL18 6 /19/81 AM1: PO=91.60MW/CM^2 NO AR COATING

ID	ISC	VOC	IP	LOG(IO)	N	R	FF	Eff	OCD	PCDa	PCDb
3R*	22.10	.549	19.63	-5.692	2.27	-1.25	.719	9.22	.00	.00	.00
1B	21.30	.550	19.39	-6.882	1.76	-.66	.749	9.27	3.90	.00	.00
2B	21.30	.550	19.63	-7.854	1.49	-.10	.760	9.42	4.03	.00	.00
3B	21.30	.549	19.68	-7.998	1.45	-.17	.766	9.47	3.90	.00	.00
4B	21.50	.548	19.30	-6.162	2.04	-1.00	.732	9.12	3.00	.00	.00
5B	21.40	.547	19.24	-6.207	2.01	-.99	.733	9.07	3.38	.00	.00
1C	19.00	.523	17.01	-6.220	1.94	-.64	.719	7.55	.65	.00	.00
2C	19.80	.524	17.49	-5.669	2.21	-.98	.704	7.73	.65	.00	.00
3C	19.60	.522	17.46	-5.972	2.04	-.82	.714	7.73	.55	.00	.00
4C	18.70	.516	16.86	-6.605	1.77	-.37	.726	7.41	.52	.00	.00
5C	20.00	.527	18.10	-6.685	1.77	-.54	.736	8.21	.91	.00	.00
6C	19.80	.525	17.71	-6.137	1.98	-.74	.720	7.91	.91	.00	.00
7C	18.90	.513	16.56	-5.445	2.30	-1.07	.693	7.10	.40	.00	.00
8C	19.80	.523	17.60	-5.828	2.12	-1.11	.717	7.85	.78	.00	.00
9C	19.00	.523	16.27	-4.659	2.97	-2.70	.683	7.17	.55	.00	.00
10C	19.30	.523	16.91	-5.342	2.41	-1.50	.699	7.47	.52	.00	.00
11C	19.30	.520	16.75	-5.117	2.55	-1.50	.686	7.28	.52	.00	.00
1S	19.80	.531	17.69	-5.990	2.07	-1.17	.725	8.07	.91	.00	.00
2S	19.30	.528	17.52	-6.789	1.74	-.72	.744	8.02	.91	.00	.00
3S	19.80	.529	17.91	-6.663	1.78	-.56	.736	8.15	.91	.00	.00
4S	19.90	.529	17.97	-6.490	1.85	-.82	.737	8.20	.91	.00	.00
5S	19.80	.523	16.83	-4.526	3.09	-2.55	.672	7.36	.65	.00	.00
1T.*	18.70	.519	16.14	-6.404	1.85	3.70	.604	6.20	.39	.00	.00
2T	19.00	.517	17.14	-6.547	1.79	-.55	.730	7.58	.52	.00	.00
3T	19.30	.520	17.30	-6.175	1.95	-.92	.726	7.71	.65	.00	.00
4T.*	18.70	.519	15.93	-4.440	3.20	-3.66	.687	7.05	.50	.00	.00
5T	18.40	.514	16.22	-5.641	2.20	-1.01	.701	7.01	.40	.00	.00
AVERAGES: 00820 BASELINE W199 00 000											
	21.36	.549	19.45	-7.021	1.75	-.58	.748	9.27	3.64	.00	.00
STD	.08	.001	.18	.783	.25	.39	.014	.16	.39	*	*
00820 W225MN009 (5.5E15)											
	19.39	.523	17.23	-5.921	2.13	-1.07	.714	7.66	.67	.00	.00
STD	.45	.005	.54	.656	.38	.61	.020	.37	.18	*	*
PERCENT OF BASELINE											
	90.8	95.2	88.6	115.7	122	17.2	95.5	82.6	18.5	*****	*****
STD%	2.5	1.1	3.6	19.8	42	295.3	4.5	5.4	7.5	*****	*****

01002 W227CR010 POLY W199 00 000
SOL18 6 /19/81 AM1: PO=91.60MW/CM^2 NO AR COATING

ID	ISC	VOC	IP	LOG(IO)	N	R	FF	Eff	OCD	PCDa	PCDb
3R*	22.10	.547	19.59	-5.634	2.30	-1.23	.715	9.14	.00	.00	.00
1B.*	21.80	.526	18.10	-4.258	3.38	-1.67	.632	7.66	.91	.00	.00
2B.*	21.70	.528	18.31	-4.474	3.14	-1.74	.653	7.91	1.30	.00	.00
3B	21.80	.544	19.84	-6.982	1.71	-.34	.742	9.31	3.90	.00	.00
4B.*	21.90	.532	18.60	-4.535	3.09	-1.97	.665	8.19	1.69	.00	.00
5B.*	21.80	.532	18.86	-4.978	2.68	-1.44	.682	8.37	2.08	.00	.00
1C	15.60	.471	13.07	-4.534	2.88	-1.98	.641	4.98	.39	.00	.00
2C	15.60	.463	13.09	-4.719	2.66	-.87	.631	4.82	1.95	.00	.00
3C	16.20	.478	14.11	-5.508	2.15	-.46	.675	5.52	.25	.00	.00
4C	16.20	.467	13.73	-4.953	2.47	-.36	.638	5.10	.20	.00	.00
5C	16.90	.480	14.52	-5.148	2.38	-.63	.659	5.65	.24	.00	.00
7C	15.90	.467	13.58	-5.133	2.34	-.23	.646	5.07	.20	.00	.00
8C.*	15.10	.451	11.33	-3.301	5.04	-5.53	.552	3.97	.16	.00	.00
9C	15.50	.469	13.54	-5.661	2.03	-.18	.674	5.18	.24	.00	.00
10C	15.70	.473	13.80	-5.915	1.92	.14	.679	5.34	.52	.00	.00
11C	16.30	.471	13.99	-5.183	2.32	-.43	.655	5.32	.26	.00	.00
1S	15.40	.476	13.58	-5.941	1.93	-.15	.687	5.33	.20	.00	.00
2S	16.90	.482	14.61	-5.206	2.34	-.96	.671	5.78	.24	.00	.00
3S	15.80	.468	13.51	-5.086	2.38	-.60	.652	5.09	.23	.00	.00
4S	16.00	.476	13.94	-5.540	2.12	-.42	.675	5.43	.20	.00	.00
5S	15.80	.472	13.78	-5.592	2.08	-.32	.675	5.32	.20	.00	.00
6S	15.70	.464	13.33	-4.958	2.46	-.57	.642	4.95	.16	.00	.00
1T	16.20	.481	13.90	-5.154	2.39	-.57	.656	5.41	.18	.00	.00
2T.*	14.70	.436	10.11	-3.314	4.87	.45	.448	3.04	.13	.00	.00
3T.*	15.10	.450	10.88	-3.092	5.81	-6.08	.518	3.72	.30	.00	.00
4T.*	15.40	.455	11.48	-3.254	5.22	-5.55	.546	4.04	.17	.00	.00
5T.*	14.80	.428	10.10	-3.294	4.83	.71	.441	2.96	1.30	.00	.00
6T	16.10	.468	13.64	-4.926	2.49	-.53	.640	5.10	.40	.00	.00
AVERAGES: 01002 BASELINE W199 00 000											
	21.80	.544	19.84	-6.982	1.71	-.34	.742	9.31	3.90	.00	.00
STD	.00	.000	.00	.000	.00	.00	.000	.00	.00	*	*
01002 W227CR010 POLY											
	15.99	.472	13.75	-5.244	2.31	-.54	.659	5.26	.36	.00	.00
STD	.42	.006	.41	.383	.25	.44	.017	.25	.41	*	*
PERCENT OF BASELINE											
	73.3	86.8	69.3	124.9	135	40.9	88.7	56.5	9.1	*****	*****
STD%	1.9	1.0	2.1	5.5	14	131.3	2.3	2.7	10.5	*****	*****

SOL19 6 /19/81

01020 W228GD001 W198 00 000
SOL19 6 /19/81 AM1: PO=91.60MW/CM^2 NO AR COATING

ID	ISC	VOC	IP	LOG(IO)	N	R	FF	Eff	OCD	PCDa	PCDb
3R*	22.10	.547	19.70	-5.846	2.18	-1.12	.722	9.23	.00	.00	.00
1B.*	21.50	.540	18.50	-4.775	2.90	-2.00	.683	8.38	2.34	.00	.00
2B.*	21.80	.555	18.86	-4.739	3.01	-2.77	.702	8.98	2.73	.00	.00
3B.*	21.80	.531	18.24	-4.382	3.26	-1.57	.640	7.83	.65	.00	.00
4B.*	21.60	.536	18.42	-4.580	3.07	-2.14	.672	8.23	1.82	.00	.00
5B.*	21.90	.544	19.08	-5.027	2.70	-1.98	.701	8.84	2.34	.00	.00
1C	21.50	.547	19.23	-5.948	2.13	-1.24	.729	9.07	3.12	.00	.00
2C	21.50	.544	18.60	-4.850	2.86	-2.18	.693	8.57	2.86	.00	.00
3C	22.00	.534	18.22	-4.070	3.69	-2.72	.643	7.98	1.20	.00	.00
4C	21.90	.539	18.63	-4.500	3.17	-2.32	.672	8.38	2.08	.00	.00
5C	22.00	.536	18.44	-4.224	3.49	-2.67	.657	8.19	1.82	.00	.00
6C	21.70	.536	18.52	-4.569	3.08	-2.25	.675	8.30	.65	.00	.00
7C	21.80	.539	19.11	-5.277	2.49	-1.47	.702	8.72	2.21	.00	.00
8C	22.10	.540	18.45	-4.174	3.58	-2.65	.651	8.22	1.43	.00	.00
1S	21.70	.536	18.18	-4.241	3.47	-2.60	.655	8.06	1.56	.00	.00
2S	22.20	.542	19.00	-4.658	3.01	-1.95	.675	8.59	1.69	.00	.00
3S	21.70	.539	18.59	-4.614	3.05	-2.40	.683	8.44	1.95	.00	.00
4S	21.70	.549	19.53	-6.311	1.97	-.78	.731	9.21	3.64	.00	.00
1T.*	22.00	.550	18.56	-4.260	3.53	-3.10	.671	8.58	2.34	.00	.00
2T	21.60	.545	19.09	-5.543	2.35	-1.34	.712	8.87	3.00	.00	.00
3T	21.80	.531	17.82	-3.963	3.85	-2.44	.622	7.62	1.30	.00	.00
4T	21.90	.541	19.07	-5.028	2.68	-1.88	.699	8.75	2.34	.00	.00
5T	21.70	.544	19.39	-5.948	2.12	-1.07	.725	9.05	3.25	.00	.00
6T	21.90	.538	18.48	-4.365	3.32	-2.40	.662	8.25	1.82	.00	.00

AVERAGES: 01020 BASELINE W198 00 000
NO BASELINE
01020 W228GD001

	21.81	.540	18.73	-4.840	2.96	-2.02	.682	8.49	2.11	.00	.00
STD	.19	.005	.45	.702	.57	.60	.031	.42	.80	*	*

01110 W229AU001 W198 00 000
SOL18 6 /19/81 AM1: PO=91.60MW/CM^2 NO AR COATING

ID	ISC	VOC	IP	LOG(IO)	N	R	FF	Eff	OCD	PCDa	PCDb
3R*	22.10	.559	19.45	-5.318	2.55	-1.75	.712	9.31	.00	.00	.00
1B*	21.90	.544	17.06	-3.297	5.52	-5.23	.597	7.52	1.82	.00	.00
2B.*	22.00	.552	19.31	-5.225	2.58	-1.86	.710	9.12	3.00	.00	.00
3B.*	22.10	.547	19.05	-4.750	2.95	-2.23	.689	8.81	2.21	.00	.00
4B	22.10	.552	19.96	-6.387	1.95	-.96	.741	9.56	3.25	.00	.00
5B.*	21.90	.550	19.26	-5.267	2.55	-1.89	.714	9.09	3.12	.00	.00
1C	17.60	.505	14.96	-4.687	2.88	-2.02	.662	6.22	.40	.00	.00
2C	18.20	.508	15.59	-4.828	2.75	-1.87	.672	6.57	.40	.00	.00
3C	17.90	.509	15.71	-5.526	2.25	-1.07	.695	6.70	.40	.00	.00
4C	17.40	.505	15.09	-5.400	2.32	-.36	.668	6.21	.43	.00	.00
5C	18.10	.505	15.57	-5.006	2.58	-1.30	.669	6.47	.40	.00	.00
6C	18.10	.498	15.05	-4.390	3.14	-1.68	.631	6.01	.33	.00	.00
7C	18.10	.503	15.43	-4.756	2.79	-1.76	.663	6.39	.42	.00	.00
8C	17.80	.498	15.00	-4.570	2.95	-1.79	.648	6.08	.30	.00	.00
9C	17.90	.506	15.48	-5.100	2.52	-1.44	.679	6.50	.43	.00	.00
1S	18.10	.510	15.78	-5.287	2.40	-1.41	.690	6.74	.50	.00	.00
2S	18.30	.508	15.64	-4.774	2.79	-1.92	.669	6.58	.34	.00	.00
3S	18.40	.510	16.18	-5.576	2.22	-1.03	.698	6.92	.43	.00	.00
4S	18.10	.511	15.73	-5.325	2.38	-.84	.677	6.63	.43	.00	.00
5S	21.20	.513	18.61	-5.391	2.31	-1.16	.699	8.04	.50	.00	.00
6S	18.20	.503	15.50	-4.821	2.73	-1.28	.656	6.35	.33	.00	.00
1T	17.40	.450	13.26	-3.911	3.49	1.09	.517	4.28	.20	.00	.00
2T	17.40	.496	14.63	-4.528	2.99	-2.00	.648	5.92	.40	.00	.00
3T	17.60	.507	15.61	-5.879	2.05	-.94	.709	6.69	.65	.00	.00
4T	17.40	.500	14.50	-4.349	3.22	-2.39	.641	5.90	.30	.00	.00
5T	17.40	.496	14.69	-4.651	2.86	-1.60	.649	5.92	3.00	.00	.00
6T	17.80	.506	15.68	-5.632	2.18	-1.04	.700	6.66	.50	.00	.00
AVERAGES: 01110 BASELINE W198 00 000											
	22.10	.552	19.96	-6.387	1.95	-.96	.741	9.56	3.25	.00	.00
STD	.00	.000	.00	.000	.00	.00	.000	.00	.00	*	*
01110 W229AU001											
	18.02	.502	15.42	-4.971	2.66	-1.32	.664	6.37	.53	.00	.00
STD	.78	.013	.94	.490	.37	.72	.039	.65	.56	*	*
PERCENT OF BASELINE											
	81.5	91.0	77.2	122.2	136	62.5	89.6	66.6	16.2	*****	*****
STD%	3.5	2.3	4.7	7.7	19	74.3	5.3	6.8	17.2	*****	*****

01112 W230AL003 W198 00 000
SOL19 6 /19/81 AM1: PO=91.60MW/CM^2 NO AR COATING

ID	ISC	VOC	IP	LOG(IO)	N	R	FF	Eff	OCD	PCDa	PCDb
3R*	22.10	.554	19.53	-5.451	2.44	-1.61	.716	9.27	.00	.00	.00
1B.*	21.60	.548	18.92	-5.211	2.58	-1.74	.705	8.82	2.47	.00	.00
2B	21.70	.552	19.82	-7.135	1.69	-.43	.750	9.50	3.90	.00	.00
3B	21.80	.547	19.57	-6.198	2.01	-.83	.728	9.19	3.12	.00	.00
4B*	21.80	.539	18.69	-4.657	3.01	-2.19	.681	8.46	1.82	.00	.00
1C	15.90	.515	13.67	-5.122	2.59	-1.07	.663	5.75	.40	.00	.00
2C	15.80	.497	13.40	-4.980	2.61	-.39	.639	5.30	.26	.00	.00
3C	15.70	.502	13.18	-4.673	2.92	-1.28	.635	5.29	.26	.00	.00
4C	15.50	.492	12.84	-4.457	3.10	-1.53	.622	5.02	.26	.00	.00
5C	16.50	.512	14.56	-5.898	2.08	-.35	.692	6.18	.30	.00	.00
6C	16.10	.502	13.84	-5.247	2.43	-.33	.655	5.60	.30	.00	.00
7C	16.80	.495	14.11	-4.813	2.72	-.20	.625	5.49	.20	.00	.00
8C	16.30	.501	13.98	-5.180	2.47	-.40	.653	5.64	.24	.00	.00
9C	15.50	.514	13.75	-6.053	2.02	-.56	.702	5.92	.33	.00	.00
10C	15.60	.502	13.41	-5.166	2.50	-.84	.661	5.47	.30	.00	.00
11C	15.50	.499	13.18	-4.996	2.62	-.63	.644	5.27	.26	.00	.00
1S	16.20	.509	13.85	-4.963	2.68	-1.29	.659	5.75	.26	.00	.00
2S	15.40	.525	14.13	-7.844	1.45	.31	.745	6.37	.40	.00	.00
3S	15.40	.492	12.86	-4.670	2.88	-.81	.624	5.00	.26	.00	.00
4S	15.50	.508	13.37	-5.203	2.50	-1.13	.669	5.57	.30	.00	.00
5S	15.50	.519	13.88	-6.447	1.87	-.25	.712	6.06	.43	.00	.00
1T	15.50	.527	13.98	-6.668	1.81	-.50	.727	6.28	.44	.00	.00
2T	16.40	.471	13.52	-4.607	2.79	.20	.599	4.89	.30	.00	.00
3T	15.30	.493	12.68	-4.614	2.94	-.47	.612	4.88	.26	.00	.00
4T	15.40	.455	12.56	-4.554	2.77	.59	.584	4.33	.21	.00	.00
5T	15.20	.494	12.77	-4.818	2.75	-.54	.629	4.99	.31	.00	.00
AVERAGES: 01112 BASELINE W198 00 000											
	21.75	.550	19.70	-6.666	1.85	-.63	.739	9.34	3.51	.00	.00
STD	.05	.002	.12	.468	.16	.20	.011	.16	.39	*	*
01112 W230AL003											
	15.76	.501	13.50	-5.284	2.50	-.55	.655	5.48	.30	.00	.00
STD	.44	.016	.54	.829	.41	.52	.041	.51	.07	*	*
PERCENT OF BASELINE											
	72.5	91.2	68.5	120.7	135	113.2	88.6	58.6	8.5	*****	*****
STD%	2.2	3.4	3.2	18.9	36	137.2	6.9	6.5	3.0	*****	*****

01216 W231MN011 (2.5E14) W199 00 000
SOL18 6 /19/81 AM1: PO=91.60MW/CM^2 NO AR COATING

ID	ISC	VOC	IP	LOG(IO)	N	R	FF	Eff	OCD	PCDa	PCDb
3R*	22.10	.559	19.52	-5.410	2.49	-1.76	.718	9.38	.00	.00	.00
1B	21.50	.552	19.46	-6.862	1.78	.11	.724	9.08	3.00	.00	.00
2B	22.00	.555	19.92	-6.652	1.86	-.54	.737	9.52	3.90	.00	.00
3B*	21.50	.543	19.02	-5.747	2.22	-.65	.701	8.66	2.34	.00	.00
4B	21.90	.551	19.83	-6.849	1.77	.01	.726	9.27	3.64	.00	.00
5B	21.50	.548	19.63	-7.543	1.56	.61	.728	9.08	3.64	.00	.00
1C	19.30	.521	16.86	-5.887	2.09	1.01	.657	6.99	.78	.00	.00
2C	20.00	.525	17.63	-6.020	2.03	.57	.676	7.50	.91	.00	.00
3C	19.90	.523	17.81	-6.403	1.86	.08	.706	7.77	.91	.00	.00
4C	19.10	.526	17.02	-6.416	1.87	.60	.691	7.34	.91	.00	.00
5C	18.60	.513	16.43	-6.019	2.00	.24	.684	6.91	.60	.00	.00
6C	19.30	.511	16.72	-5.288	2.39	-.48	.668	6.97	.46	.00	.00
7C	19.20	.515	16.89	-5.868	2.07	.22	.679	7.10	.52	.00	.00
8C	19.40	.520	17.21	-6.172	1.95	.36	.688	7.34	.91	.00	.00
9C	19.70	.515	17.30	-5.618	2.20	-.47	.687	7.37	.65	.00	.00
10C	20.00	.523	17.33	-5.210	2.49	-.77	.673	7.44	.78	.00	.00
11C	19.60	.523	17.17	-5.531	2.28	-.60	.686	7.43	.78	.00	.00
12C	19.20	.518	17.03	-5.954	2.04	-.40	.700	7.37	.78	.00	.00
1S	20.30	.525	17.67	-5.484	2.31	-.05	.668	7.53	.85	.00	.00
2S	20.40	.527	17.84	-5.470	2.33	-.59	.683	7.77	.91	.00	.00
3S	19.90	.523	17.19	-5.246	2.46	-.31	.662	7.28	.91	.00	.00
4S	19.90	.523	17.38	-5.572	2.26	-.10	.674	7.42	.91	.00	.00
5S	19.30	.519	17.14	-5.907	2.07	-.72	.708	7.50	.78	.00	.00
6S	19.70	.522	17.38	-5.614	2.23	-1.06	.704	7.65	.78	.00	.00
1T	19.30	.521	16.87	-5.641	2.22	.03	.673	7.16	.72	.00	.00
2T	20.00	.526	17.81	-6.012	2.04	-.61	.711	7.90	1.00	.00	.00
3T	19.10	.517	16.53	-5.249	2.45	-.59	.668	6.98	.52	.00	.00
4T	19.20	.520	16.16	-4.878	2.75	.28	.621	6.56	.78	.00	.00
5T	19.40	.517	17.13	-5.749	2.14	-.62	.697	7.40	.65	.00	.00
6T	19.70	.523	17.53	-5.971	2.05	-.69	.711	7.74	.91	.00	.00
AVERAGES: 01216 BASELINE W199 00 000											
	21.73	.552	19.71	-6.977	1.74	.05	.729	9.24	3.55	.00	.00
STD	.23	.002	.18	.337	.11	.41	.005	.18	.33	*	*
01216 W231MN011 (2.5E14)											
	19.56	.521	17.17	-5.716	2.19	-.20	.682	7.35	.78	.00	.00
STD	.42	.004	.43	.378	.21	.52	.020	.31	.14	*	*
PERCENT OF BASELINE											
	90.0	94.4	87.1	118.1	126	*****	93.6	79.6	22.0	*****	*****
STD%	2.9	1.2	3.0	9.6	21	*****	3.4	5.0	6.5	*****	*****

10214 W232N/TI001 (1E13) W176-00-000
SOL19 6 /19/81 AM1: PO=91.60MW/CM^2 NO AR COATING

ID	ISC	VOC	IP	LOG(IO)	N	R	FF	Eff	OCD	PCDa	PCDb
3R*	22.10	.553	19.59	-5.583	2.35	-1.45	.719	9.29	.00	.00	.00
1B	21.10	.566	19.66	-8.714	1.34	-.11	.781	9.86	9.50	.00	.00
2B*	15.20	.479	12.47	-4.627	2.85	.53	.591	4.55	.65	.00	.00
3B	21.80	.564	20.39	-9.413	1.22	.51	.775	10.07	10.40	.00	.00
4B	21.70	.563	20.12	-8.613	1.35	.57	.757	9.77	10.40	.00	.00
5B	21.10	.562	19.65	-8.607	1.35	-.20	.782	9.80	9.80	.00	.00
6B	20.90	.560	19.32	-7.909	1.50	-.49	.774	9.58	8.06	.00	.00
1C	20.30	.491	17.47	-4.924	2.54	-1.33	.674	7.10	3.38	.00	.00
2C.*	20.70	.494	15.02	-4.328	3.12	5.80	.444	4.80	3.38	.00	.00
3C	20.90	.494	19.12	-7.722	1.37	.68	.729	7.96	4.94	.00	.00
4C	20.70	.494	18.74	-6.953	1.57	.22	.722	7.81	5.20	.00	.00
5C	20.70	.494	18.89	-7.518	1.41	.53	.729	7.88	4.42	.00	.00
6C	20.70	.492	18.88	-7.370	1.45	.32	.732	7.88	4.16	.00	.00
7C	20.90	.492	19.10	-7.553	1.40	.46	.732	7.96	5.33	.00	.00
8C	21.20	.493	19.03	-6.813	1.60	.87	.694	7.68	5.20	.00	.00
1S	20.80	.496	19.01	-7.629	1.39	.60	.729	7.96	5.46	.00	.00
3S.*	16.40	.493	10.67	-6.374	1.79	16.75	.350	2.99	1.69	.00	.00
4S*	13.30	.490	7.88	-4.533	3.08	19.14	.323	2.23	1.82	.00	.00
5S.*	15.20	.491	9.23	-7.447	1.46	21.52	.318	2.51	1.95	.00	.00
6S.*	17.80	.489	11.45	-4.582	2.88	12.09	.360	3.31	3.64	.00	.00
1T.*	20.80	.492	15.24	-4.257	3.19	5.09	.454	4.91	3.12	.00	.00
3T	21.00	.491	18.97	-7.071	1.52	.79	.706	7.70	4.42	.00	.00
5T	20.50	.490	18.65	-7.212	1.48	.22	.730	7.75	4.55	.00	.00
6T	20.70	.491	18.81	-7.158	1.50	.24	.728	7.82	4.94	.00	.00
AVERAGES: 10214 BASELINE W176-00-000											
	21.32	.563	19.83	-8.651	1.35	.06	.773	9.82	9.63	.00	.00
STD	.36	.002	.38	.477	.09	.41	.009	.16	.86	*	*
10214 W232N/TI001 (1E13)											
	20.76	.493	18.79	-7.084	1.57	.33	.718	7.77	4.73	.00	.00
STD	.23	.002	.44	.737	.32	.57	.018	.23	.59	*	*
PERCENT OF BASELINE											
	97.4	87.5	94.8	118.1	116	585.7	92.9	79.2	49.1	*****	*****
STD%	2.7	.6	4.1	13.5	33	*****	3.5	3.7	11.0	*****	*****

10216 W233CR012 (2E14) W198 00 000
SOL19 6 /19/81 AM1: PO=91.60MW/CM^2 NO AR COATING

ID	ISC	VOC	IP	LOG(IO)	N	R	FF	Eff	OCD	PCDa	PCDb
3R*	22.10	.554	19.43	-5.274	2.56	-1.83	.713	9.23	.00	.00	.00
1B	20.40	.554	18.73	-7.508	1.59	-.36	.758	9.06	4.42	.00	.00
2B*	23.20	.481	20.72	-4.534	2.77	-6.79	.855	10.10	3.38	.00	.00
3B	21.90	.553	19.85	-6.584	1.88	-.89	.746	9.55	4.94	.00	.00
4B	21.60	.551	19.42	-6.100	2.08	-1.40	.741	9.33	3.64	.00	.00
6B.*	21.50	.547	18.13	-4.866	2.86	.26	.624	7.76	3.00	.00	.00
1C	20.10	.550	18.19	-6.578	1.88	-.85	.741	8.66	3.25	.00	.00
2C	19.70	.543	17.76	-6.482	1.90	-.67	.731	8.27	2.21	.00	.00
3C	21.00	.550	19.20	-7.246	1.65	-.31	.749	9.15	3.00	.00	.00
4C	20.40	.543	18.51	-6.855	1.76	-.33	.736	8.62	1.82	.00	.00
5C	21.50	.554	19.90	-8.219	1.41	.05	.764	9.63	4.42	.00	.00
6C	21.40	.554	19.85	-8.436	1.37	.12	.767	9.62	4.55	.00	.00
7C	19.70	.545	17.76	-6.376	1.95	-1.01	.737	8.37	2.60	.00	.00
8C	21.60	.554	19.91	-7.881	1.49	.00	.758	9.59	4.29	.00	.00
9C	20.60	.543	18.95	-7.838	1.47	.16	.751	8.88	2.21	.00	.00
10C	21.00	.546	19.21	-7.292	1.62	-.33	.751	9.11	3.00	.00	.00
1S	21.20	.553	19.64	-8.375	1.38	.20	.763	9.46	3.64	.00	.00
2S	21.40	.556	19.89	-8.608	1.34	.10	.772	9.71	4.81	.00	.00
3S	19.90	.550	18.28	-7.506	1.58	-.49	.761	8.81	3.25	.00	.00
5S	20.20	.549	18.36	-6.767	1.81	-.88	.749	8.79	3.90	.00	.00
6S	21.40	.551	19.83	-8.303	1.39	.00	.768	9.58	4.29	.00	.00
1T	22.50	.552	20.59	-7.433	1.59	.05	.744	9.77	3.00	.00	.00
2T	21.00	.551	19.16	-7.018	1.72	-.67	.753	9.21	3.25	.00	.00
3T	20.20	.550	18.43	-7.007	1.73	-.79	.755	8.87	3.64	.00	.00
4T	20.90	.550	19.26	-7.806	1.50	-.18	.761	9.25	3.12	.00	.00
5T	21.50	.551	19.79	-7.666	1.53	-.25	.760	9.52	3.90	.00	.00
6T	21.10	.548	19.33	-7.347	1.61	-.36	.754	9.22	3.00	.00	.00
AVERAGES: 10216 BASELINE W198 00 000											
	21.30	.553	19.33	-6.731	1.85	-.88	.748	9.31	4.33	.00	.00
STD	.65	.001	.46	.584	.20	.42	.007	.20	.53	*	*
10216 W233CR012 (2E14)											
	20.87	.550	19.13	-7.478	1.60	-.31	.754	9.15	3.39	.00	.00
STD	.71	.004	.77	.659	.18	.37	.011	.44	.80	*	*
PERCENT OF BASELINE											
	98.0	99.5	99.0	88.9	87	165.1	100.7	98.2	78.2	*****	*****
STD%	6.4	.9	6.5	20.3	20	79.6	2.4	7.0	30.3	*****	*****

10528 W234-MO-010
ROSE2 6 /19/81 AM1: PO=91.60MW/CM^2 NO AR COATING

ID	ISC	VOC	IP	LOG(IO)	N	R	FF	Eff	OCD	PCDa	PCDb
3R*	22.10	.548	19.37	-5.578	2.33	-.24	.681	8.72	.00	.00	.00
1C	19.80	.524	18.23	-7.924	1.41	.20	.751	8.24	1.11	.00	.00
2C	19.60	.523	17.88	-7.222	1.58	-.13	.741	8.04	1.37	.00	.00
3C	19.60	.522	17.87	-7.212	1.58	-.13	.741	8.02	1.11	.00	.00
4C	19.60	.524	17.94	-7.529	1.50	.12	.743	8.07	1.33	.00	.00
5C	19.60	.523	17.97	-7.800	1.43	.51	.738	8.00	1.04	.00	.00
6C	19.10	.520	17.49	-7.490	1.51	-.02	.746	7.84	.44	.00	.00
7C	19.30	.524	17.61	-7.230	1.59	-.22	.744	7.96	1.33	.00	.00
8C	19.60	.524	17.89	-7.315	1.56	.00	.740	8.04	1.30	.00	.00
9C	19.50	.524	17.84	-7.420	1.53	-.05	.745	8.05	1.37	.00	.00
10C	19.30	.522	17.61	-7.209	1.59	-.22	.744	7.92	1.11	.00	.00
11C	19.50	.524	17.85	-7.505	1.51	.08	.744	8.03	1.37	.00	.00
12C	19.40	.522	17.71	-7.353	1.55	.06	.740	7.92	1.30	.00	.00
13C	19.40	.524	17.77	-7.578	1.49	.17	.743	7.98	1.37	.00	.00
1B	21.10	.547	19.51	-8.175	1.41	.09	.762	9.30	3.38	.00	.00
2B	21.00	.546	19.38	-7.930	1.46	-.11	.762	9.24	3.25	.00	.00
3B	21.10	.547	19.54	-8.409	1.36	.29	.761	9.29	3.64	.00	.00
4B	21.20	.547	19.50	-7.777	1.50	.04	.753	9.24	3.77	.00	.00
1T	19.30	.522	17.62	-7.282	1.57	-.09	.742	7.91	1.04	.00	.00
2T	19.20	.520	17.38	-6.824	1.70	-.16	.729	7.70	1.11	.00	.00
3T	19.10	.520	17.40	-7.143	1.60	-.23	.742	7.79	1.17	.00	.00
4T	19.10	.520	17.41	-7.209	1.58	-.11	.740	7.77	1.11	.00	.00
5T	19.20	.520	17.53	-7.280	1.56	-.11	.742	7.84	1.11	.00	.00
6T	19.00	.519	17.28	-7.023	1.64	-.34	.741	7.72	1.04	.00	.00
1S	19.70	.525	17.93	-7.066	1.64	-.21	.739	8.08	1.43	.00	.00
2S	19.50	.524	17.79	-7.220	1.59	-.17	.742	8.02	1.37	.00	.00
3S	19.50	.524	17.75	-7.108	1.62	-.15	.738	7.98	1.30	.00	.00
4S	19.30	.523	17.57	-7.045	1.64	-.33	.742	7.92	1.37	.00	.00
5S	19.50	.524	17.82	-7.465	1.52	.22	.738	7.97	1.43	.00	.00
6S	19.30	.523	17.62	-7.293	1.57	-.09	.742	7.92	1.37	.00	.00
AVERAGES: 10528 BASELINE											
	21.10	.547	19.48	-8.073	1.43	.08	.760	9.27	3.51	.00	.00
STD	.07	.000	.06	.240	.05	.15	.004	.03	.21	*	*
10528 W234-MO-010											
	19.40	.523	17.71	-7.310	1.56	-.06	.741	7.95	1.22	.00	.00
STD	.21	.002	.22	.238	.06	.19	.004	.12	.21	*	*
PERCENT OF BASELINE											
	91.9	95.6	90.9	109.4	109	-72.8	97.6	85.8	34.6	*****	*****
STD%	1.3	.4	1.4	5.7	9	841.8	1.0	1.6	8.3	*****	*****

10421 W235N/V001 (1.5E14) W176 00 000
SOL19 6 /19/81 AM1: PO=91.60MW/CM^2 NO AR COATING

ID	ISC	VOC	IP	LOG(IO)	N	R	FF	Eff	OCD	PCDa	PCDb
3R*	22.10	.552	19.54	-5.555	2.36	-1.28	.712	9.19	.00	.00	.00
1B.*	15.40	.471	10.39	-3.529	4.56	4.43	.418	3.21	1.43	.00	.00
2B	21.10	.562	19.53	-8.310	1.41	.22	.761	9.55	9.88	.00	.00
3B.*	6.70	.385	4.41	-3.516	4.72	1.85	.419	1.14	.59	.00	.00
4B	21.30	.556	19.62	-8.065	1.45	.52	.745	9.33	9.88	.00	.00
5B	21.00	.563	19.53	-8.677	1.34	.15	.772	9.65	10.66	.00	.00
1T	21.40	.500	19.48	-7.851	1.35	1.48	.704	7.96	9.62	.00	.00
2T	21.10	.494	19.01	-7.319	1.46	1.59	.685	7.56	7.28	.00	.00
3T	20.90	.499	19.21	-8.182	1.28	.95	.731	8.06	8.32	.00	.00
4T.*	16.70	.469	11.39	-3.470	4.60	3.28	.428	3.55	2.73	.00	.00
5T	20.50	.485	15.84	-4.233	3.18	2.55	.513	5.39	5.98	.00	.00
6T	20.70	.495	18.98	-8.045	1.30	1.01	.726	7.86	7.80	.00	.00
1S	21.40	.502	19.65	-8.519	1.22	1.65	.713	8.10	10.66	.00	.00
2S	21.30	.500	19.62	-8.662	1.19	1.47	.723	8.14	8.58	.00	.00
3S	21.20	.496	19.52	-8.684	1.18	1.55	.720	8.01	8.32	.00	.00
4S	20.60	.494	18.95	-8.184	1.27	.81	.736	7.92	9.10	.00	.00
5S	21.10	.496	18.92	-7.127	1.52	1.68	.677	7.49	8.84	.00	.00
6S	20.70	.491	17.63	-4.822	2.61	-.80	.651	7.00	4.94	.00	.00
1C	21.30	.495	17.98	-5.421	2.21	2.18	.596	6.64	7.80	.00	.00
2C	20.30	.479	15.37	-4.067	3.37	2.69	.496	5.10	4.42	.00	.00
3C	20.70	.494	18.93	-7.868	1.33	1.02	.721	7.80	7.28	.00	.00
4C	20.40	.482	15.23	-3.906	3.63	2.45	.488	5.08	3.90	.00	.00
5C	20.90	.498	18.99	-7.744	1.37	1.53	.700	7.70	7.80	.00	.00
6C	20.90	.496	18.54	-6.840	1.61	2.09	.655	7.18	7.93	.00	.00
7C	21.10	.500	19.46	-8.561	1.21	1.17	.732	8.16	10.92	.00	.00
8C	21.00	.497	19.11	-7.754	1.37	1.39	.705	7.78	8.58	.00	.00
9C	20.80	.496	19.10	-8.264	1.26	1.19	.725	7.91	9.10	.00	.00
10C	20.60	.497	18.95	-8.393	1.24	1.19	.728	7.88	8.06	.00	.00
11C	20.70	.493	18.26	-6.392	1.75	1.52	.658	7.11	6.50	.00	.00
12C	20.70	.496	18.93	-7.893	1.33	1.02	.722	7.84	7.80	.00	.00
13C	20.70	.500	19.06	-8.403	1.24	1.12	.731	8.00	7.80	.00	.00
AVERAGES: 10421 BASELINE W176 00 000											
	21.13	.560	19.56	-8.351	1.40	.30	.759	9.51	10.14	.00	.00
STD	.13	.003	.04	.252	.05	.16	.011	.13	.37	*	*
10421 W235N/V001 (1.5E14)											
	20.88	.495	18.53	-7.214	1.69	1.44	.676	7.40	7.81	.00	.00
STD	.30	.006	1.25	1.522	.73	.69	.075	.92	1.68	*	*
PERCENT OF BASELINE											
	98.8	88.3	94.7	113.6	120	484.4	89.1	77.8	77.0	*****	*****
STD%	2.0	1.5	6.6	21.4	57	623.9	11.3	10.9	20.0	*****	*****

10422 W237CR001 (1.5E14) W198 00 000
SOL19 6 /19/81 AM1: PO=91.60MW/CM^2 NO AR COATING

ID	ISC	VOC	IP	LOG(IO)	N	R	FF	Eff	OCD	PCDa	PCDb
3R*	22.10	.550	19.47	-5.433	2.43	-1.34	.707	9.09	.00	.00	.00
1B	21.40	.553	19.78	-8.388	1.37	.62	.750	9.38	5.33	.00	.00
2B	21.40	.552	19.94	-8.932	1.27	.30	.772	9.64	4.68	.00	.00
3B	21.50	.553	20.02	-8.940	1.27	.47	.766	9.64	5.46	.00	.00
4B	21.40	.552	19.90	-8.770	1.30	.32	.768	9.59	4.68	.00	.00
5B	21.40	.550	19.80	-8.248	1.40	.13	.762	9.49	4.29	.00	.00
1T	21.30	.509	19.77	-8.883	1.18	.83	.751	8.61	5.27	.00	.00
2T	21.90	.514	20.30	-8.703	1.22	.68	.752	8.96	5.72	.00	.00
3T	22.30	.515	20.65	-8.486	1.26	.48	.755	9.17	6.70	.00	.00
4T	21.90	.510	20.31	-8.782	1.20	.80	.750	8.85	4.94	.00	.00
5T	21.60	.510	20.00	-8.550	1.24	.63	.751	8.75	5.33	.00	.00
6T	21.50	.508	19.80	-8.029	1.33	.39	.747	8.63	5.20	.00	.00
1S	21.90	.509	20.31	-8.708	1.21	.66	.753	8.88	5.59	.00	.00
2S	21.60	.509	19.72	-8.228	1.30	1.88	.699	8.13	5.46	.00	.00
3S	22.10	.509	20.47	-8.589	1.23	.65	.751	8.93	6.24	.00	.00
4S	21.60	.509	19.96	-8.352	1.27	.53	.750	8.72	5.59	.00	.00
5S	21.60	.510	19.95	-8.257	1.29	.41	.752	8.76	5.59	.00	.00
6S	22.20	.508	17.82	-4.702	2.78	2.69	.541	6.46	4.23	.00	.00
1C	22.50	.515	20.68	-7.973	1.36	.62	.738	9.04	6.24	.00	.00
2C	21.70	.510	19.84	-7.417	1.48	.15	.739	8.65	5.20	.00	.00
3C	21.90	.512	20.23	-8.326	1.28	.57	.748	8.87	7.02	.00	.00
4C	21.70	.512	20.16	-8.848	1.19	.66	.756	8.89	6.24	.00	.00
5C	21.60	.510	19.88	-8.174	1.31	.79	.737	8.58	6.63	.00	.00
6C	21.90	.513	20.35	-8.826	1.20	.53	.760	9.03	6.50	.00	.00
7C	21.60	.510	20.07	-8.984	1.16	.84	.753	8.77	6.63	.00	.00
8C	21.60	.509	19.97	-8.308	1.28	.40	.754	8.77	5.33	.00	.00
9C	21.50	.510	19.96	-8.897	1.18	.79	.753	8.73	5.33	.00	.00
10C	21.80	.512	20.17	-8.575	1.24	.74	.748	8.83	5.98	.00	.00
11C	21.90	.515	20.33	-8.791	1.21	.66	.755	9.01	6.76	.00	.00
12C	21.70	.511	20.05	-8.352	1.28	.57	.749	8.78	5.46	.00	.00
AVERAGES: 10422 BASELINE W198 00 000											
	21.42	.552	19.89	-8.656	1.32	.37	.764	9.55	4.89	.00	.00
STD	.04	.001	.09	.286	.05	.16	.008	.10	.44	*	*
10422 W237CR001 (1.5E14)											
	21.79	.511	20.03	-8.323	1.32	.75	.739	8.70	5.80	.00	.00
STD	.27	.002	.53	.835	.31	.50	.043	.51	.68	*	*
PERCENT OF BASELINE											
	101.7	92.5	100.7	103.8	100	201.7	96.8	91.1	118.6	*****	*****
STD%	1.5	.6	3.1	13.1	29	285.6	6.6	6.3	25.7	*****	*****

10713 W238MN001 (8E14) W198-00-000
SOL19 8 /18/81 AM1: PO=91.60MW/CM^2 NO AR COATING

ID	ISC	VOC	IP	LOG(IO)	N	R	FF	Eff	OCD	PCDa	PCDb
3R*	22.10	.552	19.22	-5.045	2.72	-1.67	.693	8.94	.00	.00	.00
1B	21.30	.547	18.14	-6.340	1.96	4.35	.577	7.12	4.42	.00	.00
2B	20.90	.544	18.88	-8.162	1.40	3.14	.664	7.98	3.25	.00	.00
3B	20.80	.540	18.14	-6.663	1.81	3.37	.617	7.33	3.12	.00	.00
4B	20.60	.535	17.97	-6.804	1.75	3.67	.612	7.14	2.60	.00	.00
1C	19.20	.488	17.03	-8.763	1.16	5.46	.599	5.93	1.04	.00	.00
2C	16.30	.466	11.58	-4.021	3.48	5.69	.439	3.53	.34	.00	.00
3C	18.00	.485	15.41	-7.394	1.43	6.19	.560	5.17	.68	.00	.00
4C	15.40	.485	10.66	-3.935	3.81	6.83	.422	3.33	.59	.00	.00
5C	19.00	.489	15.84	-6.472	1.72	5.84	.539	5.30	.55	.00	.00
6C	17.50	.482	13.61	-4.928	2.54	5.57	.495	4.42	.55	.00	.00
7C	18.60	.484	16.07	-8.685	1.16	7.22	.549	5.23	.81	.00	.00
8C	18.60	.488	15.68	-7.251	1.48	6.72	.538	5.17	.78	.00	.00
9C	18.50	.487	16.05	-8.409	1.22	6.72	.561	5.35	.72	.00	.00
10C	18.70	.487	15.33	-5.741	2.03	5.12	.535	5.16	.81	.00	.00
1S	19.00	.488	16.85	-8.284	1.24	4.90	.609	5.97	.91	.00	.00
2S	18.20	.481	13.83	-4.148	3.33	2.99	.499	4.62	.78	.00	.00
3S	19.70	.491	16.38	-5.864	1.97	4.48	.553	5.65	1.56	.00	.00
4S	19.40	.485	17.01	-7.527	1.39	4.43	.603	6.00	1.43	.00	.00
5S	15.70	.472	11.27	-3.506	4.61	.69	.475	3.73	.59	.00	.00
1T	17.10	.483	14.95	-8.635	1.17	6.93	.572	5.00	.46	.00	.00
2T	18.00	.486	15.83	-6.537	1.69	2.26	.646	5.98	.65	.00	.00
3T	17.90	.483	14.95	-7.169	1.49	7.26	.527	4.82	.46	.00	.00
4T	17.60	.481	14.03	-5.192	2.34	5.19	.516	4.62	.39	.00	.00
AVERAGES: 10713 BASELINE W198-00-000											
	20.90	.542	18.28	-6.992	1.73	3.63	.618	7.39	3.35	.00	.00
STD	.25	.005	.35	.696	.20	.46	.031	.35	.67	*	*
10713 W238MN001 (8E14)											
	18.02	.484	14.86	-6.445	2.07	5.29	.539	5.00	.74	.00	.00
STD	1.17	.006	1.87	1.724	1.00	1.71	.055	.79	.31	*	*
PERCENT OF BASELINE											
	86.2	89.3	81.3	107.8	120	145.7	87.2	67.6	22.1	*****	*****
STD%	6.7	1.8	12.0	36.3	79	71.3	13.7	14.4	15.6	*****	*****

APPENDIX V

Solar Cell and Materials Evaluation by DLTS

Throughout the program, we have monitored the electrically active impurity concentration of representative wafers (as-grown) and solar cells to correlate device and materials effects due to impurities. Deep levels identified in Czochralski wafers and the corresponding solar cells are listed in Table V-1. The data were obtained by deep-level transient spectroscopy as described in Volume 1 of reference 3.

Deep levels observed due to various grown-in impurities are illustrated in Figure V-1, which also includes impurities from previous phases of this program. Note that we were unable to detect deep levels due to grown-in Mn, Ag, Sn, Ni, and Cu, despite the fact that impurity content of the wafers was several orders of magnitude higher than the DLTS detection limit ($\sim 3.5 \times 10^{11}$ cm^{-3}) for these samples. Some investigators report levels[42,43] due to these impurities, but in those studies the impurities were incorporated by diffusion or other methods after the crystal growth. We also found cases such as Cr and Al for which we observed deep levels that were not in agreement with values in the literature. For example, the reported levels for Cr and $E_V+0.11eV$, $E_C-0.23eV$ and $E_C-0.41$, while for Al they are $E_V+0.057eV$, $E_V+0.214eV$, $E_V+0.312eV$, and $E_V+0.392eV$.

Some of the differences cited above are expected because deep levels depend on the site or configuration the impurity acquires and the complexes it is able to form during the growth process.

Figure V-2 depicts the fraction of total impurity content which becomes electrically active in single-crystal silicon. (We define the electrical activity to be the concentration of the trap which has the highest density. This is not necessarily the one which controls the carrier lifetime in the bulk.)

TABLE V-1

DLTS RESULTS ON PHASE IV IMPURITY-DOPED INGOTS

Ingot ID	Best Estimate of Metallurgical Impurity Concentration (N_M)	Active Impurity Concentration (cm^{-3}) In the Wafer N_{TW}	In the Cell (near junction) N_{TC}	$\frac{N_{TW}}{N_M}$
V-200-Poly	4×10^{14}	1.3×10^{14}	no data	0.32
Ti-202-Poly	2×10^{13}	1.12×10^{13}	1.15×10^{12}	0.56
V-203-Poly	4×10^{13}	1.7×10^{13}	undetectable	0.34
206-V	2.6×10^{13}	6.43×10^{12}	undetectable	0.25
207-Mo	2.0×10^{12}	2.2×10^{12}	9×10^{11}	1.1
208-Cr	1.9×10^{14}	3.91×10^{13}	undetectable	0.21
209-Ti	2.0×10^{13}	8.12×10^{12}	1.15×10^{12}	0.40
210-Ti	1.0×10^{14}	2.91×10^{13}	3.6×10^{12}	0.30
211-Cu	1.8×10^{15}	undetectable	undetectable	-
212-Cu	1×10^{16}	undetectable	undetectable	-
214-V-Poly	2×10^{14}	6×10^{13}	no data	0.30
215-Mo-Poly	2.5×10^{12}	4.5×10^{12}	no data	1.8
216-Cr-Poly	8×10^{14}	7.5×10^{12}	no data	.009
217-Ta	1.5×10^{11}	undetectable	undetectable	-
218-Ta	6.5×10^{10}	undetectable	undetectable	-
222-Ag	4.5×10^{15}	undetectable	undetectable	-
223-Ni	1.0×10^{15}	undetectable	undetectable	-
225-Mn	1.0×10^{15}	undetectable	undetectable	-
227-Cr-Poly	4.0×10^{14}	1.2×10^{13} average	undetectable	0.03
228-Gd	-	undetectable	undetectable	-
229-Au	6.0×10^{14}	8×10^{13}	undetectable	0.13
230-Al	1.2×10^{17}	2×10^{12}	6.3×10^{13}	0.000016
231-Mn-Poly		undetectable	undetectable	-
232-N/Ti	1.0×10^{13}	3.85×10^{12}	6.4×10^{11}	0.39
233-Cr	1.2×10^{14}	2.52×10^{13}	undetectable	0.21
234-Mo	5.0×10^{11}	5.5×10^{11}	5.5×10^{11}	1.1
235-N/V	6.0×10^{12}	1.4×10^{12}	4×10^{11}	0.24
236-N/Mo	3.0×10^{12}	undetectable	undetectable	-
237-Cr	2.0×10^{13}	3.0×10^{12}	undetectable	.15

The data in the figure suggest that the electrically active concentration of the grown-in impurities may be less than the metallurgical concentration of the diffusion depending on the species involved. There are several factors which may influence the electrical activity of an impurity in a crystal:

a. The ability of the impurity to produce an excited state within the bandgap (if it does not, then according to our definition the electrical activity will be zero).

b. The thermal history of the wafer. It is shown clearly in the section 3.8 that N_2, $HC\ell$, or $POC\ell_3$ treatment after the crystal growth can significantly alter the electrically active impurity concentration in the crystal.

c. The solubility of impurity in solid silicon. Following solidification, as the crystal cools, impurities will tend to precipitate out and may, therefore, become electrically inactive. The amount of impurity that can precipitate in the form of second place will depend on the difference in solubilities at two temperatures.

d. The diffusion constant of the impurity in silicon. Impurities with small diffusion constants may not obtain equilibrium with the lattice. The amount of precipitation and thus electrical activity then becomes related to the diffusion constant.

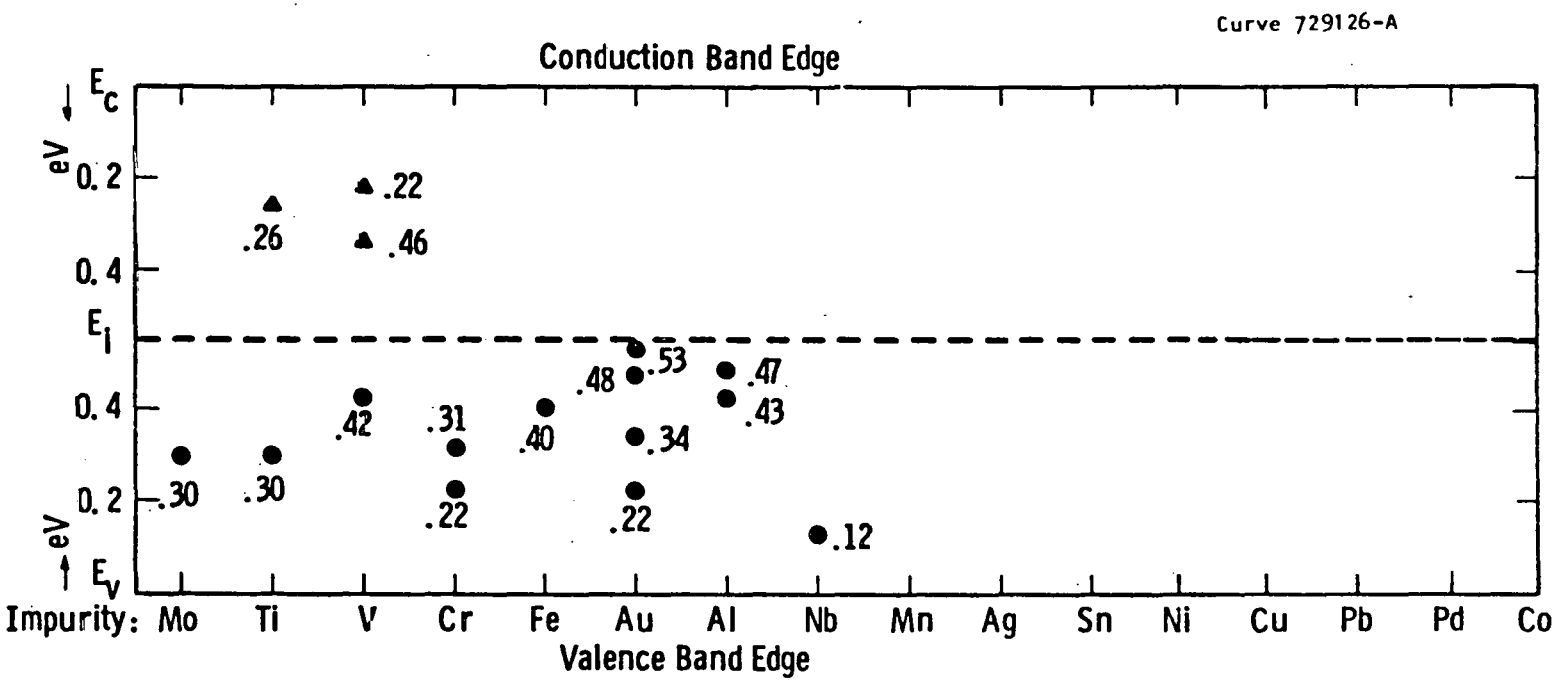

Figure V-1 Measured deep levels for impurities grown into silicon single crystals

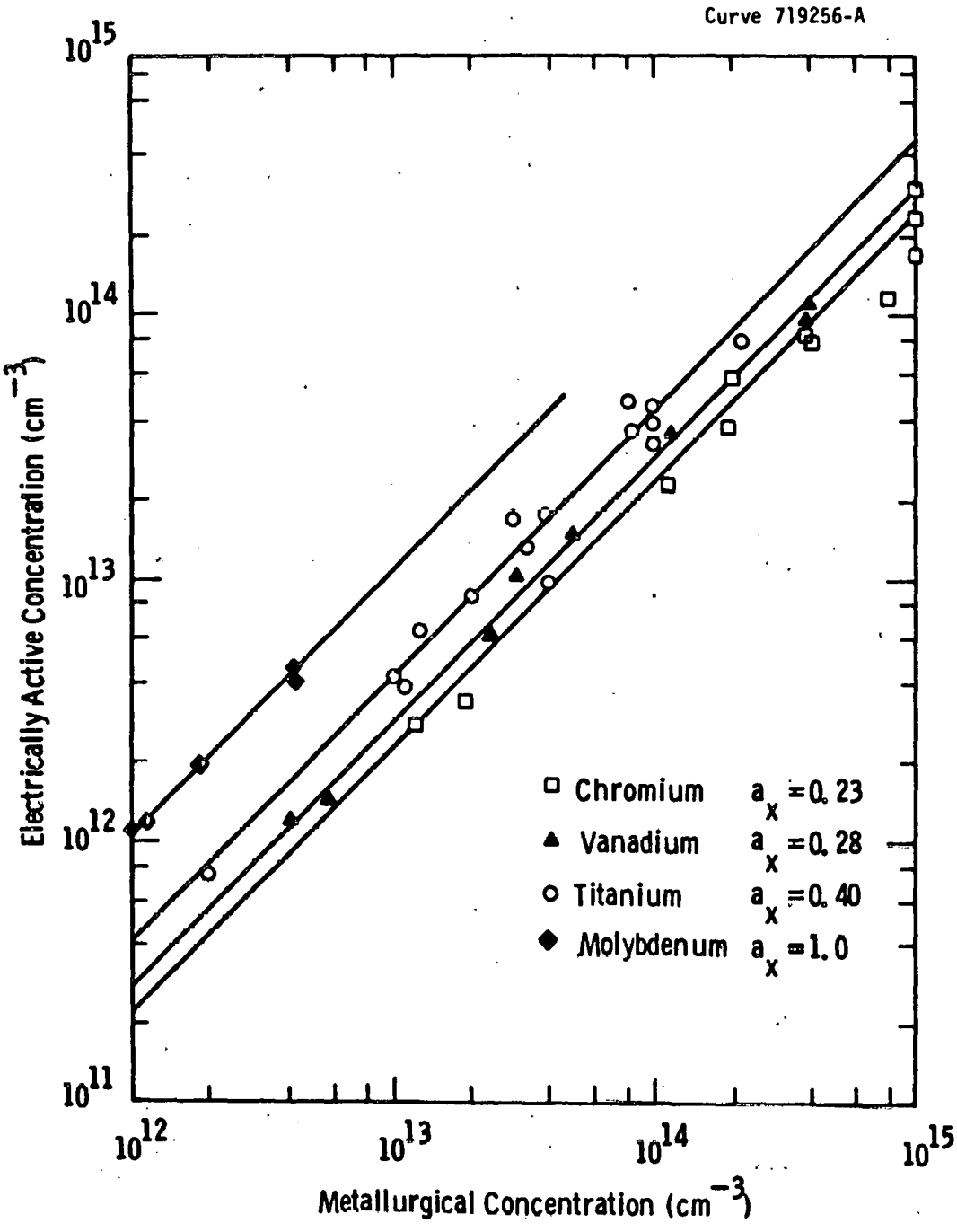

Figure V-2 Variation in electrically active impurity concentration with metallurgical doping level of silicon

APPENDIX VI

List of Related Papers on Impurity Effects

1. J. R. Davis, et al., "Silicon Solar Cells from Transition Metal-Doped Czochralski and Web Crystals," Proc. 12th PVSC, IEEE, NY (1977).

2. R. H. Hopkins, et al., "Crystal Growth Considerations in the Use of Solar Grade Silicon," J. Crystal Growth 42, 493 (1977).

3. J. R. Davis, et al., "Characterization of the Effects of Metallic Impurities on Solar Cell Performance," Proc. 13th PVSC, IEEE, NY 358 (1978).

4. R. G. Seidensticker, et al., "Solute Partitioning During Dendritic Web Growth," J. Crystal Growth 46, 51 (1979).

5. "Titanium in Silicon as a Deep Level Impurity," J. W. Chen, A. G. Milnes, and A. Rohatgi, Journal of Solid State Electronics, Vol. 22, No. 9-D, p. 801 (1979).

6. J. R. Davis, et al., "Impurity Effects in Silicon Solar Cells," Electrochemical Society, Extended Abstracts, Vol. 79-1, Abs. No. 65, p. 174 (1979).

7. A. Rohatgi, et al., "Effect of Ti, Cu, and Fe on Silicon Solar Cells," Solid St. Electr. 23 415 (1980).

8. R. G. Seidensticker and R. H. Hopkins, "Silicon Ribbon Growth by the Dendritic Web Process," J. Crystal Growth 50 221 (1980).

9. A. Rohatgi, et al., "$POCl_3$ Gettering of Titanium, Molybdenum and Iron-Contaminated Silicon Solar Cells," Proc. 14th PVSC, IEEE, NY, 908 (1980).

10. R. G. Seidensticker, et al., "Development of Processes for the Production of Low-Cost Silicon Dendritic Web for Solar Cells," Proc. 14th PVSC, IEEE, NY, 25 (1980).

11. J. R. Davis and A. Rohatgi, "Theoretical Design Considerations for Back Surface Field Solar Cells," J. R. Davis and A. Rohatgi, Proc. 14th PVSC, IEEE, NY 569 (1980).

12. J. R. Davis, et al., "Impurities in Silicon Solar Cells," IEEE Trans. of Electron Devices, ED-27, 677 (1980).

13. A. Rohatgi, "Application of DLTS Technique for the Study of Junctions and Interfaces," Proceedings of International Symposium on Science New Delhi, India, 115 (1980).

14. J. R. Davis, et al., "Impurities in Silicon," invited paper presented at the Electrochemical Society Meeting, Extended Abstracts, Vol. 80-1, Abs. No. 301, (1980).

15. A. Rohatgi, et al., "The Impact of Molybdenum on Silicon and Silicon Solar Cell Performance," Journal of Solid State Electronics, 23, 1185, (1980).

16. A. Rohatgi, et al., "The Properties of Polycrystalline Silicon Solar Cells with Controlled Titanium Additions," IEEE Transaction on Electron Devices, ED-28, 103 (1981).

17. M. H. Hanes, et al., "Thermal Stability of Impurities in Silicon Solar Cells," Proc. 15th PVSC, IEEE, NY (1981).

18. R. H. Hopkins, "Silicon Sheet: Key to Low-Cost Solar Cells," Proc. ECS Symposium on PV Materials and Processes, ECS, NY (1981).

☆ U.S. GOVERNMENT PRINTING OFFICE: 1982-546-085/3114